Electrocatalysis and Kinetics of the Direct Alcohol Fuel Cells: DEMS and ac Voltammetry Studies

Dissertation

zur

Erlangung des Doktorgrades (Dr. rer.nat)

der

Mathematisch-Naturwissenschaftlichen Fakultät

der

Rheinischen Friedrich-Wilhelms-Universität Bonn

vorgelegt von

Ehab Mostafa Othman Mostafa

aus

Mansoura, Ägypten

Bonn, 2013

Angefertigt mit Genehmigung der Mathematisch-Naturwissenschaftlichen Fakultät der Rheinischen Friedrich-Wilhelms-Universität Bonn

Promotionskommission

Erster Gutachter: Prof. Dr. Helmut Baltruschat
Zweiter Gutachter: Prof. Dr. Klaus Wandelt
Fachnaher Gutachter: Prof. Dr. Werner Mader
Fachfremder Gutachter: Prof. Dr. Karl Maier

Tag der mündlichen Prüfung:

11 . 01 .2013

Ich versichere, dass ich diese Arbeit selbständig verfasst und keine anderen als die angegebenen Quellen und Hilfsmittel benutzt sowie die Zitate kenntlich gemacht habe.

Bonn, 16.11.2012

Ehab Mostafa Othman Mostafa

To my country (Egypt),
My parents and
My family

"A Person Who Never Made a Mistake, Never Tried Anything New"

Albert Einstein

Contents

1. Introduction

2. Materials, methods and instruments

3. Electrocatalytic oxidation and adsorption rate of methanol

Notations

a	Activity	$j_{p,c}$	Current density of the cathodic peak
A	Current efficiency	j_o	Exchange current density
A^{app}	Apparent current efficiency	k_{app}	Apparent rate constant
A'	Pre-exponential factor	k_1	Rate constant of OH_{ad} formation
A_{real}	Real surface area	k_{-1}	Rate constant of H_2O formation
A_{geom}	Geometric surface area	k_2	Rate constant of CO_2 formation
b	Tafel slope	K^*	Calibration constant of DEMS
C	Concentration	K_x^o	Calibration constant of species (x)
C^*	Concentration in the bulk of the solution	m	Number of step atoms
C_{dl}	Double layer capacitance	n	Number of terrace atoms
E	Potential	N	Transfer efficiency
$E^{0'}$	Standard formal potential	Q_H	Charge of H_{ad} at Pt surface
$E_{p,a}$	Anodic peak potential	Q_F	Faradaic charge
$E_{p,c}$	Cathodic peak potential	Q_i	Ionic charge
E_0	Initial potential	Q_S^H	Charge of hydrogen desorbed from free Pt step sites
E_f	Final potential	Q_{S+T}^H	Charge of hydrogen desorbed from free Pt step and terrace sites
E_{ad}	Adsorption potential	Q_S^{Ru}	Charge of Ru deposited at Pt step sites
E_{UPD}	UPD peak potential	Q_{Sn}^H	Charge of hydrogen desorbed from Sn modified Pt surface
E_B	Thermodynamic potential of the bulk deposition	R	Universal gas constant, 8.314 $Jk^{-1}mol^{-1}$
ΔE_p	Underpotential shift = E_{UPD} - E_B	R_{el}	Electrolyte resistance
F	Faraday constant, 96500 C mol^{-1}	R_{ct}	Charge transfer resistance
f	Frequency	R_{ad}	Adsorption resistance
f_2	Collection efficiency of the detection compartment of the dual thin layer cell	r_{ads}	Adsorption rate
h	Distance between the 1st and 2nd layer of the *fcc* crystal.	T	Absolute temperature
H_{UPD}	Underpotential deposited hydrogen	t	time
I_F	Faradaic current	$t_{ad}^{\min}$	Minimum adsorption time
I_x	Ionic current of species (x)	t_{max}	Maximum time
$i_{1/2}$	Half wave current	v	Sweep rate
i_{dc}	Direct current	u_{ac}	AC voltage
i_{ac}	Alternating current	u_{dc}	DC voltage
$i_{ac\text{-}re}$	Real part of the ac current	u_{ac}^o	Total ac voltage
$i_{ac\text{-}im}$	Imaginary part of the ac current	u_{ac}^{corr}	Corrected ac voltage
i_{dl}	Double layer charging current	u	Electrolyte flow rate
i_{max}	Maximum current	u_A	AC amplitude
j	Current density	Y	Admittance
j_{max}	Maximum current density	$Y_{re\text{-}corr}$	Corrected real part of the admittance
$j_{p,a}$	Current density of the anodic peak	$Y_{im\text{-}corr}$	Corrected imaginary part of the admittance

z	Number of electron transferred
Z	Complex impedance
$\|Z\|$	Absolute value of the impedance
Z_{re}	Real part of the impedance
Z_{im}	Imaginary part of the impedance
Z_f	Faradaic impedance
Γ_{CO}	CO concentration at Pt surface
Γ_H	Number of surface active sites
φ	Phase angle
$\Delta H^{\ddagger}$	Activation enthalpy
$\Delta S^{\ddagger}$	Activation entropy
$\Delta G^{\ddagger}$	Activation free energy
α	Charge transfer coefficient (Symmetry factor)
α'	Apparent charge transfer coefficient
α'_{corr}	Corrected α'
η	Overpotential
θ^{step}	Coverage at steps
$\theta^{terrace}$	Covergae at terrace
ω	Angular frequency
μ_{ML}	Chemical potential of the metal in the monolayer
μ^0_{M}	Chemical potential of bulk metal
Φ	Work function
Ψ	Binding energy
ε_d	Average energy of the d-band
ε_F	Energy of Fermi level
ϑ_{CO}	Relative coverage of CO
ϑ_{CO}^{max}	Maximum CO coverage
τ	Time constant

Abbreviations

AC	Alternating current
AFC	Alkaline fuel cell
ATR-FTIRS	Attenuated total reflection Fourier transform infrared spectroscopy
BB-SFG	Broad band sum-frequency generation
CV	Cyclic voltammetry
CE	Counter electrode
CO_{ad}	Adsorbed CO layer
DC	Direct current
DEMS	Differential electrochemical mass spectrometry
DMFC	Direct methanol fuel cell
DAFC	Direct alcohol fuel cell
DFT	Density function theory
EIS	Electrochemical impedance spectroscopy
eV	Electron volt
fcc	Face centered cubic
FM	Frank-van-der Merwe growth mode
FTIR	Fourier transform infrared spectroscopy
LH	Langmuir-Hinshelwood
MCFC	Molten carbonate fuel cell
ML	Monolayer
MSCV	Mass spectrometric cyclic voltammogram
n.d.	Not determined
PEMFC	Polymer electrolyte membrane fuel cell
PAFC	Phosphoric acid fuel cell
Pt(Poly)	Polycrystalline platinum
ppm	Part per million
RMS	Root mean square
REF	Reference electrode
rds	Rate determining step
RHE	Reversible hydrogen electrode
SOFC	Solid oxide fuel cell
SK	Stranski-Krastanov growth mode
SERS	Surface Enhanced Raman Spectroscopy
STM	Scanning Tunneling Microscope
SE	Supporting electrolyte
UHV	Ultrahigh Vacuum
UPD	Underpotential deposition
VW	Volmer-Weber growth mode
WE	Working electrode
XPS	X-ray Photoelectron Spectroscopy

1. Introduction

1.1 Basics

1.1.1 Voltammetry techniques

Voltammetry became one of the most important methods used for studying of the electrode processes such as adsorption/desorption and the rate of electron transfer. It includes a family of techniques with the common characteristics that the potential of the working electrode is controlled (typically with a potentiostat) and the current flowing through the electrode is measured.

1.1.1.1 Potentiodynamic technique (cyclic voltammetry)

In this technique, the electrode potential is ramped between two limits, usually chosen in aqueous electrolyte to lie between hydrogen and oxygen evolution, to remove any impurities either by oxidation or reduction [1]. The applied potential is usually generated with a function generator and controlled by the potentiostat. A triangular potential sweep is applied to the working electrode as shown in Fig. 1-1, the electrode potential is varied linearly with time *(t)* with a sweep rate *($v = dE/dt$)*. The applied sweep rate can vary from few mVs^{-1} to 1000 Vs^{-1}. The current *(I)* vs. potential *(E)*, equivalent to *(I)* vs. *(t)*, is recorded. The sweep is started at a potential where no electrochemical reaction occurs *(E_0)* to the final potential *(E_f)* and returns back to *(E_0)* with a constant sweep rate.

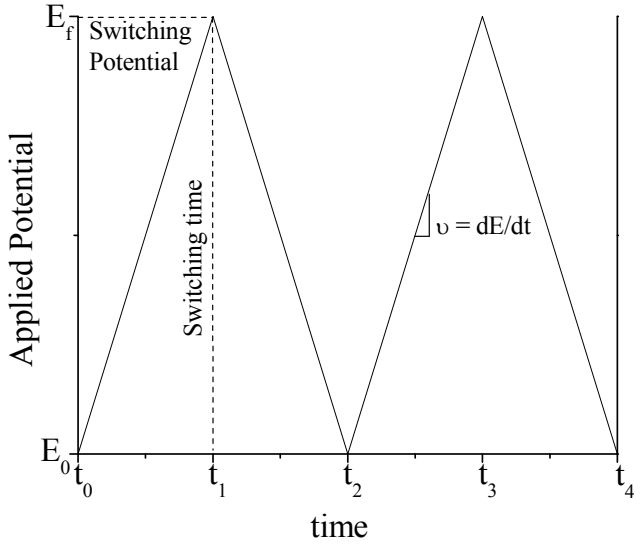

Figure 1-1 Typical potential-time wave form during cyclic voltammetry.

Assuming the presence of the redox couple *(R/O)*, in which *(R)* is oxidized to *(O)* and loses *(z)* electrons, for this couple, a non-Faradaic current will flow in the beginning of the potential sweep however, once the electrode potential reaches the standard formal potential of the couple $(E^{0'})$, the oxidation starts with a flow of a Faradaic current. With increasing the potential, the concentration of *R*, [R] decreases at the electrode surface while that of *O*, [O] increases. The oxidation current decreases due to depletion of the species *(R)* at the interface after the mass transfer rate reaches its maximum [2]. An oxidation peak will appear in the current-potential *(I-E)* curve as a result of the above process. Reversing the sweep direction, i.e. *(O)* will gain *(z)* electrons and reduce to *(R)*, a cathodic current will flow. The final *I-E* curve is called cyclic voltammogram *(CV)*.

For such a completely reversible reaction, both [R] and [O] are adjusted to a ratio according to Nernst equation:

$$E = E^{o'} + \frac{RT}{zF} \ln \frac{a_O}{a_R} \tag{1-1}$$

Taking $R = 8.314$ $JK^{-1}mol^{-1}$, $T = 298$ K and $F = 96500$ C mol^{-1}, equation (1-1) can be written as:

$$E = E^{o'} + \frac{0.059}{z} \log \frac{a_O}{a_R} \tag{1-2}$$

For reversible systems, the following can be obtained:

i. $j_{p,a} / j_{p,c} = 1$, independent of the sweep rate, switching potential or diffusion coefficients.
ii. The separation of peak potential $(E_{p,a} - E_{p,c})$ always close to $2.3RT/zF = 59/z\ mV$ at 25°C and slightly depends on switching potential.
iii. The peak current is proportional to $\sqrt{u}$.

If the species *(O)* is adsorbed at the electrode ($O^- \Leftrightarrow O_{ad} + ze^-$) and a linear sweep at rate *(v)* is applied, the current density *(j)* will be given by:

$$\frac{j}{zF} = \frac{\partial \Gamma_O}{\partial t} = \frac{\partial \Gamma_O}{\partial E} \cdot \frac{\partial E}{\partial t} = \left(\frac{\partial \Gamma_O}{\partial E} \right) \cdot u \tag{1-3}$$

Here, Γ_O is the amount of *(O)* adsorbed at time *(t)* per unit area of the electrode. The dependence of Γ_O on the potential and the concentration of O^- is described by an appropriate adsorption isotherm. Using the Langmuir adsorption isotherm, a symmetric shape of the *I-E* curve will be obtained (cf. Fig. 1-2) with the following characteristics:

i. $E_{p,a} = E_{p,c}$.

ii. The peak current is directly proportional to u.

iii. The total charge under the *I-E* curve is independent of u and equal to the charge required for the full reduction or oxidation of the adsorbed layer. The total width at half-height of the peak is $90.6/z\ mV$ at 25°C.

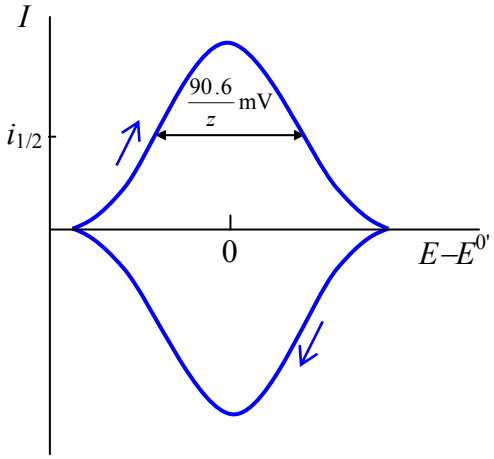

Figure 1-2 Typical CV for the oxidation and reduction of an adsorbed species assuming Langmuir adsorption. Adapted from ref. [3].

1.1.1.2 Potentiostatic technique (chronoamperometry)

In this technique, the current is measured as a function of time after application of a potential step perturbation. If the potential is stepped from E_0 (or E_1), where no current flows, to E_f (or E_2) where the current is limited by diffusion (cf. Fig. 1-3), the current flows will obey the well known Cottrell equation [2, 4]. In contrast to the steady state conditions, the current decreases with the time due to the decrease of the concentration gradient. The method is usually used to determine the diffusion coefficient [5].

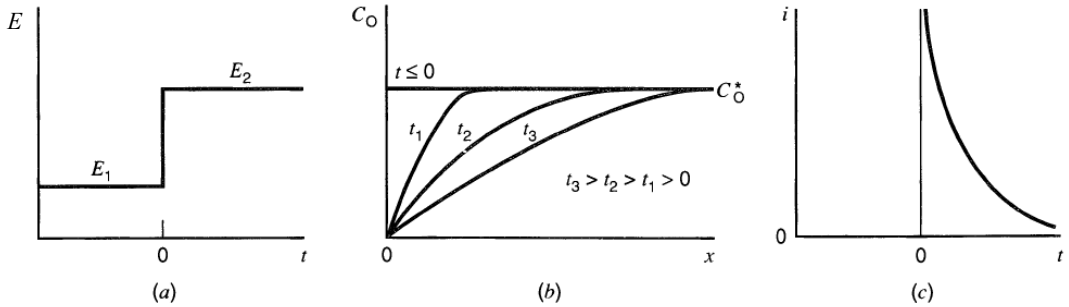

Figure 1-3 (a) potential-time waveform, (b) change in concentration profiles as time progresses and (c) the resulting current-time curve (current transient). Adopted from ref. [2].

1.1.1.3 AC voltammetry

As shown in Fig. 1-4, in ac voltammetry, a small sinusoidal ac voltage *(u_{ac})* is superimposed to the dc voltage *(u_{dc})* upon the potential sweep or potential step experiments. The phase sensitive detector (Lock-in amplifier) is usually used to extract and display the in-phase current response as a function of potential [6]. Here, the generated ac current is recorded at the same frequency (*f*) of the ac potential.

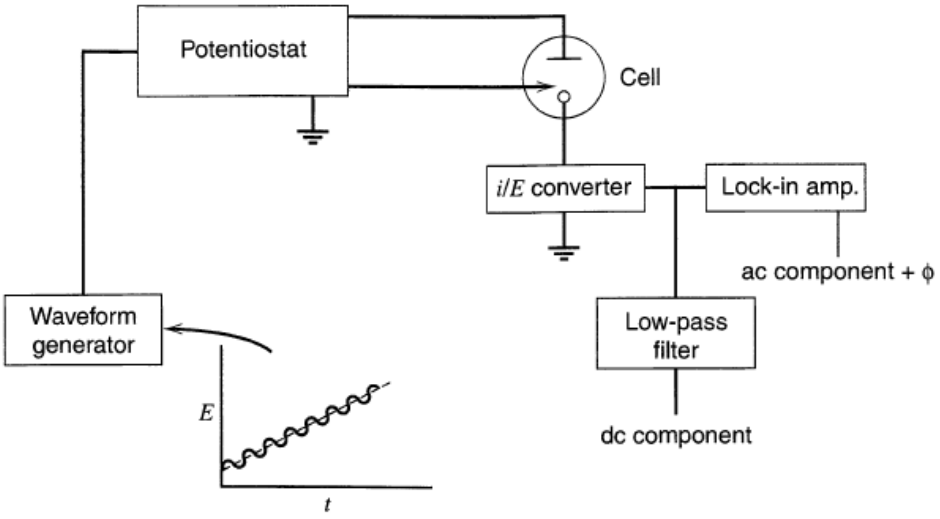

Figure 1-4 Schematic diagram of an ac voltammetry experiment. Adopted from ref. [2].

In general, the Lock-in amplifier multiplies the input signal by the reference signal then integrates it over a specific time. As a result, a dc signal will be produced and the contribution of any signal which has not the same frequency as the reference signal is attenuated to zero. In the Lock-in technique, care must be taken to calibrate the signal, because Lock-in amplifiers generally detect only the root-mean-square *(RMS)* signal of the operating frequency. For sinusoidal modulation, this would introduce a factor of $\sqrt{2}$ between the lock-in amplifier output and the peak amplitude of the signal.

1.1.2 Electrochemical impedance spectroscopy (EIS)

When an ac voltage of a small amplitude is applied to the working electrode, an ac current is obtained. The cell will act as impedance *(Z)* opposing the current flow. The characterization of the electrochemical system by measuring *(Z)* over a range of frequencies *(f)* is named as electrochemical impedance spectroscopy.

The impedance response can be described by:

$$Z = Z_{re} + jZ_{im} \quad (1\text{-}4)$$

Where Z_{re} and Z_{im} are the real and imaginary parts of Z respectively and $j = \sqrt{-1}$

In polar form (cf. Fig. 1-5), *(Z)* can be written as:

$$Z = |Z|e^{j\varphi} \text{ or } Z = |Z|(\cos\varphi + j\sin\varphi) \quad (1\text{-}5)$$

Here, $|Z| = \sqrt{(Z_{re})^2 + (Z_{im})^2}$ and $\varphi = \arctan(\frac{Z_{im}}{Z_{re}})$

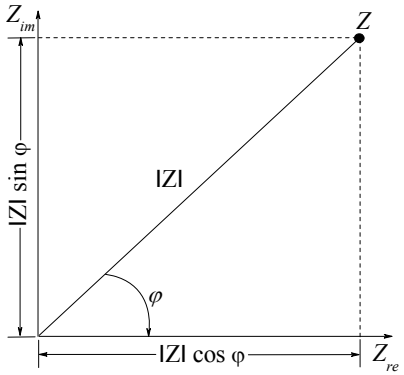

Figure 1-5 Relationships among complex impedance *(Z)*, magnitude IZI and phase angle *(φ)*.

The reciprocal of the impedance *(Z)* is the admittance *(Y)* hence; $Y = \frac{1}{|Z|}e^{-j\varphi}$ .The admittance *(Y)* is a vector with a magnitude of *(1/Z)* and a phase angle equal to that of *(Z)*, but with opposite sign.

Impedance spectra are often displayed in two different ways; *Bode plot*, in which $\log|Z|$ and φ are both displayed versus $\log f$, and *Nyquist plot*, in which the imaginary part of the impedance, Z_{im} is plotted versus the real one, Z_{re} (cf. Fig. 1-6)

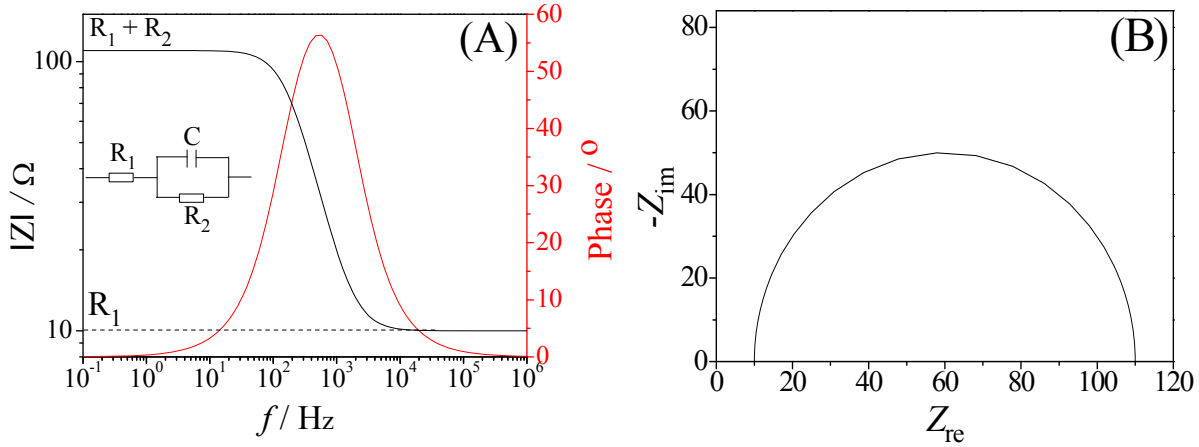

Figure 1-6 Simulated impedance spectra, (A) Bode plot and (B) Nyquist plot for the equivalent circuit in (A). The curves were calculated assuming, R_1 = 10 Ω, R_2 = 100 Ω and C = 10 µF.

1.1.3 Charge transfer coefficient and Tafel slope

For any type of electrode reaction, the rate constant can be expressed as:

$$k = A' \exp[-(\Delta H^{\ddagger} - T\Delta S^{\ddagger})/RT] = A' \exp[-\Delta G^{\ddagger}/RT] \quad (1\text{-}6)$$

Where, $\Delta H^{\ddagger}$, $\Delta S^{\ddagger}$ and $\Delta G^{\ddagger}$ are the activation enthalpy, entropy and free energy respectively and A' is the pre-exponential factor.

Fig. 1-7 represents the effect of a potential change on the standard free energies of activation for oxidation and reduction. Assuming the reduction of *(O)* to *(R)*, a change (x) in the free energy of *(O)* will result in a change ($\alpha_c x$) in the activation energy. Hence, for reduction:

$$\Delta G_c^{\neq} = \Delta G_{c,o}^{\neq} + \alpha_c zFE \quad (1\text{-}7)$$

And for oxidation,

$$\Delta G_a^{\neq} = \Delta G_{a,o}^{\neq} + \alpha_a zFE \quad (1\text{-}8)$$

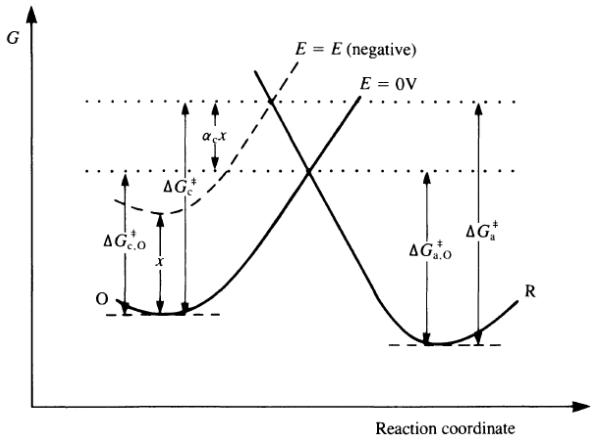

Figure 1-7 Effect of change on applied electrode potential on the reduction of *(O)* to *(R)*. adopted from ref. [7].

Here, α is a measure of the slope of the energy profile in the transition state zone. It is called charge transfer coefficient (symmetry factor) and gives the ratio of the change of the height of the energy barrier the electron has to surmount during charge transfer, with respect to the change of electrode potential. The values of α_a and $\alpha_c = 1-\alpha_a$ can vary between 0 and 1, but often they are around 0.5 which means that the activated complex is exactly halfway between reactants and products on the reaction coordinate. $\alpha = 0$ implies no influence of the electrode potential change on the barrier height and $\alpha = 1$ implies that the change of electrode potential causes an exactly equal change of barrier height.

If the concentration of *(O)* and *(R)* outside the double layer were [O] and [R], then the net current density at the electrode would be given by:

$$j = j_a - j_a = FA_a^{'}[R]\exp(-\Delta G_a^{\neq} / RT) - FA_c^{'}[O]\exp(-\Delta G_c^{\neq} / RT) \quad (1\text{-}9)$$

Substituting equations (1-7) and (1-8) into (1-9) and introducing the parameter of exchange current density *(j_0)*, which equals to j_a or j_c when the net current is zero, the deviation of the potential from its equilibrium value is given by the well known Butler-Volmer equation:

$$j = j_0\left[\exp(\frac{\alpha_a zF\eta}{RT}) - \exp(\frac{-\alpha_c zF\eta}{RT})\right] \quad (1\text{-}10)$$

At high overpotential, i.e. $|\eta|$>118 mV at 25°C, equation (1-10) can be written as:

$$\eta = -\frac{2.3RT}{\alpha_c zF}\log j_0 + \frac{2.3RT}{\alpha_a zF}\log j = a + b\log j \quad (1\text{-}11)$$

The above equation is called Tafel equation and *(b)* is the Tafel slope from which α_a can be obtained at constant temperature, i.e. at *298 K*, if $z = 1$, $\alpha = 0.5$, then $b = 118\ mV\ dec^{-1}$. The exchange current density *(j_0)* can be obtained by extrapolating the η *vs. log j* line and take the interception at $\eta = 0$.

1.2 Potential modulation technique

The potential dependence of the electrochemical reaction rate (α') can be determined in a very narrow potential range (the ac amplitude) when a small sinusoidal ac voltage is superimposed during the electrochemical reaction. Then:

$$\frac{\partial \ln i}{\partial E} = \frac{1}{i}\cdot\frac{\partial i}{\partial E} = \frac{1}{i}\cdot\frac{i_{ac}}{u_{ac}} = \frac{1}{b},$$

The Tafel slope of the reaction is then given by:

$$\frac{\partial E}{\partial \ln i} = \frac{RT}{\alpha^{'}F} \quad (1\text{-}12)$$

Here, $\frac{\partial i}{\partial E} \approx \frac{i_{ac}}{u_{ac}}$

Hence, $\alpha^{'} = \frac{RT}{F}\cdot\frac{i_{ac-re}}{u_{ac}i_{dc}}$ (1-13)

Here, the real part of the ac current is chosen since it represents the Faradaic processes occur on the surface whereas the imaginary part is due to the capacitive processes.

For the oxidation of adsorbed species (CO_{ad}) formed from CO-saturated solution or from methanol, the current (i) can be expressed as a function of potential (E) and of adsorbate coverage (θ_{CO} and θ_{OH}) as follows:

$$i = zFk_{app}(E)f(\theta_{CO}(1-\theta)), \quad (1\text{-}14)$$

where, $k_{app}(E) = k_o e^{\alpha' FE/RT}$ is the apparent rate constant depending on E, z is the number of electron transferred in the reaction, α' is the apparent charge transfer coefficient and $f(\theta)$ is the function of the fractional coverage ($\theta = \theta_{CO} + \theta_{OH}$).

Taking the logarithm on both sides of equation (1-14) and differentiation with respect to E gives:

$$\frac{\partial \ln i}{\partial E} = \frac{1}{i} \cdot \frac{\partial i}{\partial E} = \frac{\partial \ln k_{app}(E)}{\partial E} + \frac{\partial \ln f(\theta_{CO}(1-\theta))}{\partial E} \qquad (1\text{-}15)$$

Here, $\frac{\partial \ln k_{app}(E)}{\partial E} = \frac{\alpha' F}{RT}$

If a small ac voltage $u_{ac} = u_A \sin(\omega t)$ is superimposed during the electrochemical reaction then $\frac{\partial \ln f(\theta_{CO}(1-\theta))}{\partial E}$ can be ignored when the relative changes of θ_{CO} and θ_{OH} are negligible in an ac period; i.e. during an ac period (≈ 30 ms), for a total CO oxidation charge density of 350 μC cm^{-2} and an assumed high current density of ca. 300 μA cm^{-2}, the total charge density passed will be negligible. Only under these experimental conditions, the above approximation holds.

A reliable determination of the Tafel slope from a Tafel plot E(ln*i*) requires the presence of a constant slope that extends over an order of magnitude of the current. However, Wang et al. [8] reported recently that for the oxidation of CO at different Pt surfaces under stagnant conditions, a reliable determination of the Tafel slope *(b)* (in the apparent transfer coefficient $\alpha' = 2.3RT/bF$) is possible as shown above by potential modulation. Such a potential modulation method requires only k_{app} to be constant during the sampling time (one ac period).

1.3 Differential electrochemical mass spectrometry (DEMS) technique and DEMS cells

DEMS is a technique used to characterize sub-monolayer amounts of adsorbate species formed at the working electrode. It combines the electrochemical methods with the mass spectrometry (on-line analysis of the volatile products and intermediates).

Historically, Brunckenstein and Gadde [9] were the first to determine the gaseous electrochemical reaction products. The method was later improved by Wolter and Heitbaum [10, 11] by reducing the delay time of detection. Using a turbomolecular pump helped to decrease the delay time and to pump out the residual gases and solvents inside the system.

Thus, to distinguish the technique from product sampling, i.e. integrating approaches, the method was called *differential*.

As reported before in [12] and the references cited therein, significant improvements of the DEMS cells were achieved during the last decades. A thin layer cell has been used for smooth and single crystal massive electrodes [13-15]. Another development of the thin layer cell is to the dual thin layer flow through cell in combination with quartz crystal microbalance which was introduced by Baltruschat and co-workers [16]. In this cell, the Faradaic reactions, which have to be performed under continuous flow of the electrolyte, are better suited because of the rapid depletion of the reactants in the thin layer cell. (Details about the dual thin layer flow through cell together with the construction of DEMS will be given in chapter 2).

The aforementioned flow through cell could be used for single crystals without hanging meniscus arrangement or for high surface area electrodes (e.g. supported nanoparticles) [17]. Using a pinhole as the gas inlet, located at the hemispherical end of a glass tube covered by Teflon film, Kita et al. [18] applied a hanging meniscus configuration for massive electrodes. Similarly, Koper et al. [19] developed on-line mass spectrometric cell based on a small inlet Teflon tip applied for bead single crystals. This cell was not working under flow conditions and the delay time was long. Recently, Abd-El-Latif et al. [20] introduced a new DEMS cell design applicable for different bead single crystal sizes (diameter of 2-3 mm). They have used it in the usual arrangement of the single crystals (hanging meniscus) under flow through conditions.

1.4 Introduction to fuel cells

1.4.1 History

The history of fuel cells begins when Sir William Grove invented the first fuel cell in 1839 [5, 21], it took 120 years until NASA demonstrated some of his work in providing power during space flight [22]. Grove's experiment based on two Pt electrodes embedded inside two separate glass tubes and then placing these in a dilute sulfuric acid solution, as shown in the left part of Fig. 1-8. An electric current is then passed through the electrodes and causes the electrolysis of water. The resulting oxygen and hydrogen are accumulated in the two glass tube. He detected a small electric current when replacing the power supply by an amperometer.

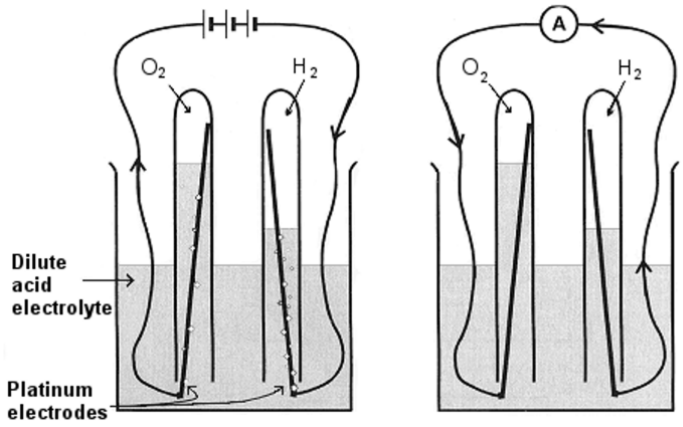

Figure 1-8 Schematic representation of the Grove fuel cell. Adopted from ref. [5].

1.4.2 Importance

Fuel cells act as an alternative to fossil fuels and diminish poisonous emission to the atmosphere. They have higher theoretical electrical efficiencies comparing to heat engines [21, 23]. Fuel cell systems are characterized by low noise and low environmental pollution. The combination between fuel cells and other renewable energy sources such as wind, water and sun might be an option for future power generation.

1.4.3 Fundamentals

A fuel cell is similar to a battery but does not need to be recharged; a battery gets recharged by using electricity which is then stored in a closed system, whereas a fuel cell uses an external supply of fuel which needs to be continuously replenished. It transforms directly the heat of combustion of a fuel (hydrogen, natural gas, methanol, ethanol, hydrocarbons, etc.) into electricity. The fuel is oxidized at the anode, without producing any pollutants (only

water and/or carbon dioxide are emitted to the atmosphere), whereas the oxidant (oxygen from air) is reduced at the cathode. Fig. 1-9 shows the principle of H_2/O_2 fuel cell which involves the production of water and heat.

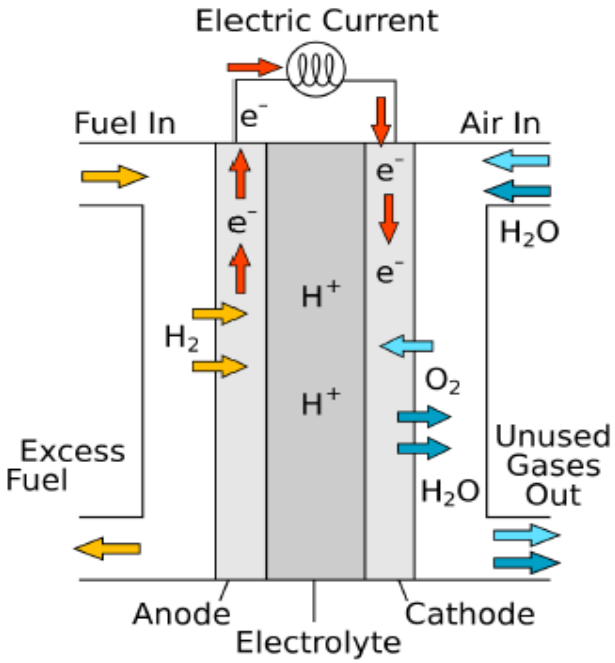

Figure 1-9 H_2/O_2 fuel cell. From: http://en.wikipedia.org/wiki/Fuel_cells (14.11.2012; 12:36 PM).

1.4.4 Types

Fuel cells are often classified according to the electrolyte used inside the cell. An exception is the direct alcohol fuel cell (DAFC) in which alcohol is directly fed to the anode. Another classification is according to the operating temperature. Thus, there are low and high temperature fuel cells. Table 1-1 (adopted from ref. [23, 24]) summarizes the well known different types of fuel cells including different cell reactions and applications.

Table 1-1 Different fuel cell types.

Fuel cell types	AFC (Alkaline)	PEMFC (Polymer Electrolyte Membrane)	DMFC (Direct Methanol)	PAFC (Phosphoric Acid)	MCFC (Molten Carbonate)	SOFC (Solid Oxide)
Operating temp. / °C	< 100	60-120	60-120	160-220	600-800	800-1000 low temp. (500-600) possible
Anode reaction	$H_2 + 2OH^- \rightarrow 2H_2O + 2e^-$	$H_2 \rightarrow 2H^+ + 2e^-$	$CH_3OH + H_2O \rightarrow CO_2 + 6H^+ + 6e^-$	$H_2 \rightarrow 2H^+ + 2e^-$	$H_2 + CO_3^{2-} \rightarrow H_2O + CO_2 + 2e^-$	$H_2 + O^{2-} \rightarrow H_2O + 2e^-$
Cathode reaction	$1/2O_2 + H_2O + 2e^- \rightarrow 2OH^-$	$1/2O_2 + 2H^+ + 2e^- \rightarrow H_2O$	$3/2O_2 + 6H^+ + 6e^- \rightarrow 3H_2O$	$1/2O_2 + 2H^+ + 2e^- \rightarrow H_2O$	$1/2O_2 + CO_2 + 2e^- \rightarrow CO_3^{2-}$	$1/2O_2 + 2e^- \rightarrow O^{2-}$
Applications	Transportation Space Military Energy storage systems			Combined heat and power for decentralized stationary power systems	Combined heat and power for stationary decentralized systems and for transportation (train, boats, ...)	
Released power	Small plants 5-150 kW modular	Small plants 5-250 kW modular	Small plants 5 kW	Small – medium sized plants (50 kW-11 MW)	Small power plants 100 kW – 2 MW	Small power plants 100-250 kW
Charge carrier	OH^-	H^+			CO_3^{2-}	O^{2-}

1.4.5 Fuels

Examples for fuels that can be directly used within fuel cell stacks are hydrogen and alcohols such as methanol and ethanol. The use of hydrogen is limited by the difficulties and risks associated with its transport and handling. As an alternative to hydrogen, liquid fuels such as methanol and ethanol are used in the direct alcohol fuel cells (DAFCs). In addition to the ease of transport, they have higher energy density. The disadvantage of using alcohols as a

fuel especially in low temperature DAFCs is the poor kinetics of their electrocatalytic oxidation which results in a low fuel cell efficiency.

1.4.6 The catalyst layer

For the electrooxidation of the fuel at the anode and electroreduction of the oxidant at the cathode, a catalyst is required. Among the catalytic important metals such as Ni, Rh, Pd, Ir,...., etc, Pt is the best fuel cell catalyst known. Polycrystalline Pt and Pt single crystals (bare or modified by foreign metal) were used in this thesis as a catalyst for the investigation of the anodic reactions as methanol and ethanol oxidation, cathodic reactions (oxygen reduction) and the oxidation of the catalyst poison (CO_{ad}).

1.5 Structure of clean catalyst surface

Since all experiments presented in this work were done either with bare Pt or with Pt modified by foreign metal deposited at its surface, only the crystal symmetry of Pt, which crystallize in the face centered cubic *(fcc)* will be discussed.

Metal surfaces are heterogeneous and polycrystalline at the atomic scale. Single crystal surfaces are found to consist of a mixture of flat regions (terraces) and defects. Two types of defects may present; line defects, such as steps and kinks and point defects, such as atomic vacancies and adatoms (cf. Fig. 1-10).

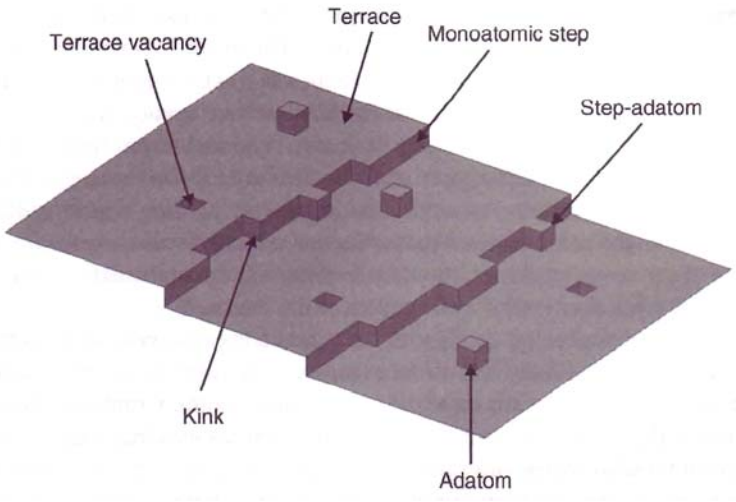

Figure 1-10 Model of the real solid surfaces with different surface sites. Adopted from ref. [25].

1.5.1 Low-Miller-index-planes

An ideal crystal is built by infinite repetition of an identical structure unit in three dimensions. The crystal structure can be described in terms of its unit cell which is composed of a single atom or a group of atoms. The unit cell is given by its lattice parameters, which are the length of the cell edges and the angles between them, while the position of the atoms inside the unit cell are described by the set of atomic positions (x_i, y_i, z_i) measured from a lattice point.

Miller indices are vectors and atomic planes in a crystal lattice can be described by a three value Miller index notation *(hkl)*. They denote a plane that intercepts the three points a_1/h, a_2/k and a_3/l. Miller indices are proportional to the reverse of the intercepts of the plane with the unit cell. If one or more of the indices is zero, this means that the planes do not intersect that axis i.e. the intercept is at infinity. The ideal structure of the low-Miller-index planes (100), (110) and (111) of the *fcc* systems are shown in Fig. 1-11 with a square, rectangular and hexagonal arrangement of the surface atoms respectively.

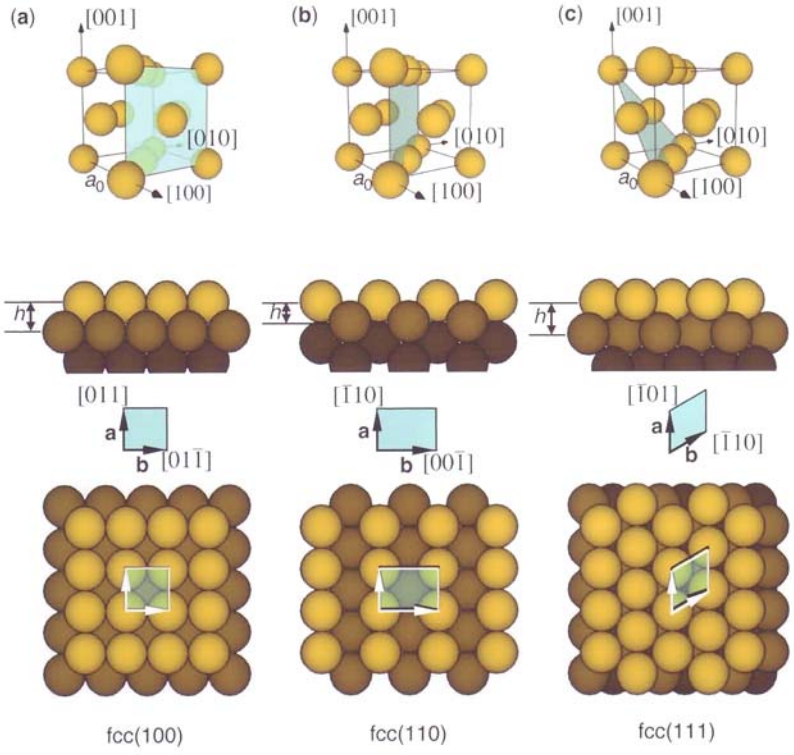

Figure 1-11 Unreconstructed surfaces of the *fcc* crystal surfaces where a_0 is the crystal lattice constant, *a* and *b* are the unit cell vectors and *h* is the distance between the first and the second layer. Adopted from ref. [25].

Low Miller index surfaces are thermodynamically favored because of the high packing density of the atoms. They have low surface free energy, high symmetries and relative stabilities [26], although reconstruction (change in configuration of the surface atoms with respect to the bulk to minimize surface energy) and relaxation (small interlayer spacing changes relative to the ideal bulk lattice of the metal surfaces) can occur.

1.5.2 High-Miller-index stepped surfaces

Single crystals can also be aligned and cut with respect to higher Miller indices. These planes have smaller atomically smooth terraces separated by steps or kinks, depending on the orientation. Fig. 1-12 illustrates the various surface structures that can be obtained by cutting and positioning an *fcc* crystal along different directions, such plot known as stereographic triangle. At the corners of the plot are the three low-index surfaces (111), (100) and (110). The three sidelines of the triangle are $[1\bar{1}0]$, [001] and $[01\bar{1}]$ crystallographic zones with planes exhibit terrace-step structure.

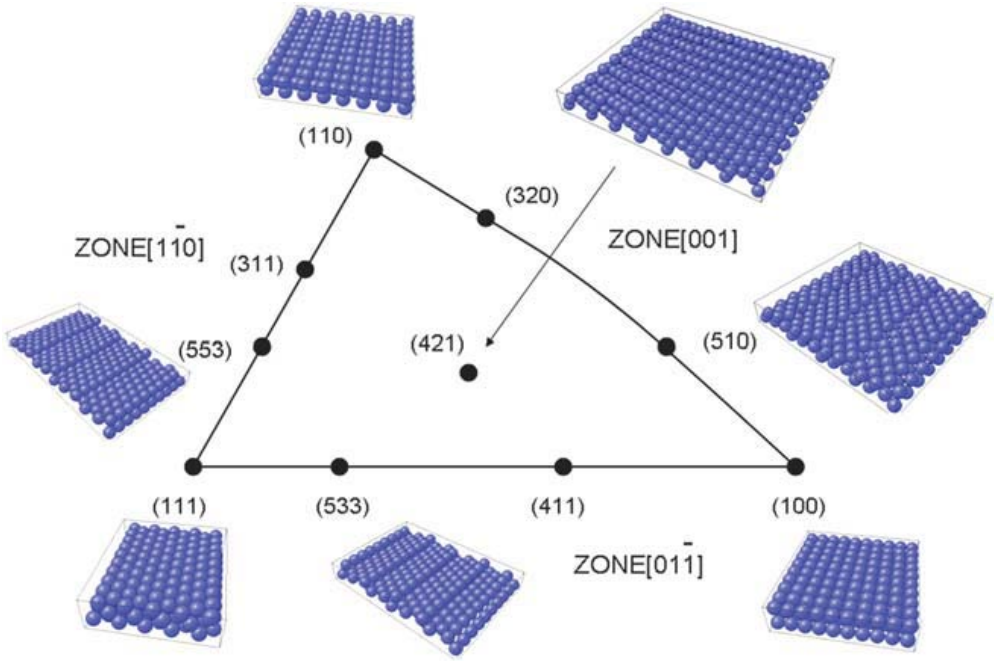

Figure 1-12 Unit stereographic triangle of fcc single-crystal surfaces and their corresponding surface atomic arrangements. Adopted from ref. [27].

Several notation systems [26] were developed to express the geometry of the surface in terms of simple low-Miller-index vectors. Lang or step notation [28] is one of the most common nomenclature systems for stepped crystals. In this system, stepped surface is written as *Pt(s) [n(hkl) × m(h'k'l')]* where *(hkl)* and *(h'k'l')* are the Miller indices assigned to terrace and step respectively; *n* and *m* are the number of atoms across the terrace and the step

respectively. As shown by Furuya et al. [29, 30] the features of the hydrogen desorption varied regularly with Miller indices (cf. Fig. 1-13). Each voltammogram acts as a finger print for the studied plane.

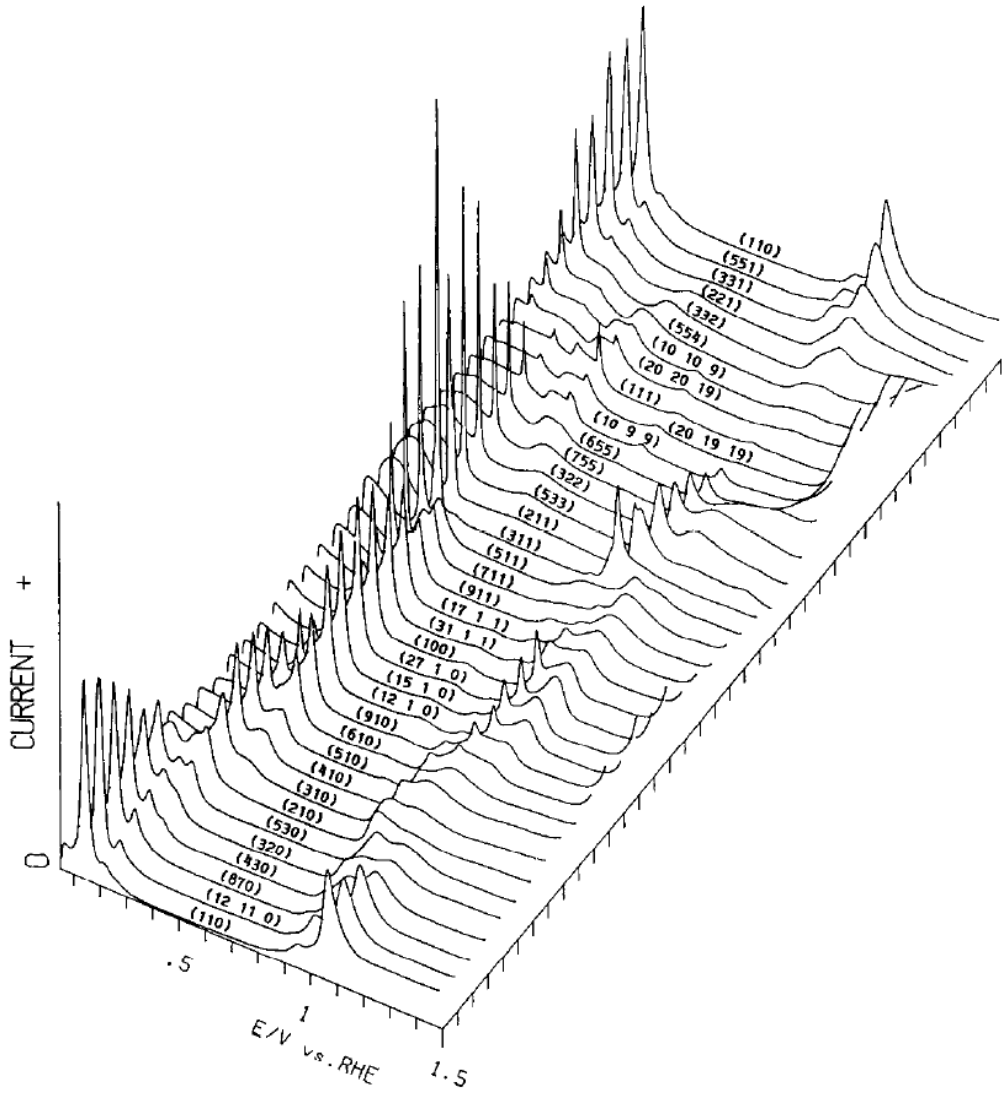

Figure 1-13 CVs for different low and higher Miller indices Pt surfaces in 0.5 M H_2SO_4 at a scan rate of 50 mV s^{-1}. Adopted from ref. [29].

Single crystals can be prepared by several ways such as UHV (by sputtering and annealing), vacuum evaporation and the most famous flame annealing and cooling technique by Clavilier et al. [31-34]. This method is very effective for removing organic contaminates in the presence of oxygen. The cooling can be carried out in inert atmosphere (Ar or N_2) or in the presence of a reductive gas as H_2 or CO.

1.6 Catalyst modification by deposition of foreign metals

1.6.1 Basics of metal deposition

The catalytic properties of the Pt catalyst can be modified by the deposition of a foreign metal. When the deposition potential of metal *(M)* on a foreign substrate *(S)* is more positive than the thermodynamic potential for the deposition of bulk metal predicted from the Nernst equation, underpotential deposition *(UPD)* occurs [35, 36]. Thermodynamically, the origin of such behavior is that the chemical potential of the metal in the monolayer (μ_{ML}) is lower than that of bulk metal (μ_M^0) [1].

The structure and number of *UPD* peaks are strongly dependent on the crystallographic orientation of the substrate and the density of surface defects. Experimentally, it was found that the sharpness and narrowness of the *UPD* peaks is strongly increased when the polycrystalline Pt substrates are replaced by single crystals. It has been found that the difference in work functions between the substrate and the bulk adsorbate ($\Delta\Phi$) related with the underpotential shift, ($\Delta E_p = E_{UPD}-E_B$) [37], where, E_{UPD} is the potential of the most positive *UPD* desorption peak and E_B is the thermodynamic potential for the bulk deposition of the adsorbate.

1.6.2 Initial stages of metal deposition

Several general mechanisms [36, 38] were found for the nucleation and growth of a metal deposit layer *(M)* on a foreign substrate *(S)*:

i. If the interaction between the adatoms with each other is stronger than that with the substrate, i.e. $\Psi_{M\text{-}M} > \Psi_{M\text{-}S}$, where Ψ is the binding energy, 3D-islands and clusters are formed from the beginning. Obviously, this cannot take place at underpotentials. This mechanism is named as Volmer-Weber (VW) or 3D-island growth (cf. Fig. 1-14, a).

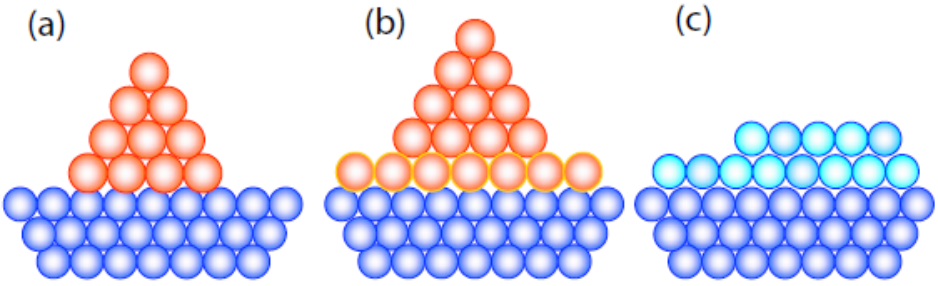

Figure 1-14 The three different growth modes of adatom (M) on a substrate (S). Adopted from ref. [38].

ii. If the binding energy $\Psi_{M\text{-}S} > \Psi_{M\text{-}M}$, the adatom can be deposited at underpotential on the substrate with two sub cases:

- With a considerable misfit in the lattice structure of *(M)* and *(S)*, Stranski-Krastanov (SK) growth mode (cf. Fig. 1-14, b) is formed: A complete 2D monolayer with internal strain (compression or expansion) will be formed followed by unstrained 3D islands above it.

- With a negligible crystallographic misfit, a commensurate monolayer is formed. Subsequent layers are also epitaxic and deposited layer-by-layer. The deposition follows the Frank-van-der-Merwe (FM) growth mode (cf. Fig. 1-14, c).

1.6.3 Ways of action of co-catalysts

In order to overcome the poisoning (deactivation) of the catalyst layer in the fuel cell, considerable interest has been devoted to compare the catalytic activities of the catalyst alone with that for a catalyst modified with some other foreign metals as Ru, Sn, Bi, As, etc during the oxidation of CO_{ad} (main Pt catalyst poison) and other small organic molecules such as formaldehyde, methanol and ethanol. The enhanced catalytic activity of such modified catalysts is usually ascribed to three different ways: a geometric (ensemble) effect, an electronic (ligand) effect and an effect according to the bifunctional mechanism. Fig. 1-15 shows an example of these effects during the oxidation of CO and methanol.

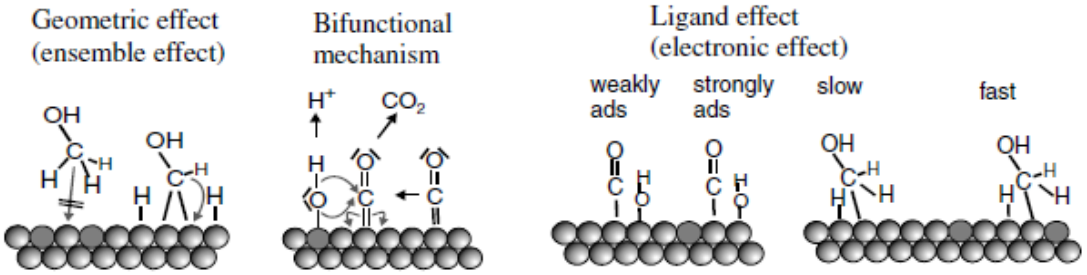

Figure 1-15 Three different ways for the action of the co-catalysts (dark spheres). Adopted from ref. [39].

The adsorption process requires the presence of an ensemble of more than one active atom. In case of methanol, for instance, it is generally accepted that an ensemble of at least three adjacent Pt atoms are necessary for the accommodation of one methanol molecule [40]. This is the reason for the inactivity of PtSn surfaces towards methanol oxidation and also for the fact that PtRu alloys with a low Ru content are the best catalyst for methanol oxidation.

An enhancement of the catalytic activity is believed to occur for the oxidation of adsorbed CO at Ru modified Pt surfaces by the bifunctional mechanism. According to this mechanism, CO_{ad} will react with an adsorbed oxygen species (such as OH^- or activated water) which adsorbed preferentially on Ru at lower potentials than at pure Pt.

In case of the ligand effect, the electronic properties of the substrate are modified by the adatom. In such modification, the strength of interaction with the adatom (adsorption energy of the substrate) is modified or the activation energy is decreased. The origin of such electronic effect is ascribed to the modification of the electronic properties of the substrate due to the presence of the second component [41, 42] (pure electronic or ligand effect) or due to lateral strain of the adsorbate layer on the primary active metal, causing a broadening and lowering or narrowing and increase of the energy of the surface d-band of the primary metal [43].

An important part of the interaction energy is that between the adsorbate states and the substrate d-states. Whereas the metal sp-bands are broad and structureless, d-bands are narrow. Small changes can change the d-states and their interaction with the adsorbate states significantly [38, 43]. If the lattice parameter of the adlayer is different from that of the surface of the bulk metal, the extent of the M-M bonding within the surface is changed (surface strain), this is followed by a shift in the d-band center. If the electronic interaction between the surface adatom and the substrate is large, the location of the d-band center is also affected by the ligand effect [44]. The average energy of the d-band (ε_d) is shifted upward or downward depending on whether the d-band becomes narrower or wider due to coupling of strain and ligand effects to maintain a constant d-band filling (cf. Fig. 1-16). Hence, when the combined effects result in a narrower d-band, its average energy increases and if the effects result in a wider d-band, its average energy decreases.

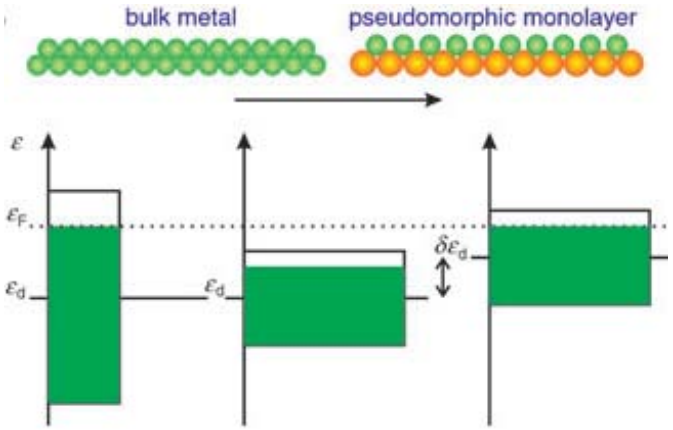

Figure 1-16 Illustration of the coupling between the bandwidth and d-band center for a band with a fixed number of d-electrons. Adopted from ref. [44].

1.7 Fuel cells electrocatalysis

1.7.1 Electrocatalytic oxidation of CO

Adsorbed CO at the anode catalyst of the low temperature fuel cells is the main reason of their low efficiency because it blocks the active sites available for the adsorption of more reactants. The Pt anodic catalyst of the H_2/O_2 fuel cell can be easily deactivated in the presence of traces of CO (10-100 ppm) [22]. In the DMFCs, CO_{ad} acts as poisoning intermediate which formed during the oxidation of methanol as studied before [45]. In both types of cells, it is necessary to oxidize CO_{ad} at low overpotential which is the aim of many ongoing studies.

The electrocatalytic oxidation of CO has been studied at different Pt surfaces including Pt(Poly) [46-50], low-Miller-index Pt single crystals [51-58] and stepped Pt(hkl) bare or modified by a second metal as alloy or adatom [59-63]. At room temperature, PtRu alloy having Ru content (10-40 %) are the best CO-tolerant anode catalyst [64]. In this alloy, a good distribution of Pt and Ru atoms is the reason of the high catalytic activity which is either explained by bifunctional mechanism or electronic effect as mentioned above.

The mechanism of CO oxidation and the assignment of the rate determining step (rds) have been widely studied. It is generally believed that the oxidation of CO at platinum occurs via the Langmuir-Hinshelwood (LH) mechanism [65] with two main reaction steps:

(i) Adsorption of oxygen species (typically OH_{ad} or activated water) with a rate constant of k_1 for the forward reaction and k_{-1} for the backward.

$$H_2O + * \rightleftharpoons OH_{ad} + H^+ + e^- \qquad (1\text{-}16)$$

(ii) Oxidation of CO_{ad} in presence of OH_{ad} to CO_2 with a rate constant k_2

$$CO_{ad} + OH_{ad} \longrightarrow CO_2 + H^+ + 2* + e^- \qquad (1\text{-}17)$$

Different values have been reported in literature for the Tafel slope, leading to different assignment of the rds in the above reaction sequence [66, 67]. A reason for differing Tafel slopes could be a potential dependent slope which is due to potential dependent rds. Such potential dependent Tafel slopes are difficult to be determined experimentally, because a reliable determination of the Tafel slope requires a constant Tafel plot over about an order of magnitude of the current. As reported recently by Wang et al. [8], a reliable determination of the Tafel slope b (or the apparent transfer coefficient $\alpha' = 2.3RT/bF$) is possible by superimposing an ac voltage to the dc voltage either in the potential step experiments or during CV even for the adsorbate. Thus, a direct, quasi continuous determination of Tafel slope is possible according to:

$$\frac{\partial \ln i}{\partial E} = \frac{1}{i}\frac{\partial i}{\partial E} = \frac{1}{i}\frac{i_{ac}}{u_{ac}} = \frac{2.3}{b} \qquad (1\text{-}18)$$

In agreement with Monte Carlo simulation by Koper et al. [68], Wang et al. [8] thus found a transition of the apparent transfer coefficient (α') from values around 1.5 at low potentials to values around 0.5 at high potentials and thus an increase of the Tafel slope from 40 mV dec^{-1} to 120 mV dec^{-1} during the oxidation of pre-adsorbed CO at Pt(Poly) under stagnant conditions. The transition occurs when $k_1+k_2>>k_{-1}$ and then reaction (1-16) would be the rate determining step [3, 8]. Using a pressure modulation technique, Wang et al. determined the volume of activation for CO_{ad} oxidation at low potentials and concluded that the transition state is highly charged ($[H^+\cdots O\cdots CO]$), supporting the conclusion that at low potentials the first step (reaction 1-16) is in equilibrium [69].

Under flow through conditions, I investigated the oxidation of pre-adsorbed CO at Pt(Poly) in the dual thin layer flow through cell. The apparent charge transfer coefficient (α') and the corresponding Tafel slopes have been calculated (cf. chapter 5, part 5.2.2) and the results were compared to that obtained before under stagnant conditions.

1.7.2 Electrocatalytic oxidation of methanol

The use of methanol as a fuel in the direct methanol fuel cells (DMFCs) is appealing [64, 70-73] because of the ease of handling, storage and transport in addition to its high energy density [50, 74]. However, the performance of such cell is still limited due to the continuous poisoning of the catalyst layer with methanol decomposition product (CO_{ad}) [64, 71, 75-77].

The dual pathway mechanism for methanol electrooxidation at platinum surfaces ,originally suggested by Bagotzky et al. [78] and later by Parsons et al. [72], became the most reliable and accepted mechanism. According to this mechanism, after oxidative adsorption of bulk methanol at platinum surface forming $(CH_xOH)_{ad}$, CO_{ad} and soluble intermediates (HCOOH and HCHO) are formed simultaneously [70] (indirect and direct pathway, respectively).

Methanol electrooxidation has been studied at different platinum surfaces including polycrystalline [75, 79-84], platinum single crystals (basal planes [85, 86] and stepped surfaces [70, 74, 79, 87-89]) and at nanoparticles [81, 90-94]. The validity of the parallel pathway mechanism for methanol oxidation at smooth Pt(Poly) has been proved recently by Wang et al. [79] and Abd-El-Latif et al. [80] as studied by DEMS. They found that CO_2 current efficiencies and the extent of CO_{ad} poisoning are independent of the convection. CO_2

can be formed through the indirect pathway while its formation through the direct pathway is negligible due to the short residence time available for the reacting species as a result of strong convection. Only in absence of convection or at rough/porous electrodes (e.g., nanoparticles), the dissolved intermediates can be further oxidized to CO_2 due to their longer residence time in the vicinity of the electrode and the desorption – readsorption reaction as suggested before [81, 90, 91, 93, 95]. They studied also the effect of methanol concentration and adsorption potentials and found that CO_2 current efficiencies increase with decreasing concentration and increasing potential whereas that of methylformate showed the opposite behavior in agreement with the results of Wang et al. [81].

By monitoring the mass fractions of CO_2 (m/z = 44) and methylformate (m/z = 60), Housmann et al. [85] found an increase in the maximum activity towards methanol oxidation at the platinum basal planes in the order Pt(111)<Pt(110)<Pt(100) which was different from findings by Herrero et al. [86] who studied the oxidation of methanol at the same surfaces by cyclic voltammetry and chronoamperometry and reported a different order: Pt(111)<Pt(100)<Pt(110). The authors attributed the difference to the differences in the electrode pre-treatment and cleanliness when they compared the maximum current density of the hydrogen adsorption/desorption peaks. They also claimed that the Pt(110) surface used by Herrero et al. was more disordered and consists mostly of (1×2) reconstructed surface which is more active toward CO oxidation [96].

The effect of step density on the oxidation of methanol has been also investigated. Wang et al. [87] compared the oxidation of methanol at smooth Pt(Poly), Pt(111) and Pt(332) electrodes and they found that methanol oxidation is enhanced with increasing step density without an appreciable increase of CO_2 current efficiency, hence they concluded that the defect sites enhance both parallel pathways of methanol oxidation. Shin and Korzeniewski et al. [88] suggested that an increase of the step density catalyzes methanol decomposition and the methanolic CO formation is inhibited on Pt(111) at the potential of the hydrogen adsorption. Tripkovic and Popovic et al. [89] reported that the initial surface activity for methanol oxidation on stepped electrodes decreases with increasing step density whereas Housmans et al. [74] found that the overall oxidation rate of methanol increases with increasing step density. Recently, Grozovski et al. [70] investigated the role of surface structure in methanol oxidation mechanism as studied by pulsed voltammetry under stagnant conditions. According to their measurements, the presence of (111) and (100) steps, both on (100) and (111) terraces respectively does not increase activity of these surfaces, while (110) steps do improve the activity towards methanol oxidation.

Ru electrodeposited on platinum or alloyed with platinum leads to better catalysts towards methanol electrooxidation than pure platinum [22, 87, 90, 94, 97-100]. Ru enhances not only the oxidation rate of adsorbed CO, but also the adsorption of methanol. The action of Ru as an alloy or adlayer during the oxidation of methanol has been ascribed to: (a) bifunctional mechanism, where Ru sites act as the center generating oxygen containing species at low potentials and thus facilitates the rates of adsorption and oxidation of Pt-CO intermediate [87, 90] and (b) an electronic or ligand effect leading a reduced Pt-CO bond strength facilitating oxidation of the CO_{ad} [41-43, 59] on one hand to; on the other hand, an increase in the dehydrogenation/adsorption rate has to be ascribed to this ligand effect. Moreover, the geometric effect also has to be considered: 3-4 adjacent platinum sites are necessary for methanol adsorption [71], and therefore, when the surface Ru concentration is too high, the rate decreases again.

Whatever the methanol oxidation pathway is, the dehydrogenation process (either C-H or O-H bond cleavage) seems to be the rate determining step (rds) [70, 86, 101, 102]. However, Jusys and Behm [92] concluded from the low kinetic H/D isotope effect that the oxidation of adsorbed CO formed from methanol is rather the rds. Thus, to investigate the reaction mechanism and the effect of different parameters on the reaction kinetics, direct measurement of the decomposition rate (methanol to adsorbed CO) is important.

Housmans et al. [74] studied the oxidation of methanol at Pt(111), Pt(554) and Pt(553) in 0.5 M H_2SO_4 by cyclic voltammetry and chronoamperometry under stagnant conditions. According to their measurements, the overall methanol oxidation rate increases with increasing step density thus, they concluded that the steps catalyzes the decomposition of methanol, i.e. methanol decomposition products are preferably adsorbed at the steps. Moreover, by comparing the chronoamperometric data, they found that surfaces with higher step density show a faster decrease of the current. A combination of chronoampermetry, fast scan cyclic voltammetry and theoretical methods was used in another study to investigate the mechanism of methanol decomposition on low Miller indices Pt surfaces [101]. In this study, it was shown that the potential where the methanol adsorption product (CO_{ad}) is stable, the decomposition proceeds through a pure dehydrogenation reaction and the dual pathway mechanism is then independent of the electrode-substrate surface structure. However, the potential at which methanol decomposition products are other than CO_{ad} depends on the surface structure. Depending on the model chosen, it was also found that the simulated rate constant can differ by orders of magnitudes [103, 104]. Thus to investigate the reaction

mechanism and the effect of different parameters on the reaction kinetics, direct measurement of the decomposition rates is important.

The rate of methanol adsorption at carbon supported platinum and smooth Pt(Poly) has been compared under flow through conditions as studied by DEMS [90]. In this previous study, 0.1 M methanol prepared in 0.5 M H_2SO_4 supporting electrolyte was adsorbed at smooth Pt(Poly) for different time at 0.5 V. The methanol adsorption rate calculated from the CO_{ad} coverages achieved after ca. 5 s of adsorption was 0.06 MLs^{-1} whereas that for platinum nanoparticels was 0.04 MLs^{-1}. However, the values of the rate achieved after shorter adsorption times were not determined. Based on the relation between CO_{ad} coverage and the IR band intensities, the kinetics of the indirect pathway of methanol oxidation has been studied recently by Liao et al. using in situ FTIR coupled with a thin-layer flow cell [105]. According to their measurements, for the oxidation of 2 M methanol prepared in 0.1 M $HClO_4$ at Pt film deposited at Si prism, the maximum rate of methanol dehydrogenation to CO_{ad} at 0.6 V is 0.4 molecule $site^{-1}$ s^{-1} which was 100 times higher than that for the oxidation of CO_{ad} formed from methanol.

In previous works [75, 79-81, 87, 90] our DEMS results proved that methanol oxidation at platinum proceeds via the parallel pathway mechanism. In chapter 3, I also studied the oxidation of methanol at Pt(331) stepped single crystal electrode with and without Ru step decoration. The aim is to investigate the effect Ru step decoration on the oxidation of methanol at this surface which has only three platinum atom wide terrace. I also studied the effect of methanol concentration, convection and degree of CO_{ad} poisoning on the current efficiencies of both CO_2 and methylformate at Pt(331) electrode. The results were compared to the values of methanol adsorption rates obtained at the same electrode under flow through conditions.

My work in chapter 3 aims also at investigation of the rate of methanol adsorption at short times when it interacts with the CO-free platinum (adsorption time $\leq$ 1 s), at smooth Pt(Poly) and platinum stepped single crystals, which will have the advantage of following up the fast poisoning rate of such reaction more accurately. At platinum stepped single crystals, the effect of adsorption potential, step density and Ru step decoration on the methanol adsorption rate will be also discussed.

Applying the potential modulation technique, my work in chapter 5 aims at determining the potential dependence (α') of the oxidation of bulk methanol and methanol adsorption product at Pt(Poly) electrode under convection conditions. The corresponding Tafel slopes have been calculated and compared to the slopes obtained by normal methods

(cf. chapter 5, part 5.2.3). The rate determining step of the reaction has been assigned according to the results of α' and Tafel slopes.

1.7.3 Electrocatalytic oxidation of ethanol

The use of ethanol as a fuel in the direct alcohol fuel cells has the advantage that it can be produced from bio-renewable sources; competition with production of food is avoided if it is produced from cellulose [106, 107]. Compared to methanol, ethanol is less toxic, easy to be stored and has a high theoretical energy content of 8 kWh kg^{-1} corresponding to 12 electrons per molecule for its total oxidation to carbon dioxide [108]. The main disadvantage of ethanol comes from the difficulty to cleave the C-C bond. Therefore, the main challenge in ethanol electrocatalysis is to find a catalyst that can help in complete oxidation at low overpotential. It is well known in literature [45, 109-112] that there are two oxidation pathways for ethanol; the first pathway via dissolved intermediates (acetaldehyde and acetic acid or acetate) that decreases the efficiency of the system and act as pollutants, the second pathway is the oxidation via the formation of adsorbed intermediates as CO and CH_x fragments [113, 114] which poison the platinum surface.

Many authors studied the electrooxidation of ethanol at different surfaces using different techniques. Kutz et al. [115] recently studied the electrooxidation of ethanol at Pt(poly) with broad band sum-frequency generation (BB-SFG) spectroscopy and electrochemistry. They found the formation of acetate adsorbate and co-adsorbed sulphuric acid anions during ethanol oxidation. In both sulphuric as well as perchloric acid solutions, surface-adsorbed CO on a top sites of platinum and acetate intermediates were observed, whereas CO molecules on bridge sites and sulphuric acid anions were found only in sulphuric acid. Schmiemann et al. reported the formation of CO_{ad} and $CH_{x,ad}$ species at Pt(Poly) as studied by DEMS [113]. Recently, Lai et al. confirmed the formation of these adsorbed species using SERS [116]. Using in situ ATR-FTIRS flow cell, Heinen et al. [117] reported the presence of both CO_{ad} and adsorbed acetyl species on the platinum surface during the adsorption of ethanol, the latter species are then decomposed to CO_{ad} and $CH_{x,ad}$ when scanning the potential to the H_{upd} region. They observed also adsorbed acetate at potentials of CO_{ad} oxidation and it was in a fast adsorption/desorption equilibrium with acetic acid in the solution.

Using a mixture of perchloric and sulphuric acids as supporting electrolyte, Abd El Latif et al. [109] found the production of acetaldehyde as the only product of ethanol electrooxidation at Pt(Poly) using DEMS. As found by in situ FTIRS and/or DEMS, the

production of acetaldehyde and acetic acid exceeded that of CO_2 when ethanol was oxidized at carbon supported platinum alloy catalysts [112] or binary catalysts as PtRu/C, Pt_3Sn/C [118-120].

The electrooxidation of ethanol on platinum single crystal surfaces has been a subject of interest to many authors. Iwasita et al. [121] reported, form FTIR spectroscopic studies that CO_2 and the soluble products (acetaldehyde and acetic acid) are formed during ethanol oxidation on Pt(111), Pt(110) and Pt(100). Weaver et al. [45] and Korzeniewski et al. [122] reported that ethanol undergoes primarily four-electron oxidation to acetic acid on Pt(111) and surfaces vicinal to the (111) plane. As step density increases, the formation of acetic acid on the surfaces vicinal to (111) plane decreases [123]. According to DEMS results [109], acetaldehyde is formed above 0.6 V as the only product of ethanol oxidation on Pt(19,1,1) where a simple dehydrogenation reaction takes place, the formation of other products however require the presence of step sites and (111) terraces. For different platinum stepped single crystals with different (111) terraces width, Colmati et al. [124] found that there was no significant improvement of the activity towards ethanol oxidation for surfaces vicinal to (100) steps when compared to that vicinal to (110). This was attributed to a very small amount of CO adsorbed on those surfaces leading to very small oxidation currents.

After the first report on the co-catalytic effect of Pb on formic acid oxidation [125], it has been shown that also modification of the electrode surface with adatoms such as Sn [62, 126-130], Ru [90, 131], Bi [132, 133], As [134, 135] etc, can enhance the catalytic properties of platinum electrode. Many authors [119, 136] reported the catalytic activity of Pt_3Sn/C catalyst for ethanol oxidation with different techniques. In general, the anticipated but unproven reason behind the strong catalytic activity was the ease of C-C bond breaking at sufficiently low overpotential. The deposition of Sn on Pt(111) was also studied by cyclic voltammetry (CV) and scanning tunnelling microscopy (STM) [137]. According to this study, adsorbed Sn was not directly observed by STM due to its high mobility except when coadsorbed with Cu, CO or sulphate anions. In that case, Sn segregated in observable 2D islands implying a repulsive interaction with these species. Sn not only facilitates the oxidation of weakly adsorbed CO at low potentials due to electronic effect but also produces weakly adsorbed CO states at the surface due to the electronic repulsion between Sn atoms and CO molecules. Step decoration of stepped single crystals vicinal to (111) by Sn leads to a better distribution and much enhanced activity [60, 127]. Recently, Del Colle et al. reported the catalytic effect of Sn adsorbed at Pt(s)[n(111)×(111)] surfaces during the oxidation of ethanol as studied by voltammetry, chronoamperometry and FTIR [138]. They found that Sn

partially covering (111) steps can promote the C-C bond breaking and the oxidation of the resulting CO_{ad} as well as the oxidation of ethanol to acetic acid.

It is the aim of my work in chapter 4 to analyse in detail the contributions of the possible reaction products, in particular CO_2, to the overall current. In order to model the conditions of continuous oxidation in a fuel cell, the continuous mass transfer to the electrode surface is necessary. Therefore, our mass spectrometric measurements using the thin layer flow through cell is much better suited than the typical FTIR measurements under stagnant conditions.

However, such a quantitative determination is not trivial and a careful analysis of the convection behaviour is necessary. In the dual thin layer flow through cell, the collection efficiency is dependent on the flow rate [12]. At low flow rates (< 1 μLs^{-1}), a homogeneous distribution of the species formed in the electrochemistry compartment during their transfer through the capillaries (complete mixing) occurs before entering to the detection compartment due to a sufficiently long residence time leading to actual current efficiency values. At higher flow rates, however, incomplete mixing occurs due to shorter residence times in the capillaries before entering the detection compartment. The product concentration at the entrance in the vicinity of the Teflon membrane will be higher than the average. Since in the usual calibration experiment the concentration at the entrance of the detection compartment is homogeneous, this leads to current efficiencies which are too high.

Therefore, I present a simple method for the correction of the current efficiencies due to incomplete mixing. Oxidation of i-propanol at Pt(Poly) was performed under the same experimental conditions as that of ethanol in 0.5 M H_2SO_4. Acetone (the only product of i-propanol oxidation on platinum) and acetaldehyde have similar transfer characteristics and diffusion coefficients [139]. The calculated acetone current efficiencies at each flow rate were used to correct the apparent current efficiency values in each case.

The electrochemical behaviour of the secondary C_3 alcohol was investigated before [140]. From FTIR spectra, it was concluded before that there is no absorption band due to an adsorbed CO species [141]. As a general agreement in all of the previous literature, the cleavage of C-C bonds is negligible during the adsorption of i-propanol or acetone on Pt(Poly) [142, 143].

I also investigated the oxidation of ethanol on platinum single crystals before and after deposition of Sn. The aim is a semi-quantitative analysis of the volatile product and an estimate of the current efficiencies for soluble intermediate of ethanol oxidation at Sn modified electrodes.

1.7.4 Electrocatalytic reduction of oxygen

In the proton-exchange membrane fuel cell (PEMFC), the main problem that arises at the cathode is the voltage drop due to sluggish ORR kinetics. Far from equilibrium potential (1.2 V), the limiting state-of-the-art operating potential is 0.7 V [144]. This is due to strong inhibition of the cathodic ORR, resulting in high overpotentials and therefore, significant deterioration in the energy conversion efficiency of the cell [145]. The difficulty stems from the exceptionally strong (O=O) bond (498 kJ mol^{-1}). Thus, activation of this bond is typically kinetically slow [146]. Several studies have been performed to find the best catalyst for ORR at poly- or single crystal platinum surfaces. Currently the best cathode catalysts are platinum or alloys of platinum with Co or Ni [147-150] in 0.1 M $HClO_4$.

The modified Wroblowa et al. [151] scheme for ORR still the most effective scheme that describe the complicated ORR pathway at a metal surface [152](cf. Fig. 1-17). It can be summarized as follows: Oxygen can be reduced directly to water without the production of hydrogen peroxide through the direct 4-electron pathway or through a series 2-electron pathway involves hydrogen peroxide production as an intermediate and/or a combination between these two pathways.

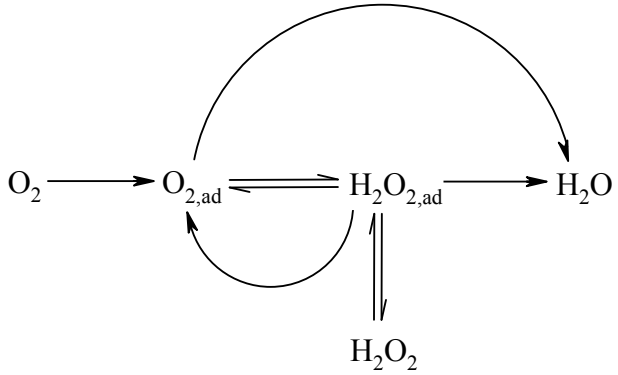

Figure 1-17 The purposed scheme for oxygen reduction reaction.

The ORR proceeds on platinum via a direct 4-electron pathway with a small amount ca. 1 % of H_2O_2 formed at low overpotentials (0.1 – 0.4 V) [153]. On other electrodes, for instant, gold, ORR proceeds via a 2-electron pathway at low overpotentials in acidic medium. However, in alkaline medium Au(100) exhibit 4-electron pathway for ORR [146, 154, 155]. On platinum, O_2 binds to the metal surface and then transforms to superoxide following the first electron transfer with a possible coupled proton transfer, namely associative mechanism. Oxygen can also dissociates upon platinum coordination followed by reaction with H^+, namely dissociative mechanism [156, 157].

ORR has been studied before at polycrystalline platinum [158, 159], Pt/C nanoparticles [152, 160-163] and platinum single crystals [152, 164-168]. Markovic et al. [169] studied the ORR at platinum low index single crystal surfaces in perchloric acid solutions in a hanging meniscus rotating ring disk technique. By comparing the half-wave potentials, the ORR activity was at Pt(110) > Pt(111) > Pt(100). In sulphuric acid, however, the order of the activity increased in the sequence Pt(110) > Pt(100) > Pt(111) [167] and the differences in the activity was attributed to the structural sensitivity to the bisulphate adsorption and its inhibiting effect.

At polycrystalline platinum, low index platinum single crystals and platinum alloys [159, 169], a Tafel slope of (-RT/F = -60 mV dec^{-1}) has been reported at high potentials and high coverage by adsorbed oxygenated species. The adsorbed intermediates are in quasi equilibrium and their surface concentration varies linearly with potential and pH according to Temkin isotherm. At low potentials and low coverage, however, a Tafel slope of (-2RT/F = -120 mV dec^{-1}) has been detected and the Langmuir isotherm explains the variation of the adsorbate surface concentration. Antoine et al. studied the kinetics and mechanism of ORR on Pt nanoparticles inside Nafion [161]. In all cases, the rate determining step was assigned to be the first electron addition to the adsorbed oxygen $(O_2)_{ad}$ including the protonation of the O_2 molecule [71, 153].

As an application of the potential modulation method described in chapter 5, my work in chapter 6 aims at investigation of the kinetics of ORR at Pt(Poly) under convection conditions. Also the apparent transfer coefficient and the corresponding Tafel slope have been calculated. Tafel slopes obtained from ac voltammetry method were compared to that obtained by normal methods and the rds of the reaction has been assigned.

References

[1] C. Hamann, A. Hamnett, and W. Vilestich, Electrochemistry, second completely revised and updated edition, Verlag GmbH & Co. KGaA, Weinheim, 2007.

[2] A. J. Bard and L. R. Faulkner, Electrochemical Methods: Fundamentals and Applications, John Wiley & Sons Inc., New York, Weinheim, 2001.

[3] H. Wang, in Mathematisch-Naturwissenschaftlichen Fakultät, Rheinischen Friedrich-Wilhelms-Universität Bonn, Bonn, 2009.

[4] A. J. Bard, G. Inzelt, and F. Scholz, Electrochemical Dictionary, Springer-Verlag Berlin Heidelberg, 2008.

[5] X. Z. Yuan, C. Song, H. Wang, and J. Zhang, Electrochemical Impedance Spectroscopy in PEM Fuel Cells - Fundamentals and applications, Springer London Dordrecht Heidelberg New York, 2010.

[6] D. Pletcher, R. Greef, R. Peat, L. M. Peter, and J. Robinson, Instrumental Methods In Electrochemistry (Southampton Electrochemistry Group), Horwood Publishing Limited, 1985.
[7] C. M. A. Brett and A. M. O. Brett, Electrochemistry: Principles, Methods and Applications, Oxford University Press, Oxford, 1993.
[8] H.-C. Wang, S. Ernst, and H. Baltruschat, Physical Chemistry Chemical Physics 12:2190 (2010).
[9] R. R. Bruckenstein and J. Gadde, Journal of the American Chemical Society 93:793 (1971).
[10] O. Wolter and J. Heitbaum, Ber. Bunsenges. Phys. Chem. 88:2 (1984).
[11] O. Wolter and J. Heitbaum, Ber. Bunsenges. Phys. Chem. 88:6 (1984).
[12] H. Baltruschat, Journal of the American Society for Mass Spectrometry 15:1693 (2004).
[13] T. Hartung and H. Baltruschat, Langmuir 6:953 (1990).
[14] T. Hartung, U. Schmiemann, I. Kamphausen, and H. Baltruschat, Analytical Chemistry 63:44 (1991).
[15] H. Baltruschat and U. Schmiemann, Ber. Bunsenges. Phys. Chem. 97:452 (1993).
[16] Z. Jusys, H. Massong, and H. Baltruschat, Journal of the Electrochemical Society 146:1093 (1999).
[17] Z. Jusys, J. Kaiser, and R. J. Behm, Electrochimica Acta 47:3693 (2002).
[18] Y. Gao, H. Tsuji, H. Hattori, and H. Kita, Journal of Electroanalytical Chemistry 372:195 (1994).
[19] A. H. Wonders, T. H. M. Housmans, V. Rosca, and M. T. M. Koper, Journal of Applied Electrochemistry 36:1215 (2006).
[20] A.-E.-A. Abd-El-Latif, J. Xu, N. Bogolowski, P. Königshoven, and H. Baltruschat, Electrocatalysis 3:9 (2012).
[21] F. Vigier, S. Rousseau, C. Coutanceau, J.-M. Leger, and C. Lamy, Topics in Catalysis 40:111 (2006).
[22] Abd-El-Latif, Vol. PhD, in Mathematisch-Naturwissenschaftlichen Fakultät, Rheinischen Friedrich-Wilhelms-Universität Bonn, Bonn, 2011, p. 185.
[23] L. Carrette, K. A. Friedrich, and U. Stimming, Fuel Cells 1:5 (2001).
[24] L. Carrette, K. A. Friedrich, and U. Stimming, ChemPhysChem 1:162 (2000).
[25] G. A. Somorjai and Y. Li, Introduction to surface chemistry and catalysis, John Wiely & Sons, Inc., Hoboken, New Jersey, 2010.
[26] F. Hernández, Vol. PhD, in Mathematisch-Naturwissenschaftlichen Fakultät, Rheinischen-Friedrich-Wilhelms-Universität Bonn, Bonn, 2006.
[27] M. T. M. Koper, Nanoscale 3:2054 (2011).
[28] B. Lang, R. W. Joyner, and G. A. Somorjai, Surface Science 30:440 (1972).
[29] N. Furuya and S. Koide, Surface Science 220:18 (1989).
[30] N. Furuya and M. Shibata, Journal of Electroanalytical Chemistry 467:85 (1999).
[31] J. Clavilier, R. Faure, G. Guinet, and R. Durand, Journal of Electroanalytical Chemistry 107:205 (1980).
[32] J. Clavilier, K. El Achi, and A. Rodes, Chemical Physics 141:1 (1990).
[33] A. Rodes, K. El Achi, M. A. Zamakchardi, and J. Clavilier, Journal of Electroanalytical Chemistry 284:245 (1990).
[34] J. Clavilier, A. Rodes, K. E. Achi, and M. A. Zamakhchari, J. Chim. Phys. 88:1291 (1991).
[35] A. J. Bard, H. D. Abruña, C. E. Chidsey, L. R. Faulkner, S. W. Feldberg, K. Itaya, M. Majda, O. Melroy, R. W. Murray, M. D. Porter, M. P. Soriaga, and H. S. White, Journal of Physical Chemistry 97:7147 (1993).

[36] E. Budevski, G. Staikov, and W. J. Lorenz, Electrochemical Phase Formation and Growth, VCH, Weinheim, 1996.
[37] D. M. Kolb, M. Przasnyski, and H. Gerischer, Journal of Electroanalytical Chemistry 54:25 (1974).
[38] W. Schmickler and E. Santos, Interfacial Electrochemistry, Springer Heidelberg Dordrecht London New York, 2010.
[39] H. Baltruschat, E. Siegfried, and N. Bogolowski, in Catalysis in Electrochemistry, From Fundamentals to Strategies for Fuel Cell Development (E. S. a. W. Schmickler, ed.), John Wiley & Sons, Inc., Hoboken, New Jersey, Canada, 2011.
[40] A. Cuesta, Journal of the American Chemical Society 128:13332 (2006).
[41] J. R. Kitchin, J. K. Norskov, M. A. Barteau, and J. G. Chen, Physical Review Letters 93:156801 (2004).
[42] J. R. Kitchin, J. K. Norskov, M. A. Barteau, and J. G. Chen, Journal of Chemical Physics 120:10240 (2004).
[43] M. Mavrikakis, B. Hammer, and J. K. Norskov, Physical Review Letters 81:2819 (1998).
[44] L. A. Kibler, A. M. El-Aziz, R. Hoyer, and D. M. Kolb, Angewandte Chemie-International Edition 44:2080 (2005).
[45] S.-C. Chang, L.-W. H. Leung, and M. J. Weaver, Journal of Physical Chemistry 94:6013 (1990).
[46] R. J. Bellows, E. P. MarucchiSoos, and D. T. Buckley, Industrial & Engineering Chemistry Research 35:1235 (1996).
[47] H. Wang, Z. Jusys, R. J. Behm, and H. D. Abruña, The Journal of Physical Chemistry C 116:11040 (2012).
[48] A. Cuesta, A. Couto, A. Rincon, M. C. Perez, A. Lopez-Cudero, and C. Gutierrez, Journal of Electroanalytical Chemistry 586:184 (2006).
[49] G. Stalnionis, L. Tamasuskaite-Tamasiunaite, V. Pautieniene, and Z. Jusys, Journal of Electroanalytical Chemistry 590:198 (2006).
[50] G. García, J. Florez-Montano, A. Hernandez-Creus, E. Pastor, and G. A. Planes, Journal of Power Sources 196:2979 (2011).
[51] E. A. Batista, T. Iwasita, and W. Vielstich, Journal of Physical Chemistry B 108:14216 (2004).
[52] C. Saravanan, M. T. M. Koper, N. M. Markovic, M. Head-Gordon, and P. N. Ross, Physical Chemistry Chemical Physics 4:2660 (2002).
[53] I. Villegas and M. J. Weaver, Journal of Chemical Physics 101:1648 (1994).
[54] A. Cuesta, Electrocatalysis 1:7 (2010).
[55] A. Cuesta, M. a. Escudero, B. Lanova, and H. Baltruschat, Langmuir 25:6500 (2009).
[56] A. Lopez-Cudero, A. Cuesta, and C. Gutierrez, Journal of Electroanalytical Chemistry 586:204 (2006).
[57] A. Cuesta, M. d. C. Pérez, A. Rincón, and C. Gutiérrez, ChemPhysChem 7:2346 (2006).
[58] A. Lopez-Cudero, A. Cuesta, and C. Gutierrez, Journal of Electroanalytical Chemistry 579:1 (2005).
[59] G. Samjeské, X.-Y. Xiao, and H. Baltruschat, Langmuir 18:4659 (2002).
[60] H. Massong, H. S. Wang, G. Samjeske, and H. Baltruschat, Electrochimica Acta 46:701 (2000).
[61] S. Wasmus and A. Küver, Journal of Electroanalytical Chemistry 461:14 (1999).
[62] H. A. Gasteiger, N. A. Markovic, and J. Philip. N. Ross, Journal of Physical Chemistry 99:8945 (1995).

[63] H. A. Gasteiger, N. A. Markovic, and J. Philip. N. Ross, Journal of Physical Chemistry 99:8290 (1995).
[64] T. Iwasita, Electrochimica Acta 47:3663 (2002).
[65] S. Gilman, Journal of Physical Chemistry 68:70 (1964).
[66] E. Santos, E. P. M. Leiva, and W. Vielstich, Electrochimica Acta 36:555 (1991).
[67] E. Herrero, J. M. Feliu, S. Blais, Z. Radovic-Hrapovic, and G. Jerkiewicz, Langmuir 16:4779 (2000).
[68] M. T. M. Koper, A. P. J. Jansen, R. A. v. Santen, J. J. Lukien, and P. A. J. Hilbers, Journal of Chemical Physics 109:6051 (1998).
[69] H.-C. Wang and H. Baltruschat, ChemPhysChem 11:2798 (2010).
[70] V. Grozovski, V. Climent, E. Herrero, and J. M. Feliu, Journal of Electroanalytical Chemistry 662:43 (2011).
[71] N. M. Markovic and P. N. Ross, Surface Science Reports 45:117 (2002).
[72] R. Parsons and T. VanderNoot, Journal of Electroanalytical Chemistry 257:9 (1988).
[73] T. Iwasita-Vielstich, in Advances in Electrochemical Science and Engineering, Vol. 1 (H. Gerischer and C. W. Tobias, eds.), VCH, Weinheim, New York, 1990, p. 127.
[74] T. H. M. Housmans and M. T. M. Koper, Journal of Physical Chemistry B 107:8557 (2003).
[75] H. Wang, T. Löffler, and H. Baltruschat, Journal of Applied Electrochemistry 31:759 (2001).
[76] R. Parsons and T. VanderNoot, Journal of Electroanalytical Chemistry 257:9 (1988).
[77] T. D. Jarvi, S. Sriramulu, and E. M. Stuve, Journal of Physical Chemistry B 101:3649 (1997).
[78] V. S. Bagotzky, Y. B. Vassiliev, and O. A. Khazova, Journal of Electroanalytical Chemistry 81:229 (1977).
[79] H. Wang and H. Baltruschat, in DMFC Symposium, Meeting of the Electrochemical Society 2001 (S. R. Narayanan, ed.), The Electrochemical Society, Washington D.C., 2001.
[80] A. A. Abd-El-Latif and H. Baltruschat, Journal of Electroanalytical Chemistry 662:204 (2011).
[81] H. S. Wang, C. Wingender, H. Baltruschat, M. Lopez, and M. T. Reetz, Journal of Electroanalytical Chemistry 509:163 (2001).
[82] K.-I. Ota, Y. Nakagawa, and M. Takahashi, Journal of Electroanalytical Chemistry 179:179 (1984).
[83] T. Iwasita and W. Vielstich, Journal of Electroanalytical Chemistry 201:403 (1986).
[84] E. A. Batista, G. R. P. Malpass, A. J. Motheo, and T. Iwasita, Journal of Electroanalytical Chemistry 571:273 (2004).
[85] T. H. M. Housmans, A. H. Wonders, and M. T. M. Koper, Journal of Physical Chemistry B 110:10021 (2006).
[86] E. Herrero, K. Franaszczuk, and A. Wieckowski, Journal of Physical Chemistry 98:5074 (1994).
[87] H. Wang and H. Baltruschat, Journal of Physical Chemistry C 111:7038 (2007).
[88] J. Shin and C. Korzeniewski, Journal of Physical Chemistry 99:3419 (1995).
[89] A. V. Tripkovic and K. D. Popovic, Electrochimica Acta 41:2385 (1996).
[90] B. Lanova, H. Wang, and H. Baltruschat, Fuel Cells 6:214 (2006).
[91] Z. Jusys, J. Kaiser, and R. J. Behm, Langmuir 19:6759 (2003).
[92] Z. Jusys and R. J. Behm, Journal of Physical Chemistry B 105:10874 (2001).
[93] Y. E. Seidel, A. Schneider, Z. Jusys, B. Wickman, B. Kasemo, and R. J. Behm, Langmuir 26:3569 (2010).
[94] H. Wang, L. R. Alden, F. J. DiSalvo, and H. D. Abruna, Langmuir 25:7725 (2009).

[95] Y. E. Seidel, A. Schneider, Z. Jusys, B. Wickman, B. Kasemo, and R. J. Behm, Faraday Discussions 140:167 (2008).
[96] N. M. Markovic, B. N. Grgur, C. A. Lucas, and P. N. Ross, Surface Science 384:L805 (1997).
[97] M. Watanabe and S. Motoo, Journal of Electroanalytical Chemistry 60:275 (1975).
[98] T. Iwasita, F. C. Nart, and W. Vielstich, Ber. Bunsenges. Phys. Chem. 94:1030 (1990).
[99] R. Ianniello, V. M. Schmidt, U. Stimming, J. Stumper, and A. Wallau, Electrochimica Acta 39:1863 (1994).
[100] M. Krausa and W. Vielstich, Journal of Electroanalytical Chemistry 379:307 (1994).
[101] D. Cao, G. Q. Lu, A. Wieckowski, S. A. Wasileski, and M. Neurock, Journal of Physical Chemistry B 109:11622 (2005).
[102] E. Herrero, W. Chrzanowski, and M. J. Weaver, Journal of Physical Chemistry 99:10423 (1995).
[103] J. L. Cohen, D. J. Volpe, and H. D. Abruna, Physical Chemistry Chemical Physics 9:49 (2007).
[104] G. Q. Lu, W. Chrzanowski, and A. Wieckowski, Journal of Physical Chemistry B 104:5566 (2000).
[105] L. W. Liao, S. X. Liu, Q. Tao, B. Geng, P. Zhang, C. M. Wang, Y. X. Chen, and S. Ye, Journal of Electroanalytical Chemistry 650:233 (2011).
[106] S.-Z. Li and C. Chan-Halbrendt, Applied Energy 86, Supplement 1:S162 (2009).
[107] R. Cascone, in SBE Special Section - Biofuels, 2008.
[108] F. Vigier, C. Coutanceau, F. Hahn, E. M. Belgsir, and C. Lamy, Journal of Electroanalytical Chemistry 563:81 (2004).
[109] A. A. Abd-El-Latif, E. Mostafa, S. Huxter, G. Attard, and H. Baltruschat, Electrochimica Acta 55:7951 (2010).
[110] J. Willsau and J. Heitbaum, Journal of Electroanalytical Chemistry 194:27 (1985).
[111] G. A. Camara and T. Iwasita, Journal of Electroanalytical Chemistry 578:315 (2005).
[112] H. Wang, Z. Jusys, and R. J. Behm, Journal of Physical Chemistry B 108:19413 (2004).
[113] U. Schmiemann, U. Müller, and H. Baltruschat, Electrochimica Acta 40:99 (1995).
[114] T. Iwasita and E. Pastor, Electrochimica Acta 39:531 (1994).
[115] R. B. Kutz, B. Braunschweig, P. Mukherjee, D. D. Dlott, and A. Wieckowski, The Journal of Physical Chemistry Letters 2:2236 (2011).
[116] S. C. S. Lai, S. E. F. Kleyn, V. Rosca, and M. T. M. Koper, The Journal of Physical Chemistry C 112:19080 (2008).
[117] M. Heinen, Z. Jusys, and R. J. Behm, The Journal of Physical Chemistry C 114:9850 (2010).
[118] H. Wang, Z. Jusys, and R. J. Behm, Journal of Power Sources 154:351 (2006).
[119] Q. Wang, G. Q. Sun, L. H. Jiang, Q. Xin, S. G. Sun, Y. X. Jiang, S. P. Chen, Z. Jusys, and R. J. Behm, Physical Chemistry Chemical Physics 9:2686 (2007).
[120] L. Colmenares, H. Wang, Z. Jusys, L. Jiang, S. Yan, G. Q. Sun, and R. J. Behm, Electrochimica Acta 52:221 (2006).
[121] X. H. Xia, H.-D. Leiss, and T. Iwasita, Journal of Electroanalytical Chemistry 437:233 (1997).
[122] J. Shin, W. J. Tornquist, C. Korzeniewski, and C. S. Hoaglund, Surface Science 364:122 (1996).
[123] D. J. Tarnowski and C. Korzeniewski, Journal of Physical Chemistry B 101:253 (1997).
[124] F. Colmati, G. Tremiliosi-Filho, E. R. Gonzalez, A. Berna, E. Herrero, and J. M. Feliu, Physical Chemistry Chemical Physics 11:9114 (2009).

[125] E. Schwarzer and W. Vielstich, Chemie Ingenieur Technik 45:201 (1973).
[126] S. Tillmann, A. Friedrich, H. Massong, and H. Baltruschat, in The 195th Meeting of the Electrochemical Society, Vol. Abstracts 99-1, The Electrochemical Society, Seattle, 1999, p. 1097.
[127] H. Massong, S. Tillmann, T. Langkau, E. A. Abd El Meguid, and H. Baltruschat, Electrochimica Acta 44:1379 (1998).
[128] K. Wang, H. A. Gasteiger, N. M. Markovic, and P. N. Ross, Electrochimica Acta 41:2587 (1996).
[129] M. Shibata and N. Furuya, Journal of Electroanalytical Chemistry 269:217 (1989).
[130] S. Motoo, M. Shibata, and M. Watanabe, Journal of Electroanalytical Chemistry 110:103 (1980).
[131] H. Wang, Z. Jusys, and R. J. Behm, Journal of Applied Electrochemistry 36:1187 (2006).
[132] G. Samjeské, H. Wang, T. Löffler, and H. Baltruschat, Electrochimica Acta 47:3681 (2002).
[133] E. Herrero, J. Feliu, and A. Aldaz, Journal of Catalysis 152:264 (1995).
[134] X. Y. Xiao and H. Baltruschat, Langmuir 19:7436 (2003).
[135] E. Herrero, A. Rodes, J. M. Pérez, J. M. Feliu, and A. Aldaz, Journal of Electroanalytical Chemistry 393:87 (1995).
[136] V. Rao, C. Cremers, U. Stimming, L. Cao, S. G. Sun, S. Y. Yan, G. Q. Sun, and Q. Xin, Journal of the Electrochemical Society 154:B1138 (2007).
[137] X. Xiao, S. Tillmann, and H. Baltruschat, Physical Chemistry Chemical Physics 4:4044 (2002).
[138] V. Del Colle, J. Souza-Garcia, G. Tremiliosi-Filho, E. Herrero, and J. M. Feliu, Physical Chemistry Chemical Physics 13:12163 (2011).
[139] D. Bayer, C. Cremers, H. Baltruschat, and J. Tubke, ECS Transactions 41:1669 (2011).
[140] E. Pastor, S. Gonzalez, and A. Arvia, Journal of Electroanalytical Chemistry 395:233 (1995).
[141] L.-W. H. Leung, S.-C. Chang, and M. J. Weaver, Journal of Electroanalytical Chemistry 266:317 (1989).
[142] T. Hartung, Universität Witten/Herdecke, 1989.
[143] B. Bänsch, T. Hartung, H. Baltruschat, and J. Heitbaum, Journal of Electroanalytical Chemistry 259:207 (1989).
[144] J. Rossmeisl, G. S. Karlberg, T. Jaramillo, and J. K. Norskov, Faraday Discussions 140:337 (2008).
[145] K. J. J. Mayrhofer, D. Strmcnik, B. B. Blizanac, V. Stamenkovic, M. Arenz, and N. M. Markovic, Electrochimica Acta 53:3181 (2008).
[146] A. A. Gewirth and M. S. Thorum, Inorganic Chemistry 49:3557 (2010).
[147] V. R. Stamenkovic, B. Fowler, B. S. Mun, G. Wang, P. N. Ross, C. A. Lucas, and N. M. Markovic, Science 315:493 (2007).
[148] Y. Sha, T. H. Yu, B. V. Merinov, P. Shirvanian, and W. A. Goddard, The Journal of Physical Chemistry Letters 2:572 (2011).
[149] V. Stamenkovic, B. S. Mun, K. J. J. Mayrhofer, P. N. Ross, N. M. Markovic, J. Rossmeisl, J. Greeley, and J. K. Norskov, Angewandte Chemie-International Edition 45:2897 (2006).
[150] V. R. Stamenkovic, B. S. Mun, M. Arenz, K. J. J. Mayrhofer, C. A. Lucas, G. F. Wang, P. N. Ross, and N. M. Markovic, Nature Materials 6:241 (2007).
[151] H. S. Wroblowa, P. Yen Chi, and G. Razumney, Journal of Electroanalytical Chemistry and Interfacial Electrochemistry 69:195 (1976).

[152] N. M. Markovic, T. J. Schmidt, V. Stamenkovic, and P. N. Ross, Fuel Cells - From Fundamentals to Systems 1:105 (2001).
[153] R. Adzic, in Electrocatalysis (J. Lipkowski and P. N. Ross, eds.), New York u.a., 1998, p. 197.
[154] R. R. Adzic, N. M. Markovic, and V. B. Vešović Journal of Electroanalytical Chemistry and Interfacial Electrochemistry 165:105 (1984).
[155] S. Strbac and R. R. Adžić Electrochimica Acta 41:2903 (1996).
[156] J. K. Norskov, J. Rossmeisl, A. Logadottir, L. Lindqvist, J. R. Kitchin, T. Bligaard, and H. Jonsson, Journal of Physical Chemistry B 108:17886 (2004).
[157] A. U. Nilekar and M. Mavrikakis, Surface Science 602:L89 (2008).
[158] S. Strbac, Electrochimica Acta 56:1597 (2011).
[159] V. Stamenković , T. J. Schmidt, P. N. Ross, and N. M. Marković, Journal of Electroanalytical Chemistry 554-555:191 (2003).
[160] N. Alexeyeva, K. Tammeveski, J. Solla-Gullón, and J. M. Feliu, Electrochimica Acta 55:794 (2010).
[161] O. Antoine, Y. Bultel, and R. Durand, Journal of Electroanalytical Chemistry 499:85 (2001).
[162] T. Nishimura, T. Morikawa, M. Yokoi, C. Iwakura, and H. Inoue, Electrochimica Acta 54:499 (2008).
[163] D. W. Banham, J. N. Soderberg, and V. I. Birss, The Journal of Physical Chemistry C 113:10103 (2009).
[164] R. Subbaraman, D. Strmcnik, A. P. Paulikas, V. R. Stamenkovic, and N. M. Markovic, ChemPhysChem 11:2825 (2010).
[165] B. B. Blizanac, P. N. Ross, and N. M. Markovic, Journal of Physical Chemistry B 110:4735 (2006).
[166] J. X. Wang, N. M. Markovic, and R. R. Adzic, Journal of Physical Chemistry B 108:4127 (2004).
[167] N. M. Markovic, H. A. Gasteiger, and P. N. Ross, Journal of Physical Chemistry 99:3411 (1995).
[168] A. Kuzume, E. Herrero, and J. M. Feliu, Journal of Electroanalytical Chemistry 599:333 (2007).
[169] N. Markovic, R. Adzic, B. Cahan, and E. Yeager, Journal of Electroanalytical Chemistry 377:249 (1994).

2. Materials, methods and instruments

This chapter provides a description of different materials, methods and instruments used in the present thesis. The first part gives an overview of the chemicals and cleanliness of the glassware in addition to a description of the cleaning and preparation procedures of the platinum single crystal electrodes. The second part describes different electrochemical techniques which were used here. Finally, the last part describes the electrochemical instrumentation especially, the construction of the dual thin layer flow through cell and the procedures of DEMS calibration.

2.1 Chemicals, cleanliness and electrodes

2.1.1 Chemicals

All solutions were prepared using Millipore-Q® water with a specific resistance of 18.2 MΩ cm and TOC < 3 ppb. Highly pure argon was used for deaeration of solutions prior to each experiment. Tables 2-1 and 2-2 summarize the gases, chemicals and working electrodes used in this thesis.

Table 2-1 List of chemicals and gases

Name	***Formula***	***Company***	***Purity***
Acetaldehyde	CH_3CHO	Fluka	> 99.5 %
Acetone	CH_3COCH_3	Aldrich	99.9 %
Ammonium solution	NH_3 / H_2O	ChemSolute	25 % p.a.
Argon	Ar	Praxair	99.999 %
Carbon monoxide	CO	Praxair	99.997 %
Chromium(VI) oxide	CrO_3	Merck	puriss. p.a.
Ethanol	C_2H_5OH	Merck	99.9 %
Hydrogen	H_2	Air Liquide	99.999 %
Hydrogen peroxide	H_2O_2	Merck	30 %
i-propanol	$CH_3CHOHCH_3$	Aldrich	99.9 %
Methanol	CH_3OH	Merck	99.9 %
Methylformate	$HCOOCH_3$	Merck	97 %
Nitric acid	HNO_3	VWR	AnalaR 65 %
Oxygen	O_2	Air Liquide	99.9995 %
Potassium hydroxide	KOH	Aldrich	Semiconductor grade
Ruthenium (III) chloride	$RuCl_3$	Aldrich	99.98 %
Sulfuric acid	H_2SO_4	Merck	Suprapure, 95-97 %
Tin (II) sulphate	$SnSO_4$	Acros	99 %

Table 2-2 List of working electrodes

Crystals and Lang notation	*Company*	*Diameter*	*Zone*	*Miller indices*
Polycrystalline platinum (Pt(Poly))	Metal crystals	1 cm	--	--
Pt(100)	Metal crystals	1 cm	--	--
Pt(331) = Pt(s)[3(111)×(111)] ≡ Pt(s)[2(111)×(110)]	Metal crystals & oxides Goodfellow	1 cm	$[1\,\bar{1}\,0]$	Pt(n,n,n-2)
Pt(332) = Pt(s)[6(111)×(111)] ≡ Pt(s)[5(111)×(110)]				
Pt(11,1,1) = Pt(s)[6(100)×(111)]	Metal crystals & oxides	1 cm	$[01\,\bar{1}]$	Pt(2n-1,1,1)
Pt(311) = Pt(s)[2(100)×(111)] ≡ Pt(s)[2(111)×(100)]	Metal crystals & oxides			

n is the number of terrace atoms

2.1.2 Cleanliness of solutions and glassware

Careful cleaning processes have been performed prior to each experiment due to the sensitivity of platinum surfaces (especially single crystals) towards impurities such as organic compounds or strongly adsorbing anions which can be easily adsorbed at platinum. All glassware was first cleaned overnight in 5 M KOH solution to remove possible anions and/or organic contaminations. Cationic compounds and/or metal residues can be removed by soaking the glassware in chromic acid bath overnight (640 ml conc. H_2SO_4 + 360 ml H_2O + 21.4 gm CrO_3). Afterwards, all cleaning parts were rinsed by Millipore-water. Due to the carcinogenic and toxic properties of the hexavalent chromium compounds, cleaning in a water steam system for at least four hours was an alternative.

As supporting electrolyte, 0.5 M sulfuric acid has been used in all cases because the hydrogen adsorption peaks are sharper and more prominent in the presence of sulfate anions; this help in the control of cleanliness and surface structure. To test the cleanliness of the electrolyte, glassware and electrochemical cells, the adsorption test has been performed as follows: in the supporting electrolyte, the potential applied to Pt(Poly) was cycled between 0.05 and 1.5 V at a sweep rate of 50 mVs^{-1}. After the CV reached stable shape, the potential was stopped in the beginning of the double layer region i.e. at about +0.35 V (where no hydrogen or oxygen adsorption/desorption takes place) for 3 minutes, then the potential sweep was started again. If the CVs before and after the potential hold were the same (cf. Fig. 2-1), then the system and the solutions are clean enough and if not, the electrochemical cell and the glassware were cleaned again and a fresh electrolyte was prepared.

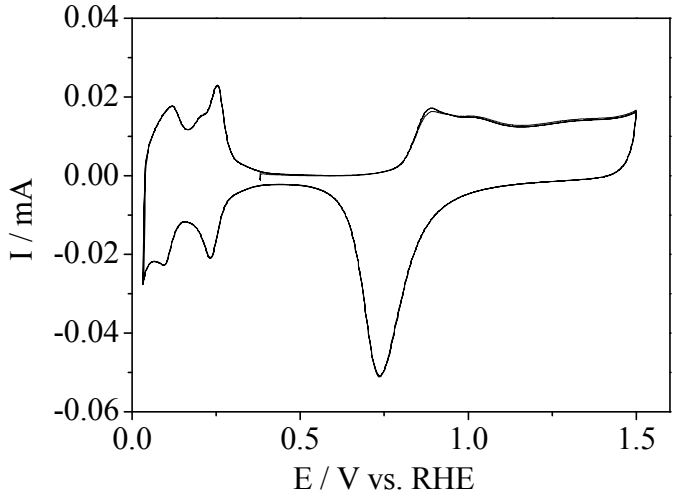

Figure 2-1 Typical CV recorded in the DEMS cell for Pt(Poly) during the adsorption test in 0.5 M H_2SO_4. Sweep rate = 50 mVs^{-1}. Electrolyte flow rate = 5 μLs^{-1}.

Not only the cleanliness of the system has been checked by adsorption test but also, the active (real) surface area of the Pt(Poly) electrode and consequently its roughness factor can be calculated by under-potential deposition of hydrogen (H_{UPD}), assuming 210 $\mu C\ cm^{-2}$ for the total charge in the hydrogen adsorption region (0.05-0.35 V) after subtraction of the double layer charging current [1].

$$A_{real} = \frac{Q_H}{210 \mu C cm^{-2}}, \tag{2-1}$$

where, Q_H is the total charge of hydrogen desorbed from platinum surface.

Knowing the geometric surface area of Pt(Poly) electrode $A_{geom} = \pi r^2$, the roughness factor can be calculated as follows:

$$Roughness\ factor = \frac{A_{real}}{A_{geom}} \tag{2-2}$$

2.1.3 Single crystal electrodes

2.1.3.1 Chemical cleaning

Due to the impurities contained in the single crystal electrodes, chemical cleaning was necessary especially when the crystal is new. The crystal was first immersed in conc. HNO_3 then in a mixture of NH_3/H_2O_2 (1:1) each for 5 min followed by roughening and annealing (see below). This procedure repeated several times until the characteristic CV was obtained.

2.1.3.2 Roughening and annealing

The electrochemical cleaning of the single crystals was done by sweeping the potential from 0.05 to 1.5 V (roughening) in a normal H-cell containing the supporting electrolyte until the CV is stable (cf. Fig. 2-2).

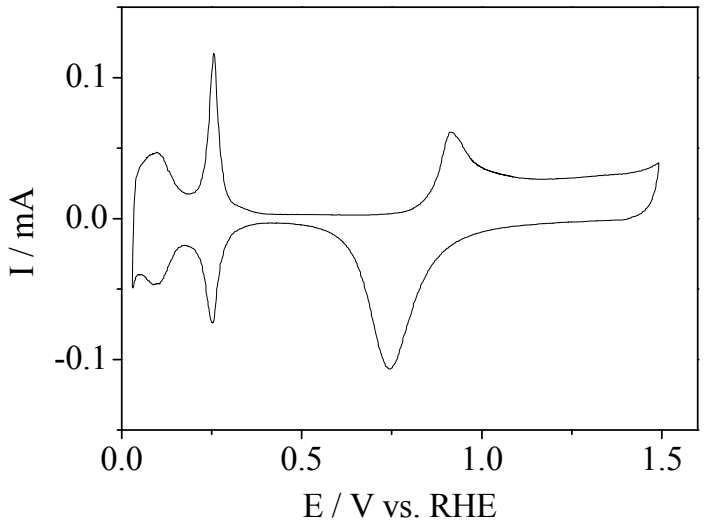

Figure 2-2 Typical CV recorded in the H-cell during roughening of Pt(311) in 0.5 M H_2SO_4. Sweep rate = 50 mVs^{-1}.

After roughening, the stepped single crystals were prepared according the method of Clavilier [2]: annealing was achieved by heating the crystal over a butane flame; after it turned to a faint red color, it was left over the flame for about 30 s and then transferred into the conventional H-cell, where it was allowed to cool down to room temperature over Millipore-Q water for about 4 min in an atmosphere of H_2/Ar mixture [3]. The crystal was then transferred with a droplet of water, to protect it from contamination, to another H-cell containing the supporting electrolyte where it kept in contact with the supporting electrolyte deaerated with highly pure argon (99.999 %) in a hanging meniscus configuration. The quality of the single crystal surface after preparation was checked by recording the CV in the potential range of 0.05 to 0.85 V. The potential should not exceed 0.9 V, because at higher potentials, roughening starts and the adsorbed oxygen destroys the single crystal structure and the arrangement of the Pt atoms at the surface. The crystal was then (or after deposition of Ru or Sn) transferred quickly to the DEMS cell while being protected by a droplet of electrolyte. Before DEMS measurement, the cleanliness of the electrode and the integrity of the single crystal structure was checked by recording the CV between 0.05 - 0.85 V in the DEMS cell (cf. Fig. 2-3). In general, the CVs in both cells showed almost similar features, this fact demonstrates the quality of the transfer and the cleanliness of DEMS cell. The small

difference in the shape of the CVs in both cells is partially due to electrolyte flow and transport of evolved hydrogen away from the electrode surface [4] but mainly due to high iR drop in the DEMS cell with a high electrolyte resistance [5, 6].

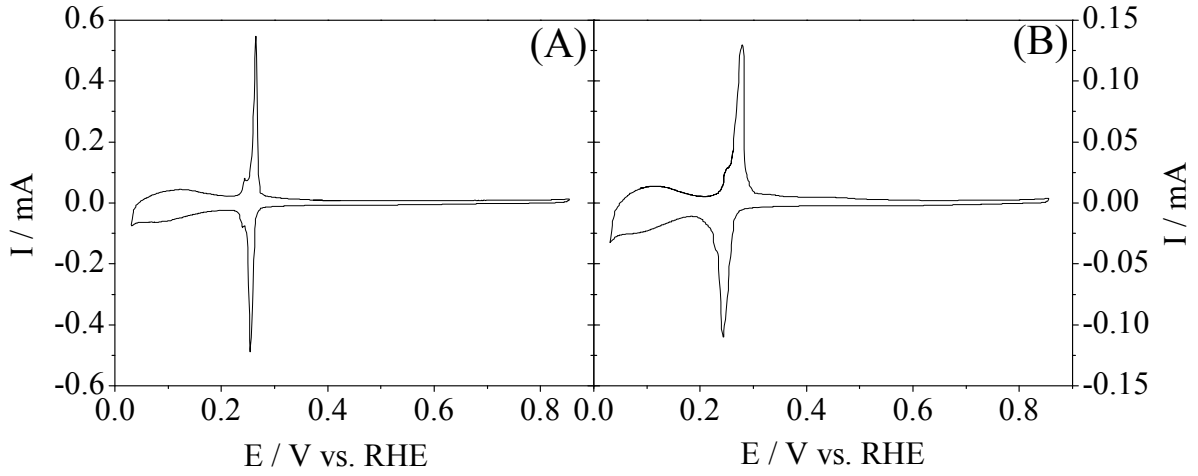

Figure 2-3 Typical characteristic CV for Pt(311) in 0.5 M H_2SO_4 at 50 mVs^{-1} (A) in H-cell, (B) in the dual thin layer flow through cell (DEMS cell).

2.1.4 Reversible hydrogen electrode (RHE)

A reversible hydrogen electrode (RHE) [7] as shown in Fig. 2-4 was used as a reference electrode in this thesis. For its preparation, the electrode was first rinsed with Millipore-Q water and the supporting electrolyte (0.5 M H_2SO_4) was removed and then filled again simply by using water suction pump. Afterwards, another Pt wire was dipped into the supporting electrolyte and a potential difference of about 1.6 V was applied between the Pt wire (anode) and the RHE electrode (cathode). H_2 is generated by electrolysis at the cathode to partially fill the bulb. This process should be repeated at least three times to ensure the purity of the H_2. Finally, the bulb was half-filled with H_2 so that the Pt wire has contact with both H_2 gas and the electrolyte.

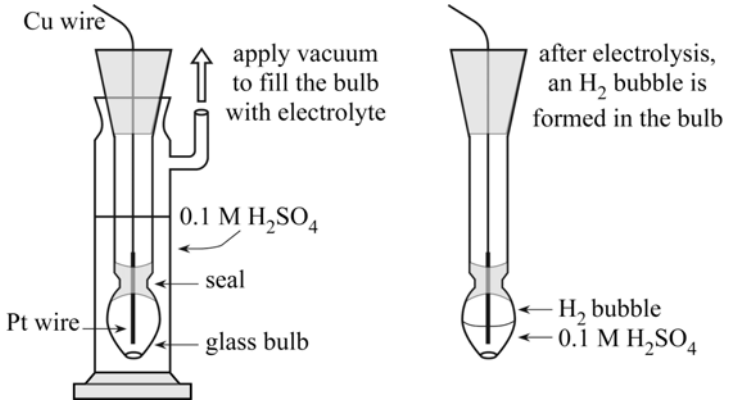

Figure 2-4 Construction of the reversible hydrogen electrode. Adopted from ref. [8].

2.2 Electrochemical techniques

2.2.1 Potentiodynamic technique

Potentiodynamic alcohol oxidation presented in this thesis was done according to the potential program shown in Fig. 2-5 as follows: first the potential was held at 0.05 V (the potential at which alcohol do not yet adsorb [9, 10]) in the supporting electrolyte, which was then exchanged by a supporting electrolyte containing alcohol. Afterwards, the potential was swept in the anodic direction at 10 mVs^{-1} for three cycles. In case of Ru and Sn-free platinum single crystal electrodes, three cycles were recorded with an upper potential limit of 0.85 V followed by potential stop for less than 1 min at 0.05 V; then, further sweeps were recorded with an upper potential limit of 1.5 V. In case of Ru or Sn modified single crystals, the upper potential limit was 0.8 V and 0.6 V respectively because the oxidation of these adatoms starts at higher potentials as will be shown in chapters 3 and 4.

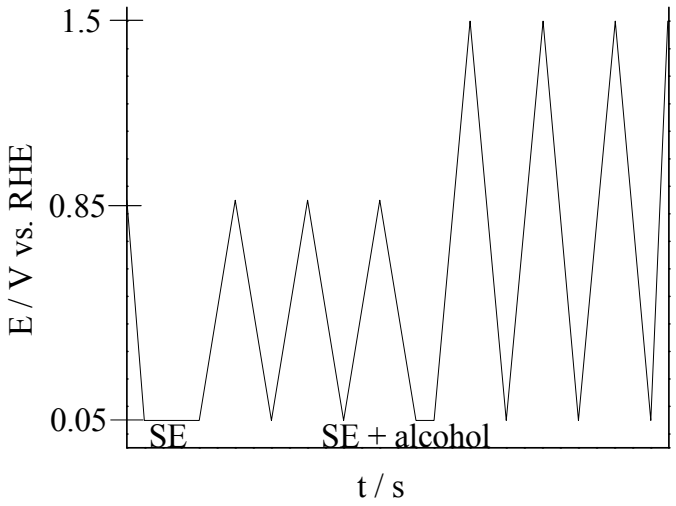

Figure 2-5 The potential program used in the potentiodynamic alcohol oxidation.

2.2.2 Potentiostatic technique

2.2.2.1 Potentiostatic alcohol oxidation

In another set of experiments, after exchanging the supporting electrolyte for the methanol solution at 0.05 V as shown above, the potential was stepped to various positive potentials to record the current transients during methanol potentiostatic oxidation (cf. chapters 3 and 4).

2.2.2.2 Formation and oxidation of alcohol adsorbate

For the formation of the alcohol adsorption product, the potential program shown in Fig. 2-6 was applied; the potential was first held at 0.05 V (E_0, the potential at which alcohol does not yet adsorb, cf. chapters 3 and 4) in the base electrolyte, which was then replaced by alcohol containing solution under potential control. Afterwards, the potential was stepped to more positive potential, E_{ads}, at which alcohol could adsorbs, for 2 min, t_2. Then, the potential was stepped back to 0.05 V, E_0. After replacing the alcohol containing solution with an alcohol free solution, which takes ca. 5 minutes, t_3, the potential was swept in the anodic direction; t_4 to oxidize the alcohol adsorbate (CO_{ads}) potentiodynamically or stepped to various positive potentials to oxidize it in a series of potentiostatic experiments.

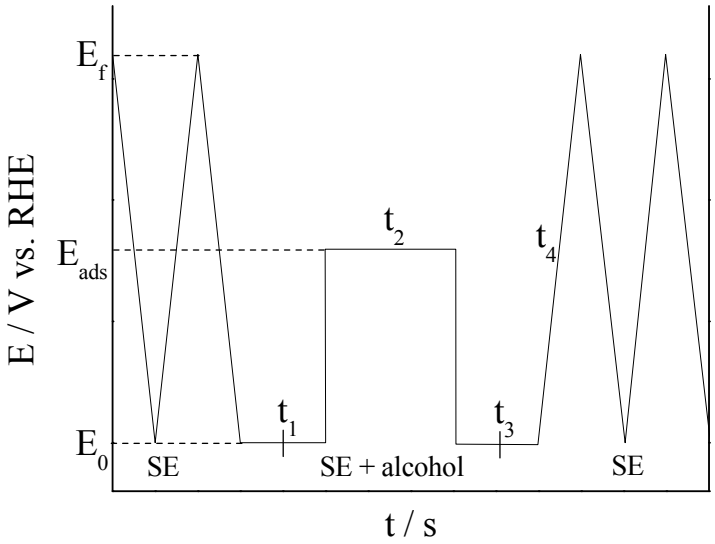

Figure 2-6 The potential program used in the formation and oxidation of alcohol adsorbate.

2.2.2.3 Potentiostatic CO oxidation

CO was adsorbed at a constant electrode potential of 0.06 V by replacing the supporting electrolyte (0.5 M H_2SO_4) solution with the same solution saturated with CO (ca. 10^{-3} M) which last for ca. 3 min. After the formation of a CO monolayer, the solution was exchanged for pure supporting electrolyte under potential control (E = 0.06 V) to maintain the CO free solution. The adsorbed CO was then either oxidized in a series of potential step experiments in which the potential was stepped from 0.06 V to higher oxidation potentials or by sweeping the potential to more positive values (shown later).

2.2.3 Deposition of Ru or Sn sub-monolayer at platinum stepped single crystals

2.2.3.1 Electrochemical deposition of Ru

A solution of 0.02 M $RuCl_3$ + 0.5 M H_2SO_4 was prepared as a stock solution. By dilution, a solution of 5 mM $RuCl_3$ + 0.5 M H_2SO_4 is freshly prepared before each deposition experiment. In the H-cell, after preparation of the single crystal electrode, it was transferred to another cell containing the above deposition solution. After ensuring potential control at 0.35 V, the electrode was kept in contact with the electrolyte in a hanging meniscus configuration at 0.4 or 0.6 V for 5 min. The amount of Ru deposited on the surface depends on the applied potential according to ref. [11] as shown in Fig. 2-7.

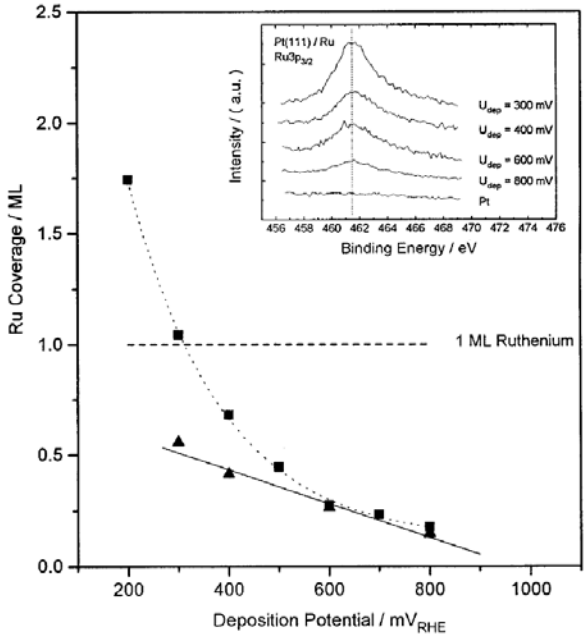

Figure 2-7 Ru coverage determined by XPS as a function of deposition potential for Pt(Poly) (*squares*) and Pt(111) (*triangles*). The inset shows the XPS spectra (Ru $3p_{3/2}$ emission) of Ru-modified Pt(111) at various deposition potentials. The dotted line in the insert indicates the value of 461.4 eV. Adopted from ref. [11].

The Ru coverage at platinum stepped single crystals with (111) steps and (111) terraces can be calculated as follows:

$$\theta_{Ru}^{step} = \frac{Q_s^H - Q_s^{Ru}}{Q_s^H} \tag{2-3}$$

$$\theta_{Ru}^{s+T} = \frac{Q_s^H - Q_s^{Ru}}{Q_{s+T}^H} \tag{2-4}$$

Here, θ_{Ru}^{step} is the Ru coverage at Pt step sites, $\theta_{\mathrm{Ru}}^{\mathrm{s+T}}$ is the Ru coverage at Pt (steps + terraces), only as long as the steps are decorated, Q_s^H is the charge of hydrogen desorbed from free Pt step sites, Q_{s+T}^H is the charge of hydrogen desorbed from free Pt step and terrace sites and Q_s^{Ru} is the charge of hydrogen desorbed from Ru deposited at Pt step sites.

2.2.3.2 Diffusion controlled deposition of Sn

Diffusion controlled deposition of Sn at platinum stepped single crystals was done as follows: after preparation of the single crystal electrode, it was transferred to another cell containing freshly prepared 2×10^{-5} M $SnSO_4$ + 0.5 M H_2SO_4 (to avoid the autocatalytic oxidation of Sn^{+2} to Sn^{+4} by dissolved oxygen [12]). The potential is controlled at 0.35 V and then cycled in the range of 0.05 – 0.6 V vs. RHE. Under such conditions, the deposition of Sn is a slow, mass transfer-controlled process. The surface concentration of the adatom increases progressively with time; from the shape of the voltammertric profile, we can monitor the increase of the surface coverage.

By the help of a CO oxidation experiment at the Sn modified platinum electrode (cf. chapter 4, part 4.2.2.1), assuming that CO only adsorbs at the free Pt sites, the relative Sn coverage is given by:

$$\theta_{Sn} = 1 - \theta_{CO} \tag{2-5}$$

Coverage of adsorbed CO formed either from CO saturated electrolyte or from alcohol was calculated from the amount of CO_2 formed during the oxidation in the supporting electrolyte:

$$\vartheta_{\mathrm{CO}} = \Gamma_{\mathrm{CO}} / \Gamma_{\mathrm{H}} \tag{2-6}$$

Then θ_{CO} is given by:

$$\theta_{CO} = \frac{\vartheta_{CO}}{\vartheta_{CO}^{max}} = \frac{\Gamma_{CO}/\Gamma_H}{\vartheta_{CO}^{max}}, \tag{2-7}$$

where, θ_{CO} is the CO coverage compared to ϑ_{CO}^{max} which is the maximum CO coverage obtained from CO saturated solution (0.5 M H_2SO_4) at clean Pt electrode ≈ 0.6, Γ_{CO} is the surface concentration in mol cm^{-2} of adsorbed CO, Γ_{H} represents the number of active sites per surface area as determined from the charge of adsorbed hydrogen in the characteristic CV in the supporting electrolyte.

The relative Sn coverage at the surface can be also obtained simply by comparing the charge of the hydrogen adsorption before and after Sn deposition at the platinum surface [13-15].

$$\theta_{Sn} = \frac{Q_o^H - Q_{Sn}^H}{Q_o^H}, \tag{2-8}$$

where, Q_o^H is the total charge of hydrogen desorbed from platinum surface and Q_{Sn}^H is the total charge of hydrogen desorbed from Sn-modified platinum surface.

2.3 Electrochemical instrumentation

2.3.1 Data collection

2.3.1.1 In DEMS measurements

Computers with integrated A/D converter boards were used for data collection. For detection of the Faradaic current, a computer operated under DOS system was used with Potmadash software developed in our group. For detection of the ion current during mass spectrometric measurements, a computer operated under WIN98 system was used with a Quadstar™ 422-software (Pfeiffer-Vacuum GmbH), which makes it possible to detect the ion current for each m/z separately. A home-made potentiostat, function and potential step generators were used for recording the data.

2.3.1.2 In AC and EIS measurements

A computer operated under WIN2000 system with a measuring board, data acquisition card and LabView software from National Instruments® was used. A potentiostat, model 273 A (EG&G, Princeton Applied Research) is employed for I-E measurements. A lock-in amplifier, type 5210 (EG&G), combined with the potentiostat, was used for the ac voltammetry measurements to generate the ac voltage and to record the phase sensitive ac signal. In EIS measurements, Solartron SI 1260 Impedance/Gain-Phase analyzer was used for recording impedance spectrum and zPlot-zView® software from Scribner Associates was used for the evaluation of the impedance spectrum and for data fitting. Origin 7.0 software (OriginLab®) and Excel 2010 (Microsoft®) were used for data evaluation.

2.3.2 Electrochemical cells

2.3.2.1 The conventional electrochemical H-cell

In a normal voltammetry experiment, e.g. preparation of the single crystals, and deposition of metals, the conventional three electrode cell (H-cell) was used (cf. Fig. 2-8). In this cell the reference electrode, immersed in the supporting electrolyte, is connected to the cell body with a Luggin capillary while separated to some extent with a grounded glass stopcock so that electroactive species such as metal ions cannot diffuse to the reference electrode compartment. On the cell body, there are several ports serving as a gas inlet, gas outlet and solution inlet. The working electrode was kept in contact with the electrolyte in a hanging meniscus configuration. A platinum sheet immersed in the supporting electrolyte served as the counter electrode, which is separated by a fritted glass disk from the main part of the cell.

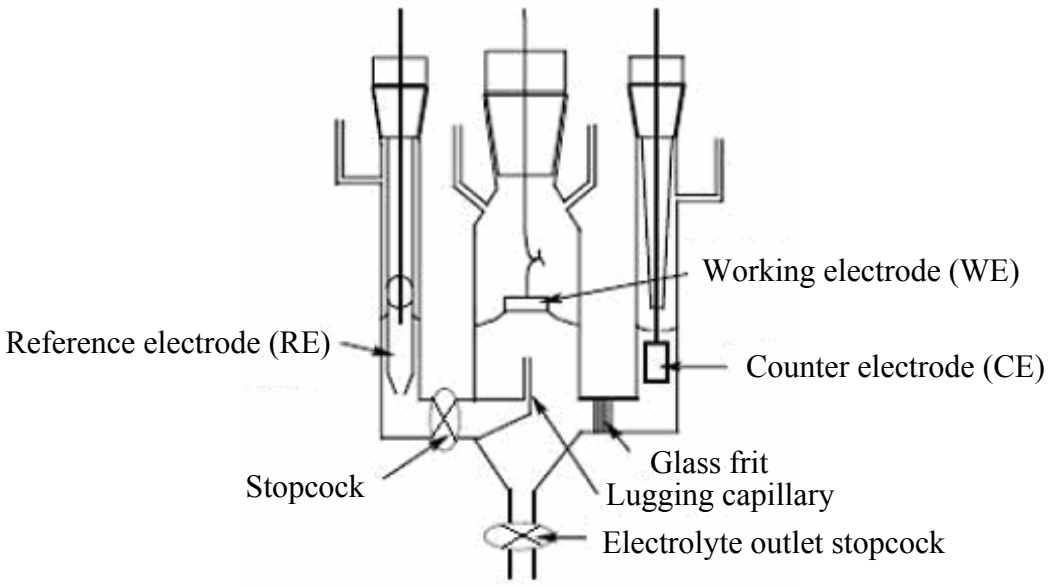

Figure 2-8 The conventional electrochemical H-cell. Adopted from ref. [4].

2.3.2.2 The dual thin layer flow through cell

For all of the Faradaic reactions which have to be performed under a continuous flow of the electrolyte, the dual thin layer flow through cell has been used. The construction of the cell is shown in Fig. 2-9 and described also in ref. [5]: The electrolyte first flows through a thin layer compartment (electrochemistry compartment) containing the working electrode placed directly on a four Teflon ring spacer (Gore-Tex®) with a thickness of ca. 50 μm, mean pore size of 0.02 μm, inner diameter of 6 mm a porosity of 50 % which leaves an electrolyte layer thickness of 200 μm. Through six capillaries, each one has a diameter of ca. 0.5 mm, the

electrolyte then flows to the second thin layer (detection compartment). In this compartment, a porous Teflon membrane from the same company was supported on a stainless steel frit and served as the interface between the electrolyte and the vacuum.

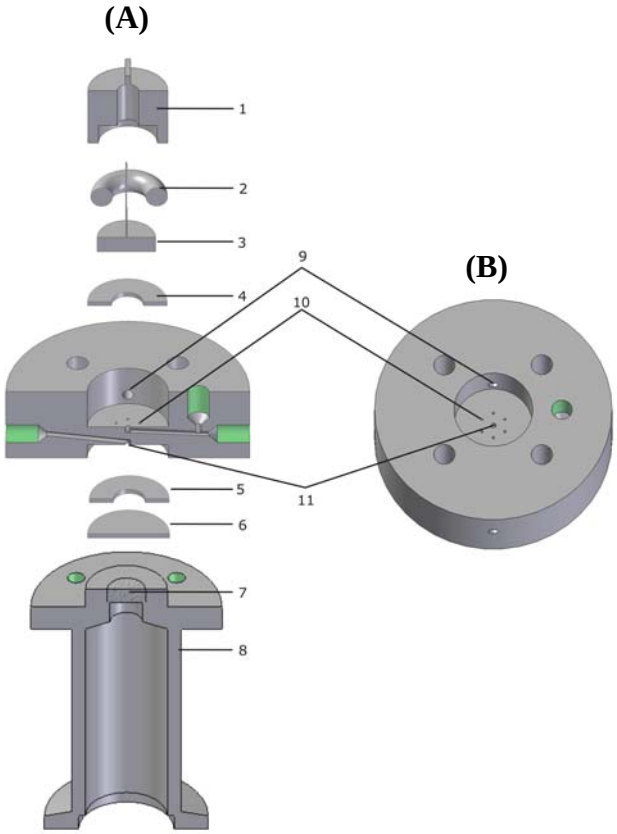

Figure 2-9 Sketch for the dual thin-layer flow through cell (Kel F) (1) Kel-F support; (2) Kalrez; (3) disc working electrode; (4), (5) Teflon gasket; (6) porous Teflon membrane; (7) stainless steel frit; (8) stainless steel connection to MS; (9) capillaries for flushing with Ar; (10) inlet-outlet capillaries; (11) connecting capillaries. (A) Side view of Kel-F body of the cell, (B) Top view of the cell.

Under continuous flow of the electrolyte, products were transported from the working electrode surface to the mass spectrometer by convection. Only the volatile ones can evaporate through the porous Teflon membrane into the vacuum system of the mass spectrometer. Different flow rates of the electrolyte were adjusted by a peristaltic pump at outlet of the cell. The reference electrode was a reversible hydrogen electrode (RHE) connected to the electrolyte inlet. Two Pt wires were used as counter electrodes with different applied resistances (100 kΩ and 1100 Ω) in the inlet and outlet respectively to optimize the current distribution and decrease the ohmic resistance. This cell was fixed over a metal holder and only the electrochemistry compartment was used in case of ac voltammetry and EIS

measurements or connected to the differential electrochemical mass spectrometry (DEMS) through a valve as will be shown in the next section and the two compartments were used.

2.3.3 DEMS setup and calibration

2.3.3.1 DEMS setup

The dual thin layer flow through cell was connected to the quadruple mass spectrometer (Balzer QMG-422) via a valve at position 1 as shown in Fig. 2-10. The produced volatile species during the electrochemical reaction will evaporate through the hydrophobic porous Teflon membrane to the mass spectrometer where the m/z ratio of different species can be known.

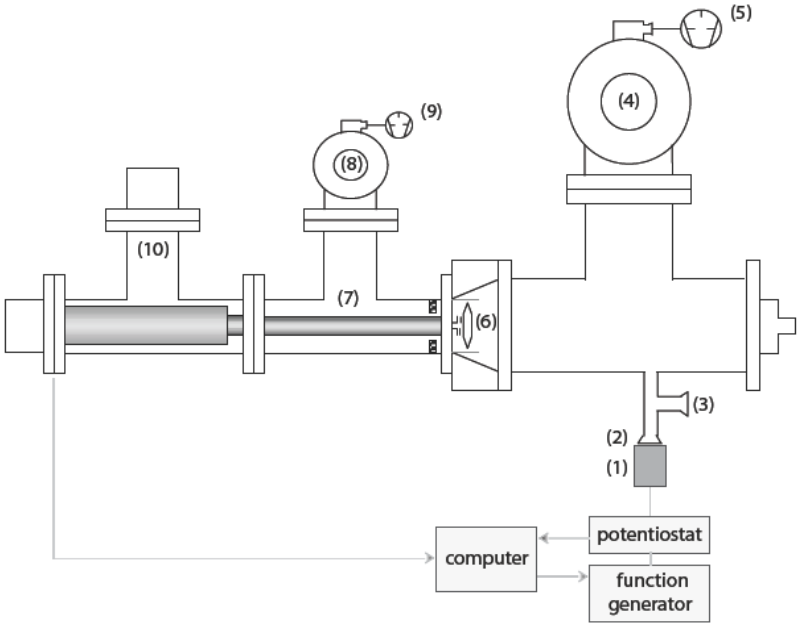

Figure 2-10 Schematic representation of a typical experimental DEMS setup; (1) electrochemical cell, (2) MS connection to the electrochemical cell, (3) connection to the calibration leak, (4) turbomolecular pump, (5) rotary pump, (6) ion source, (7) quadruple rods, (8) turbomolecular pump, (9) rotary pump, (10) secondary electron multiplier. Adopted from refs. [4, 5].

2.3.3.2 Calibration of DEMS by the oxidation of pre-adsorbed CO

Using a known electrochemical reaction with a current efficiency of 100 %, e.g. the oxidation of pre-adsorbed CO to CO_2 at Pt(Poly) surface [16], DEMS can be calibrated. Under flow conditions, simply after ensuring the cleanliness of the platinum surface by cycling the potential from 0.05 to 1.5 V in the dual thin layer cell at a sweep rate 50 mVs^{-1},

the potential range was kept constant at 0.06 V and about 2 ml of CO saturated supporting electrolyte (≈ 10^{-3} M) was injected into the cell from inlet to form a monolayer of CO at the Pt surface. Afterwards, a fresh electrolyte is introduced to the cell to remove the excess (bulk) CO and the potential was swept in the anodic direction at a sweep rate = 10 mVs^{-1}. As shown in Fig. 2-11, the hydrogen desorption peaks disappeared in the first cycle where the surface was blocked with adsorbed CO molecules. The onset of CO oxidation starts at about 0.4 V and the current efficiency was about 80 % after background subtraction. The total Faradaic charge was corrected by a factor of 0.8 corresponding to 20 % of non- Faradaic remaining charges (assigned to adsorption of anions like sulfate, bisulfate, hydroxides…etc) at the Pt surface [17-19].

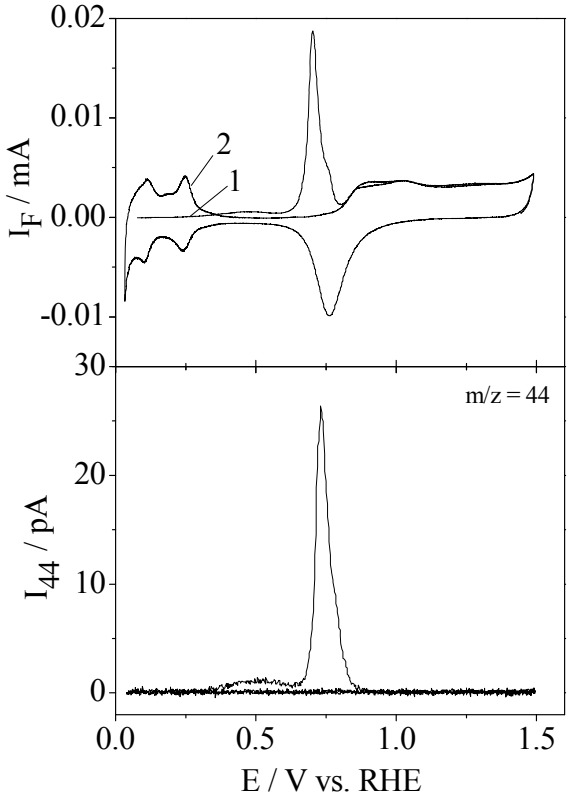

Figure 2-11 The Faradaic current (I_F) and the mass spectrometric ionic current (I_{44}) recorded simultaneously during the electrooxidation of pre-adsorbed CO at smooth Pt(Poly) electrode in 0.5 M H_2SO_4 at sweep rate of 10 mVs^{-1} and electrolyte flow rate of 5 μLs^{-1}. Number 1 and 2 indicate the first and second cycles respectively.

Both faradaic charges (Q_f^{total}) and ionic charge for the formation of m/z = 44 (Q_i^{44}) were used to calculate the calibration constant (K^*) according to the following equation:

$$K^* = \frac{zQ_i^{44}}{0.8Q_f^{total}} \tag{2-8}$$

Here, z is the number of electron transferred during the oxidation of one CO molecule to CO_2 = 2 electrons.

2.3.3.3 Approximate calibration for acetaldehyde, acetone and methylformate

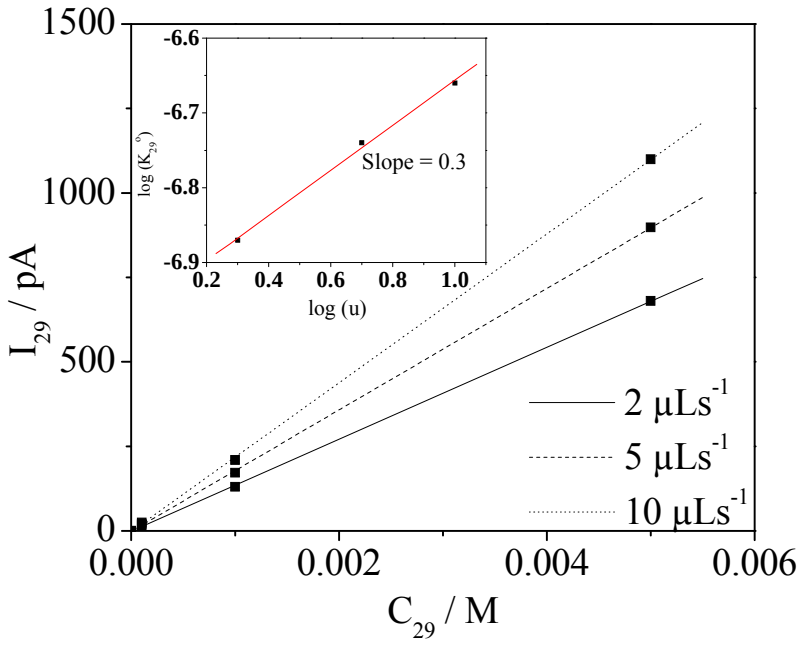

Figure 2-12 The linear relationship between the concentration of acetaldehyde (C_{29}) and the ionic current (I_{29}) recorded at different electrolyte flow rate. Inset: the flow rate dependence on acetaldehyde calibration constant (K_{29}^o).

Calibration for acetaldehyde, acetone and methylformate was done as follows: different concentrations of them in the range of 0.1-5 mM were prepared and the ionic signal of m/z = 29 (acetaldehyde), m/z = 58 (acetone) or m/z = 60 (methylformate) was monitored for each concentration at 2, 5 and 10 µLs^{-1}. As shown in Fig. 2-12, the slope of the linear relationship of the ionic current (I_x) vs. the concentration (C_x) gives the calibration constants for acetaldehyde (K_{29}^o) (or acetone (K_{58}^o) and methylformate (K_{60}^o)) times the flow rate dependent collection efficiency of the dual thin layer cell (f_2) and the electrolyte flow rate (u) [5]:

$$I_x = f_2 u K_x^o C_x \tag{2-9}$$

Here, K_x^o is defined from: $I_x = K_x^o \cdot \frac{dn}{dt}$ with $\frac{dn}{dt} = f_2 u C_x$ which is the incoming flow of the species x in mol s^{-1}. At very low flow rate (< 1 µLs^{-1}), the residence time will be long enough for the species to reach to the Teflon membrane and in this case, $K_x^o \propto u^1$ i.e. no diffusion

limitation. However, at higher flow rates, $K_x^o \propto u^{0.3}$ suggesting diffusion limitation to the Teflon membrane [5] (cf. inset in Fig. 2-12).

Following the above procedures, the actual current efficiencies will be only obtained at very low flow rate ($u < 1$ μLs^{-1}) i.e. in case of complete mixing of the species before entering the detection compartment. At high flow rates, however, the product concentration at the entrance in the vicinity of the Teflon membrane will be higher than the average. Since in the usual calibration experiment the concentration at the entrance of the detection compartment is homogeneous, this leads to apparent current efficiencies which are too high. A correction for that will be described in chapter 4.

References

[1] T. Biegler, D. A. J. Rand, and R. Woods, Journal of Electroanalytical Chemistry 29:269 (1971).
[2] J. Clavilier, D. Armand, S. G. Sun, and M. Petit, Journal of Electroanalytical Chemistry 205:267 (1986).
[3] J. Clavilier, K. Elachi, M. Petit, A. Rodes, and M. A. Zamakhchari, Journal of Electroanalytical Chemistry 295:333 (1990).
[4] Abd-El-Latif, Vol. PhD, in Mathematisch-Naturwissenschaftlichen Fakultät, Rheinischen Friedrich-Wilhelms-Universität Bonn, Bonn, 2011, p. 185.
[5] H. Baltruschat, Journal of the American Society for Mass Spectrometry 15:1693 (2004).
[6] E. Mostafa and H. Baltruschat, submitted to Journal of Electrochimica Acta.
[7] F. G. Will, Journal of the Electrochemical Society 133:454 (1986).
[8] F. Hernández, Vol. PhD, in Mathematisch-Naturwissenschaftlichen Fakultät, Rheinischen-Friedrich-Wilhelms-Universität Bonn, Bonn, 2006.
[9] E. Pastor, S. Gonzalez, and A. Arvia, Journal of Electroanalytical Chemistry 395:233 (1995).
[10] M. Krausa and W. Vielstich, Journal of Electroanalytical Chemistry 379:307 (1994).
[11] S. Cramm, K. A. Friedrich, K. P. Geyzers, U. Stimming, and R. Vogel, Fresenius Journal of Analytical Chemistry 358:189 (1997).
[12] Z. D. Wei, L. L. Li, Y. H. Luo, C. Yan, C. X. Sun, G. Z. Yin, and P. K. Shen, Journal of Physical Chemistry B 110:26055 (2006).
[13] H. Massong, S. Tillmann, T. Langkau, E. A. Abd El Meguid, and H. Baltruschat, Electrochimica Acta 44:1379 (1998).
[14] P. Berenz, S. Tillmann, H. Massong, and H. Baltruschat, Electrochimica Acta 43:3035 (1998).
[15] X. Xiao, S. Tillmann, and H. Baltruschat, Physical Chemistry Chemical Physics 4:4044 (2002).
[16] O. Wolter and J. Heitbaum, Ber. Bunsenges. Phys. Chem. 88:2 (1984).
[17] H. Baltruschat and U. Schmiemann, Ber. Bunsenges. Phys. Chem. 97:452 (1993).
[18] J. Willsau and J. Heitbaum, Electrochimica Acta 31:943 (1986).
[19] J. Clavilier, R. Albalat, R. Gómez, J. M. Orts, J. M. Feliu, and A. Aldaz, Journal of Electroanalytical Chemistry 330:489 (1992).

3. Electrocatalytic oxidation and adsorption rate of methanol

3.1 Introduction

The first part of this chapter includes the electrocatalytic oxidation of CO as well as methanol at Pt(331) stepped single crystal electrode in the dual thin layer flow through cell as studied by DEMS. The effect of flow rate, methanol concentration, potential and Ru step decoration on the obtained CO_2 and methylformate current efficiencies during the oxidation of methanol has been investigated.

Crucial for the use in fuel cells is the complete oxidation to CO_2 which can be achieved if the reactants first adsorb at the electrode surface along the reaction path with adsorbed CO as an intermediate. Therefore, in the second part of this chapter I determined the methanol adsorption rates at different Pt surfaces including smooth Pt(Poly), Pt(332), Pt(331), Ru step decorated Pt(331), Pt(100) and Pt(11,1,1) electrodes. The effects of different parameters such as methanol concentration, adsorption potentials, step density and Ru step decoration on the obtained values of adsorption rate have been examined. Finally, the oxidation of methanol adsorption product formed at smooth Pt(Poly), Ru/Pt(331), Pt(100) and Pt(11,1,1) at different adsorption potentials or times was investigated and the shape of the adsorbate oxidation was discussed.

3.2 Results and discussion

3.2.1 Electrooxidation of pre-adsorbed CO at Ru/Pt(331) single crystal electrodes

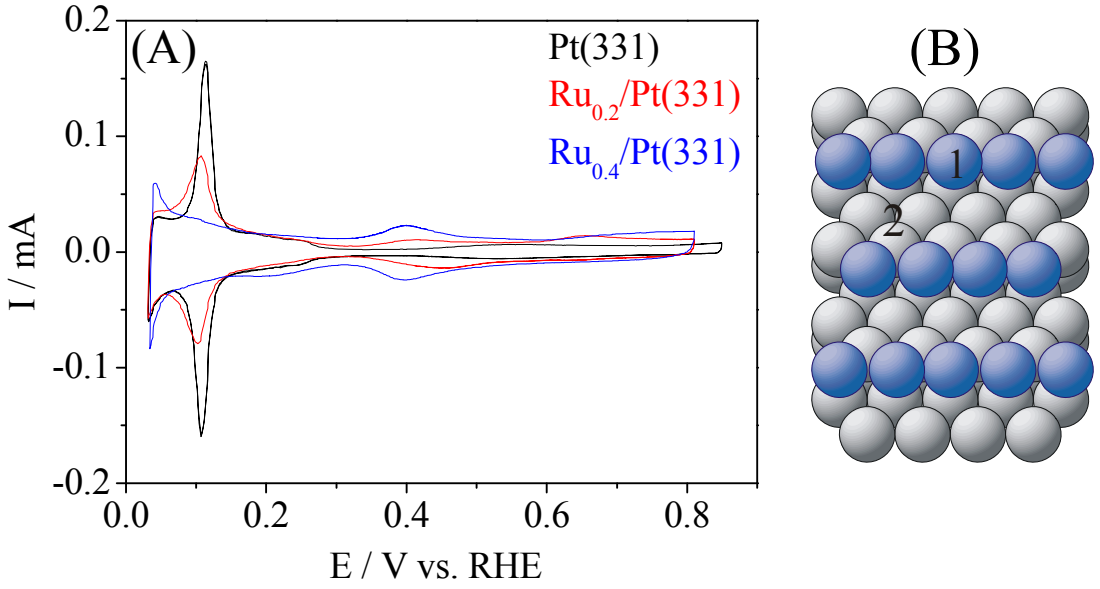

Figure 3-1 (A) CV of Pt(331) electrode before and after Ru deposition in 0.5 M H_2SO_4 solution. Scan rate: 50 mVs^{-1}. $Ru_{0.2}$/Pt(331): θ_{Ru} = *50 % of steps, 20 % of the step + terrace* and $Ru_{0.4}$/Pt(331): θ_{Ru} = *90 % of steps, 40 % of the step + terrace.* (B) Model for Ru step decoration at Pt(331) electrode adopted from ref. [1], the numbers imply step site (1) and terrace site (2).

Fig. 3-1 shows typical CV of Pt(331) in 0.5 M H_2SO_4 solution before and after deposition of Ru. For bare Pt(331), the sharp peak at 0.1 V is attributed to hydrogen adsorption/desorption at the (111) step sites, whereas the broad region between 0.05 and 0.35 V is due to hydrogen adsorption at terrace sites. The signal between 0.35 and 0.85 V is ascribed to anions (sulphate/bisulphate) adsorption at terrace sites [2, 3]. The high current in the double layer region (0.35-0.85 V) at Ru modified surface is due to OH adsorption at Ru atoms [4]. Ru deposition leads to partial or complete suppression of the Pt(331) step sites, whereas terrace sites remain not affected which imply step decoration in accordance with references [5-7].

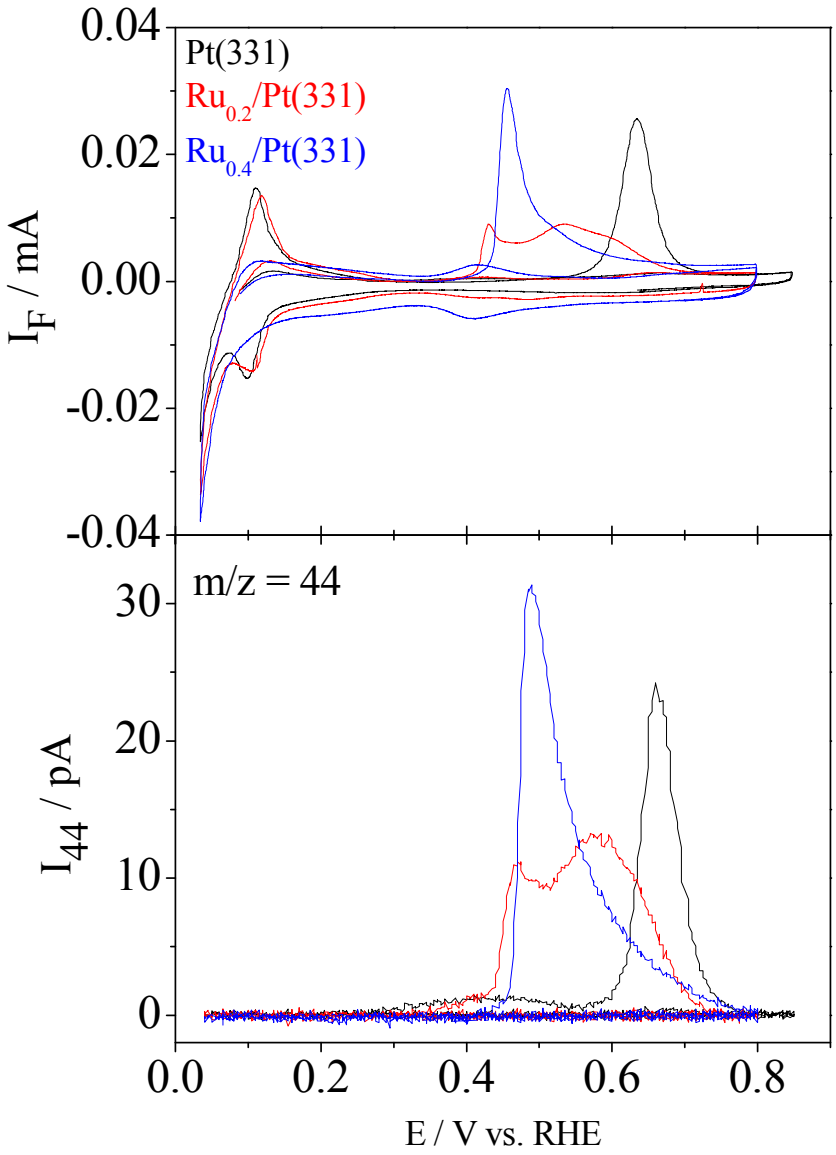

Figure 3-2 The Faradaic current (I_F) and the mass spectrometric ionic current (I_{44}) recorded simultaneously during the oxidation of pre-adsorbed CO at Pt(331) and Ru step decorated Pt(331) electrode with different Ru coverage in 0.5 M H_2SO_4 at 10 mVs^{-1} and 5 μLs^{-1}.

After preparation of the single crystals, they were then (or after deposition of Ru) transferred to the DEMS cell, in which they were cleaned by adsorption and subsequent oxidation of CO. The Faradaic current (I_F) and the mass spectrometric ionic current (I_{44}) recorded simultaneously during the oxidation of adsorbed CO at Ru free and Ru step decorated Pt(331) are shown in Fig. 3-2. At bare Pt(331), the pre-peak of CO_{ad} oxidation starts at 0.2 V whereas the main peak was located at 0.63 V. At $Ru_{0.2}$/Pt(331) (i.e. Ru half coverage of the step sites), the main peak was shifted to lower potential (0.43 V) with the appearance of a new peak (or shoulder) at 0.53 V. In this case, the main peak overlaps with the pre-peak. At $Ru_{0.4}$/Pt(331) (i.e. Ru complete coverage of the step sites), the main peak was also shifted to

0.46 V without a second peak at more positive potential. All of the above observations are in agreement with the previous literature for CO oxidation at free and Ru modified Pt(332), Pt(331) in a mixture of 0.1 M H_2SO_4 + 0.5 M $HClO_4$ [1], at Pt(665) and facetted Pt(332) in 0.5 M H_2SO_4 [6-8].

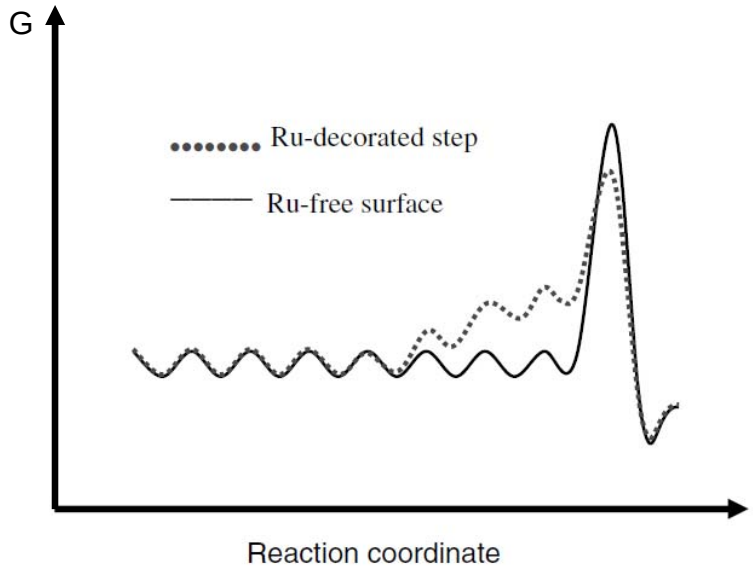

Figure 3-3 Influence of Ru step decoration on adsorption enthalpy of CO_{ad} with respect to the reaction coordinate. Adopted from ref. [9].

As explained before by Baltruschat and coworkers for Pt(665) and $Pt(332)_{fac}$, the presence of two different oxidation peaks for CO_{ad} is due to different adsorption enthalpies (cf. Fig. 3-3). Due to the electronic effect of Ru, the adsorption enthalpy for Pt atoms in the neighborhood of Ru is increased. This effect extends over at least four rows of atoms. In case of Pt(665), about 1/3 of terrace sites are not affected and the diffusion of CO from these sites to the step sites is slowed down by the higher adsorption enthalpy of these sites. Therefore, the oxidation peak at low potential is due to the oxidation of CO_{ad} molecules directly influenced by the electronic effect of Ru. The second peak at more positive potential is ascribed to the oxidation of CO adsorbed at a large distance to Ru and affected only by the bifunctional effect of Ru.

When the steps are almost completely covered by Ru (in case of $Ru_{0.4}$/Pt(331)), CO can adsorb only at Ru or close to Ru. All CO_{ad} are affected by the bifunctional and the electronic effects of the Ru atoms at the steps.

3.2.2 Electrooxidation of methanol at platinum single crystal electrodes

3.2.2.1 Potentiodynamic measurements at Ru/Pt(331)

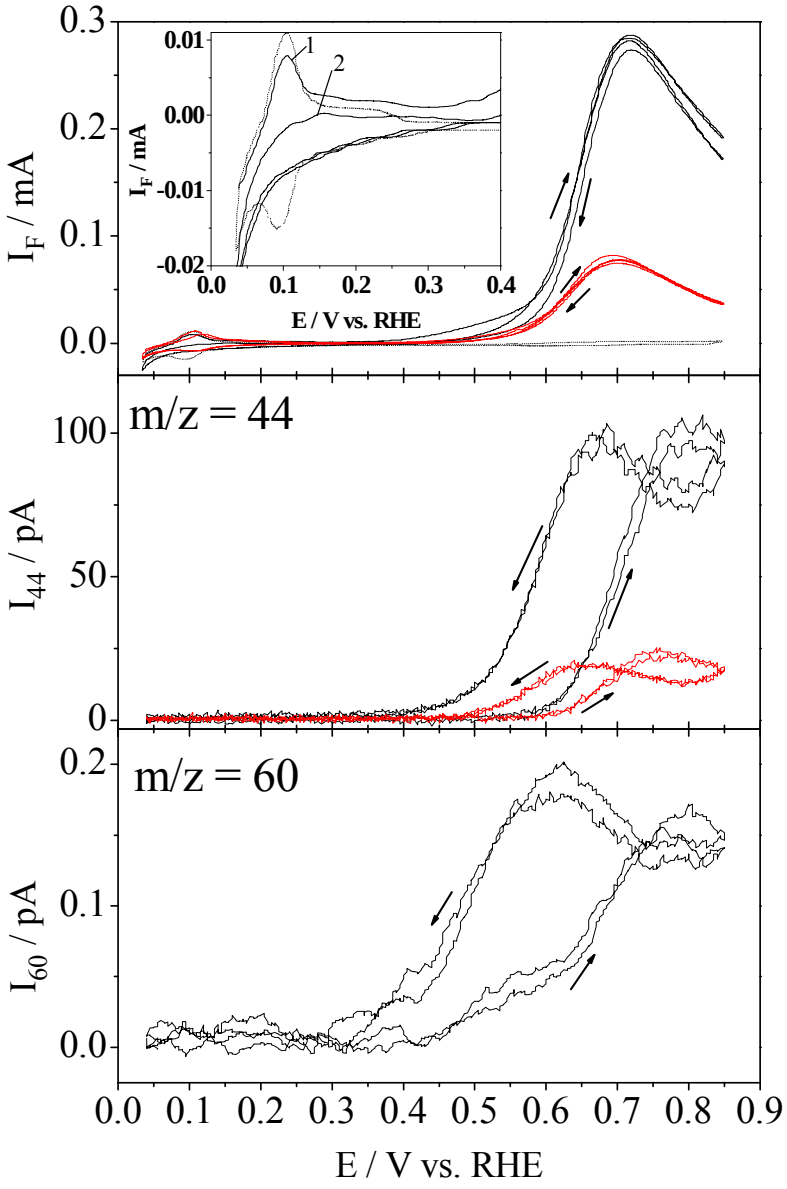

Figure 3-4 The Faradaic currents (I_F) and the mass spectrometric ionic currents for m/z = 44 (CO_2) and m/z = 60 ($HCOOCH_3$) recorded simultaneously during the potentiodynamic oxidation of methanol at smooth Pt(331) in 0.5 M H_2SO_4 solution + 0.1 M (black) and 0.01 M (red) methanol. Dotted line: CV in the supporting electrolyte. Scan rate: 10 mVs^{-1}. Electrolyte flow rate: 2 μLs^{-1}. Two cycles are shown. Inset: Expanded view of the Faradaic currents during the first and second anodic sweep in 0.1 M methanol. Arrows indicate the direction of sweep.

To investigate the effect of Ru step decoration on the oxidation of methanol at Pt(331) electrode, one should compare that to the behavior at bare surface. Therefore, the same reaction at bare Pt(331) will be first discussed. Fig. 3-4 shows the potentiodynamic oxidation of two different methanol concentrations (0.1 M and 0.01 M) in 0.5 M H_2SO_4 at Pt(331) electrode. The Faradaic currents (I_F) are recorded simultaneously with the mass spectrometric ionic currents for m/z = 44 (CO_2) and m/z = 60 ($HCOOCH_3$) in case of 0.1 M methanol or only m/z = 44 in case of 0.01 M methanol, where in the later the amount of methylformate was too low to be detected. The inset of Fig. 3-4 shows that the hydrogen desorption peaks are still visible in the first cycle where methanol is irreversibly adsorbed only at potentials above 0.1 V after replacing the supporting electrolyte by methanol containing solution giving rise to a shoulder around 0.5 V. Similar to Pt(Poly) [4, 10], this shoulder is not parallel by a signal for CO_2 (m/z = 44), but is due to the oxidative adsorption of methanol according to: ($CH_3OH \rightarrow CO_{ad} + 4H^+ + 4e^-$). Small hysteresis between the positive- and negative-going sweeps is due to small amount of CO_{ad} being formed at low potentials as suggested before [11]. In the positive going scan the oxidation starts at ca. 0.5 V, as indicated by the onset of CO_2 and methylformate formation. Afterwards, the Faradaic currents start to increase sharply during the anodic sweep leading to an oxidation peaks at 0.72 V and 0.7 V for 0.1 M and 0.01 M methanol respectively. Although the surface is free from CO, currents significantly decrease above 0.7 V mainly due to adsorption of water and anions [11-13]. During the negative going scan, an oxidation peak is observed at 0.7 V for both concentrations followed by a decrease in the current below 0.7 V; this might be due to decrease of surface activity with decreasing potential and/or strong accumulation of CO_{ad} at the surface at low potentials [11]. In case of 0.1 M methanol, the anodic and cathodic oxidation peaks for m/z = 44 located at 0.82 and 0.68 V respectively whereas those for 0.01 M methanol are at 0.76 and 0.65 V. This shift in the ionic peak potentials with respect to those of the Faradaic ones are due to the delay time in the dual thin layer flow through cell (ca. 5 seconds at 2 μLs^{-1}). Methylformate is detected at 0.1 M methanol at approximately the same ionic peak potentials as CO_2. Increasing methanol concentration leads to a significant increase in both Faradaic and ionic currents due to higher adsorption rate at higher concentration (shown later).

Three cycles with an upper potential limit of 1.5 V have been recorded simultaneously with the corresponding ionic currents during the oxidation of 0.1 M and 0.01 M methanol at Pt(331) electrode as shown in Fig. 3-5. The first cycle of this series starts with a smooth surface, while during the next ones, the surface is being roughened. Here, the hydrogen desorption peaks are still visible in the first cycle for both methanol concentrations similar to

smooth surface (cf. inset of Fig. 3-5). Similar results of the same reaction at Pt(Poly) were also reported by Wang et al. [14]. The onset of oxidation is about 0.5 V during the positive going scan followed by two anodic oxidation peaks; the first one is at 0.73 V or 0.7 V for 0.1 M and 0.01 M respectively and the second one is parallel to the oxygen region. During the negative going scan, an oxidation peak is observed at 0.66 V in both cases. Abd-El-Latif et al. [1] found the increase of both Faradaic and ionic currents after roughening by about 25 % when they performed the oxidation of 0.01 M methanol at Pt(331) using a mixture of 0.5 M $HClO_4$ + 0.1 M H_2SO_4 as a supporting electrolyte. In the present work, using 0.5 M H_2SO_4 as a supporting electrolyte on one hand, has the advantage of sharper peaks in the hydrogen region but on the other hand, high concentration of sulfate reduces the reactivity of the platinum surface due to its high adsorpitivity [4]. The later is the reason for non significant increase of the oxidation current after roughening observed here for both methanol concentrations.

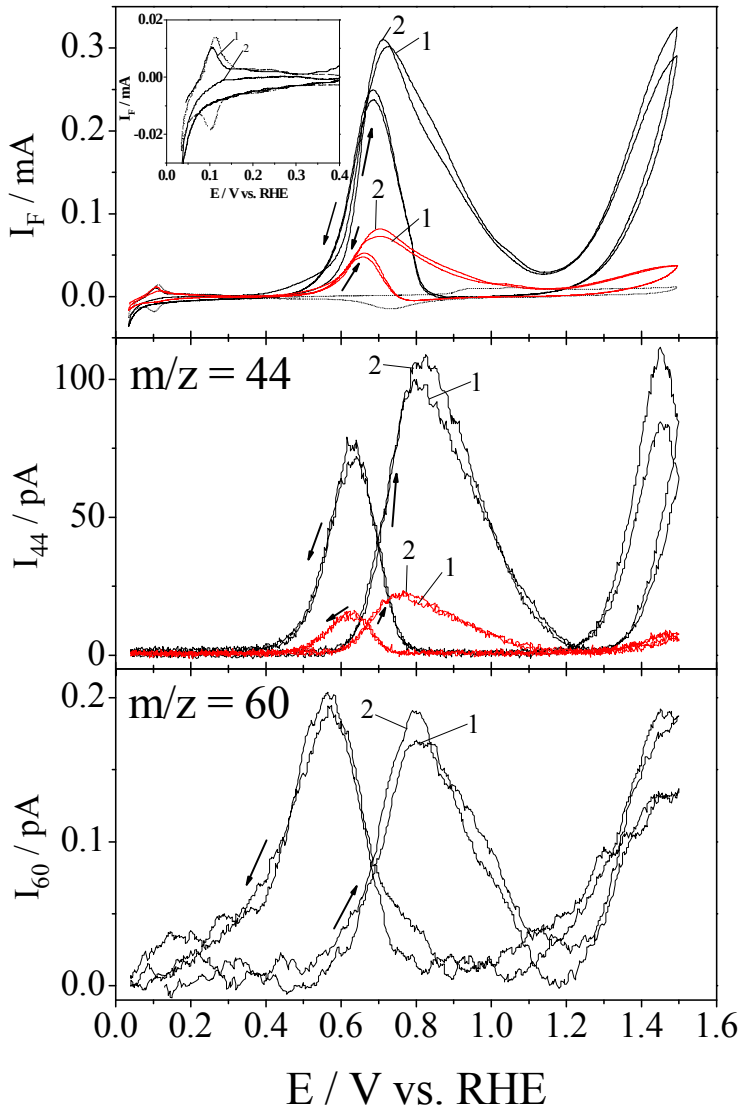

Figure 3-5 The Faradaic currents (I_F) and the mass spectrometric ionic currents for m/z = 44 (CO_2) and m/z = 60 ($HCOOCH_3$) recorded simultaneously during the potentiodynamic oxidation of methanol at roughened Pt(331) in 0.5 M H_2SO_4 solution + 0.1 M (black) and 0.01 M (red) methanol. Dotted line: CV in the supporting electrolyte. Scan rate: 10 mVs^{-1}. Electrolyte flow rate: 2 μLs^{-1}. Two cycles are shown. Inset: Expanded view of the Faradaic currents during the first and second anodic sweep in 0.1 M methanol. Arrows indicate the direction of sweep.

The Faradaic current (I_F) is the sum of the corresponding currents of many products: CO_2, formic acid, formaldehyde and methylformate. The CO_2 current efficiency (A_{44}) was calculated as follows:

$$A_{44} = \frac{6.I_{CO_2}}{K^*.I_F} \qquad (3\text{-}1)$$

Where, 6 is the number of electrons transferred during the oxidation of one methanol molecule, I_{CO_2} is the ionic signal of m/z = 44.

The apparent methylformate current efficiency, which differs from the true current efficiency, due to incomplete mixing in the dual thin layer cell, is given by:

$$A_{60}^{app} = \frac{I_F^{60}}{I_F} \tag{3-2}$$

Here,

$$I_F^{60} = \frac{I_{60} zF}{f_2 K_{60}^o} \tag{3-3}$$

This difference is smaller at low flow rates. Because of the low values of A_{60}, I did not perform any correction.

The current efficiencies with respect to CO_2 and methylformate for different methanol concentrations at three different flow rates calculated at the anodic peak potential are shown in Table 3-1. The current efficiency with respect to CO_2 is independent of the flow rate whereas with increasing flow rate the apparent current efficiency with respect to methylformate increases due to incomplete mixing in the dual thin layer flow through cell [15]. Low values of CO_2 current efficiencies indicate that a large amount of other products (HCHO and HCOOH) are formed in all conditions. With increasing methanol concentration, the current efficiency for CO_2 decreases [16]. As reported in ref. [16], the oxidation path via adsorbed CO is not much dependent on concentration but depends on the oxidation rate of CO_{ad} whereas the second reaction path via dissolved intermediate is largely depends on concentration; therefore, with increasing methanol concentration the second oxidation path becomes predominant. Under convection conditions, a large amount of intermediate is formed and then transported away from the electrode surface without reaction, this results in a low CO_2 current efficiency. After roughening, the current efficiencies for both CO_2 and methylformate were in the same range where the presence of defects promotes the oxidation of methanol via the two pathways simultaneously [17].

Table 3-1 Current efficiencies with respect to CO_2 and methylformate during the electrooxidation of 0.1 M and 0.01 M methanol at smooth (s) and roughened (r) Pt(331) surfaces.

u / μLs^{-1}	Cycle No.	0.1 M methanol				0.01 M methanol	
		A_{44} % (s)	A_{60} % (s)	A_{44} % (r)	A_{60} % (r)	A_{44} % (s)	A_{44} % (r)
2	1	22	0.15	22	0.17	30	31
	2	21	0.18	19	0.2	29	27
	3	21	0.16	19	0.14	22	27
5	1	20	0.34	22	0.35	35	34
	2	20	0.33	19	0.34	33	29
	3	19	0.31	18	0.29	34	29
10	1	18	0.45	18	0.44	34	35
	2	17	0.46	16	0.46	32	29
	3	17	0.48	16	0.31	32	29

Wang et al. [4] investigated the effect of surface structure during the oxidation of methanol at Pt(111) and Pt(332) electrodes in 0.5 M H_2SO_4 under flow through conditions. According to their measurements, although the Faradaic current increases with increasing step density, the current efficiency for CO_2 formation was approximately the same (ca. 25 %). This is now further proven when performing the oxidation at Pt(331) electrode. Again, though the Faradaic current is higher at Pt(331) as compared to Pt(332), the CO_2 current efficiencies are in the same range. This implies that the (110) steps catalyze the oxidation of methanol not only via adsorbed CO but also via HCHO and HCOOH as reported before [14, 16] and that the rate determining step is common for both paths.

The Faradaic currents as well as the ionic currents of m/z = 44 and m/z = 60 are recorded simultaneously during the oxidation of 0.1 M methanol + 0.5 M H_2SO_4 solution at Ru half or complete step decorated smooth Pt(331) together with the first and second extension of the sweep to 1.5 V as shown in Fig. 3-6 A and B respectively. The general characteristic of the CV and the mass spectrometric CV (MSCV) remain the same like bare Pt(331) as explained above. The catalytic activity towards methanol oxidation decreases with increasing Ru coverage at the steps implying that methanol is preferentially adsorbed and oxidized at the steps. Increase blocking of the steps with increasing Ru coverage leads to a decrease in the overall catalytic activity due to the lack of free Pt step sites. At least three adjacent platinum atoms are required for the decomposition of methanol to adsorbed CO on Pt(111) as reported by Cuesta et al. [18]. Step decoration with Ru leads to a shift of the onset

of oxidation by about 0.1 V to the negative direction in both smooth and roughened surfaces due to electronic and bifunctional effects [4].

As depicted in Fig. 3-6 B, slow dissolution of Ru up on extension of the sweep to more positive potential (roughening) leads to a shift in the onset of oxidation to less positive potential. Both the Faradaic and ionic currents increase in the second cycle compared to the first one (i.e. when the surface is still smooth). Not only the currents have increased after roughening but also the CO_2 current efficiency, this increase reaches its maximum in case of 40 % Ru coverage on the surface (cf. Table 3-2). This enhancement of the catalytic activity has been found before for PtRu/C [19] and Pt(Poly) [17] and it was attributed to the formation of platinum-rich surface by dissolving some Ru atoms.

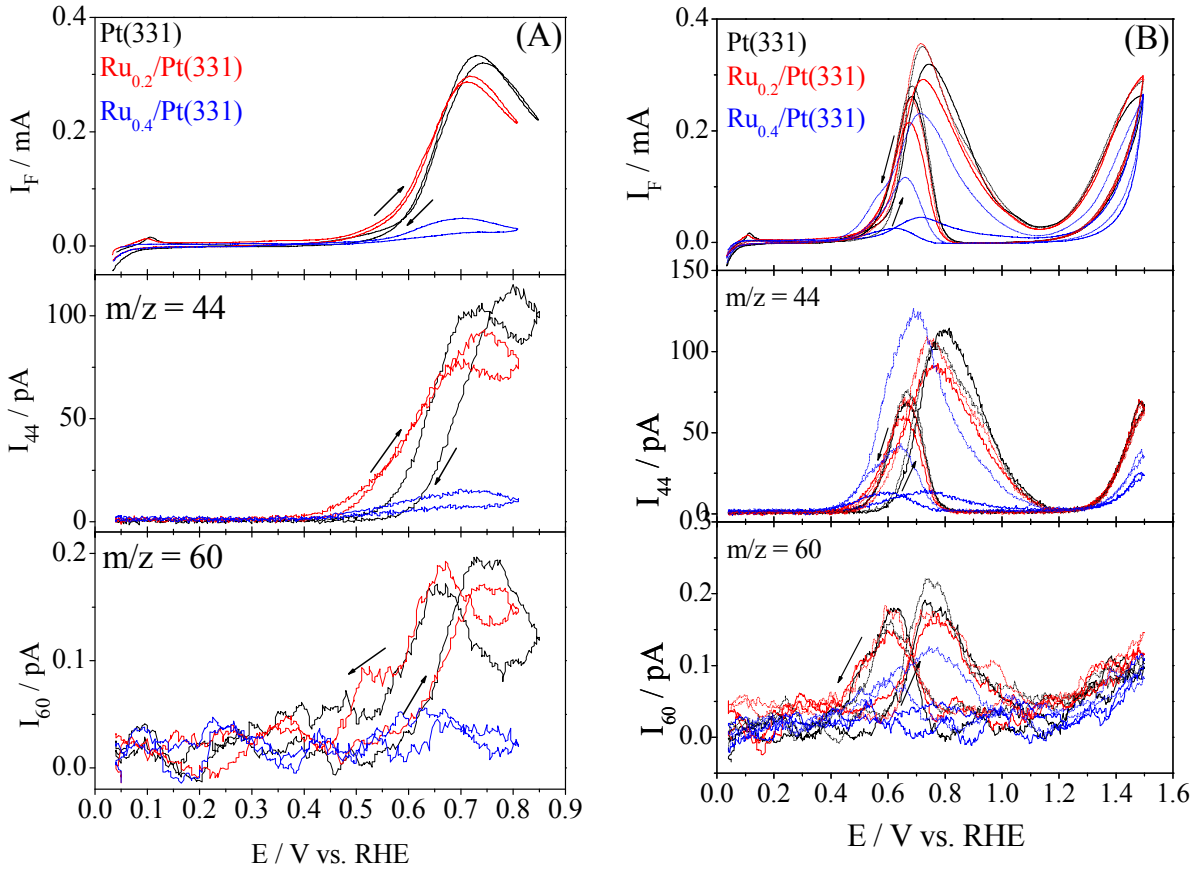

Figure 3-6 The Faradaic currents (I_F) and the ionic currents for m/z = 44 and m/z = 60 recorded simultaneously during the potentiodynamic oxidation of methanol at Ru modified smooth Pt(331) (A) (only the first cycle is shown) and roughened (B) (the first cycle and the second cycle "dotted line" are shown) in 0.1 M methanol + 0.5 M H_2SO_4 solution. The CV and MSCV recorded at bare Pt(331) are also shown for comparison. Scan rate: 10 mVs^{-1}. Electrolyte flow rate: 5 μLs^{-1}. Arrows indicate the direction of the sweep.

Table 3-2 Current efficiencies with respect to CO_2 and methylformate during the electrooxidation of 0.01 M and 0.1 M methanol at Ru step decorated smooth (s) and roughened (r) Pt(331) electrodes.

Surface		$Ru_{0.2}$/Pt(331)						$Ru_{0.4}$/Pt(331)					
u / μLs^{-1}	Cycle no.	0.1 M methanol				0.01 M methanol		0.1 M methanol				0.01 M methanol	
		A_{44} % (s)	A_{60} % (s)	A_{44} % (r)	A_{60} % (r)	A_{44} % (s)	A_{44} % (r)	A_{44} % (s)	A_{60} % (s)	A_{44} % (r)	A_{60} % (r)	A_{44} % (s)	A_{44} % (r)
2	1	18	0.15	19	0.16	27	29	16	0.26	15	0.27	23	24
	2	17	0.15	19	0.15	26	31	15	0.2	30	0.15	25	37
	3	17	0.14	17	0.15	26	25	15	0.21	23	0.14	25	28
5	1	16	0.3	16	0.3	25	25	13	0.53	14	0.55	21	20
	2	16	0.3	15	0.25	25	28	13	0.28	41	0.32	20	23
	3	16	0.3	15	0.25	25	23	12	0.3	30	0.26	20	16
10	1	15	0.46	16	0.45	27	27	13	0.91	13	1	20	19
	2	15	0.48	17	0.5	26	30	13	1	32	0.51	20	22
	3	14	0.4	16	0.37	26	22	12	0.52	27	0.36	19	15

The results of CO_2 and methylformate current efficiencies calculated at different flow rates for 0.1 M and 0.01 M methanol at the anodic oxidation peak for Pt(331)/$Ru_{0.2}$ and Pt(331)/$Ru_{0.4}$ are summarized in Table 3-2. As at bare Pt(331), the current efficiency with respect to CO_2 decreases with increasing methanol concentration whereas it is independent of the flow rate. Due to incomplete mixing in the dual thin layer cell, the apparent current efficiency with respect to methylformate increases with increasing flow rate of the electrolyte. With increasing Ru coverage at the step sites of Pt(331), CO_2 current efficiency decreases in agreement with literature [1]. The results in ref. [1] and also here are different from the results of Wang et al. at $Ru_{0.2}$/Pt(332) electrode [17]; there, even with complete Ru step decoration, the current efficiency for CO_2 increases from 25 % to 46 %. In case of $Ru_{0.2}$/Pt(331), ca. 4 free Pt rows are still available for methanol adsorption and oxidation. Here, however, Ru modified Pt(331) has a 1.5 atoms wide free terrace leading to much lower CO_2 current efficiencies because this atomic ensemble is not sufficient for methanol adsorption and oxidation [20, 21]. Therefore, here, the formation of soluble intermediates (HCHO and HCOOH) through the non-CO-pathway exceeds the CO pathway. Step decoration with Ru leads to faster adsorption (shown later) but no increase in the Faradaic current or CO_2 current efficiency at high potentials. In this case one could expect the change of the rate determining step from the

oxidative removal of CO_{ad} to the formation of CO_{ad} at the steps where there is no corresponding increase in the CO_{ad} oxidation current with increasing Ru coverage.

3.2.2.2 Potentiostatic measurements

To start the reaction at un-poisoned surface at constant potential, a series of potential step experiments were done first at bare Pt(331) and compared afterwards to the Ru modified Pt(331). To do so, after checking the cleanliness of the electrode by CV, the potential is stepped from 0.05 V (where the methanol containing solution is introduced to the cell) to different adsorption potentials from 0.5 to 0.8 V for 0.1 M and 0.01 M methanol as shown in Fig. 3-7 A and B respectively. The Faradaic current transients are recorded simultaneously with the ionic current transients in all cases. For both concentrations, at 0.5 and 0.6 V the current is constant after 10 s, whereas at higher potentials the current decreases over the whole oxidation period due to deactivation of the platinum surface caused by slow adsorption of OH or O at potentials higher than 0.7 V. A similar behavior has been observed before with smooth Pt(Poly) and platinum single crystal electrodes [4, 22-24].

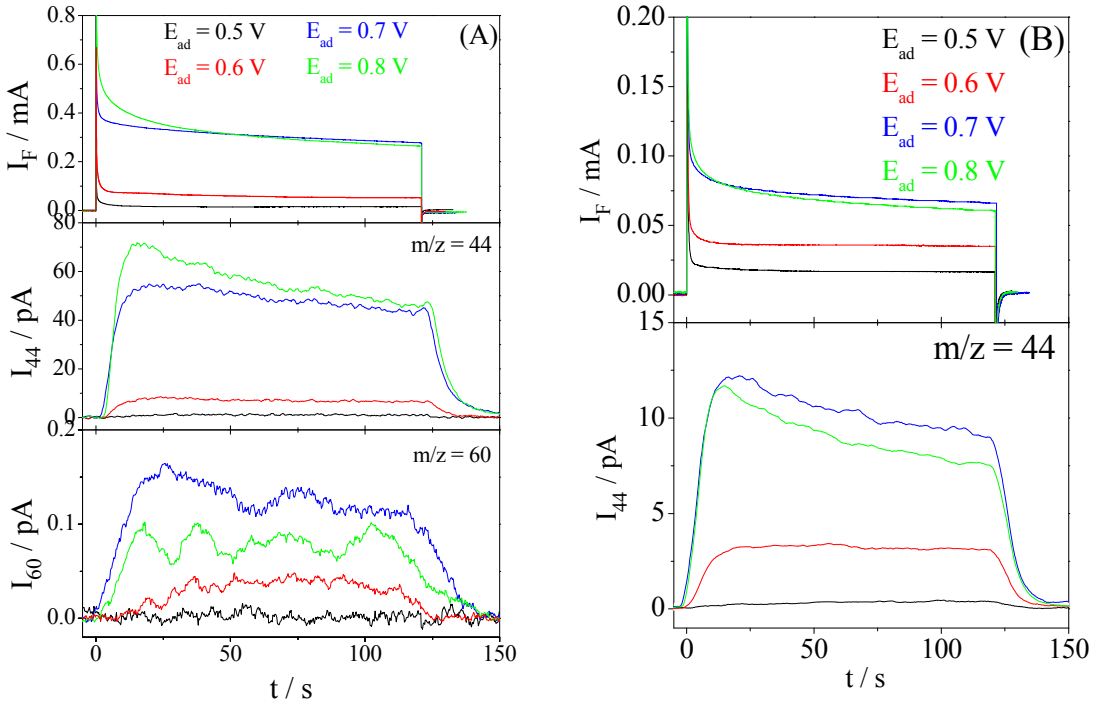

Figure 3-7 The Faradaic current transients (I_F) and the mass spectrometric ionic current transients for m/z = 44 and m/z = 60 recorded simultaneously during 2 min of methanol potentiostatic oxidation of methanol at smooth Pt(331) in 0.5 M H_2SO_4 solution + (A) 0.1 M and (B) 0.01 M methanol after the step of the potential from 0.05 V to different potentials.

Table 3-3 shows the current efficiencies with respect to both CO_2 and methylformate or only CO_2 during the potentiostatic oxidation of methanol at smooth Pt(331) for different step potentials, methanol concentration and flow rates. At 0.1 M methanol, the current efficiency with respect to CO_2 increases with increasing potential due to faster oxidation of methanol adsorbate (CO_{ad}). At 0.01 M methanol, however, the same behavior is observed only until 0.7 V and then CO_2 current efficiency decreases at 0.8 V.

With increasing methanol concentration, CO_2 current efficiency decreases in a good agreement with the results of the potentiodynamic experiments shown above. A similar behavior was observed before in case of Pt(Poly) electrode [16, 24]. ϑ_{CO} increases with increasing methanol concentration while it decreases in all cases with increasing adsorption potential due to the increased rate of adsorbate oxidation. ϑ_{CO} is independent of the flow rate; formation of CO from soluble intermediates is therefore negligible. If it was not, more CO adsorbate would be formed at lower flow rates due to longer residence times [24]. An adsorbate coverage of less than 2 % is calculated at 0.8 V for 0.01 M and of ca. 5 % for 0.1 M. Hence, lowering of concentration leads to lower adsorbate coverage and thus consequently lower methanol oxidation current transients and CO_2 current efficiencies observed at 0.8 V (cf. Fig. 3-7 B and Table 3-3).

The coverage of CO_{ad} as well as CO_2 current efficiency are not affected by increasing flow rate of the electrolyte, both confirms the parallel pathway mechanism. The apparent methylformate current efficiency increases with increasing convection due to incomplete mixing in the dual thin layer flow through cell [15] which corroborates with results of the potentiodynamic oxidation shown above. With increasing potential, CO_2 current efficiencies increase whereas that of methylformate decreases as reported before [16, 19, 23-25].

Table 3-3 Current efficiencies with respect to CO_2 and methylformate during the potentiostatic oxidation of methanol at Pt(331) together with the corresponding CO coverages at different applied potentials, methanol concentration and flow rates.

u / μLs^{-1}	E_{ad} / V vs. RHE	0.1 M Methanol			0.01 M Methanol	
		A_{44} %	A_{60} %	ϑ_{CO} %	A_{44} %	ϑ_{CO} %
2	0.5	7	0.45	17	10	15
	0.6	18	0.4	13	23	7
	0.7	23	0.21	6.5	27	2
	0.8	27	0.13	4.5	18	1.5
5	0.5	10	0.87	22	15	18.5
	0.6	16	0.45	15	20	6.5
	0.7	21	0.4	6	30	3
	0.8	26	0.34	3	17	1.7
10	0.5	13	2.3	21	20	11.5
	0.6	16	0.6	12.5	22	5
	0.7	19	0.55	4.5	28	1.3
	0.8	22	0.4	1.5	16	0.5

The effect of Ru step decoration was also studied during the potentiostatic oxidation of methanol at Ru half or completely step decorated Pt(331) electrode using two different methanol concentrations as shown in Fig. 3-8 (A-D). The Faradaic current and the ionic current transients of m/z = 44 and m/z = 60 (in case of 0.1 M methanol) or only m/z = 44 (in case of 0.01 M methanol) were also recorded simultaneously similar to bare Pt(331). At the Ru/Pt(331) surface an oxidation current transient is already detectable at 0.4 V, i.e. lower by 0.1 V than at the bare surface in accordance with the results of the potentiodynamic measurements. The lowering of the methanol oxidation current transients increases in the following order: $Ru_{0.4}$/Pt(331) > $Ru_{0.2}$/Pt(331) > Pt(331) and the reason for inhibition is that methanol is preferably adsorbed and oxidized at steps; hence, when blocking them by Ru, i.e., only one row of Pt in the terrace will be available, the oxidation current is largely inhibited due to absence of the contiguous adsorption sites.

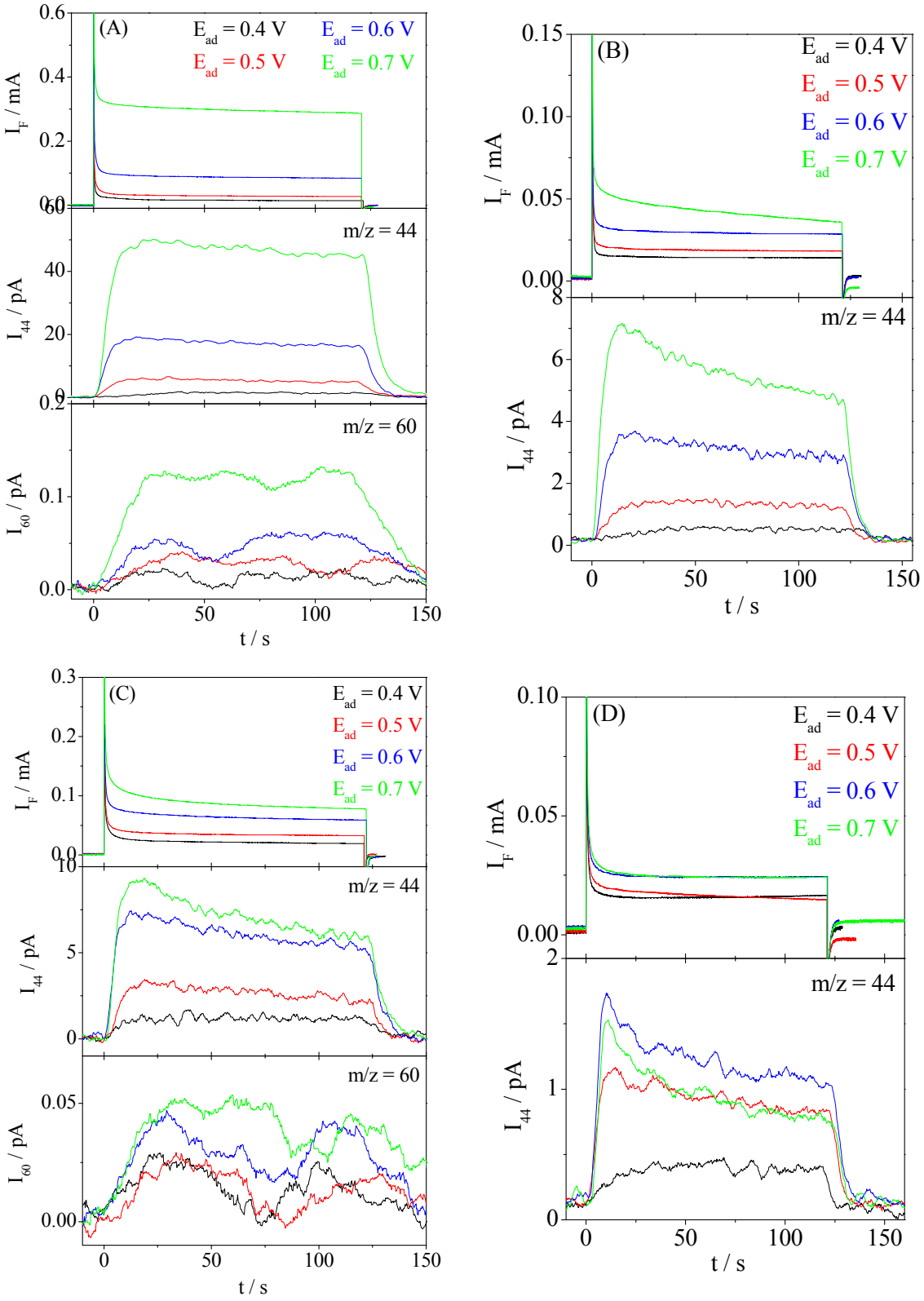

Figure 3-8 The Faradaic current transients (I_F) and the mass spectrometric ionic current transients for m/z = 44 and m/z = 60 recorded simultaneously during 2 min of potentiostatic oxidation of 0.1 M and 0.01 M methanol at $Ru_{0.2}$/Pt(331) (A, B) and $Ru_{0.4}$/Pt(331) (C, D) respectively after the step of the potential from 0.05 V to different potentials.

The current efficiencies for CO_2 and methylformate produced during the oxidation of methanol at Ru/Pt(331) electrode are also calculated and summarized in Table 3-4. At $Ru_{0.2}$/Pt(331) and $Ru_{0.4}$/Pt(331), the current efficiencies with respect to CO_2 are higher than bare Pt(331) at low potentials (< 0.7 V) and then decrease at 0.7 V. Ru promotes methanol oxidation at low potentials by the electronic effect (high methanol adsorption rate (shown later) and higher ϑ_{CO}, compare Tables 3-3 and 3-4). At high potentials, however, the co-catalytic activity decreases due to the transformation of an active Ru hydrous oxide to an inactive anhydrous oxide as reported before [4]. Complete blocking of the platinum step sites at high Ru coverage (40 %) shifts the oxidation reaction to the non-CO-pathway in agreement with the results of the potentiodynamic experiments shown above. This means that the free step sites are most important for methanol adsorption and oxidation and the decrease of the CO_{ad} coverage is accompanied by a decrease in the CO_2 current efficiencies and the formation of high amount of soluble intermediates.

Table 3-4 Current efficiencies with respect to CO_2 and methylformate during the potentiostatic oxidation of methanol at Ru step decorated Pt(331) together with the corresponding CO coverages at different applied potentials, methanol concentration and flow rates.

Surface		$Ru_{0.2}$/Pt(331)					$Ru_{0.4}$/Pt(331)				
u / μLs^{-1}	E_{ad} / V vs. RHE	0.1 M methanol			0.01 M methanol		0.1 M methanol			0.01 M methanol	
		A_{44} %	A_{60} %	ϑ_{CO} %	A_{44} %	ϑ_{CO} %	A_{44} %	A_{60} %	ϑ_{CO} %	A_{44} %	ϑ_{CO} %
2	0.4	13	0.63	31	20	25	10	0.53	20	15	14
	0.5	20	0.5	24	25	20	12	0.42	11	13	3.5
	0.6	25	0.4	14	30	8.5	15	0.36	5	20	2
	0.7	20	0.25	8	24	4	12	0.37	4	18	1
5	0.4	18	0.9	28	22	23	8.5	0.75	19	10	12.5
	0.5	25	0.8	22	30	10	19	1.24	10	15	3
	0.6	30	0.5	11	35	4	22	0.55	3.5	28	1
	0.7	22	0.3	5	30	1.2	13	0.78	2.5	20	0.7
10	0.4	13	1.4	24	18	18	8	2	15.6	12	13.5
	0.5	23	1.3	13	29	10.5	14	1.4	6	16	4
	0.6	27	1.2	7	33	3.5	18	0.93	2.5	22	3
	0.7	20	0.4	3	30	0.8	10	0.85	1.5	19	1.5

3.2.3 Methanol adsorption rate at platinum single crystal electrodes

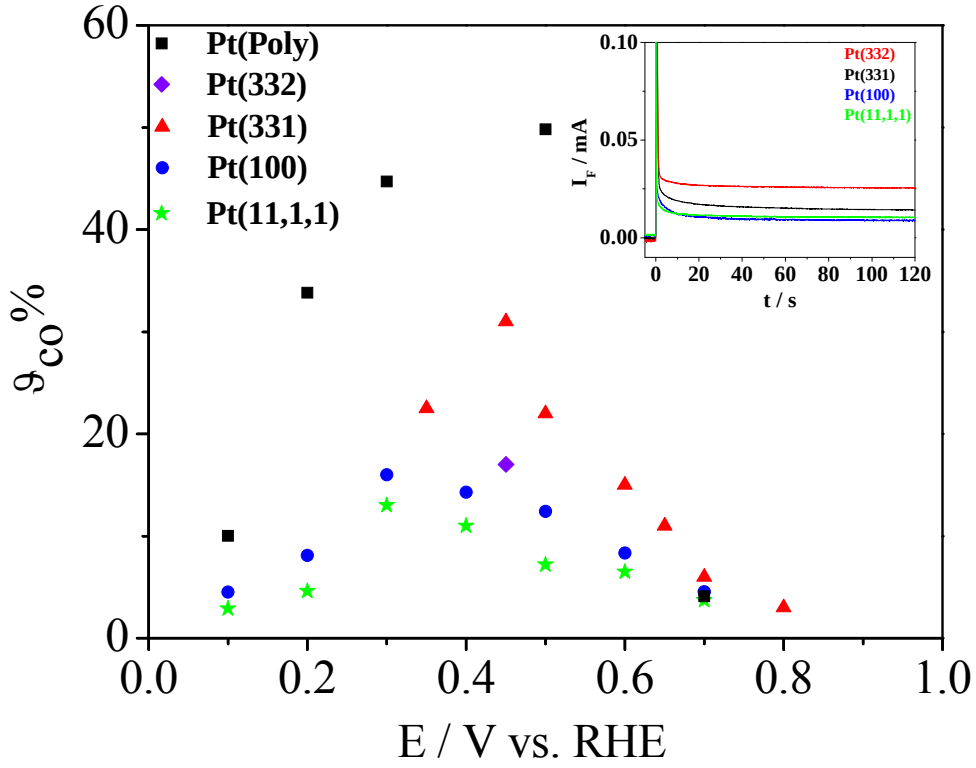

Figure 3-9 Variation of the relative coverage of methanol adsorbate (ϑ_{CO}) with adsorption potential at different platinum single crystal electrodes. The adsorption of methanol was carried out for 2 min in 0.1 M CH_3OH + 0.5 M H_2SO_4 solution. Results at Pt(Poly) are also shown for comparison. Inset: The Faradaic current transients recorded during the adsorption of methanol at 0.45 V for Pt(331) and Pt(332), and at 0.3 V for Pt(100) and Pt(11,1,1) for 2 min.

In order to investigate the potential dependence of the maximum CO coverage formed during methanol adsorption at Pt(331), Pt(100) and Pt(11,1,1) electrodes, a number of potential step experiments were performed starting from clean surface (at 0.05 V) to different adsorption potentials. As depicted in Fig. 3-9, at low potentials the limiting coverage of methanol adsorbate increases with increasing adsorption potentials, and at high potentials (above 0.45 V, at Pt(331) and above 0.3 V, at both Pt(100) and Pt(11,1,1)), it decreases again where the oxidation of methanol adsorbate occurs at these potentials. Therefore, the coverages obtained at 0.45 V (ca. 31 %, for Pt(331)) and at 0.3 V (ca. 16 %, for Pt(100) and ca. 13 %, for Pt(11,1,1)) are the steady state coverage during methanol adsorbate oxidation at these surfaces compared to a coverage of 50 % obtained at 0.5 V for Pt(Poly). Lanova et al. also reported a coverage of 56 % [8, 26] whereas a coverage of 30 % was reported by Wang et al.

[17]. At Pt(332), a coverage of 17 % was obtained at 0.45 V in agreement with a value of 15 % obtained before in literature [17] at 0.35 V.

The influence of adsorption time and adsorption potential on the relative coverage of methanol adsorbate were investigated at Pt(331) and Pt(332) as shown in Fig. 3-10. At both electrodes, at E_{ad} = 0.45 V, the maximum adsorption time, where I got the saturation coverage, is 2 min. It is obvious that, depending on the adsorption potential the saturation time will change. At E_{ad} = 0.35 V, i.e. lower than the saturation potential, the maximum coverage is obtained after 5 min of adsorption. On the other hand, at E_{ad} = 0.65 V, i.e. higher than the saturation potential, the maximum coverage is obtained after 5 s.

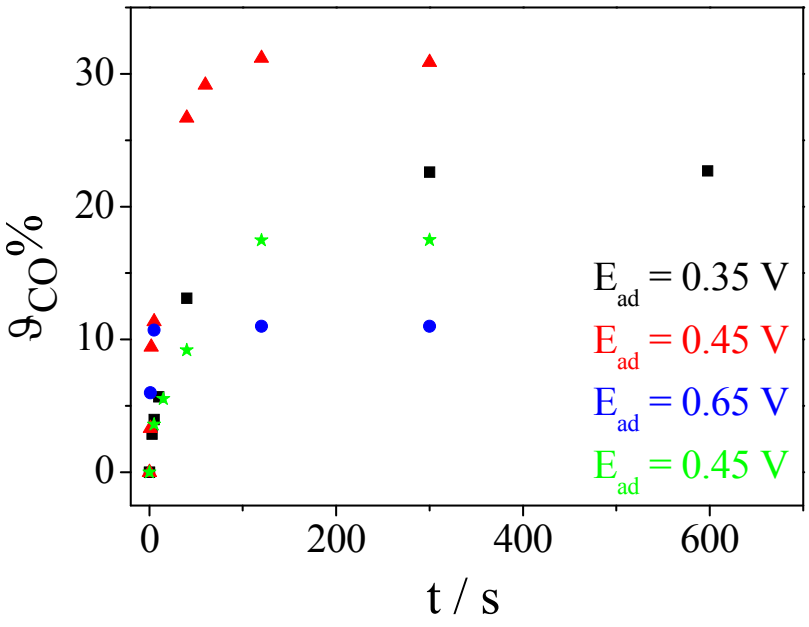

Figure 3-10 Effect of adsorption time on the relative coverage of methanol adsorbate (ϑ_{CO}), at smooth Pt(331) and Pt(332) electrodes. Adsorption of methanol was carried out in 0.1 M CH_3OH + 0.5 M H_2SO_4 solution at 0.35 V (squares), 0.45 V (triangles) and 0.65 V (cycles) for Pt(331) and at 0.45 V (stars) for Pt(332).

Appropriate rates of methanol adsorption are calculated from the slope of the line taken at coverages achieved after short adsorption times (≤ 1 s). The results are shown in Table 3-5 together with the maximum adsorption coverage, ϑ_{CO}^{max}% of methanol adsorbate at each surface. At Pt(331), the methanol adsorption rate is 10 fold higher when increasing the potential from 0.35 to 0.45 V corresponding to a Tafel slope of approximately 100 mV dec^{-1}.

Whereas the methanol adsorption rates increases with adsorption potential the maximum saturation coverage decreases above 0.5 V: at the potential of adsorption also

oxidation occurs and hence results in a decrease of the steady state coverage. Both the adsorption rate and maximum saturation coverage decreases with decreasing step density from Pt(331) to Pt(332). This indicates that Pt(331) is more active for methanol adsorbate adsorption and oxidation and methanol adsorbate is preferably formed and oxidized on the steps.

Table 3-5 The rates of methanol adsorption (determined for $t_{ad}^{\min}$ = 1 s) and the maximum adsorption coverages at different platinum surfaces for different adsorption potentials

Surface	E_{ad} / V vs. RHE	r_{ads} / MLs^{-1}	ϑ_{CO}^{max} %
Pt(331)	0.35	0.003	22.5
	0.45	0.03	31
	0.65	0.06	12
Pt(332)	0.45	0.01	17.5
$Ru_{0.2}$/Pt(331)	0.35	0.03	37
$Ru_{0.4}$/Pt(331)		0.04	19
Pt(100)	0.3	2.2	16
Pt(11,1,1)		1.8	13
Pt(Poly)	0.3	0.083	44.7
	0.4	0.19	n.d.

n.d.: not determined

As depicted in Table 3-5, step decoration with Ru have a significant effect on both the adsorption rate of methanol as well as ϑ_{CO}^{max} %. A comparison between the relative coverage of methanol for bare Pt(331) and Ru step decorated Pt(331) with different Ru coverage on the surface is shown in Fig. 3-11. With increasing Ru coverage, the rate of methanol adsorption increases due to electronic effect of Ru; where the electronic properties of the substrate (Pt atom) are modified by the second component (Ru adatom) either by modification of the adsorption enthalpy of CO_{ad} or lowering of the activation energy [7, 27-29].

On the other hand, the steady state saturation coverage of methanol adsorbate is also affected by Ru step decoration. Up to 20 % of Ru on the surface, the saturation coverage is increased from 22.5 to 37 % however with increasing Ru coverage to 40 % the coverage decreases to 19 %. 3-4 contiguous platinum sites are necessary for methanol adsorption as reported before [21]. In case of 20 % Ru on the surface (i.e. ca. 50 % Ru on the steps) the CO_{ad} coverage increases due to electronic effect of Ru atoms on the platinum sites in the vicinity of them. At short distances (40 % Ru on the surface corresponding to ca. 90 % on the

steps) a repulsive interaction between Ru adatom and the adsorbed CO molecules leads to a decrease of the CO coverage at these surfaces. Also in this case, only one row Pt atoms will be only available for methanol adsorption and this also lead to a decrease of the coverage.

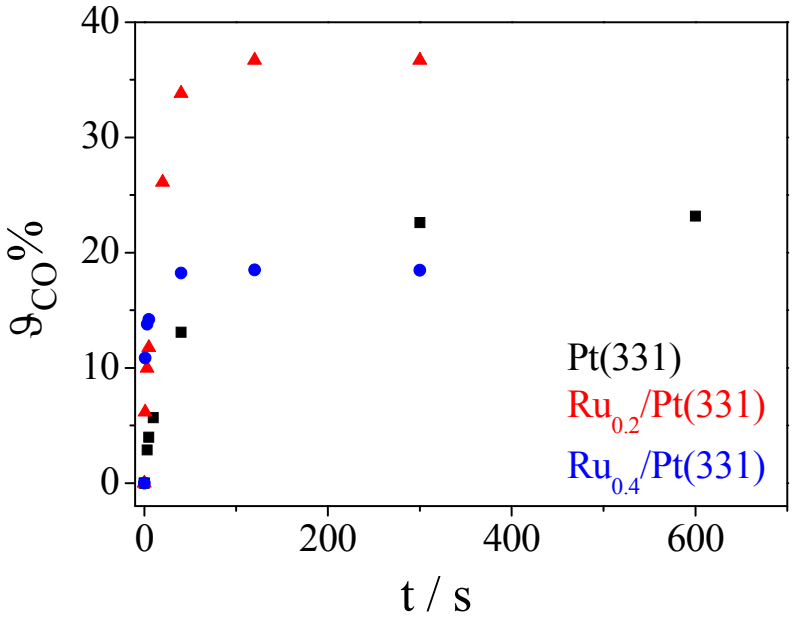

Figure 3-11 Effect of Ru step decoration on the relative coverage of methanol adsorbate (ϑ_{CO}). Adsorption of methanol was carried out in 0.1 M CH_3OH + 0.5 M H_2SO_4 solution at 0.35 V for 2 min on bare Pt(331) (squares), $Ru_{0.2}$/Pt(331) (triangles) and $Ru_{0.4}$/Pt(331) (cycles).

The rate of methanol adsorption was also determined at Pt(100) and Pt(11,1,1) electrodes (cf. Fig. 3-12). As depicted in Table 3-5, unlike Pt(331) and Pt(332) electrodes, at these surfaces, an increasing step density leads to a decrease in the rate of methanol adsorption implying that at these surfaces methanol adsorption is not preferred at step sites. The surface with limited number of terrace sites (Pt(11,1,1)), due to the presence of step edge has the lower adsorption rate as well as lower steady state coverage comparing to Pt(100) with infinite number of terrace sites. Moreover, the saturation coverage is achieved after 10 s at Pt(100) compared to 1 min at Pt(11,1,1) implying a very fast poisoning rate at Pt(100) electrode in consistence with the results of Xu et al. [30] who reported a decrease in the CO_2 current efficiency during methanol oxidation at Pt(100), Pt(15,1,1) and Pt(711) by increasing step density and attributed that to the geometric ensemble effect.

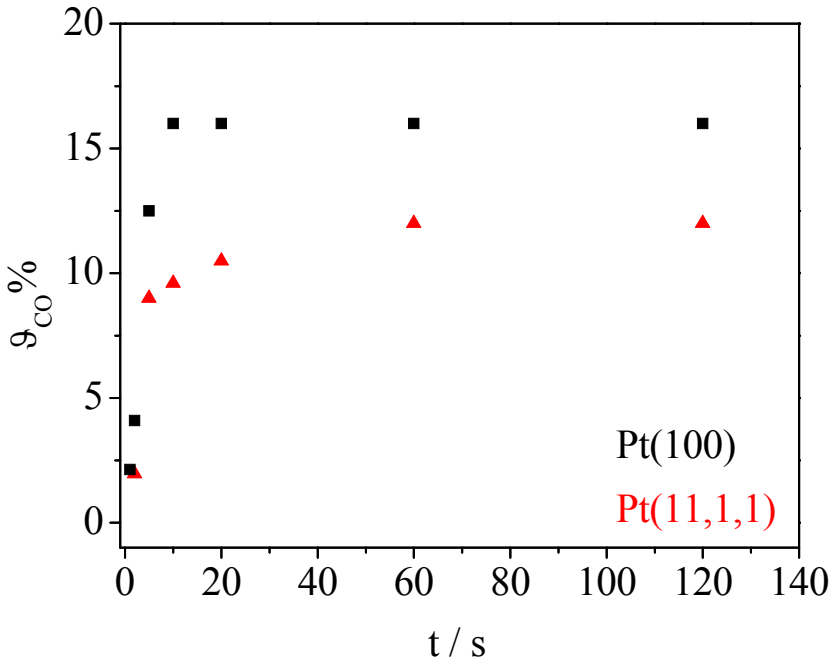

Figure 3-12 Effect of adsorption time on relative coverage of methanol adsorbate (ϑ_{CO}), at Pt(100) (squares) and Pt(11,1,1) (triangles) electrodes. Adsorption of methanol was carried out in 0.1 M CH_3OH + 0.5 M H_2SO_4 solution at 0.3 V for 2 min.

3.2.4 Methanol adsorption rate at smooth Pt(Poly) electrode

For a smooth Pt(Poly) electrode, the methanol adsorption rates were also determined at shorter adsorption times using two different methanol concentrations (0.1 M and 0.01 M). Measuring the rate at shorter time has the advantage of following up the fast poisoning rate of such reaction more accurately. To do so, after cleaning the electrode by cyclic voltammetry in the supporting electrolyte, the potential was stopped at 0.05 V, where the methanol containing solution was introduced to the cell then, the potential was stepped to 0.3, 0.4, 0.5 and 0.6 V (in case of 0.1 M methanol, cf. Fig. 3-13 A) or to 0.4, 0.5 and 0.6 V (in case of 0.01 M) where methanol is allowed to adsorb for different adsorption time ($t_{ad} \leq 5$ s). The Faradaic current and the mass spectrometric ion current for m/z = 44 (CO_2) were recorded simultaneously. Obviously, from the current transients, the oxidation of methanol adsorbate is only started at 0.5 V.

After 5 s, the potential was stepped back to 0.05 V to perform another electrolyte exchange. The Faradaic current and the mass spectrometric ion current of m/z = 44 (CO_2) during the oxidation of methanol adsorption product formed after potential step experiments at different applied potentials for t_{ad} = 5 s are shown in Fig. 3-13 B. With decreasing coverage, the oxidation peak shifts to more negative potentials whereas the onsets of all oxidation peaks

overlap, demonstrates zero order reaction with respect to the coverage in accordance with literature [26].

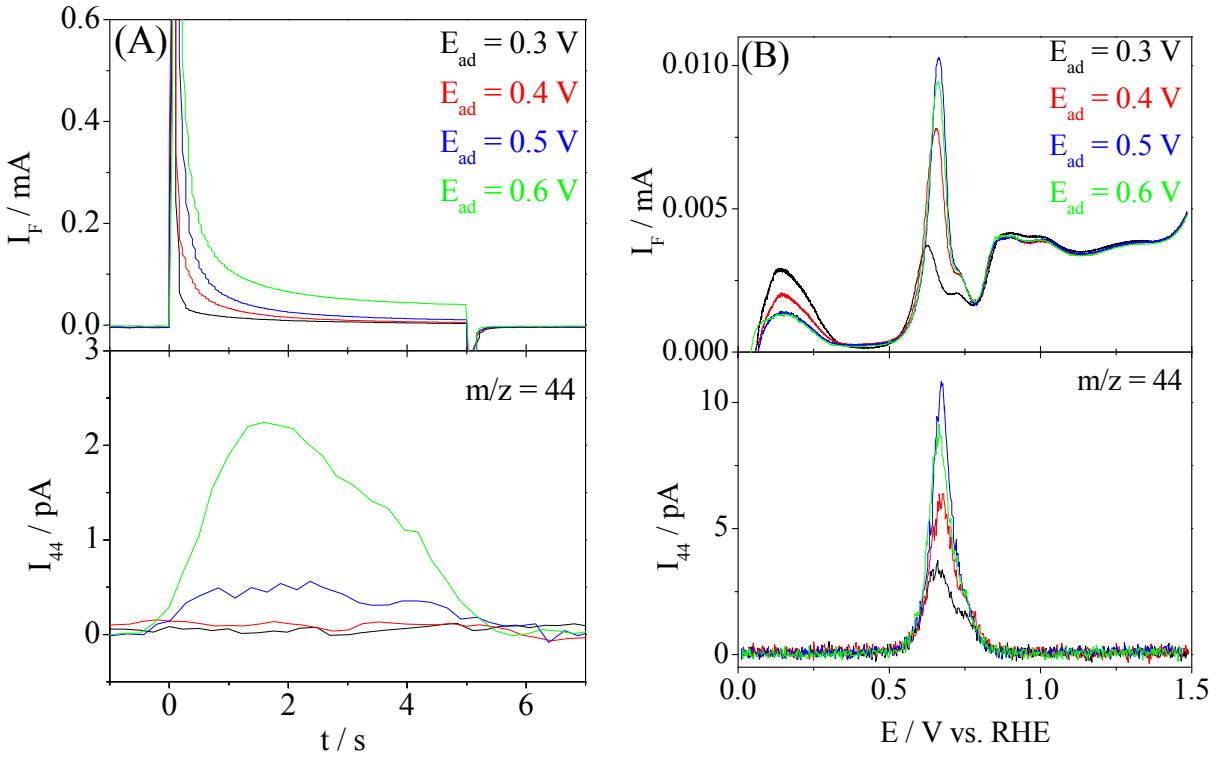

Figure 3-13 (A) The Faradaic current transients (I_F) and the mass spectrometric ionic current transients for m/z = 44 recorded simultaneously during the adsorption of methanol at smooth Pt(Poly) in 0.5 M H_2SO_4 solution + 0.1 M methanol after the step of the potential from 0.05 V to 0.3 V, 0.4 V, 0.5 V and 0.6 V, t_{ad} = 5 s (B) Oxidation of the methanol adsorption product, scan rate: 10 mVs^{-1} and electrolyte flow rate: 5 μLs^{-1}.

According to equation (2-6), the relative coverage of methanol adsorbate (ϑ_{CO}) was calculated from the integrated charge of CO_2 and plotted against adsorption time for 0.1 M and 0.01 M methanol (Fig. 3-15 A and B respectively). For both concentrations, methanol adsorption is very fast at short time, i.e. when the majority of the surface is free. The appropriate initial rate of adsorption ($d\theta/dt$ at $t_{ad} = 0$) is therefore calculated at a coverage achieved after short adsorption time ($t_{ad} \leq 1$ s) which were different and obviously more reliable than those reported before in literature [26] because here the initial rate calculated from the slope at shorter adsorption times.

After 5 s, saturation coverage was not yet achieved at potentials ≤ 0.5 V (cf. Fig. 3-14 C). At 0.6 V, the saturation coverages 31 %, in case of 0.1 M methanol and 21 %, in case of 0.01 M was achieved after 2 s. The steady state coverage obtained at 0.6 V is lower than 56 %

where at this potential, a part of the adsorbate is already oxidized to CO_2 (cf. m/z = 44 signal in Fig. 3-13 B).

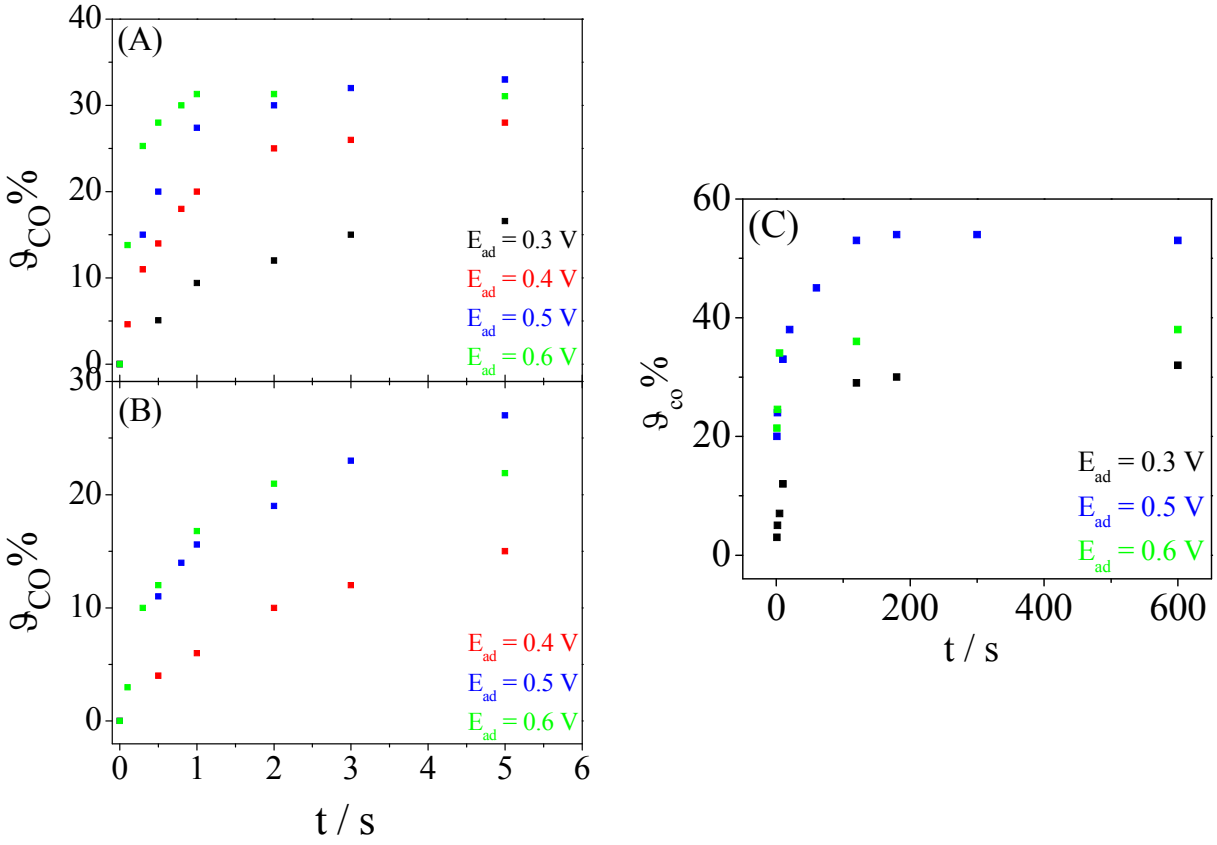

Figure 3-14 Variation of the relative coverage of methanol adsorbate (ϑ_{CO}) with methanol concentration (A), (C) 0.1 M and (B) 0.01 M, adsorption time and adsorption potentials (0.3 V, 0.4 V, 0.5 V and 0.6 V) at smooth Pt(Poly) electrode. (C) Results of the same experiment but with longer adsorption times adopted from ref. [8] are shown for comparison.

As depicted in Table 3-6, methanol adsorption rate increases with increasing methanol concentration since the amount of the reacting species reach the surface of the electrode are higher at higher concentration. As the adsorption potential increases, the rate of methanol adsorption also increases in accordance with literature [31-35]. The later is explained by the potential-dependent Tafel slope according to Tafel equation and then the rate should increase according to:

$$r_{ads} = \left.\frac{d\theta}{dt}\right|_{t=0} = ke^{\alpha zF\eta/RT} = ke^{E/b} \qquad (3\text{-}4)$$

Here, Tafel slope (b) = $2.3RT/\alpha zF$ where, α is the transfer coefficient and z is the number of electron transferred in the rds.

Table 3-6 The rates of methanol adsorption at smooth Pt(Poly) for different adsorption potentials and methanol concentrations.

E_{ad}/V vs. RHE	r_{ads} / MLs^{-1}	
	0.1 M Methanol	0.01 M Methanol
0.3	0.1	n.d.
0.4	0.26	0.08
0.5	0.7	0.2
0.6	1	0.35

n.d.: not determined

The logarithm of the adsorption rates as a function of adsorption potentials is plotted in Fig. 3-15. Tafel slopes of 237 and 250 mV dec^{-1} are obtained in case of 0.1 M and 0.01 M methanol respectively which is higher than the usual slope of 118 mV dec^{-1} predicted from the Tafel equation for an rds involving one electron transfer with a transfer coefficient of ca. 0.5. A slope of approximately 100 mV dec^{-1} was obtained above at the Pt(331) single crystal electrode. Different Tafel slopes might be due to a different potential dependence of the rate due to different surface structure. Recently, Shao et al. reported a Tafel slope of 440±30 mV dec^{-1} for the dehydrogenation of 2 M methanol at platinum film deposited at Silicon prism as studied by ATR-FTIR spectroscopy under flow conditions [31]. In their calculations, they consider the slope of the line from 0.3 up to 0.7 V. In fact, at potentials ≥ 0.6 V, the oxidation of methanol adsorbate will start. In Fig. 3-15, however, I consider only the slope until E < 0.6 V. Evaluating their data for low coverages and low potentials, also a Tafel slope of ca. 200 mV dec^{-1} is obtained. According to their measurements, the reasons for the unusual slopes are: (i) the rds for methanol dehydrogenation is the heterolytic break of C-H bond associated with one electron transfer but with small apparent transfer coefficient ($\alpha = 0.13$) i.e. only a small amount of the interfacial potential difference is contributed to the reduction of the activation barrier for the rds in agreement with DFT calculations [36, 37] (ii) the rds is the homolytic splitting of C-H bond followed by a fast discharge of H_{ad}; i.e. no charge transfer is involved in the rds.

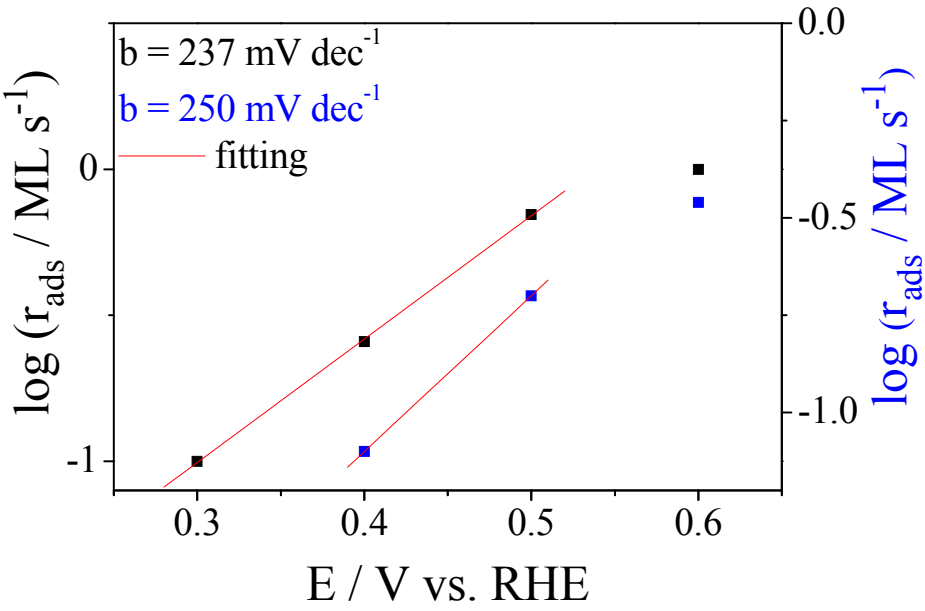

Figure 3-15 Tafel plots of the methanol adsorption rate as a function of adsorption potentials at smooth Pt(Poly). Black squares (0.1 M methanol) and blue squares (0.01 M methanol).

3.2.5 Oxidation of methanol adsorption product

In the following, the stripping peaks of the methanol adsorption products obtained in the previous experiments (cf. Fig. 3-16 and 3-17) shall be explained in detail. The disappearance of the hydrogen desorption peaks in the first anodic cycle is due to blocking of the platinum sites with adsorbed methanol.

As shown above in Fig. 3-13 B, with decreasing coverage, the oxidation peak shifts to more negative potentials whereas the onsets of all oxidation peaks overlap demonstrating a zero order reaction with respect to the coverage. In ref. [26], the authors attributed that to the presence of special active sites to which CO_{ad} diffuses. As shown in Fig. 3-16 A, different from the shape of methanol adsorbate stripping peaks at Pt(Poly), both the onset potential and the peak potential shift in the anodic direction with decreasing methanol adsorbate coverage. On Pt(331), the same result is also obtained when varying the coverage by adsorption of methanol at different adsorption times (cf. Fig. 3-16 B). Here, as reported before for the same reaction at Ru modified Pt(Poly) [26], it is hardly to imagine a reason for a reaction order higher than 1; rather, the behavior signifies the presence of different adsorption sites with different adsorption enthalpies. Pt(331) is a surface with a 2 Pt atoms narrow terrace and one monoatomic Pt step. At low coverage, the sites leading to the most stable adsorbate (step sites) are populated, at higher coverage those with high positive adsorption enthalpies (terrace

sites) are also populated and the onset of oxidation and the peak potentials are shifted to lower values.

As depicted in Fig. 3-16 (C, D), at $Ru_{0.2}$/Pt(331) electrode, the onset potential of methanol adsorbate oxidation was shifted by ca. 0.1 V to the negative direction when compared to bare Pt(331). Again, this is due to the electronic and bifunctional effects of Ru [4]. Both the onset potential and the peak potential of methanol adsorbate oxidation were also shifted to more positive potential with decreasing coverage. This behavior was reported before for Ru modified Pt(Poly) and platinum nanoparticles electrodes [26] and also on Ru modified platinum single crystals [6, 7] when the oxidation of CO at these surfaces results in a distinct two oxidation peaks at different potentials. Two different methanol adsorbate (CO_{ad}) oxidation peaks can be also visible in Fig. 3-16 (C, D) at $Ru_{0.2}$/Pt(331) electrode. The interpretation for that is, as pointed out above, the presence of two different adsorption sites with two different adsorption enthalpies; at low methanol adsorbate coverage, the oxidation will occur at potentials similar to bare Pt(331) because the adsorbate will be populated at the most stable sites away from Ru. At high adsorbate coverage, Pt sites in the close vicinity of Ru will be also populated and the oxidation of CO_{ad} formed at these sites results in a shift in both the onset potential and the peak potential to the negative direction.

At $Ru_{0.4}$/Pt(331), the same shift (by ca. 0.1 V to the negative direction) is observed (cf. Fig. 3-16 (E, F)) similar to $Ru_{0.2}$/Pt(331), but without the two distinct methanol adsorbate oxidation peaks; rather, a very broad oxidation peak is observed. Here, as pointed out above, for the oxidation of pre-adsorbed CO at $Ru_{0.4}$/Pt(331) electrode, the concept of two different adsorption sites is no more valid when the steps are almost completely blocked by Ru. Similar to CO adsorbed from CO saturated electrolyte, CO_{ad} formed from methanol can only adsorbed at the uncovered terrace sites (one row of Pt) and on Ru. These molecules, however, are still affected by the bifunctional effect of Ru atoms at the steps, hence, methanol adsorbate oxidation peaks were also shifted to more negative potentials compared to bare surface.

The oxidation of methanol adsorption product at Pt(100) and Pt(11,1,1) electrodes at different adsorption potentials and times is shown in Fig. 3-17 (A, B) and (C, D) respectively. Both the onset potential and the peak potential of methanol adsorbate oxidation shift to more positive values with increasing adsorption potential. Here, it seems that different adsorption potentials lead to methanol adsorption at different sites (defects or terrace sites). At potentials $\leq$ 0.3 V, methanol adsorption occurs at most active sites and then the adsorbate formed at those sites will be oxidized at low potentials. However, at potentials > 0.3 V, simultaneous

oxidation during adsorption occurs and only methanol adsorbate formed at stable sites survives and oxidized at more positive potentials.

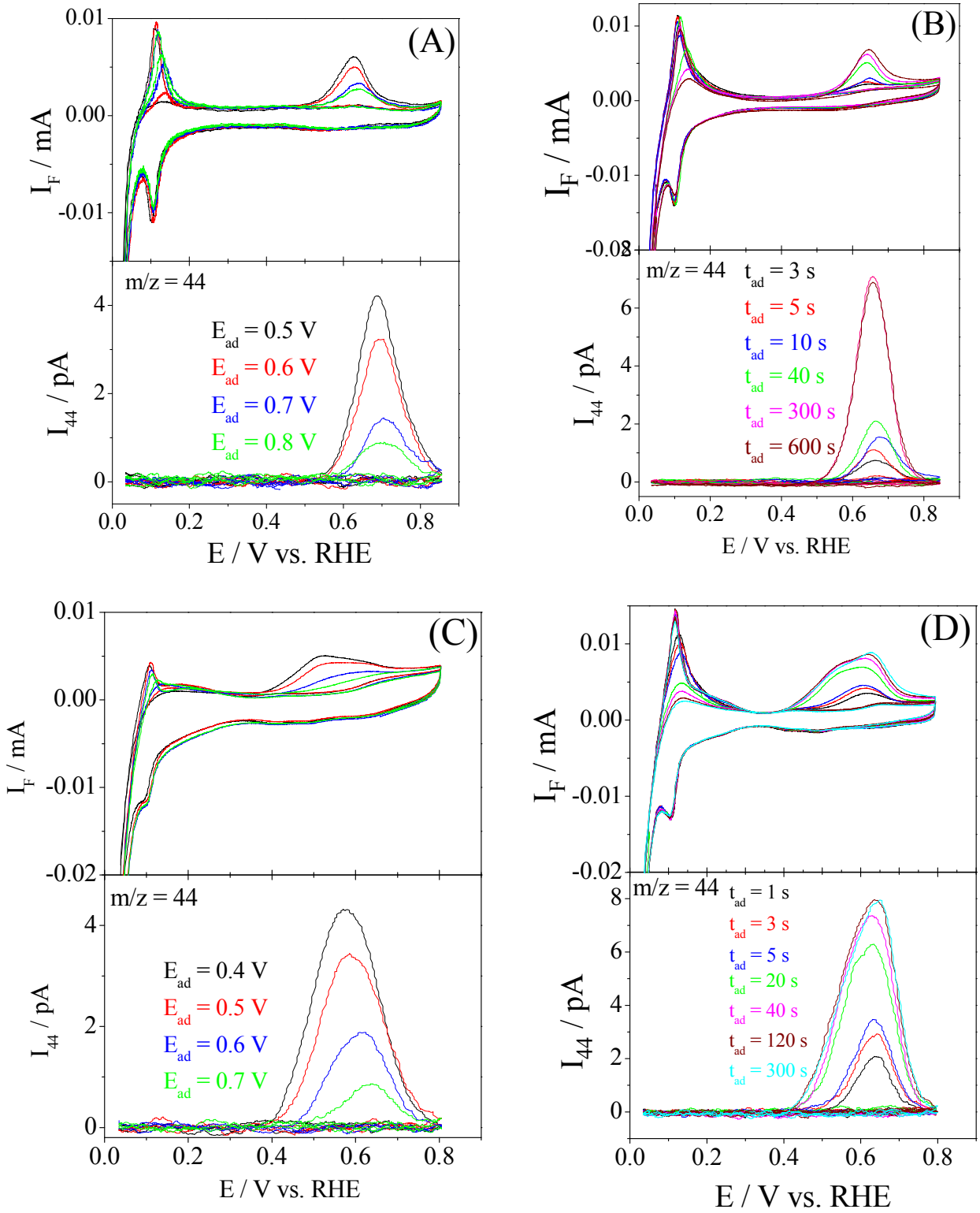

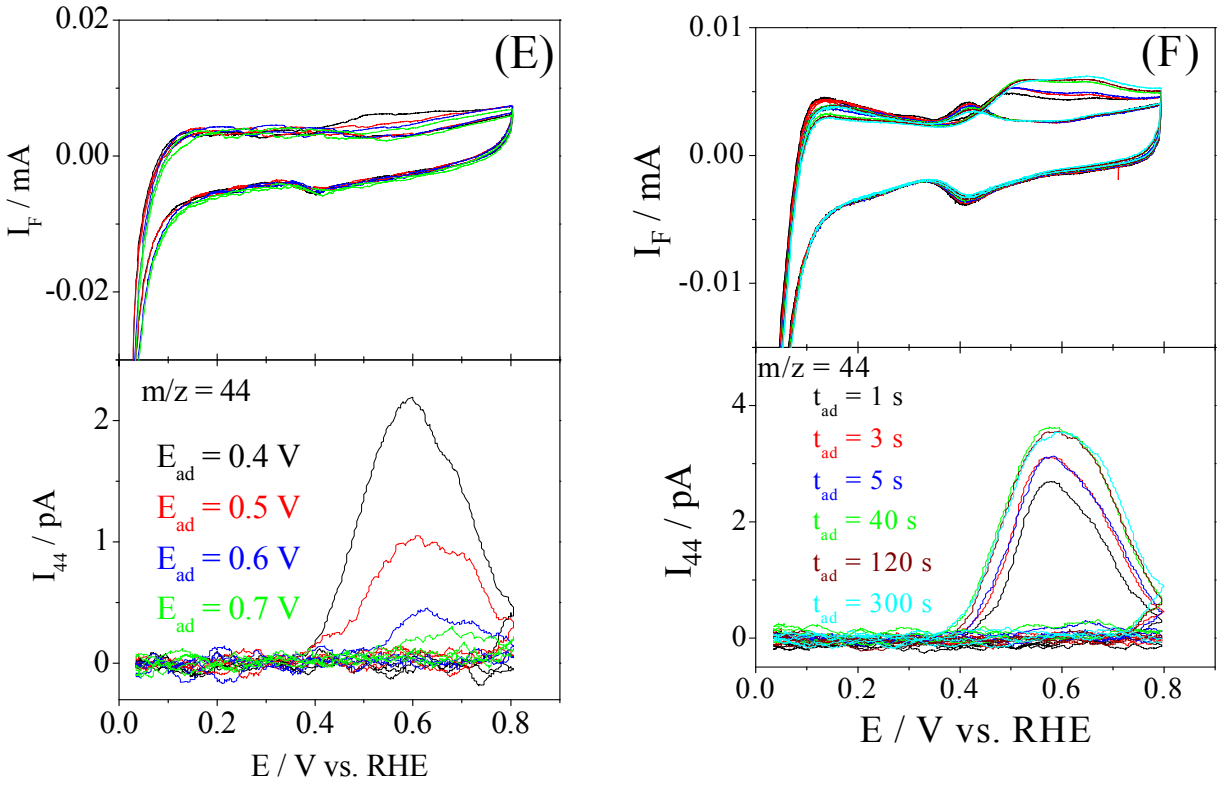

Figure 3-16 The Faradaic currents (I_F) and the mass spectrometric ionic currents for m/z = 44 recorded simultaneously during the electrooxidation of methanol adsorbate after step of the potential from 0.05 V to different adsorption potentials or times (E_{step} = 0.35 V) at Pt(331) (A, B), $Ru_{0.2}$/Pt(331) (C, D) and $Ru_{0.4}$/Pt(331) (E, F) respectively in 0.1 M methanol + 0.5 M H_2SO_4 solution. Scan rate: 10 mVs^{-1}. Electrolyte flow rate: 5 μLs^{-1}.

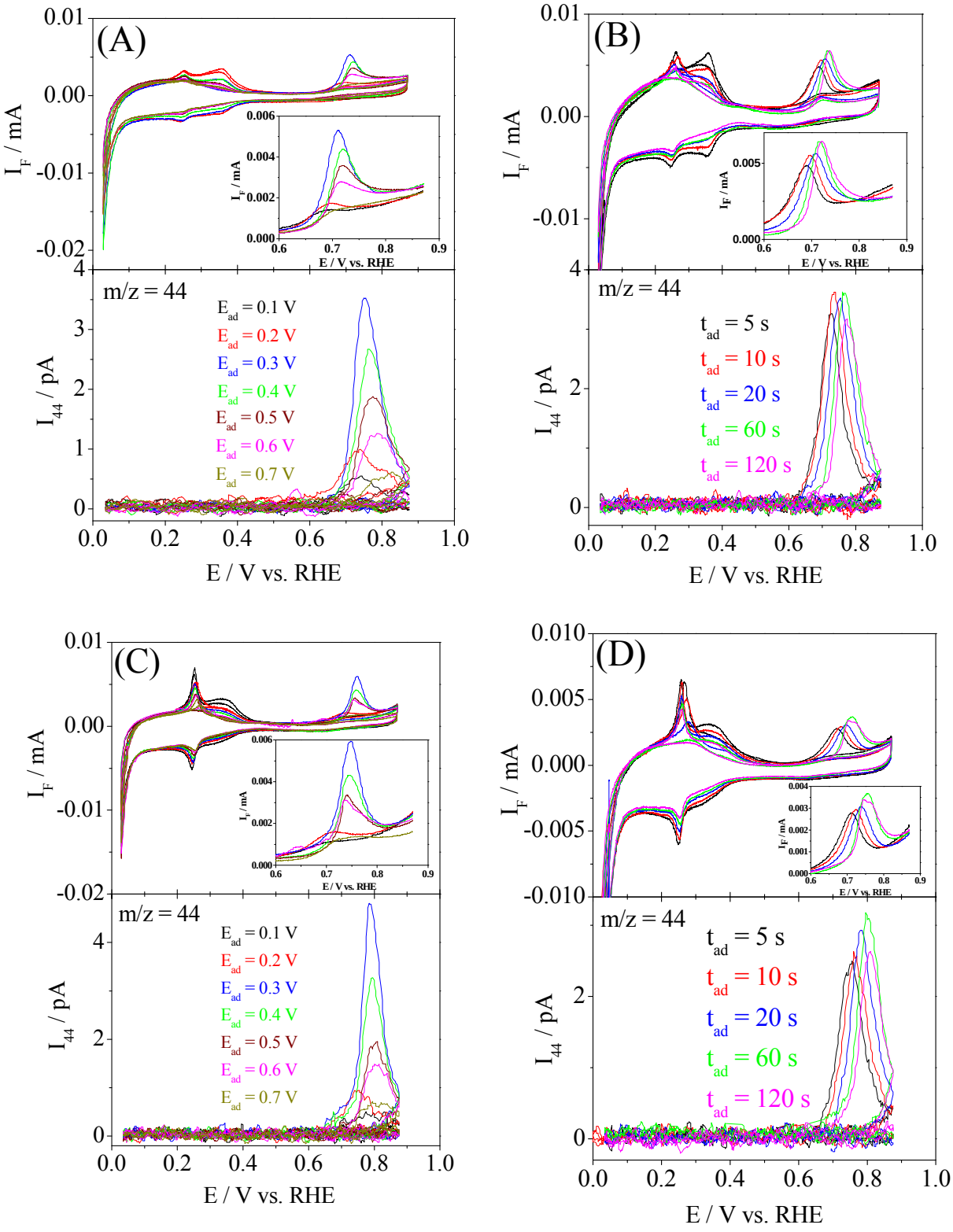

Figure 3-17 The Faradaic currents (I_F) and the mass spectrometric ionic currents for m/z = 44 recorded simultaneously during the electrooxidation of methanol adsorbate after step of the potential from 0.05 V to different adsorption potentials or times (E_{step} = 0.3 V) at Pt(100) (A, B) and Pt(11,1,1) (C, D) respectively in 0.1 M methanol + 0.5 M H_2SO_4 solution. Scan rate: 10 mVs^{-1}. Electrolyte flow rate: 5 μLs^{-1}.

3.3 Conclusions

In the present chapter, the effect of Ru step decoration during the potentiodynamic and potentiostatic oxidation of methanol at Pt(331) single crystal electrode has been studied and compared to the same reaction at bare surface. Also, the effect of methanol concentration, flow rate and potential on the obtained CO_2 and methylformate current efficiencies was investigated. At Ru/Pt(331) electrodes with different Ru coverages at the steps (from 0 to 40 %), CO_2 current efficiencies and the degree of surface poisoning with CO_{ad} are independent of flow rate; both confirm the parallel pathway mechanism for the electrooxidation of methanol at platinum electrode. CO_2 current efficiencies decrease with increasing methanol concentration and increase with increasing potential, whereas that of methylformate shows the reverse trend. Ru electrodeposited at Pt(331) step sites promotes the adsorption and oxidation of CO_{ad} formed from methanol at low potentials according to electronic and bifunctional mechanisms. At high potentials, however, Ru loses its co-catalytic activity. Complete blocking of the platinum step sites with Ru shifts the oxidation to the indirect pathway (non-CO-pathway) and thus results in low CO_2 current efficiencies. It leads also to inhibition of methanol oxidation due to blocking of the most platinum active sites necessary to the first step of methanol adsorption and oxidation.

Some methanol adsorption rates obtained during methanol adsorption at smooth Pt(Poly) and platinum stepped single crystals have been presented. At Pt(Poly), the adsorption rate increases with increasing methanol concentration and adsorption potentials. A Tafel slope between 237 mV dec^{-1} (in case of 0.1 M methanol) and 250 mV dec^{-1} (in case of 0.01 M methanol) obtained here at potentials < 0.6 V is more reliable than the values of ca. 400 mV dec^{-1} reported before in literature [31] where the Tafel slope at a potential ≥ 0.6 V was calculated during the dehydrogenation of 2 M methanol and where the oxidation of methanol adsorbate already starts. At Pt(331) and Pt(332) electrodes, methanol adsorption rate is doubled with doubled step density, higher with higher Ru coverage and increases by a factor of 10 per 0.1 V (Tafel slope of ca. 100 mV dec^{-1}). I attributed the difference in the adsorption rates and consequently the difference in potential dependence of the rate to the difference in surface structure. Increasing the step density from Pt(100) to Pt(11,1,1) however, leads to a decrease in the steady state coverage and the methanol adsorption rate due to the geometric ensemble effect .

The stripping peaks during the oxidation of the methanol adsorption product formed at Pt(Poly), Ru/Pt(331), Pt(100) and Pt(11,1,1) electrodes were also compared. At Pt(Poly), with

decreasing coverage, the methanol adsorbate oxidation peaks shifts to more negative potentials whereas, the onsets of all peaks overlaps, signifying a zero order reaction with respect to the coverage. The zero order kinetics of methanol adsorbate oxidation at Pt(Poly) was attributed before [26] to the presence of special active sites (defects) to which the CO_{ad} diffuses. Further improvements of such interpretation will be mentioned in chapter 5, part 5.2.4 of this thesis. Different from the behavior of methanol adsorbate oxidation at Pt(Poly), at Ru/Pt(331), with decreasing coverage, both the onset potential and the peak potential of methanol oxidation were shifted to more positive values. Such behavior was rather attributed to the presence of different adsorption sites with different adsorption enthalpies. Similar to Ru/Pt(331) electrodes, at Pt(100) and Pt(11,1,1), the shift was also observed. Here, different adsorption sites are rather due to different adsorption potentials; at low potentials ($E \leq 0.6$ V), only the most active sites are populated by methanol adsorbate (CO_{ad}) and thus the adsorbate formed at those sites will be oxidized at low potentials. At high potentials, however, the simultaneous oxidation/adsorption reaction will occur and only CO_{ad} at stable sites survives and then oxidized at high potentials.

References

[1] Abd-El-Latif, Vol. PhD, in Mathematisch-Naturwissenschaftlichen Fakultät, Rheinischen Friedrich-Wilhelms-Universität Bonn, Bonn, 2011, p. 185.

[2] J. Mostany, E. Herrero, J. M. Feliu, and J. Lipkowski, Journal of Physical Chemistry B. 106:12787 (2002).

[3] V. Del Colle, A. Berna, G. Tremiliosi-Filho, E. Herrero, and J. M. Feliu, Physical Chemistry Chemical Physics 10:3766 (2008).

[4] H. Wang and H. Baltruschat, Journal of Physical Chemistry C 111:7038 (2007).

[5] S. G. Sun, A. C. Chen, T. S. Huang, J. B. Li, and Z. W. Tian, Journal of Electroanalytical Chemistry 340:213 (1992).

[6] H. Massong, H. S. Wang, G. Samjeske, and H. Baltruschat, Electrochimica Acta 46:701 (2000).

[7] G. Samjeské, X.-Y. Xiao, and H. Baltruschat, Langmuir 18:4659 (2002).

[8] B. Lanova, in Institute für Physikalische und Theoretische Chemie, Abteilung Elektrochemie, Vol. Ph.D., Rheinische Friedrich-Wilhelms Universität Bonn, Germany, 2009.

[9] H. Baltruschat, E. Siegfried, and N. Bogolowski, in Catalysis in Electrochemistry, From Fundamentals to Strategies for Fuel Cell Development (E. S. a. W. Schmickler, ed.), John Wiley & Sons, Inc., Hoboken, New Jersey, Canada, 2011.

[10] M. Krausa and W. Vielstich, Journal of Electroanalytical Chemistry 399:7 (1995).

[11] V. Grozovski, V. Climent, E. Herrero, and J. M. Feliu, Journal of Electroanalytical Chemistry 662:43 (2011).

[12] K. Franaszczuk, E. Herrero, P. Zelenay, A. Wieckowski, J. Wang, and R. I. Masel, Journal of Physical Chemistry 96:8509 (1992).

[13] E. Herrero, K. Franaszczuk, and A. Wieckowski, Journal of Physical Chemistry 98:5074 (1994).
[14] H. Wang, T. Löffler, and H. Baltruschat, Journal of Applied Electrochemistry 31:759 (2001).
[15] H. Baltruschat, Journal of the American Society for Mass Spectrometry 15:1693 (2004).
[16] H. S. Wang, C. Wingender, H. Baltruschat, M. Lopez, and M. T. Reetz, Journal of Electroanalytical Chemistry 509:163 (2001).
[17] H. Wang, Vol. PhD, Beijing Normal University, Beijing, 2001.
[18] A. Cuesta, Journal of the American Chemical Society 128:13332 (2006).
[19] H. Wang, L. R. Alden, F. J. DiSalvo, and H. D. Abruna, Langmuir 25:7725 (2009).
[20] H. A. Gasteiger, N. Markovic, P. N. Ross, and E. J. Cairns, Journal of Physical Chemistry 97:12020 (1993).
[21] N. M. Markovic and P. N. Ross, Surface Science Reports 45:117 (2002).
[22] H. Wang and H. Baltruschat, in DMFC Symposium, Meeting of the Electrochemical Society 2001 (S. R. Narayanan, ed.), The Electrochemical Society, Washington D.C., 2001.
[23] Y. E. Seidel, A. Schneider, Z. Jusys, B. Wickman, B. Kasemo, and R. J. Behm, Langmuir 26:3569 (2010).
[24] A. A. Abd-El-Latif and H. Baltruschat, Journal of Electroanalytical Chemistry 662:204 (2011).
[25] Z. Jusys, J. Kaiser, and R. J. Behm, Langmuir 19:6759 (2003).
[26] B. Lanova, H. Wang, and H. Baltruschat, Fuel Cells 6:214 (2006).
[27] M. Mavrikakis, B. Hammer, and J. K. Norskov, Physical Review Letters 81:2819 (1998).
[28] J. R. Kitchin, J. K. Norskov, M. A. Barteau, and J. G. Chen, Physical Review Letters 93:156801 (2004).
[29] J. R. Kitchin, J. K. Norskov, M. A. Barteau, and J. G. Chen, Journal of Chemical Physics 120:10240 (2004).
[30] J. Xu, A.-E.-A. Abd-El-Latif, and H. Baltruschat, to be submitted (2012).
[31] S. X. Liu, L. W. Liao, Q. Tao, Y. X. Chen, and S. Ye, Physical Chemistry Chemical Physics 13:9725 (2011).
[32] K. Kunimatsu, H. Hanawa, H. Uchida, and M. Watanabe, Journal of Electroanalytical Chemistry 632:109 (2009).
[33] D. Cao, G. Q. Lu, A. Wieckowski, S. A. Wasileski, and M. Neurock, Journal of Physical Chemistry B 109:11622 (2005).
[34] G. Q. Lu, W. Chrzanowski, and A. Wieckowski, Journal of Physical Chemistry B 104:5566 (2000).
[35] T. H. M. Housmans and M. T. M. Koper, Journal of Physical Chemistry B 107:8557 (2003).
[36] P. Ferrin, A. U. Nilekar, J. Greeley, M. Mavrikakis, and J. Rossmeisl, Surface Science 602:3424 (2008).
[37] Y. Sun, Y. Liu, Z. Liang, L. Xiong, A. Wang, and S. Chen, The Journal of Physical Chemistry C 113:9878 (2009).

4. Electrocatalytic oxidation of ethanol

4.1 Introduction

Due to the difficulties and risks associated with the transport and handling of hydrogen, the direct use of alcohols as a fuel in fuel cells is an alternative. Comparing to methanol, ethanol can be produced easily from biomass, is less toxic, easy to be stored and has a higher mass energy density. In this chapter, using the dual thin layer flow through cell, I investigated the electrooxidation of ethanol at Pt(Poly), smooth, roughened and Sn modified Pt(11,1,1), Pt(311) single crystal electrodes by on-line differential electrochemical mass spectroscopy (DEMS). In addition to the current efficiency of CO_2, that of acetaldehyde was determined as a function of flow rate. The aim is to analyze in detail the contribution of the possible reaction products, in particular CO_2, to the overall current and to investigate the effect of single crystal surface modification with Sn during the oxidation of ethanol. At high flow rates, the apparent acetaldehyde current efficiencies are too high due to incomplete mixing in the dual thin layer flow through cell. To obtain reliable values of acetaldehyde current efficiencies, I present here a new calibration procedure based on the oxidation of i-propanol at Pt(Poly) under the same experimental conditions to that of ethanol. Assuming a product (acetone) current efficiency of 100 %, the true acetaldehyde current efficiencies can be calculated.

4.2 Results and discussion

4.2.1 Electrooxidation of ethanol at smooth Pt(Poly)

4.2.1.1 Potentiodynamic measurements

The potentiodynamic oxidation of 0.01 M ethanol in 0.5 M H_2SO_4 supporting electrolyte at smooth Pt(Poly) is shown in Fig. 4-1A, it includes the Faradaic current (I_F) and the ion currents for m/z = 44 (CO_2 + CH_3CHO) and m/z = 29 (acetaldehyde) for ethanol oxidation. The appearance of the hydrogen desorption peaks in the first anodic sweep is due to the fact that ethanol does not adsorb at 0.05 V, the potential at which ethanol containing solution is replacing the supporting electrolyte (cf. Fig. 4-1B).

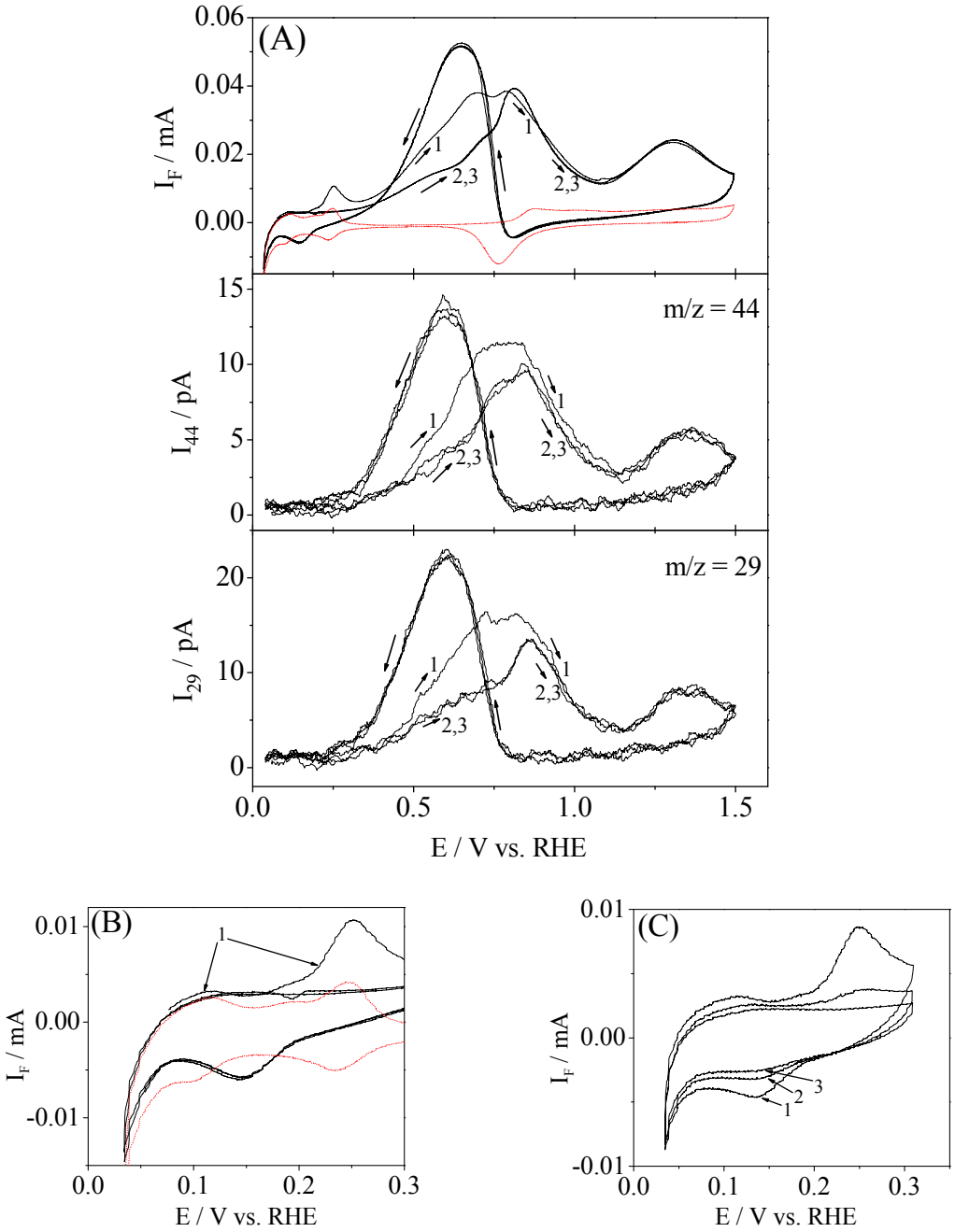

Figure 4-1 (A) Potentiodynamic oxidation of 0.01 M ethanol + 0.5 M H_2SO_4 solutions at smooth Pt(Poly). The Faradaic current (I_F) was recorded simultaneously with the ionic currents at sweep rate = 10 mVs^{-1} and electrolyte flow rate = 5 μLs^{-1}. For comparison, the CV recorded in pure supporting electrolyte (red line) is shown. (B) Enlarged view of I_F in the hydrogen region. (C) Three potential cycles in ethanol containing solution up to 0.3 V.

The charge observed at 0.25 V in the first positive going sweep of ethanol oxidation is due to hydrogen desorption and alcohol oxidative adsorption [1]. Afterwards, three different oxidation peaks were observed at 0.7 V, 0.8 V and the third peak in the oxygen region at 1.3

V [2-4]. Heinen et al. reported recently the same behaviour during the oxidation of ethanol at a thin platinum film as studied by ATR-FTIRS [5]. According to their measurements, the onset of the formation of linearly bonded CO coincides with this peak at 0.25 V; therefore, this current is due to the oxidation of ethanol to acetaldehyde which then decomposes to CO_{ad} and $CH_{x,ad}$ fragments. The increase in the oxidation current corresponds indeed to the formation of acetaldehyde at these low potentials (cf. Fig 4-1A, m/z = 29) whereas the adsorbed acetyl species are hardly detected by IR [5].

After complete desorption of adsorbed oxygen during the cathodic going sweep, an oxidation peak at 0.65 V in addition to a reduction peak at 0.15 V were observed. The hydrogen desorption charges during the second anodic sweep are completely suppressed due to complete blocking of the platinum surface by ethanol adsorbed intermediates formed in the preceding cathodic sweep. Because of these adsorbates, which are only oxidized at higher potential, the oxidation current was lower in the second cycle.

The nature of the ethanol reduction peak at 0.15 V was not discussed before. This peak does not correspond to either of the hydrogen adsorption peaks. In order to check whether it is related to the oxidation peak at 0.25 V, in an additional experiment, a CV between 0.05 V and 0.3 V was recorded (cf. Fig. 4-1C). The reduction peak is still visible, but smaller than the anodic peak. Both anodic and cathodic peaks decrease from cycle to cycle, obviously, due to the aforementioned formation of adsorbed CO and CH_x fragments. After an electrolyte exchange at 0.3 V and potential cycles down to -0.1 V and then to +1.5 V, the formation of methane and an oxidation peak for adsorbed CO were detected respectively (cf. Fig. 4-2). I have to conclude that the process leading to the anodic peak at 0.25 V is partially reversible. A possibility is the reversible formation of weakly adsorbed ethoxy species ($-OCH_2CH_3$), which is either further oxidized to acetyl [5] or, in the cathodic sweep, desorbs as ethanol. Such ethoxy species are formed when alcohols are adsorbed in UHV [6]; they are also presumably formed at Au electrodes [7].

During all anodic cycles for ethanol oxidation, the mass spectrometric ion currents of m/z = 29 were similar to the Faradaic currents. Therefore, acetaldehyde seems to be produced over the whole potential range independent of the applied potential [4] but the ion current of m/z = 44 showed an additional shoulder at 0.7 V in the second and third cycles which was not visible in m/z = 29, and therefore is an indication for CO_2 production.

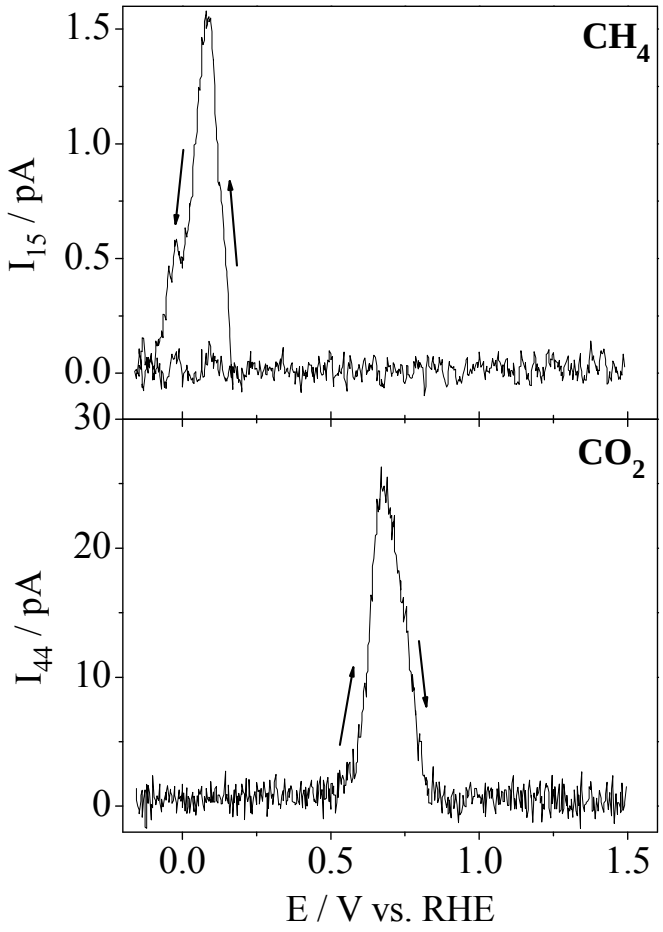

Figure 4-2 The formation of methane and CO_2 from adsorbates (formed at smooth Pt(Poly) during potential sweep between 0.05 and 0.3 V in ethanol containing solution) while sweeping the potential to -0.1 V and then to 1.5 V in 0.5 M H_2SO_4 after an electrolyte exchange at 0.3 V. Sweep rate = 10 mV s^{-1} and electrolyte flow rate = 5 µL s^{-1}.

4.2.1.2 Potentiostatic measurements

More important than the potential sweep experiments are the potential step ones, in which each potential step starts with a clean surface. A series of potential step experiments in 0.01 M ethanol was done in 0.5 M H_2SO_4. The potential was stepped from 0.05 V to different adsorption potentials (0.5-0.8 V) during which ethanol was allowed to adsorb for two minutes as shown in Fig. 4-3A. The Faradaic and ionic current transients were recorded simultaneously in each case. They increase with increasing potentials up to 0.7 V and then decrease at 0.8 V due to surface deactivation by adsorbed oxygen species at high potentials. In all transients the oxidation current was high in the beginning and then it decreases with time due to deactivation of the platinum surface by accumulation of the adsorbed intermediates that block the platinum active sites. After recording current transients, an electrolyte exchange

with the supporting electrolyte was performed at 0.05 V and the potential was swept in the positive direction (cf. Fig. 4-3B). CO_2 was formed at a potential where usually CO_{ad} is oxidized. With increasing potential of the step, the CO_{ad} oxidation peak decreases since at such high potentials ethanol adsorbate oxidation already starts.

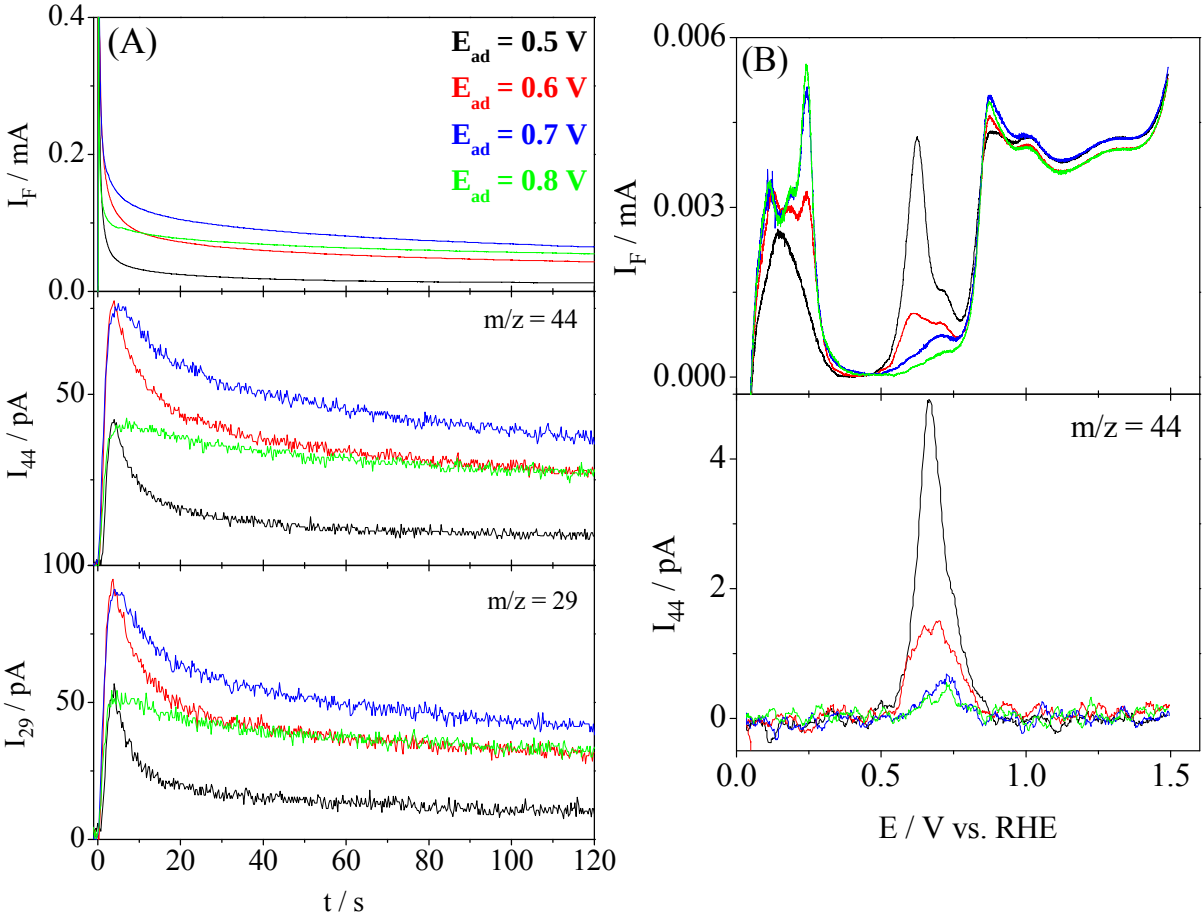

Figure 4-3 (A) Potentiostatic oxidation of 0.01 M ethanol + 0.5 M H_2SO_4 solution at smooth Pt(Poly) and different potential steps. (B) Oxidation of ethanol adsorbate formed previously in (A). The Faradaic currents (I_F) were recorded simultaneously with the ionic currents in each case with electrolyte flow rate = 5 μLs^{-1}, in (B) sweep rate = 10 mVs^{-1}.

As shown above and demonstrated earlier [8], CO_{ad} is mainly formed from α-carbon atom of ethanol, whereas a $CH_{x,ad}$ species is mainly formed from the β-carbon atom; which depending on potential is slowly oxidized to CO_{ad} as well or (at low potentials) desorbed as CH_4. Therefore, there is no "ideal" potential for the electrolyte exchange, i.e. a potential at which the adsorption reaction is not proceeding any further and at which the adsorbate is stable. In the experiment of Fig. 4-2, the reaction continues at the potential of the electrolyte exchange. Therefore, I choose 0.05 V for this electrolyte exchange: Here, the adsorption reaction is stopped, CO_{ad} is stable, but any adsorbed CH_x-fragment might desorb.

The coverage of CO_{ad} decreases with increasing the adsorption potential due to an increase of the oxidation rate of ethanol adsorption product. As depicted in Table 4-1, the calculated coverages hardly depend on the flow rate of the electrolyte, demonstrating that the adsorption reaction is not diffusion limited and that the adsorption of acetaldehyde formed as an intermediate is also negligible under these conditions. In principle, at a low flow rate, an intermediate has a higher chance to reabsorb.

Calculation of carbon dioxide current efficiency (A_{CO_2})

For the oxidation of ethanol the Faradaic current is given by the sum of the oxidation ratio of the various products:

$$I_F = I_F^{CO_2} + I_F^{CH_3CHO} + I_F^{CH_3COOH} + I_F^{CH_3CH_2OCOCH_3} + ... + etc \quad (4\text{-}1)$$

The ionic current corresponds only to the formation of CO_2 ($I_{44}^{CO_2}$) is given by the difference between the total recorded ionic current of m/z = 44 ($I_{44}^{Recorded}$) and the contribution of acetaldehyde ionic current ($0.55\, I_{29}^{CHO}$):

$$I_{44}^{CO_2} = I_{44}^{Recorded} - 0.55 I_{29}^{CHO} \quad (4\text{-}2)$$

Hence, A_{CO_2} is given by:

$$A_{CO_2} = \frac{I_F^{CO_2}}{I_F} = \frac{6 \cdot I_{44}^{CO_2}}{K^* I_F} \quad (4\text{-}3)$$

Here, *6* is the number of electron transferred per one carbon atom during the complete oxidation of ethanol to CO_2 and K^* is the calibration constant calculated from CO calibration experiment (cf. chapter 2, part 2.3.3.2).

Calculation of the true acetaldehyde current efficiency (A_{29})

Due to incomplete mixing occurs in the dual thin layer cell at high flow rate, as pointed out before in chapter 1, part 1.7.3, the experimental current efficiencies of acetaldehyde will be too high if calibration is simply achieved by an electrolyte with a known product concentration. To find out the reliable current efficiencies, the oxidation of 0.05 M i-propanol in 0.5 M H_2SO_4 at smooth Pt(Poly) was done (cf. Fig. 4-4A) under identical experimental conditions to that of ethanol for which the Faradaic current efficiency is 100 %; the product (acetone) has a similar diffusion coefficient and volatility as acetaldehyde.

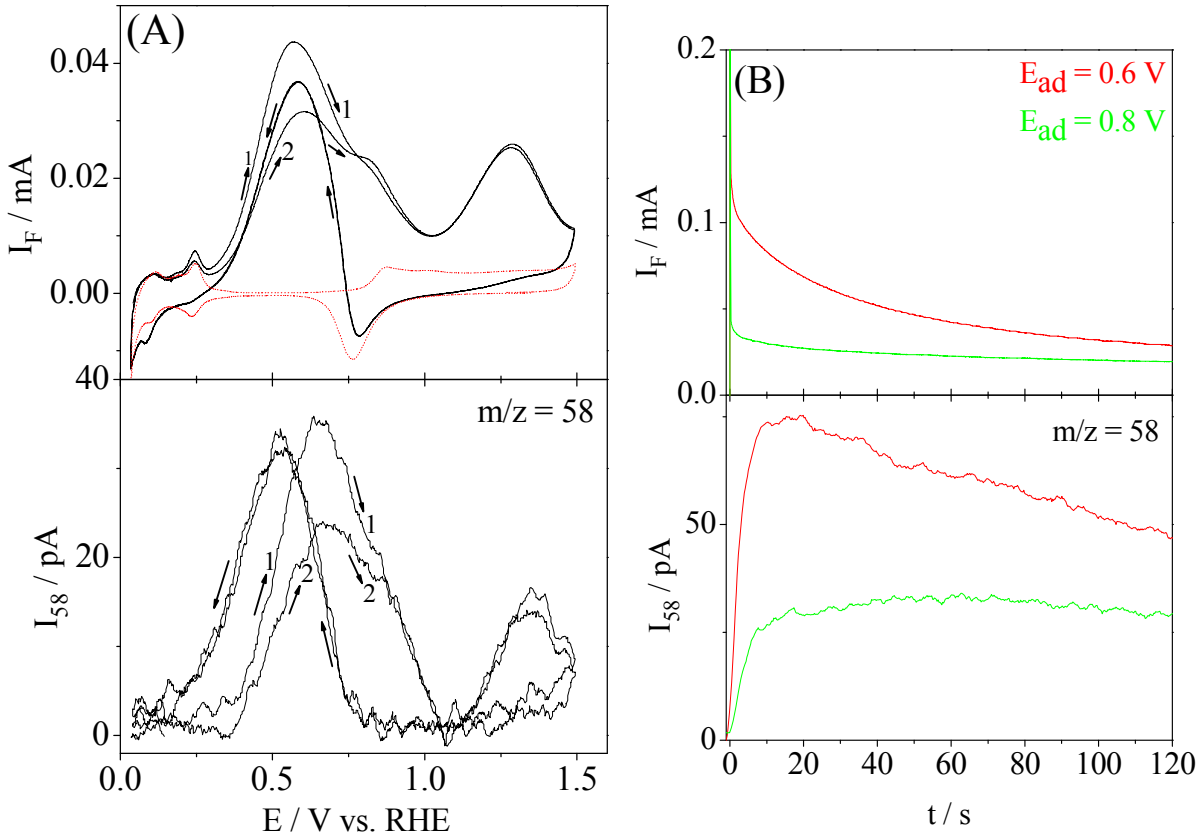

Figure 4-4 (A) Potentiodynamic and (B) Potentiostatic oxidation of 0.05 M i-propanol + 0.5 M H_2SO_4 solution at smooth Pt(Poly). The Faradaic currents were recorded simultaneously with the ionic currents in each case at flow rate = 5 μLs^{-1}, sweep rate = 10 mVs^{-1} (in A). For comparison, the CV recorded in pure supporting electrolyte is shown in (A) (red line).

During the positive going sweep, the broad oxidation peak at 0.6 V starts at 0.35 V was followed by another peak in the oxygen region at 1.3 V [9] while an oxidation peak at 0.58 V was observed during the negative going sweep after complete electroreduction of platinum oxides. No ionic currents corresponds to the formation of CO_2 (m/z = 44) was detected during i-propanol oxidation rather, acetone (m/z = 58) was the only detected ionic current in agreement with references [9-11]. The Faradaic and ionic currents transients recorded at 0.6 V and 0.8 V for i-propanol oxidation as shown in Fig. 4-4B were less steeper at 0.6 V and almost constant with time at 0.8 V when compared to the corresponding transients recorded at the same potentials in case of ethanol oxidation (cf. Fig. 4-3A). This is obviously due to much higher degree of surface poisoning with adsorption products (including CO_{ad}) in case of ethanol while acetone is formed as the main adsorbate in case of i-propanol.

As mentioned in chapter 2, the slope of the linear relationship between the ionic current (I_x) and the concentration (C_x) gives the calibration constants for acetaldehyde or acetone times the flow rate dependent collection efficiency (f_2) of the detection compartment and the flow rate of the electrolyte (u) [12] according to:

$$I_x = f_2 u K_x^o C_x \tag{4-4}$$

In the limiting case of very low flow rate, $f_2 = 1$ and in the calibration experiment I_x is proportional to u. At high flow rates, also f_2 depends on u. Here, $x = 29$ (acetaldehyde), 58 (acetone), I_x is the ionic current of x species, f_2 is the collection efficiency of the detection compartment and C_x is the concentration of x species, K_x^o is defined from: $I_x = K_x^o \cdot \frac{dn}{dt}$ with $\frac{dn}{dt} = f_2 u C_x$ which is the incoming flow of the species x in mol s^{-1}.

In an electrochemical experiment, the concentration C_x in the detection compartment is determined by the product formation rate in the electrochemical compartment:

$$C_x = \frac{I_F A}{zFu} \tag{4-5}$$

Here, I_F is the Faradaic current, A is the current efficiency, z is the number of electrons transferred and F is the Faraday's constant.

This, however, is the average concentration which only identical to the concentration at the surface of the Teflon membrane (which determines the flow into the mass spectrometer and thus the ion current) if a complete mixing occurs in the electrolyte before it enters the detection compartment (this is only the case at flow rates below 1 $\mu L s^{-1}$ [13, 14]). At higher flow rates, the concentration close to the Teflon membrane is higher than the average due to laminar flow and incomplete mixing in the electrolyte.

In case of complete mixing, the transfer efficiency N (the ratio of the species entering the mass spectrometer ($\frac{dn}{dt} = f_2 u C_x$) to the amount of species formed at the electrode ($I_F A/zF$) is identical to the collection efficiency f_2 of the detection compartment (ratio of the number of species entering the mass spectrometer to the amount entering the detection compartment).
In that case,

$$I_x = f_2 u K_x^o \cdot (I_F A/zFu) = f_2 K_x^o I_F A/zF\ , \tag{4-6}$$

and calibration as described before holds (cf. chapter 2, part 2.3.3.3); the current efficiency is given by:

$$A = \frac{I_x zF}{f_2 K_x^o I_F}$$

At high flow rate, the residence times in the connecting capillaries is not sufficient for a complete mixing or inter diffusion to occur, and therefore:

$I_x = NK_x^o I_F A/zF$, with $N>f_2$ (4-7)

Or $A^{true} = \frac{I_x zF}{NK_x^o I_F}$

Whereas in that case, $\frac{I_x zF}{f_2 K_x^o I_F} = A^{app} > A^{true} = A$

In order to determine the ratio between N and f_2, we used the electrooxidation of i-propanol to acetone, which is occurring with a current efficiency of 100 %: For similar species, in which the nearly diffusion limited rate of evaporation into the mass spectrometer is similar, the ratio of the transfer efficiency to the collection efficiency will be similar:

$$\frac{N^{acetone}}{f_2^{acetone}} = \frac{N^{acetaldehyde}}{f_2^{acetaldehyde}} \quad (4\text{-}8)$$

The calibration experiment with a solution of acetone gives $f_2 K_{58}^o$ according to equation (4-4):

$$f_2 K_{58}^o = \frac{I_{58}^a}{C_{58} u} \quad (4\text{-}9)$$

I_{58}^a is the ionic current of acetone recoded during acetone calibration.

Electrooxidation of i-propanol leads to a value of $N^{acetone} K_{58}^o$ according to equation (4-7):

$$N^{acetone} K_{58}^o = \frac{I_{58}^b zF}{I_F} \quad (4\text{-}10)$$

I_{58}^b is the ionic current of acetone produced during i-propanol oxidation.

Hence, $\frac{N^{acteone}}{f_2^{acetone}} = \frac{I_{58}^b zF}{I_F} \cdot \frac{C_{58} u}{I_{58}^a}$ (4-11)

The current efficiency for the oxidation of ethanol to acetaldehyde is then given by:

$$A_{29} = \frac{I_{29} zF}{\frac{N^{acetone}}{f_2^{acetone}} f_2^{acetaldehyde} K_{29}^o I_F} = \frac{I_{29} zF}{N^{acetaldehyde} K_{29}^o I_F} \quad (4\text{-}12)$$

Whereas the apparent acetaldehyde current efficiency is given by:

$$A_{29}^{app} = \frac{I_{29} zF}{f_2 K_{29}^{o} I_F}, \tag{4-13}$$

and that for i-propanol to acetone:

$$A_{58}^{app} = \frac{I_{58} zF}{f_2 K_{58}^{o} I_F} \tag{4-14}$$

The correction factor is then:

$$\frac{A_{29}}{A_{29}^{app}} = \frac{N^{acetaldehyde}}{f_2} = \frac{1}{A_{58}^{app}}, \tag{4-15}$$

since I assume that $A_{58} = 100\ \%$.

Apparent current efficiencies for acetone of *171 %* at 2 μLs^{-1}, *290 %* at 5 μLs^{-1} and *400 %* at 10 μLs^{-1} calculated after the potentiostatic i-propanol oxidation at Pt(Poly) electrode at 0.6 V (peak potential in the CV, Fig. 4-4A) were used to calculate the true acetaldehyde current efficiencies at each flow rate for polycrystalline as shown in Table 4-1 and at single crystal platinum electrodes as will be shown later.

Table 4-1 summarizes the values of current efficiencies with respect to CO_2 ($A_{CO_2}\%$) and acetaldehyde ($A_{29}\%$) calculated during the potentiodynamic and potentiostatic oxidation of ethanol at smooth Pt(Poly), together with the coverage of ethanol adsorbate calculated using equation (2-6). In general, there was no production of CO_2 but the small CO_2 current efficiencies in the second cycle at 0.7 V may be due to the oxidation of adsorbed intermediates (accompanied by C-C bond splitting) during the first cathodic sweep as mentioned above. In the potentiostatic experiments, there was no production of CO_2. This is in agreement with a previous study [4], where d_6-ethanol was used to better distinguish between the formation of CO_2 and acetaldehyde. The corrected current efficiencies of acetaldehyde are around 100 %, therefore, I concluded that under convection conditions, acetaldehyde is the only ethanol oxidation product at Pt(Poly) and the amount of acetic acid is negligible.

The low current efficiency values for CO_2 seem to be at variance with results obtained by FTIR [5, 15, 16]. For such a comparison, however, the different conditions have to be taken into account: Typically, in FTIR measurements a thin (1 μm), stagnant electrolyte layer with dissolved ethanol is comprised between the electrode and the window. At a concentration of 0.1 mol L^{-1}, the total amount of ethanol in this layer is only 10 nmol cm^{-2} and therefore corresponds roughly to 10 monolayers. This means that a large part of these molecules can adsorb and then be oxidized to CO_2. This situation is completely different in

our thin layer cell (thickness 200 µm) and when working under convection: the number of molecules reaching the surface are much larger, but only a small percentage is strongly adsorbed and oxidized to CO_2, the larger part is oxidized via weakly adsorbed intermediates to acetaldehyde and acetic acid. The above results (negligible current efficiency for CO_2) confirm that CO_2 is only evolved from the strongly bound adsorbate in cyclic voltammetry, whereas at constant potential, the reaction to acetaldehyde and acetic acid is occurring continuously and no CO_2 is formed.

Table 4-1 Carbon dioxide and acetaldehyde current efficiencies calculated during the potentiodynamic and potentiostatic oxidation of ethanol at smooth Pt(Poly) at different flow rates and potentials together with the corresponding CO_{ad} coverage for the oxidation of ethanol adsorbate.

u / µLs^{-1}	Potentiodynamic measurements						Potentiostatic measurements				
	E / V vs. RHE	1st cycle			2nd cycle		E / V vs. RHE	I_F /mA	A_{CO_2} %	ϑ_{CO} %	A_{29} %
		A_{CO_2} %	A_{29}^{app} %	A_{29} %	A_{CO_2} %	A_{29} %					
2	0.55[a]	n.d.	n.d.	n.d.	0	100	0.5	0.013	1.4	18	102
	0.7[a]	0	163	95	10	78	0.6	0.04	0	8	100
	0.8[a]	0	157	92	0.8	69	0.7	0.066	0	4	105
	1.3[a]	0	134	78	0	70	0.8	0.055	0	2	92
	0.65[c]	0	147	86	0	85					
5	0.55[a]	n.d.	n.d.	n.d.	0	100	0.5	0.016	0	16	99
	0.7[a]	0	237	82	15	80	0.6	0.046	0	7	97
	0.8[a]	0.6	226	78	0	67	0.7	0.068	0	2	99
	1.3[a]	1.3	198	68	0	73	0.8	0.06	0	1	90
	0.65[c]	0	247	85	0	82					
10	0.55[a]	n.d.	n.d.	n.d.	0	92	0.5	0.018	0.6	20	102
	0.7[a]	2	309	77	19	71	0.6	0.048	0	7.5	103
	0.8[a]	5	279	69	0.3	56	0.7	0.07	0	2.8	95
	1.3[a]	0.1	294	74	0.1	60	0.8	0.06	0	1.6	91
	0.65[c]	0	281	70	0	70					

a: anodic c: cathodic "n.d.": not determined.

A_{29}^{app} : Example of the apparent acetaldehyde current efficiencies.

4.2.2 Electrooxidation at Pt(11,1,1) and Pt(311) stepped single crystal electrodes

4.2.2.1 Electrooxidation of pre-adsorbed CO

Effect of Sn surface modification

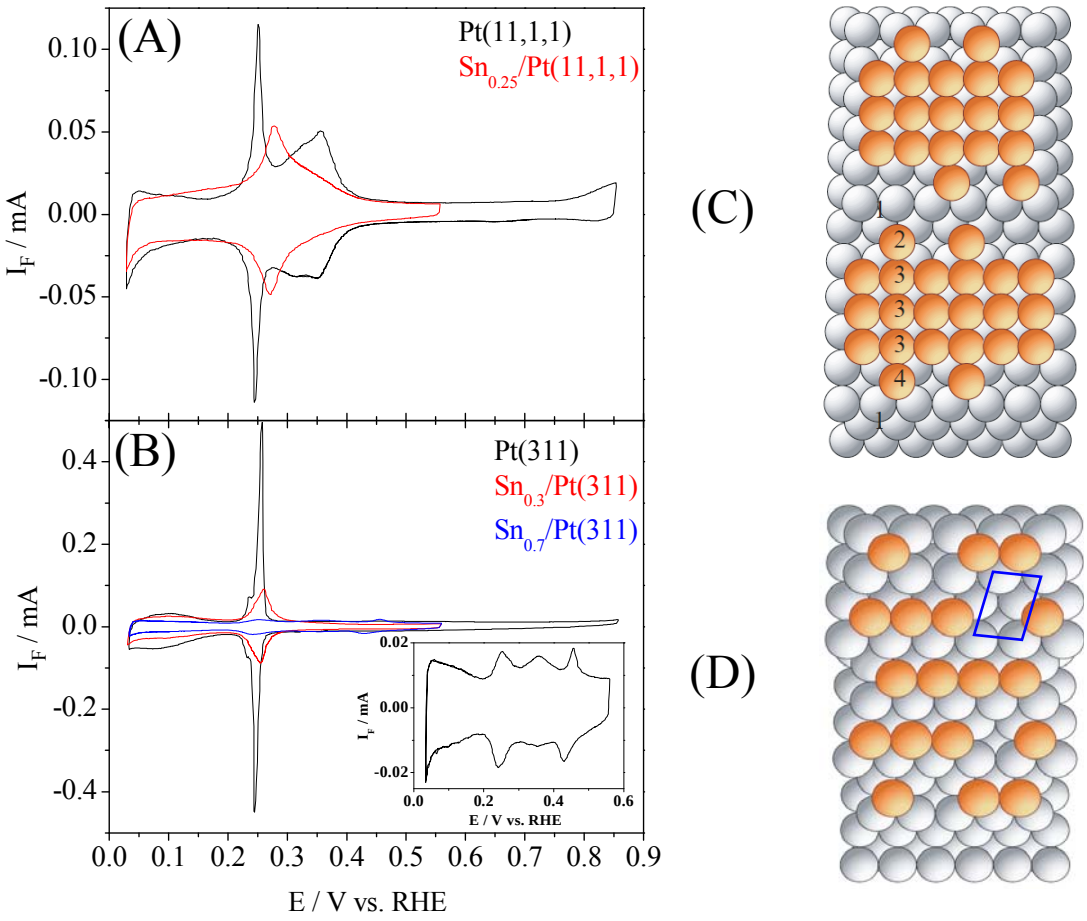

Figure 4-5 (A) CVs of Pt(11,1,1) and (B) Pt(311) before and after Sn deposition in 0.5 M H_2SO_4 solution in the conventional H-cell with sweep rate of 50 mVs^{-1}. Inset in (B): Enlarged view of the CV in case of $Sn_{0.7}$/Pt(311) surface. (C) and (D) Model for Sn deposition at Pt(11,1,1) and Pt(311) respectively, the numbered sites in (C) involve step sites (2) terrace sites (3) and step edge site (4). The adsorption position for hydrogen at (111) sites is indicated by (1). The surface unit cell is shown in (D).

Fig. 4-5A and B shows the typical CVs for Pt(11,1,1) and Pt(311) electrodes respectively recorded in H-cell before and after deposition of Sn. The current below 0.2 V in the CV of clean Pt(11,1,1) is due to hydrogen adsorption at (111) step sites and the sharp peak at about 0.25 V is attributed to hydrogen and anion adsorption at terrace atoms adjacent to (111) step sites (terrace edge) [17]. This peak was followed by a small peak at 0.35 V attributed to the hydrogen adsorption at (100) terraces. Comparing to Pt(11,1,1), with

increasing step density in case of Pt(311), the peak at 0.35 V diminishes while that at 0.25 V and the current below 0.2 V increases [17].

The peaks at 0.25 V and 0.35 V in the CV of Sn modified Pt(11,1,1) were partially and completely suppressed respectively, this is due to filling of the (100) terrace sites with Sn before the step sites (cf. Fig. 4-5C). Similar behavior has been observed before for Cu-UPD on surfaces vicinal to (100) terraces [17, 18]. Cu atoms were preferentially deposited on Pt(100) terrace sites in which one copper atom is coordinated by four platinum atoms due to square symmetry while on Pt(111) it coordinates only to three due to hexagonal symmetry. Interesting is the positive shift of the first peak at 0.25 V to about 0.28 V when the Sn coverage is in the range of 25 %, this behaviour was reported before for Pt(100) electrode modified with about 24 % of Sn by El-Shafei et al. [19] and also for Pt(100) modified by Cu-UPD [17]. This might be due to the effect of Sn atoms deposited on terrace edge which can influence the electronic character of unoccupied sites results in the H-UPD peak shift.

The peak at 0.25 V (H_{ads} at (100) terrace sites) as well as the current below 0.2 V (H_{ads} at (111) step sites) decreases with increasing Sn coverage at Pt(311) surface. As shown in Fig. 4-5D, there is only one type of sites for Sn deposition; the four-fold terrace site is identical to the step site. This explains the simultaneous decrease of the peaks for hydrogen adsorption at (111) step sites and at (100) terrace sites. Again, in agreement with Sn modified Pt(11,1,1) by decreasing the terrace width, a small shift of the potential occurs for the first peak at 0.25 V to about 0.27 V after deposition of Sn. At high Sn coverage (ca. 70 %), two new reversible peaks were developed in the CV of Pt(311), which might be due to the adsorption/desorption of anions close to Sn on the step sites (cf. inset in Fig. 4-5B) [20, 21].

After preparation of the single crystals, they were then (or after deposition of Sn) transferred to the DEMS cell, in which they were cleaned by adsorption and subsequent oxidation of CO. The Faradaic current (I_F) and the mass spectrometric ionic current (I_{44}) recorded simultaneously during the oxidation of adsorbed CO at Sn free and Sn modified Pt(11,1,1) and Pt(311) are shown in Fig. 4-6A and B respectively. In both surfaces, a significant shift of the main oxidation peak and the prepeak was observed in presence of Sn, the shift also increases with increasing Sn coverage on the surface of Pt(311) from $\theta_{Sn} = 0$ ML to $\theta_{Sn} = 0.75$ ML (cf. Fig. 4-6B).

CO oxidation in two peaks in presence of Sn has been also found before [22, 23] at Sn modified Pt(111) and Pt(332) single crystal electrodes. There and also here in case of Sn modified Pt(11,1,1) and Pt(311) electrodes, the prepeak was not only shifted negatively with increasing Sn coverage but also largely increased due to the change of the electronic

properties of Pt when Sn adsorbed. While the main peak is hardly shifted in case of Sn modified Pt(11,1,1), it is significantly shifted in case of Pt(311) for the case of the very high Sn coverage.

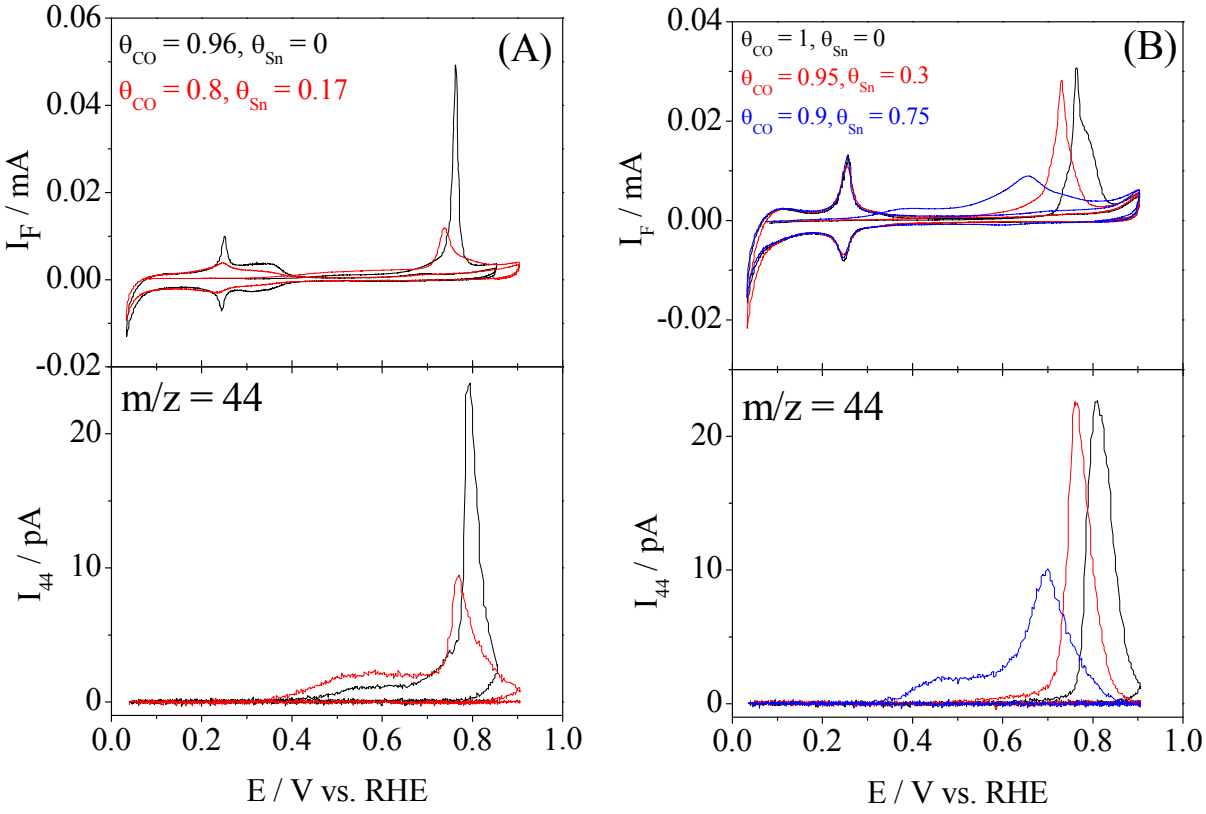

Figure 4-6 The Faradaic current (I_F) and the mass spectrometric ionic current for m/z = 44 recorded simultaneously during the oxidation of pre-adsorbed CO at Sn free and Sn modified Pt(11,1,1) (A) and Pt(311) (B) electrodes with different coverage in 0.5 M H_2SO_4 at 10 mVs^{-1} and 5 μLs^{-1}.

The coverage of Sn was calculated from the charge of adsorbed hydrogen at bare and Sn modified surfaces according to equation (2-8); values are given in Fig. 4-6A and B. Whereas on Pt(11,1,1) the sum of θ_{CO} and θ_{Sn} is approximately 1, as expected, this is not the case for Pt(311): for the surface highly covered by Sn, $\theta_{Sn} + \theta_{CO} = 0.75 + 0.9 = 1.65$. The reason may become clear from the model in Fig. 4-5D: a full monolayer of Sn corresponds to complete monoatomic rows of Sn on the terraces, which are not in direct contact to each other. Deposition of further Sn in the underpotential region could in principle be possible, but would be energetically much less favourable, because such Sn atoms would only coordinate to 2 instead of 5 Pt atoms. In ref. [24], it was shown that one Sn atom suppresses the adsorption of 3 hydrogen atoms. Therefore, it is not astonishing that the relatively open ad-lattice shown in Fig. 4-5D leads to a suppression of 70 % of the hydrogen adsorption charge

(or a coverage of terraces by complete rows of Sn leads to a complete suppression of hydrogen adsorption).

In the above model, complete coverage of Sn corresponds to a surface concentration of Sn of $\Gamma_{Sn} = 1/(S.N_A) = 1.44$ nmol cm^{-2}, (with, S = d^2 (n-1/2)), whereas from the hydrogen adsorption charge ($Q_H = 275$ μC cm^{-2}), the number of adsorption sites is calculated to be $\Gamma_H = 2.85$ nmol cm^{-2}. (Here, S is the area of the surface unit cell, d is the the atomic diameter, n is the number of atomic rows per terrace and N_A is the Avogadro's number = 6.022×10^{23} mol^{-1}) [17]. The theoretical density of adsorption sites is $\Gamma_H = 2.88$ nmol cm^{-2}, assuming 2 adsorption sites per unit cell. Now assuming that CO can adsorb at all sites between the atomic rows of Sn, a coverage of $\Gamma_{CO} = 1.44$ nmol cm^{-2} is calculated corresponding to $\vartheta_{CO} = 0.5$ ML or $\theta_{CO} = 0.83$ ML for a surface fully covered by Sn as stated above. Therefore, a CO coverage of θ = 0.9 ML for a Sn coverage of 0.75 ML is completely reasonable.

4.2.2.2 Electrooxidation of ethanol

Effect of surface structure

The potentiodynamic oxidation of 0.01 M ethanol at smooth Pt(11,1,1) and Pt(311) electrodes is shown in Fig. 4-7A and B respectively. The Faradaic current (I_F) was recorded simultaneously with the ionic currents of m/z = 44 and m/z = 29 in all cases. Similar to Pt(Poly), also at these surfaces ethanol does not adsorb at 0.05 V therefore the hydrogen desorption peak was still visible in the first cycle. This has been examined in an independent experiment by checking the coverage of ethanol adsorbate after stopping the potential at 0.05 V for 2 min followed by electrolyte exchange and sweeping the potential to more positive values.

For Pt(11,1,1), the peak at 0.32 V in the first positive going sweep was larger than in the supporting electrolyte; thus the corresponding change is again not only due to hydrogen desorption but also due to the oxidative adsorption of ethanol (cf. inset of Fig. 4-7A). A small oxidation current of ca. 7 μA leading to the formation of acetaldehyde was visible already at 0.4 V and might have to be ascribed to the oxidation of ethanol at defects. The current increases rapidly at 0.7 V until its maximum at 0.75 V and then decreases again. In the reverse sweep the cathodic peak was centred at about 0.7 V where it gets its maximum value. Due to poisoning of the surface with adsorbed intermediates during the first sweep, the oxidation currents decrease in the second and third cycles.

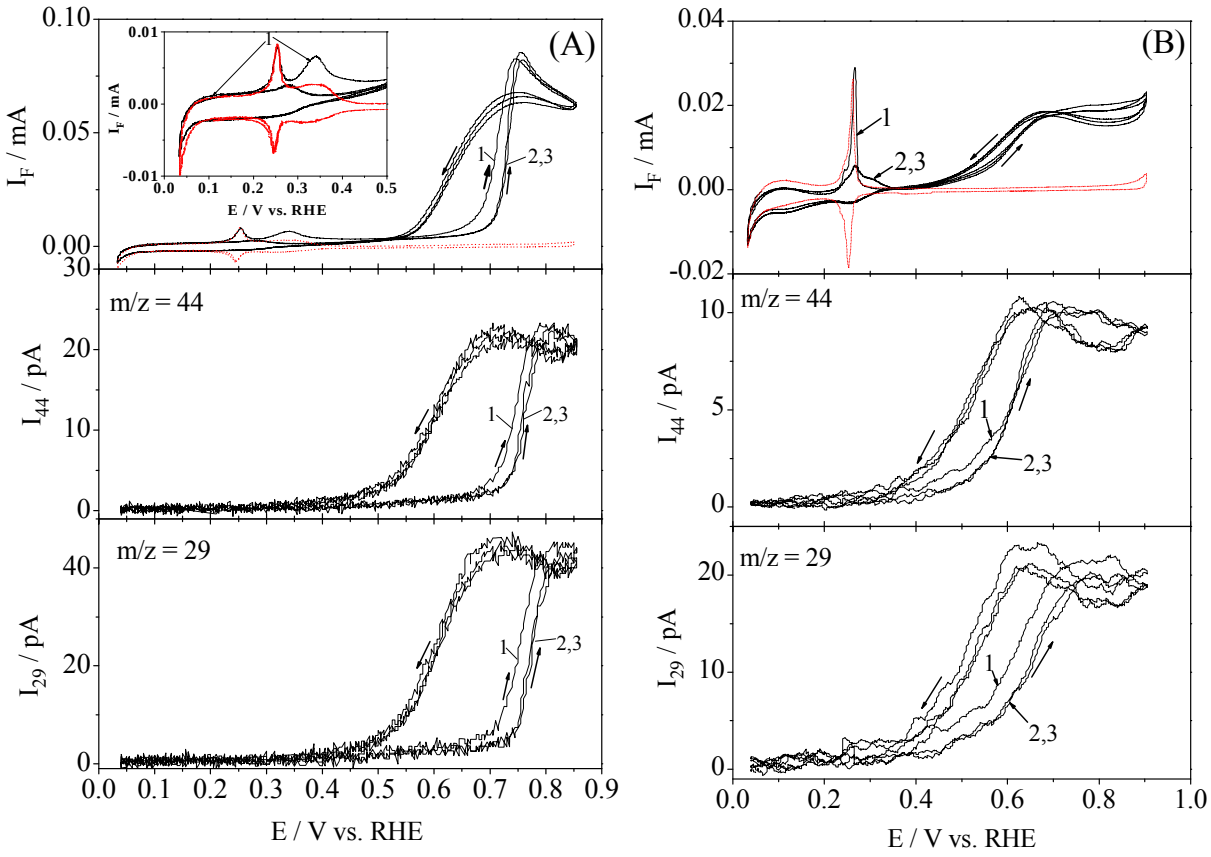

Figure 4-7 Potentiodynamic oxidation of 0.01 M ethanol + 0.5 M H_2SO_4 solutions at smooth Pt(11,1,1) (A) and smooth Pt(311) (B). The Faradaic current was recorded simultaneously with the ionic currents in each case with a sweep rate = 10 mVs^{-1} and electrolyte flow rate = 5 μLs^{-1}. Inset in (A): Enlarged view of I_F in the hydrogen region. For comparison, the CV recorded in the supporting electrolyte is shown (red lines).

At smooth Pt(311), the onset oxidation potential is 0.5 V, similar to surfaces vicinal to the (111) plane (but different from Pt(11,1,1) where it is 0.7 V) [4, 25]. Both the Faradaic and ionic currents at the peak were lower than that for Pt(11,1,1). Colmati et al. [26] reported the low activity behaviour of Pt(211) towards ethanol oxidation compared to Pt(533) and Pt(17,15,15) electrodes. According to their measurements under stagnant conditions, with increasing the (100) steps vicinal to (111) terraces, a decrease in the Faradaic current was observed. By the help of FTIR, they ascribed the small hysteresis between the positive and negative going sweep to a small amount of CO being accumulated at these surfaces.

When extending the sweep above 0.85 V, the deactivation of the surface due to oxygen adsorption above 0.9 V was observed for both surfaces as shown in Fig. 4-8A and B, followed by a broad peak at 1.3 V. At Pt(11,1,1), during the negative going sweep, an oxidation peak

was observed at 0.65 V. Surface poisoning by the adsorbed intermediates formed in the preceding cathodic sweep suppresses the hydrogen desorption peaks in the subsequent anodic sweeps. In the second and third cycles, the oxidation rate and consequently the current increase due to introduction of defects into the surface. Only after roughening, as observed before for Pt(19,1,1) [4], a small oxidation current becomes visible around 0.5 V which is due to acetaldehyde formation.

Only at Pt(311) in the first cycle, the onset of oxygen adsorption was paralleled by an additional peak in the Faradaic and ionic currents at 0.94 V. Comparing the shape and the height of this peak in the Faradaic current to the ionic currents suggests the formation of some acetic acid at this potential. Previous results indicate that the (111) plane is very active in the formation of acetic acid and it can be detected above 0.4 V [27]. During the cathodic sweep, an oxidation peak was present at 0.6 V. In the second and third sweeps, the hydrogen desorption peaks were also suppressed. The onset oxidation potential decreases and the oxidation rate increases due to surface roughening. In addition to the three oxidation peaks observed in the first cycle, another new peak develops in the subsequent cycles located at about 0.77 V.

Carbon dioxide and acetaldehyde current efficiencies calculated during the potentiodynamic oxidation of ethanol at smooth and roughened Pt(11,1,1) and Pt(311) electrodes are listed in Table 4-2. The presented current efficiency values are either calculated at the peak potentials or from the integrated Faradaic and ionic charges during the positive going sweep; integration limits (smooth surface, 0.4-0.85 V) and (roughened surface, 0.4-1 V, to avoid the contribution from the charge of oxygen adsorption above 1 V). For comparison, current efficiencies calculated from the integration of the whole cycle are also presented.

At smooth and roughened Pt(11,1,1), the steep increase of the Faradaic current at 0.7 V makes the comparison of the ionic currents difficult due to the long time constant of the ion detection (3-5 seconds). More reliable current efficiencies are then the ones calculated from the integrated charge. From these results, it is clear that the main ethanol oxidation product is acetaldehyde in accordance with the same reaction at Pt(19,1,1) [4].

Different from Pt(11,1,1) and similar to Pt(poly), CO_2 is produced at Pt(311) electrode as depicted in Table 4-2. Here, the recorded ionic current of m/z = 44 (CO_2 + CH_3CHO) was higher than that due to the contribution of acetaldehyde to m/z = 44 (= 0.55 I_{29}) and hence CO_2 is being formed. It is worth mentioning that after roughening, CO_2 current efficiencies were higher due to the increase of surface defects (compare values at 0.7 V in Table 4-2).

Since the current efficiency for CO_2 and acetaldehyde do not add to 100 %, acetic acid is also produced at smooth and roughened Pt(311) electrode.

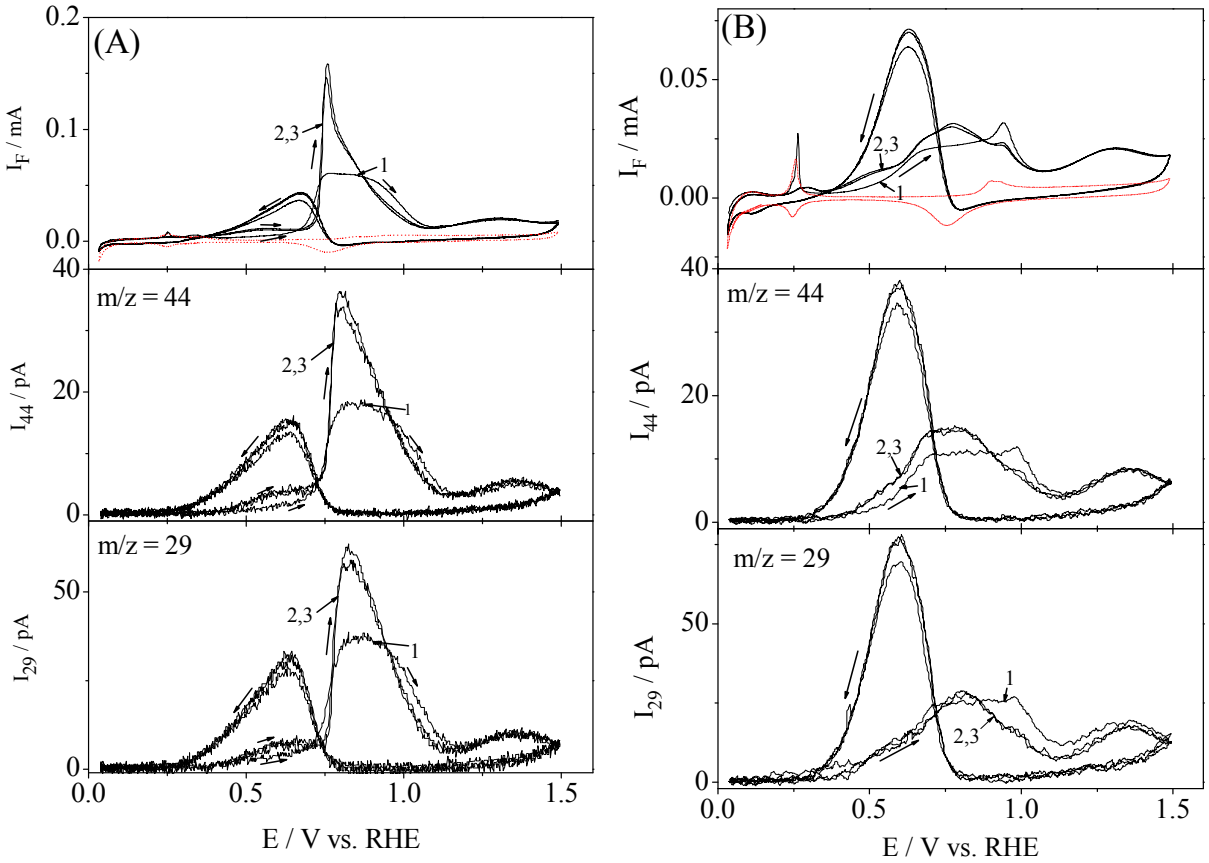

Figure 4-8 Potentiodynamic oxidation of 0.01 M ethanol + 0.5 M H_2SO_4 solutions on Pt(11,1,1) (A) and Pt(311) (B) with an upper potential limit of 1.5 V. The Faradaic current was recorded simultaneously with the ionic currents in each case with a sweep rate = 10 mVs^{-1} and electrolyte flow rate = 5 μLs^{-1}. For comparison, the CV recorded in the supporting electrolyte is shown (red lines).

Table 4-2 Carbon dioxide and acetaldehyde current efficiencies calculated during the potentiodynamic oxidation of ethanol on smooth (s) and roughened (r) Pt(11,1,1) and Pt(311) at different peak potentials or from the oxidation charge at 5 μLs^{-1}.

Surface	Cycle no.	E / V vs. RHE	$A^{p}_{CO_2}$ %	$A^{app,p}_{29}$ %	A^{p}_{29} %	$A^{a}_{CO_2}$ %	$A^{q}_{CO_2}$ %	A^{a}_{29} %	A^{q}_{29} %
s-Pt(11,1,1)	1	0.85	0	296	102	0	0	102	107
	2	0.84	0	296	102	0	0	96	109
	3	0.85	0	294	101	0	0	105	98
r-Pt(11,1,1)	1	0.85	0	315	108	0	n.d.	105	n.d.
		1.3	0	277	96				
	2	0.55	0	295	102	0	n.d.	107	n.d.
		0.75	n.d.	n.d.	n.d.				
		1.3	n.d.	n.d.	n.d.				
	3	0.55	0	298	103	0	n.d.	108	n.d.
		0.75	n.d.	n.d.	n.d.				
		1.3	n.d.	n.d.	n.d.				
s-Pt(311)	1	0.7	0	200	69	1.5	0	86	82
		0.74	0	214	74				
	2	0.7	11	159	55	4	0	67	69
		0.74	3	182	63				
	3	0.7	10	151	52	3	0	65	55
		0.74	7	174	60				
r-Pt(311)	1	0.7	0	220	76	0.7	n.d.	88	n.d.
		0.74	0	232	80				
		0.77	0	217	75				
		0.94	0	174	60				
		1.3	0	176	61				
	2	0.7	14	145	50	3	n.d.	68	n.d.
		0.74	4	153	53				
		0.77	9	162	56				
		0.94	0	140	48				
		1.3	0	168	58				
	3	0.7	19	145	50	3	n.d.	70	n.d.
		0.74	6	153	53				
		0.77	8	159	55				
		0.94	0	156	54				
		1.3	0	168	58				

A^{p}, A^{a} and A^{q} are the current efficiencies calculated at the peak potentials, from the integration of the whole anodic cycle or the whole cycle respectively.
"n.d.": not determined

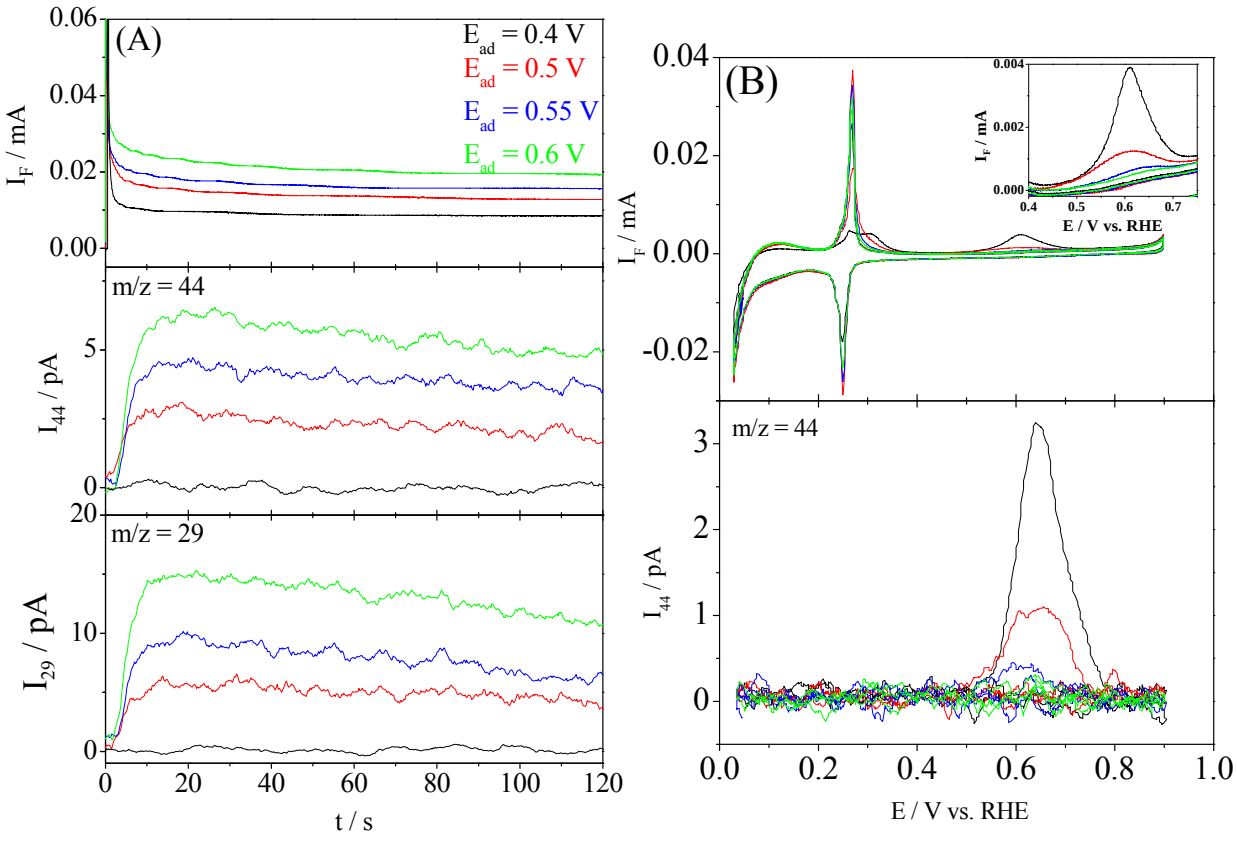

Figure 4-9 (A) Potentiostatic oxidation of 0.01 M ethanol + 0.5 M H_2SO_4 solutions on smooth Pt(311) at different step potentials, the potential was stepped from 0.05 V to different potentials (0.4-0.6 V). (B) The Faradaic and ionic current recorded in 0.5 M H_2SO_4 during the oxidation of ethanol adsorbate at smooth Pt(311) after each potential step experiment. In (B): sweep rate = 10 mVs^{-1}, electrolyte flow rate = 5 μLs^{-1} and inset is an expanded view of the Faradaic current in the ethanol adsorbate oxidation region.

In order to check whether in the CV CO_2 is only due to the oxidation of ethanol adsorption product which had been formed in the preceding cathodic sweeps or is really due to bulk oxidation of ethanol, I performed additional potential step experiments (cf. Fig. 4-9A). The Faradaic and ionic current transients increase with increasing potential. As a general trend for all of the potential step experiments, A_{CO_2} was always zero (cf. Table 4-3) which proves that CO_2 in the potentiodynamic experiments was formed from the oxidation of ethanol adsorbate species. It is worth mentioning that CO_{ad} coverage calculated at Pt(311) surface is lower than that for Pt(Poly) at the same potential (compare ϑ_{CO} in Tables 4-1 and 4-3). As mentioned above, formation of a small amount of CO at Pt(211) has been found before from IR spectra [26]. Here however, DEMS allowed us also to determine the amount of steady state

coverage of CO_{ad}. Again, acetaldehyde current efficiencies in the range of 50-70 % imply the formation of some amount of acetic acid.

It is well known that Pt(311) surface is in the turning point of (2n-1,1,1) series; it can be designated as Pt(s)[2(100)×(111)] or Pt(s)[2(111)×(100)]. The terrace-step model is no longer valid when the terraces are very short. The terrace atoms are affected by the change in the electronic properties caused by the presence of the steps leading to a unique behavior [26]. At Pt(111) under stagnant conditions, it has been found that acetic acid is the main product of ethanol oxidation and acetaldehyde is the secondary one [27]. Recently, the formation of acetic acid on roughened Pt(332) at E < 0.8 V was concluded under flow conditions from the comparison between the Faradaic current due to acetaldehyde formation and the total Faradaic current [4]. Hence, similar to Pt(111) and surfaces vicinal to (111) plane, the formation of acetic acid at Pt(311) was observed.

As shown in Fig. 4-9B, the oxidation of ethanol adsorption product is done after electrolyte exchange with a solution free from ethanol. Again, CO_2 was formed at a potential where usually CO_{ad} is oxidized and the corresponding coverage decrease with increasing the adsorption potential due to increase of their oxidation rate. During the oxidation of ethanol adsorption product formed at 0.4 V, a new peak emerges at 0.33 V in the first positive going sweep and then disappears in the next ones. This peak might be due to anion adsorption on sites adjacent to CO adsorbed on steps. A similar peak was observed during the stripping of Cu at Pt(11,1,1) electrode. It has been also observed during copper deposition at Pt(s)[n(111)×(110)] surfaces and it was ascribed also to anion adsorption on sites adjacent to copper adsorbed on steps (cf. ref. [17] and the references cited therein). Alternatively, partial coverage of some sites by CO changes the adsorption energy for hydrogen adsorbed at sites remaining uncovered by CO.

Table 4-3 Carbon dioxide and acetaldehyde current efficiencies for the potentiostatic oxidation of ethanol on smooth Pt(311) electrode at 5 μLs^{-1} and different step potentials together with the corresponding CO_{ad} coverage for the oxidation of ethanol adsorbate.

E / V vs. RHE	I_F/mA	A_{CO_2} %	ϑ_{CO} %	A_{29} %
0.4	0.008	n.d.	10	n.d.
0.5	0.013	0	7	52
0.55	0.016	0	2	53
0.6	0.02	0	0.8	71

Effect of Sn surface modification

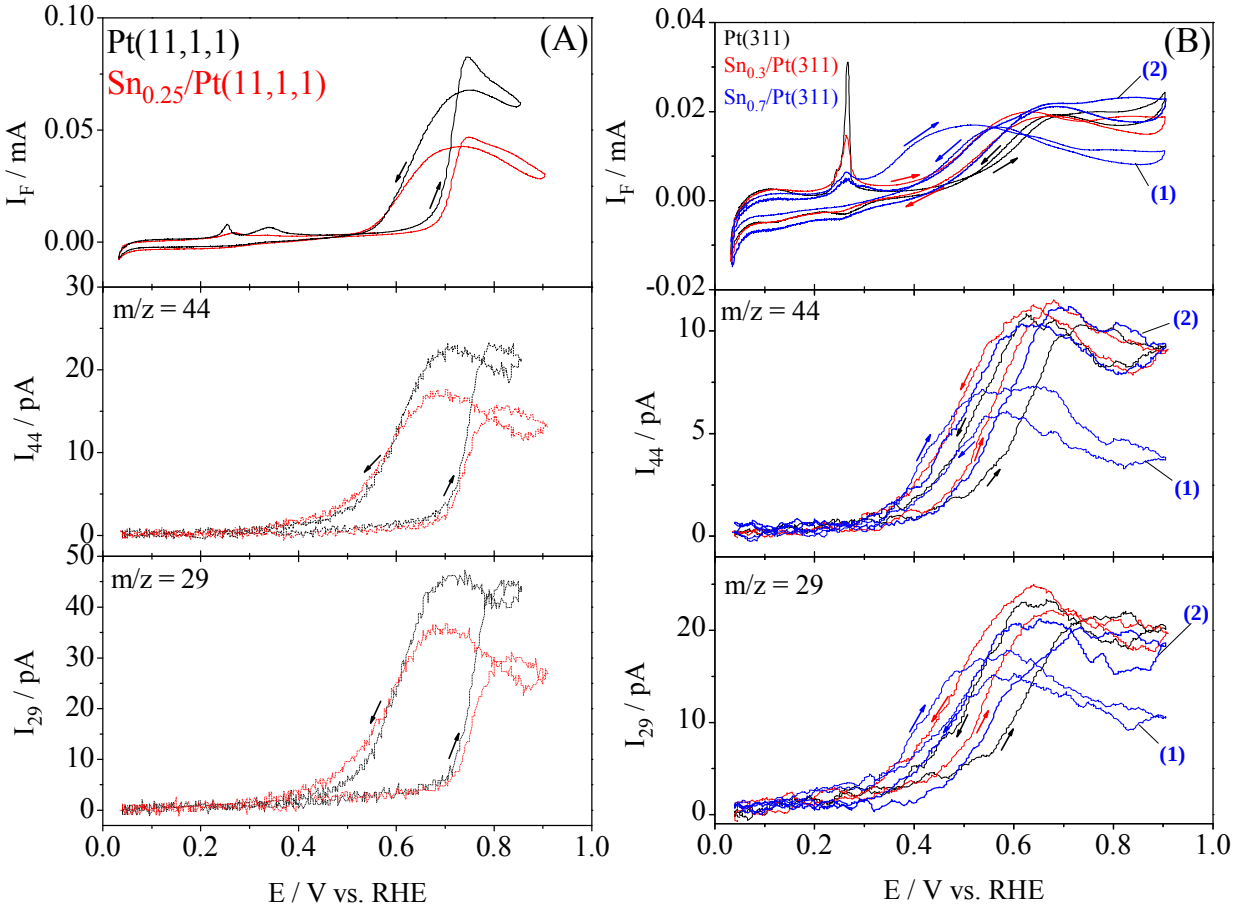

Figure 4-10 Potentiodynamic oxidation of 0.01 M ethanol + 0.5 M H_2SO_4 solutions on Sn modified (A) Pt(11,1,1) and (B) Pt(311) electrodes. The Faradaic currents recorded simultaneously with the ionic currents in each case with sweep rate = 10 mVs^{-1}, electrolyte flow rate = 5 μLs^{-1}. For comparison, the CV recorded in case of bare electrodes is shown. Arrows indicate the direction of sweep. Numbers between brackets indicate the first and second cycles in case of $Sn_{0.7}$/Pt(311) electrode.

The potentiodynamic oxidation of ethanol on Sn modified stepped single crystals is shown in Fig. 4-10A and B for Pt(11,1,1) and Pt(311) respectively. The Sn modified Pt(11,1,1) electrode was less active toward ethanol oxidation than bare Pt(11,1,1). Both Faradaic and ionic currents were inhibited in presence of Sn. The oxidation current of about 7 µA starting at 0.4 V was not affected by the presence of Sn; this is an indication that this current is due to the oxidation of adsorbed ethanol molecules on the nearly uncovered defect sites where Sn is preferentially deposited at terraces.

For Sn modified Pt(311), a significant shift of the onset potential of oxidation to much lower potentials was observed. At higher potentials (0.6 V), the current decreases again because at such high potentials Sn is oxidized [23, 28] (compare cycles 1 and 2 in case of $Sn_{0.7}$/Pt(311) electrode, Fig. 4-10B). At $Sn_{0.7}$/Pt(311) surface, the shift in the onset potential of ethanol oxidation is highest comparing to $Sn_{0.3}$/Pt(311) or bare Pt(311). Also, only at $Sn_{0.7}$/Pt(311), the current increase in the anodic scan occurs at lower potentials than the current decrease in the cathodic sweep. The Faradaic current is increased at low potentials much more than the ionic currents. This implies qualitatively that acetic acid is being produced (See also acetaldehyde current efficiencies in Table 4-4).

The effect of Sn modification on ethanol oxidation was also studied using bead Pt crystals for various surface orientations (notably Pt(100), Pt(110), Pt(111), Pt(11,1,1), Pt(311), Pt(976) and kinked Pt) and different Sn surface coverages in 0.1 M ethanol solution. Of all these surfaces, Pt(311) modified with 70 % to 100 % Sn was the one with the lowest onset potential. This is most likely due to the fact that for adsorbed metal atoms there is only one kind of ad-atom position on this surface, and only monoatomic rows are possible. On other faces, in particular Pt(11,1,1), 2D islands may form on the terraces since step decoration is not favored.

Table 4-4 presents a comparison of the current efficiencies with respect to CO_2 and acetaldehyde calculated for bare and Sn modified Pt(11,1,1) and Pt(311) surfaces either at the peak potentials or from the oxidation charge. Surface modification with Sn hardly affects the product distribution or the current efficiencies comparing to bare surfaces.

In order to check the steady state oxidation products, I performed the potential step experiment as shown in Fig. 4-11, in which the potential was stepped from 0.05 V to different oxidation potentials (0.4-0.6 V). Both Faradaic and ionic current transients increase for 0.4 and 0.5 V and then decrease at 0.55 and 0.6 V due to the dissolution of Sn. Here, comparing to bare Pt(311), a signal for both m/z = 44 and m/z = 29 can be detected at 0.4 V (cf. Fig. 4-9 and 4-11).

Table 4-4 Carbon dioxide and acetaldehyde current efficiencies calculated during the potentiodynamic oxidation of ethanol on Sn modified smooth Pt(11,1,1) and Pt(311) electrodes at different peak potentials or from the oxidation charge at 5 μLs^{-1}.

Surface	Cycle no.	E / V vs. RHE	$A^{P}_{CO_2}$ %	A^{P}_{29} %	$A^{a}_{CO_2}$ %	A^{a}_{29} %
Pt(11,1,1)	1	0.7[c]	0	98	0	102
	2	0.7[c]	0	101	0	104
	3	0.7[c]	0	105	0	107
$Sn_{0.25}$/Pt(11,1,1)	1	0.7[c]	0	104	0	106
	2	0.7[c]	0	103	0	104
	3	0.7[c]	0	97	0	103
Pt(311)	1	0.7	0	69	1.5	86
	2	0.7	11	55	4	67
	3	0.7	10	52	3	65
$Sn_{0.3}$/Pt(311)	1	0.63	3	73	1	68
	2	0.7	6	65	4	65
	3	0.7	4	60	2	58
$Sn_{0.7}$/Pt(311)	1	0.5	2	63	0.8	82
	2	0.7	8	68	3.6	69
	3	0.7	6	57	4	61

A^{p} and A^{a} are the current efficiencies calculated at the peak potentials or from the integration of the whole anodic cycle respectively.
"c": cathodic peak potential.

The above observations imply that Sn adsorbed at the Pt(311) surface facilitates the adsorption and oxidation of ethanol at low potentials. This was proved by comparing the calculated CO_{ad} coverage after the oxidation of ethanol adsorption product formed at low potentials (0.4 and 0.5 V) at $Sn_{0.7}$/Pt(311) and Pt(311) surfaces (Tables 4-3 and 4-5). The coverage were higher at Sn modified Pt(311) while at potentials ≥ 0.55 V, Sn is oxidized and the coverage were similar to bare surface. All CO_2 current efficiencies for Sn modified surfaces were zero and those for acetaldehyde were in the range of 50-70 %; this implies that the co-catalytic effect of Sn was not associated with CO_2 production; rather, acetic acid as well as acetaldehyde are the main oxidation products.

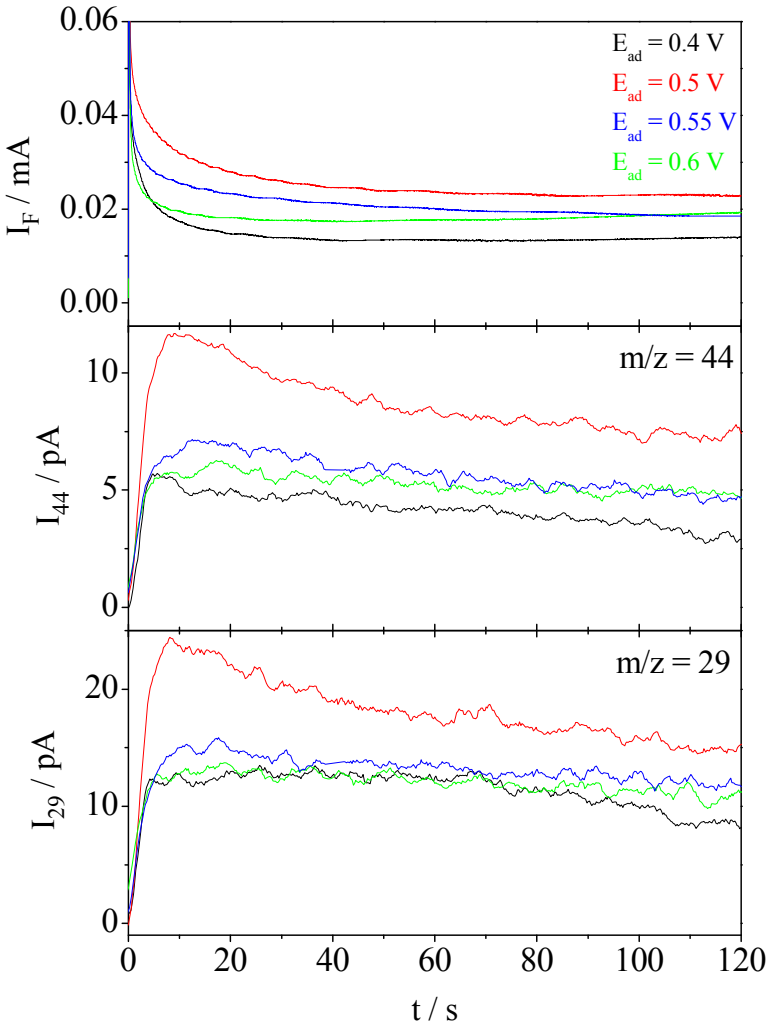

Figure 4-11 Potentiostatic oxidation of 0.01 M ethanol + 0.5 M H_2SO_4 solutions at smooth $Sn_{0.7}$/Pt(311) at different step potentials. The Faradaic and ionic current transients were recorded simultaneously with an electrolyte flow rate = 5 μLs^{-1}.

Table 4-5 Carbon dioxide and acetaldehyde current efficiencies for the potentiostatic oxidation of ethanol on $Sn_{0.7}$/Pt(311) electrode at 5 μLs^{-1} and different step potentials. The corresponding CO_{ad} coverage for the oxidation of ethanol adsorbate was also included.

E / V vs. RHE	I_F/mA	A_{CO_2} %	ϑ_{CO}%	A_{29} %
0.4	0.001	0	17	46
0.5	0.02	0	12	60
0.55	0.013	0	3	55
0.6	0.013	0	1	68

4.3 Conclusions

I have presented a detailed evaluation of the current efficiencies for CO_2 and acetaldehyde during ethanol oxidation at polycrystalline platinum, Pt(11,1,1) and Pt(311) as well as the same single crystal surfaces modified by Sn. Under potentiostatic conditions, the amount of CO_2 is negligible at all surfaces; this is particularly noticeable for the Pt(311) surface modified by Sn, which is particularly active as judged solely from the onset potential of the Faradaic current. To obtain reliable values of the current efficiency for acetaldehyde, a new calibration procedure had to be used: due to incomplete mixing of the electrolyte between electrochemical and detection compartments, experimental current efficiencies are too high if calibration is simply achieved by an electrolyte with a known concentration of the product. I corrected for this by performing additional experiments with i-propanol, for which the Faradaic current efficiency is 100 %; the product (acetone) has a similar diffusion coefficient and volatility as acetaldehyde.

Acetaldehyde was the only product of ethanol oxidation at smooth and roughened Pt(11,1,1). A small oxidation current of ca. 7 μA leading to acetaldehyde formation becomes visible already at 0.4 V. I ascribed this current to the oxidation of ethanol at defect Pt(11,1,1) sites.

At smooth and roughened Pt(311) electrode, a small amount of CO_2 is observed due to the oxidation of the ethanol adsorption product and not due to bulk oxidation of ethanol as proved by a separate potential step experiments. Acetaldehyde current efficiencies are about 50 %; I therefore attributed the rest and the difference in the shapes of CV and mass spectrometric CV to the formation of acetic acid similar to surfaces vicinal to (111) plane.

Both Faradaic and ionic currents of ethanol oxidation at Sn modified Pt(11,1,1) electrode are inhibited in presence of Sn. At Sn modified Pt(311), the onset potential of ethanol oxidation is shifted negatively whereas Sn has no effect at low potentials in case of Pt(11,1,1) electrode. This behavior may be attributed to the easier adsorption and oxidation of ethanol at Sn modified Pt(311) surface. The zero current efficiency for CO_2 in the potential step experiments proves that the effect of Sn is not associated with CO_2 production; rather, both acetic acid and acetaldehyde are the main (only) products of oxidation. Nevertheless, from fundamental point of view, the large cocatalytic effect of Sn is remarkable; it may be due to the formation of monoatomic rows of Sn only on Pt(311), as depicted in Fig. 4-5D.

References

[1] A. A. Abd-El-Latif and H. Baltruschat, Journal of Electroanalytical Chemistry 662:204 (2011).
[2] G. A. Camara and T. Iwasita, Journal of Electroanalytical Chemistry 578:315 (2005).
[3] H. Wang, Z. Jusys, and R. J. Behm, Fuel Cells 4:113 (2004).
[4] A. A. Abd-El-Latif, E. Mostafa, S. Huxter, G. Attard, and H. Baltruschat, Electrochimica Acta 55:7951 (2010).
[5] M. Heinen, Z. Jusys, and R. J. Behm, The Journal of Physical Chemistry C 114:9850 (2010).
[6] A. F. Lee, D. E. Gawthrope, N. J. Hart, and K. Wilson, Surface Science 548:200 (2004).
[7] G. Tremiliosi-Filho, E. Gonzalez, A. Motheo, E. Belgsir, J. Leger, and C. Lamy, Journal of Electroanalytical Chemistry 444:31 (1998).
[8] U. Schmiemann, U. Müller, and H. Baltruschat, Electrochimica Acta 40:99 (1995).
[9] E. Pastor, S. Gonzalez, and A. Arvia, Journal of Electroanalytical Chemistry 395:233 (1995).
[10] T. Hartung, Universität Witten/Herdecke, 1989.
[11] B. Bänsch, T. Hartung, H. Baltruschat, and J. Heitbaum, Journal of Electroanalytical Chemistry 259:207 (1989).
[12] H. Baltruschat, Journal of the American Society for Mass Spectrometry 15:1693 (2004).
[13] J. Fuhrmann, H. Zhao, E. Holzbecher, H. Langmach, M. Chojak, R. Halseid, Z. Jusys, and J. Behm, Physical Chemistry Chemical Physics 10:3784 (2008).
[14] J. Fuhrmann, A. Linke, H. Langmach, and H. Baltruschat, Electrochimica Acta 55:430 (2009).
[15] T. Iwasita and E. Pastor, Electrochimica Acta 39:531 (1994).
[16] V. Del Colle, J. Souza-Garcia, G. Tremiliosi-Filho, E. Herrero, and J. M. Feliu, Physical Chemistry Chemical Physics 13:12163 (2011).
[17] R. Francke, V. Climent, H. Baltruschat, and J. M. Feliu, Journal of Electroanalytical Chemistry and Interfacial Electrochemistry 624:228 (2008).
[18] N. Bogolowski, S. Huxter, A.-E.-A. A. Abd-El-Latif, G. A. Attard, and H. Baltruschat, Journal of Electroanalytical Chemistry 646:68 (2010).
[19] A. A. El-Shafei and M. Eiswirth, Surface Science 604:862 (2010).
[20] E. Herrero, V. Climent, and J. M. Feliu, Electrochemistry Communications 2:636 (2000).
[21] E. A. Abd El Meguid, P. Berenz, and H. Baltruschat, Journal of Electroanalytical Chemistry 467:50 (1999).
[22] H. Massong, H. S. Wang, G. Samjeske, and H. Baltruschat, Electrochimica Acta 46:701 (2000).
[23] H. Massong, S. Tillmann, T. Langkau, E. A. Abd El Meguid, and H. Baltruschat, Electrochimica Acta 44:1379 (1998).
[24] S. Tillmann, G. Samjeske, A. Friedrich, and H. Baltruschat, Electrochimica Acta 49:73 (2003).
[25] S. C. S. Lai and M. T. M. Koper, Faraday Discussions 140:399 (2008).
[26] F. Colmati, G. Tremiliosi-Filho, E. R. Gonzalez, A. Berna, E. Herrero, and J. M. Feliu, Physical Chemistry Chemical Physics 11:9114 (2009).
[27] F. Colmati, G. Tremiliosi-Filho, E. R. Gonzalez, A. Berna, E. Herrero, and J. M. Feliu, Faraday Discussions 140:379 (2009).

[28] Q.-W. Zheng, C.-J. Fan, C.-H. Zhen, Z.-Y. Zhou, and S.-G. Sun, Electrochimica Acta 53:6081 (2008).

5. Determination of the apparent transfer coefficient of methanol oxidation by potential modulation technique under convection conditions

5.1 Introduction

In this chapter, the apparent transfer coefficient for methanol oxidation and for the oxidation of the methanol adsorption product was determined using the recently introduced ac voltammetry method [1]. To ensure fast convectional transport and avoid interference with reaction intermediates, I used the dual thin layer flow through cell, which is typically used for DEMS. Potential sweep and potential step experiments have been performed at Pt(Poly), superimposing a small sinusoidal voltage to the normal dc voltage and the components of the ac current have been recorded. The potential dependence of the electrochemical reaction rate, described by the apparent transfer coefficient (α'), has been recorded quasi continuously as a function of potential or time and the corresponding Tafel slopes have been calculated. In control experiments, using adsorbed CO, values previously determined (cf. chapter 1, part 1.7.1) using the H-cell were reproduced. This demonstrates that the method is applicable to the thin layer cell despite of the high electrolyte resistance which was subtracted by applying a simple mathematical correction to the ac voltage.

5.2 Results and discussion

5.2.1 Electrochemical impedance spectroscopy in the dual thin layer cell

In order to obtain an idea about the possibility of performing ac measurements in the thin layer cell, impedance spectra were recorded for bare Pt(Poly) in the dual thin layer flow though cell (cf. Fig. 5-1) and the R(CR) model was employed to fit the recorded values; fitting data are shown in Table 5-1.

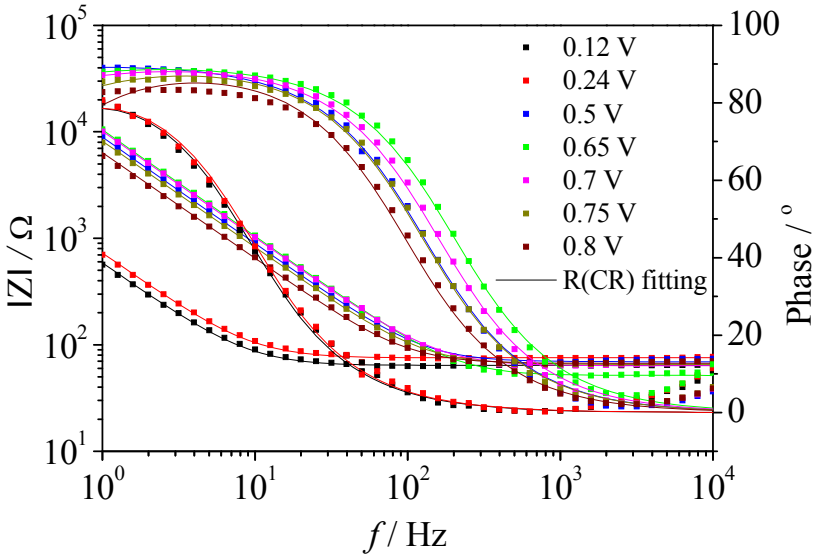

Figure 5-1 The EIS of Pt(Poly) in 0.5 M H_2SO_4 at various potentials. Sweep rate = 50 mVs^{-1} and electrolyte flow rate = 5 μLs^{-1}.

The shape of EIS spectra is as expected for the equivalent circuit of Fig. 5-2 except for low frequencies and high frequencies (> 3×10^3 Hz). The high electrolyte resistance and the bad current distribution may cause this deviation. A comparison between capacitance values calculated from the CV with those obtained after the fitting shows a good agreement (cf. Table 5-1); the reliability of the data was demonstrated by the constant electrolyte resistance and very high charge transfer resistance, which in pure supporting electrolyte should theoretically be infinite. The phase at low frequency changes from 90° to 75° at high potentials. This probably has to be attributed to a slow anion (hydroxide) adsorption at such high potentials which is not included in the simple equivalent circuit shown in Fig. 5-1. These data show that meaningful impedance and ac data can be obtained using the thin layer cell configuration in the above mentioned frequency range.

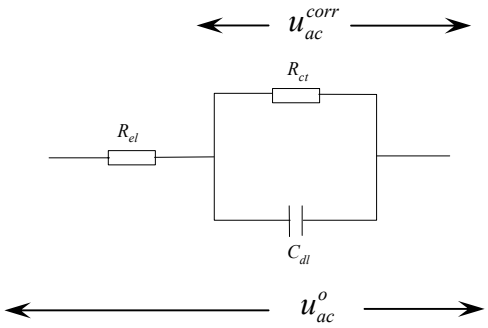

Figure 5-2 Equivalent circuit used for fitting of EIS data during CO and methanol oxidation at Pt(Poly) in the dual thin layer cell.

Table 5-1 The fitting data for EIS on Pt(Poly) using R(CR) model.

E / V vs. RHE	R_{el} / Ω	C_{dl} / F from fitting	C_{dl} / F from CV	R_{ct} / Ω
0.12	64.04	2.7×10^{-4}	3.8×10^{-4}	6373
0.24	75	2×10^{-4}	3.4×10^{-4}	7534
0.5	69.35	1.79×10^{-5}	1.5×10^{-5}	145670
0.65	55.21	1.8×10^{-5}	1.3×10^{-5}	339960
0.7	65.6	1.6×10^{-5}	1.7×10^{-5}	222290
0.75	65.6	1.94×10^{-5}	2.5×10^{-5}	91346
0.8	67.03	2.46×10^{-5}	5×10^{-5}	36919

During CO or methanol oxidation at Pt(Poly), the real part of the ac current is not only given by the charge transfer current and the ad/desorption of ions but also affected by the potential drop in the electrolyte. EIS spectra of Pt(Poly) in the dual thin layer cell showed an electrolyte resistance of about 65-75 Ω cm^2 (cf. Fig. 5-1). This high value, which leads to a high $i_{ac}R$ drop during the superimposed ac potential is due to the high resistance of the thin electrolyte layer and the thin capillary to the inlet as compared to the H-cell with its negligible electrolyte resistance of about 2 Ω cm^2 as reported before [1]. Therefore, I applied an ac potential correction in order to subtract this resistance. Fig. 5-2 shows the simple equivalent circuit which I used for the correction. It consists of a resistance (R_{el}) representing the electrolyte resistance in series with a parallel combination of a capacitor (C_{dl}) representing the double layer capacitance and another resistance (R_{ct}) which represents the charge transfer resistance.

In the equivalent circuit shown above the corrected ac voltage is given by:

$$u_{ac}^{corr} = u_{ac}^{o} - R_{el} i_{ac} \tag{5-1}$$

And the ac current is given by:

$$i_{ac} = \frac{u_{ac}^{corr}}{R_{ct}} + \frac{u_{ac}^{corr}}{Z_c}, \text{ Rearrangement gives, } \frac{i_{ac}}{u_{ac}^{corr}} = \frac{1}{R_{ct}} + \frac{1}{Z_c} \text{ where, } Z_c = 1/j\omega C \tag{5-2}$$

Equation (5-2) can also be written as:

$$\frac{i_{ac}}{u_{ac}^{corr}} = \frac{i_{ac}^{re} + ji_{ac}^{im}}{u_{ac}^{o} - R_{el}(i_{ac}^{re} + ji_{ac}^{im})}$$

$$= \frac{i_{ac}^{re}(u_{ac}^{o} - i_{ac}^{re}R_{el})}{(u_{ac}^{o})^2 - 2u_{ac}^{o}R_{el}i_{ac}^{re} + (R_{el}i_{ac}^{re})^2 + (R_{el}i_{ac}^{im})^2} + j\frac{i_{ac}^{im}(u_{ac}^{o} - i_{ac}^{im}R_{el})}{(u_{ac}^{o})^2 - 2u_{ac}^{o}R_{el}i_{ac}^{re} + (R_{el}i_{ac}^{re})^2 + (R_{el}i_{ac}^{im})^2}$$

$$= Y_{re-corr} + jY_{im-corr}$$

Here, $Y_{re\text{-}corr}$ and $Y_{re\text{-}corr}$ are the corrected real and imaginary parts of the admittance.

In chapter 1, part 1.2 it was shown that the potential dependence of the rate (α') can be calculated in a very narrow potential range (the ac amplitude) as follows:

$$\alpha' = \frac{RT}{F} \cdot \frac{i_{ac-re}}{u_{ac} i_{dc}} \tag{5-3}$$

By replacing (u_{ac}) in equation (5-3) by (u_{ac}^{corr}), the corrected apparent transfer coefficient can be determined by:

$$\alpha_{corr}' = \frac{RT}{F} \cdot \frac{i_{ac}}{i_{dc} u_{ac}^{corr}} = \frac{RT}{F} \cdot \frac{Y_{re\text{-}corr}}{i_{dc}} \tag{5-4}$$

And the Tafel slope is then given by:

$$\frac{\partial E}{\partial \ln i} = \frac{RT}{\alpha_{corr}' F} \tag{5-5}$$

As an appropriate ac frequency, I chose (33.5 Hz) in accordance with literature [1] in order to meet the requirements mentioned before in chapter 1, part 1.2; i.e. the relative changes of CO and OH coverage remain constant during the sampling time (one ac period, ca. 30 ms). At ac frequencies considerably lower than 33.5 Hz, the relative changes in the function $f(\theta_{CO}(1-\theta)$ would not be negligible, at considerably higher frequencies, the influence of the slow anion adsorption/desorption process discussed before by Wang et al. [1, 2] would become too large. Moreover, the frequency should be so low that the capacitive current through C_{dl} is not too large.

5.2.2 Electrooxidation of CO at Pt(Poly) in the dual thin layer cell

5.2.2.1 Potential sweep experiments

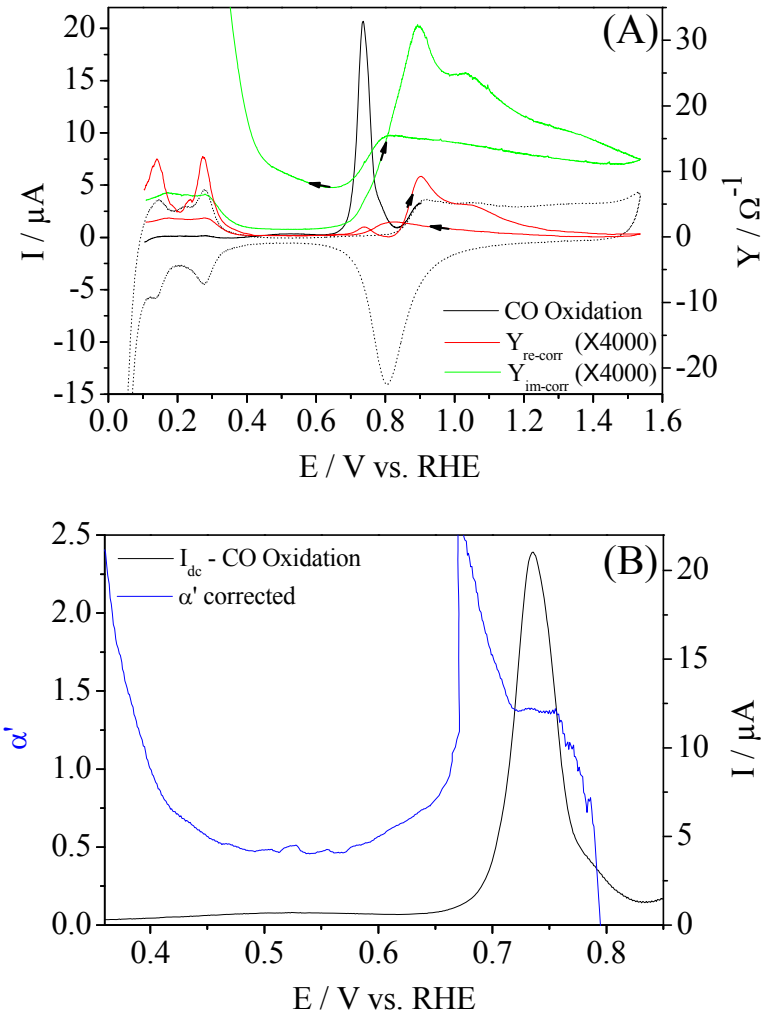

Figure 5-3 (A) The oxidation of adsorbed CO at Pt(Poly) in 0.5 M H_2SO_4. Black: dc current; Red: corrected real part of the admittance; Green: corrected imaginary part of the admittance; Dotted line: CV in CO-free electrolyte. (B) Blue: Apparent transfer coefficients (α') calculated from corrected ac voltage; Black: expanded view of the dc current in the CO oxidation region. u_{ac} = 1 mV, f = 33.5 Hz, sweep rate = 10 mVs^{-1} and electrolyte flow rate = 5 μLs^{-1}.

Fig. 5-3A displays the dc current and the corrected real and imaginary parts of the admittance recorded during the oxidation of adsorbed CO at Pt(Poly) as a function of potential. A pre-peak at about 0.5 V and a main peak at about 0.73 V can be observed similar to those observed before [1, 3-7]. The total charge density for CO oxidation, calculated by integration from 0.3-0.8 V, is 351 µC cm^{-2} including the double layer charging [8].

The corrected real part of the admittance *($Y_{re\text{-}corr}$)*, which represents the ratio between the real part of the ac current and the corrected ac voltage, is expanded by a factor of (4000) for better comparison. $Y_{re\text{-}corr}$ is somewhat high in the hydrogen region (0.1-0.4 V) due to incomplete correction (compensation) of the high electrolyte resistance in this region A control experiment, in the H-cell (cf. Fig. 5-4) shows that, under the condition of low electrolyte resistance, the real part of the ac current is almost zero at a potential lower than 0.45 V. Small values of $Y_{re\text{-}corr}$ are obtained in the region (0.4-0.6 V) i.e. below the onset of the main peak; afterwards, a peak at the same potential as for the dc current is observed (cf. Fig. 5-3A). (A further large peak at 0.9 V is due to the oxygen adsorption reaction).

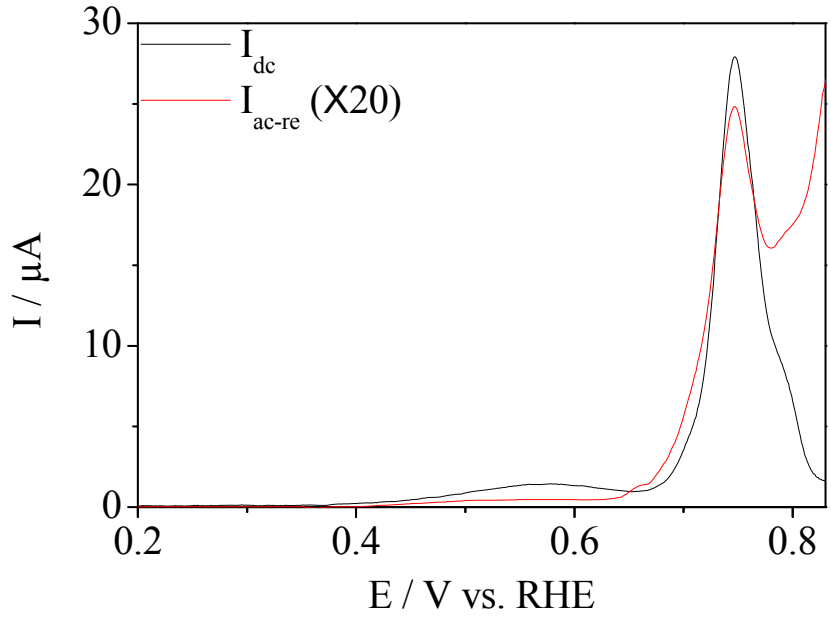

Figure 5-4 The oxidation of adsorbed CO at Pt(Poly) in the H-cell in 0.5 M H_2SO_4. Sweep rate = 50 mVs^{-1}.

The blue lines in Fig. 5-3B show the apparent transfer coefficient calculated according to equation (5-4) with a correction for the ac iR drop. The value of α' after correction around the pre-peak at 0.5 V is 0.48 (corresponding to a Tafel slope of 123 mV dec^{-1}) and around the main peak at 0.73 V is 1.4 (Tafel slope of 42 mV dec^{-1}). Wang et al. [1] reported apparent transfer coefficients of 0.53 at 0.54 V for the pre-peak and 1.39 at 0.69 V for the main-peak when he performed the same experiment in the normal H-cell under stagnant conditions. The constant coefficient measured around the main peak i.e., for CO coverage between ca. 0.3 and 0.7, is most reliable since the corresponding signal of both ac and dc current are higher than that at higher or lower coverage, where contributions from background may be dominating. (values calculated for α' are shown here for the complete potential range, although, of course,

they are not meaningful at potentials where the dc current is small or dominated by processes other than CO oxidation). What is not clear at this point is the large value of α' between 0.65 V and 0.7 V, which is also observed before by Wang et al. [1]. This might be related to the initial nucleation period (formation of the first CO free sites)

5.2.2.2 Potential step experiments

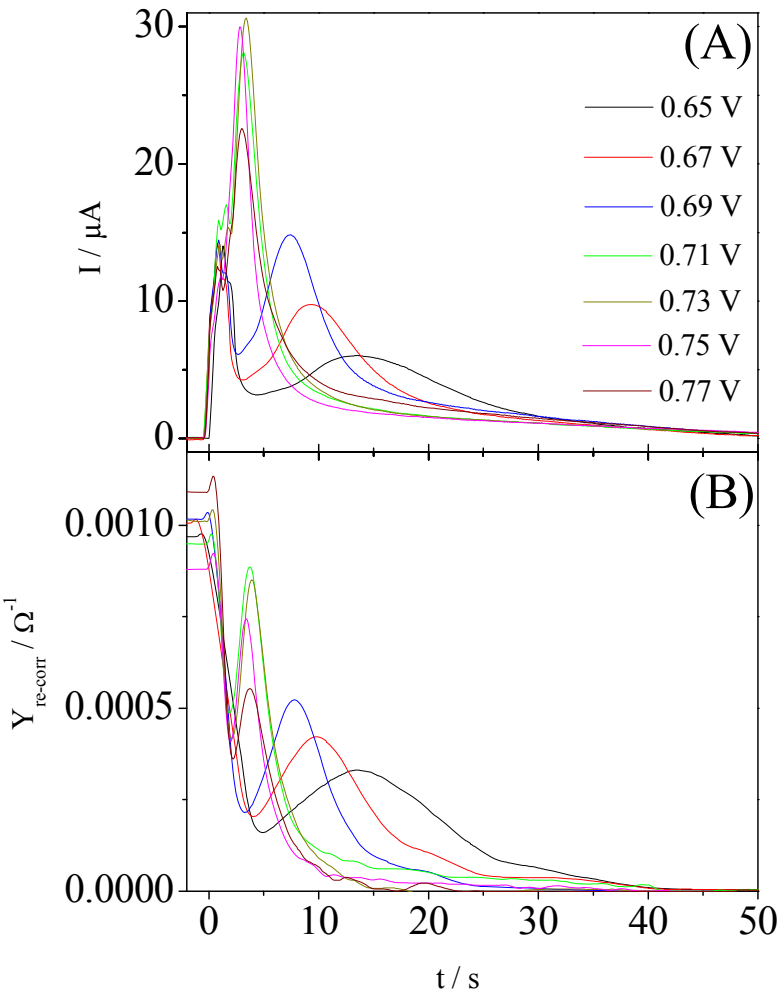

Figure 5-5 (A) The dc current transients, (B) corrected real part of the admittance transients for the oxidation of CO at Pt(Poly) at various stepped potentials in 0.5 M H_2SO_4. u_{ac} = 3 mV, f = 33.5 Hz and electrolyte flow rate = 5 µLs^{-1}.

Fig. 5-5A shows the dc current transients recorded during the oxidation of CO after potential steps to various potentials on Pt(Poly) in the dual thin layer flow through cell. The corrected real part of the admittance transients are displayed in Fig 5-5B. As a general trend, with increasing potential, i_{max} increases and t_{max} decreases. As expected, for high step potentials there is no clear trend, because of the large iR drop and the inhomogeneous current distribution which limit the time resolution.

All transients in Fig. 5-5A, start with high and quickly decaying current corresponding to the oxidation of weakly adsorbed CO molecules. This initial current has the same origin as the prepeak in the CV and was identified as being due to CO oxidation by DEMS [9, 10]. Then the current increases rapidly due to an increased availability of free surface sites for oxygen/OH^- adsorption according to the (LH) mechanism.

The corrected transfer coefficients for CO oxidation at Pt(Poly) at various potentials are plotted separately in Fig. 5-6 (A-G) together with the plot of the real part of the corrected admittance transient ($Y_{re\text{-}corr}$) as a function of time. For the CO oxidation at the low potential of 0.65 V, the apparent transfer coefficient after correction around the dc current maximum is calculated to be about 1.3. At relatively high potential of 0.75 V, the coefficient after correction is 0.5. Again, as already discussed in the context of Fig. 5-3, α' is reliable only when the oxidation current is large, i.e. in the vicinity of the peak of i_{dc}.

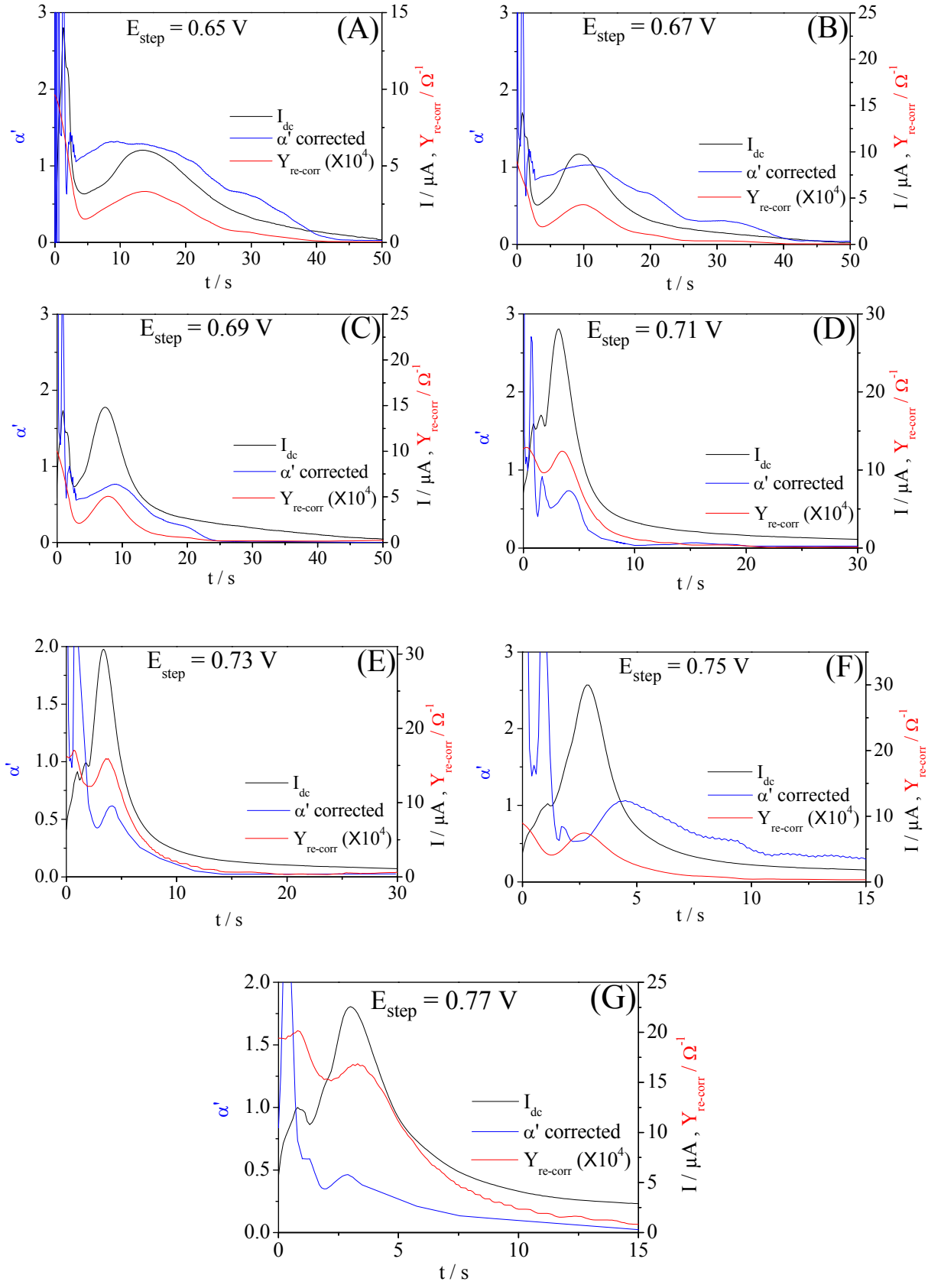

Figure 5-6 The corrected apparent transfer coefficient for the oxidation of pre-adsorbed CO at Pt(Poly) in 0.5 M H_2SO_4 at different potentials together with the dc and the corrected real part of the admittance transients, u_{ac} = 3 mV, f = 33.5 Hz and electrolyte flow rate = 5 μLs^{-1}.

α' values calculated after correction at the dc current peak maximum is plotted versus the step potential in Fig. 5-7. The increase of α' behind the oxidation peak is an artifact caused by the above mentioned slow adsorption of anions (hydroxide). As a general trend, with increasing potential, α' decreases from values around 1.3 to about 0.5. The Tafel slope calculated from the corrected α' values is 45 mV dec^{-1} at 0.65 V, and increases to 120 mV dec^{-1} at 0.75 V. These observations are in a good agreement with Wang et al. [1] except that the α' values after correction are ca. 10 % lower at all potentials, this is again due to the differences between the dual thin layer cell used in this work and the normal H-cell used by Wang et al.

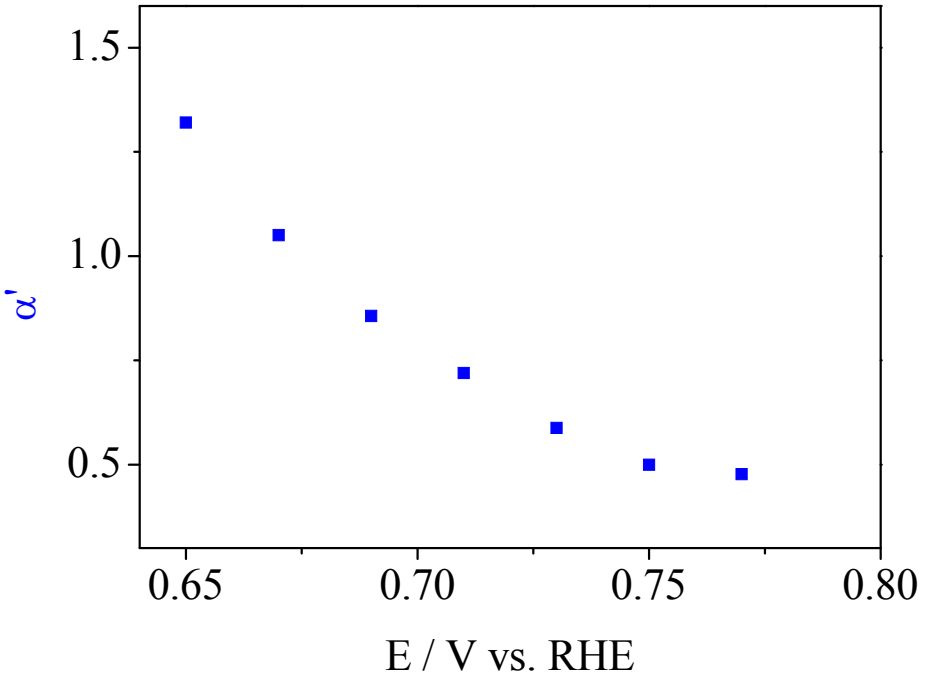

Figure 5-7 The apparent transfer coefficient for the oxidation of pre-adsorbed CO at Pt(Poly) at various potentials determined in the maximum of the current transients of potential step experiments and calculated after correction.

For comparison, the apparent transfer coefficient values were also calculated by plotting *log* t_{max} vs. E_{step} [6, 11, 12] (t_{max} is the time recorded at the maximum current) or by plotting the peak potential in linear sweep experiments vs. the logarithm of the sweep rate [13, 14]. The plot of *log* j_{max} vs. E_{step} also has been used to get the Tafel slope [6] (j_{max} is the maximum current density). The peak current density (j_{max}) and the time of the current maximum (t_{max}) recorded during the above potential step experiments are listed in Table 5-2. From the plot of *log* (j_{max}) and $-log(t_{max})$ versus the potentials, Tafel slopes can be obtained (cf. Fig. 5-8). A Tafel slope of 166.7 mV dec^{-1} was obtained for all the potential range from the plot of $-log(t_{max})$ versus the potential, which is in a good agreement with refs. [1] and [2].

At low potentials, both plots give values of 91.72 mV dec^{-1} and 100 mV dec^{-1} respectively. At high potentials, the slope is much lower and not reasonable due to the change of the surface conditions as suggested before [2] and the high iR drop.

Table 5-2 t_{max} and j_{max} for CO oxidation at Pt(Poly) at various potentials.

E / V vs. RHE	t_{max} / s	-log t_{max}	j_{max} / µA cm^{-2}	log j_{max}	α' corrected
0.65	13.7	-1.13672	21.28	1.32797	1.32
0.67	9.3	-0.96848	34.99	1.54394	1.05
0.69	7.4	-0.86923	52.37	1.71908	0.82
0.71	3.2	-0.50515	99.19	1.99647	0.72
0.73	3.4	-0.53148	108.23	2.03435	0.62
0.75	2.8	-0.44716	105.94	2.02506	0.5
0.77	3	-0.47712	79.79	1.90195	0.5

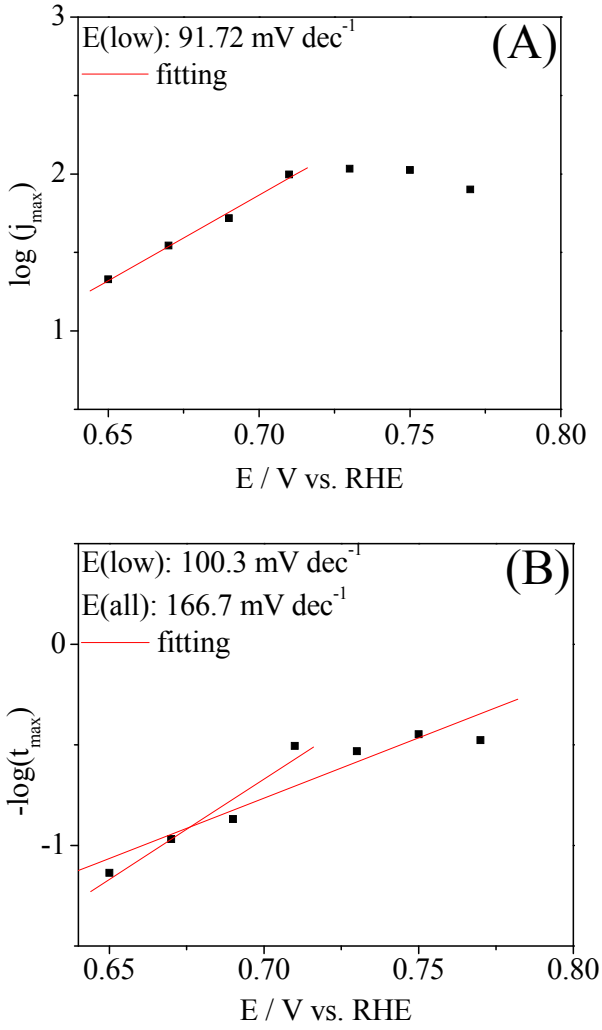

Figure 5-8 Tafel slopes for CO oxidation at Pt(Poly) obtained by plotting log(j_{max}) vs. E (A) and –log(t_{max}) vs. E (B).

5.2.3 Electrooxidation of methanol at Pt(Poly) in the dual thin layer cell

5.2.3.1 Potential sweep experiments

Fig. 5-9 shows the dc and ac cyclic voltammograms recorded during bulk oxidation of 10^{-2} M methanol + 0.5 M H_2SO_4 solution at Pt(Poly) in the dual thin layer flow through cell. In the positive going scan the oxidation starts at 0.4 V giving rise to a shoulder due to oxidative adsorption of methanol [15-17]. Above 0.6 V, the Faradaic current starts to increase sharply during the first anodic sweep, leading to an oxidation peak at 0.75 V. During the negative-going scan, an oxidation peak centered at 0.72 V is observed. The methanol adsorbate formed during the first cathodic sweep below 0.7 V acts as a poison; therefore, in the subsequent anodic cycle the oxidation peak is smaller than in the first cycle. The real part of the corrected admittance recorded in the first and second sweep is also shown here and shows very small values below 0.6 V.

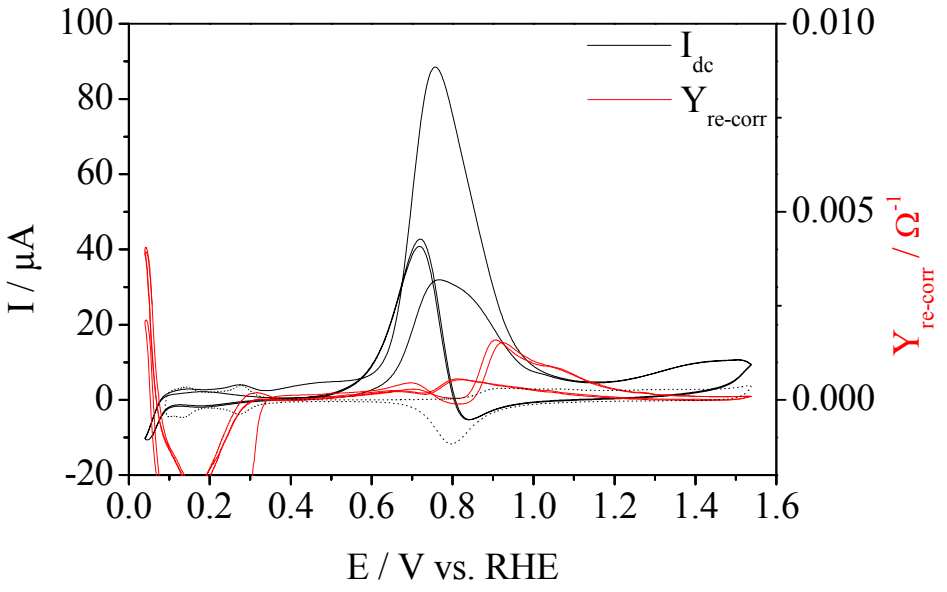

Figure 5-9 Bulk oxidation of 10^{-2} M methanol + 0.5 M H_2SO_4 solution at Pt(Poly). Black: dc current; Red: real part of the corrected admittance, Dotted line: CV in methanol-free electrolyte. Two cycles are shown. u_{ac} = 1 mV, f = 33.5 Hz. Sweep rate = 10 mVs^{-1} and electrolyte flow rate = 5 μLs^{-1}.

The apparent transfer coefficients calculated after ac potential correction together with the corrected real part of the admittance during the first and second cycles of methanol bulk oxidation are displayed in Fig. 5-10 (A and B) for the first and the second cycles respectively. All $Y_{re\text{-}corr}$ calculated below 0.6 V are very small (almost zero) which proves the validity of the ac correction method. At the onset of methanol oxidation, the corrected α' values around

0.5 is calculated (Tafel slope of 118 mV dec^{-1}). Contrary to the case of CO oxidation, the peak in the Faradaic current does not coincide with the peak in the admittance. The reason is the different nature of the peak: positive of the peak, the current decreases due to blocking of the surface with oxygen species and not due to a depletion of the reactant as for adsorbed CO.

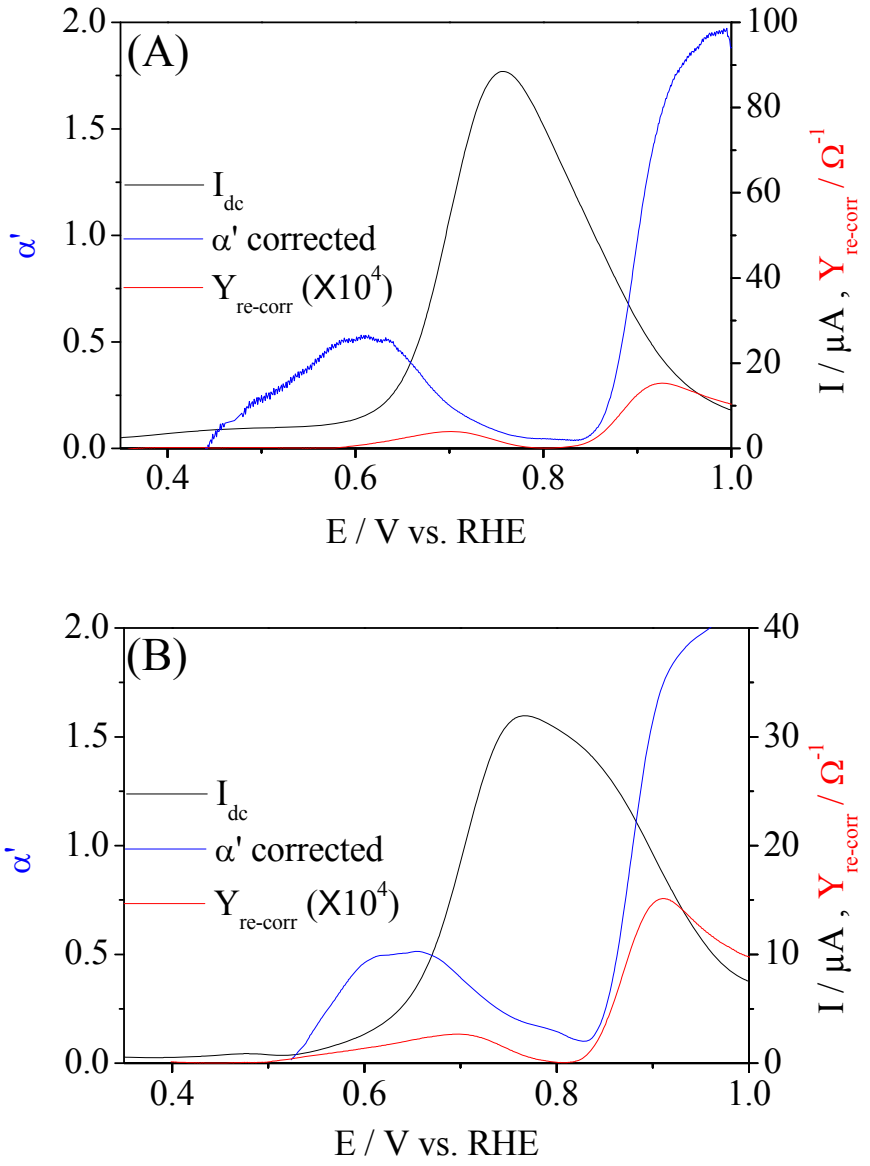

Figure 5-10 The corrected apparent transfer coefficient calculated in the first (A) and second (B) cycles of methanol bulk oxidation at Pt(Poly) together with the dc current and the corresponding real part of the corrected admittance. u_{ac} = 1 mV, f = 33.5 Hz. Sweep rate = 10 mVs^{-1} and electrolyte flow rate = 5 μLs^{-1}.

5.2.3.2 Potential step experiments

A series of potential step experiments are also performed in the dual thin layer cell in the onset potential region stating form 0.63 to 0.71 V. Fig. 5-11 (A-E) shows the apparent transfer coefficient calculated after correction and taken during 2 minutes of methanol oxidation at different potentials together with the dc and real part of the ac current transients; α' stays essentially constant during these 2 min.

As depicted in Fig 5-11F, α' values of 0.5 are obtained only at low potentials (0.63, 0.65 V) in agreement with the results of the potential sweep experiments. At higher potentials, α' decreases and obviously, the oxidation rate constant is no longer (or less) potential dependant in the vicinity of the peak potential. Such a potential independent rate would be expected for diffusion limited processes. However, it is well known that methanol oxidation is not diffusion limited [18]; the oxidation current increases with increasing potential (cf. Fig. 5-11G), the linear instead of exponential increase reflects the decreasing value of α' shown in Fig. 5-11F. The current decrease at potentials positive of the peak is rather caused by adsorption of an oxygen species that blocks the platinum active sites, which also leads to a reduced potential dependence of the oxidation rate. Obviously, and not astonishingly, the adsorption of these species occurs fast enough at high potentials to influence the adsorption of methanol on the time scale of the potential modulation. This situation is different from the case of oxidation of adsorbed CO as described above or that of methanol adsorbate oxidation described below; there, the current decrease positive of the oxidation peak is caused by decreasing coverage with CO, whereas the rate constant is increasing with potential and thus also the apparent transfer coefficient should remain constant.

A transfer coefficient of 0.5 for methanol oxidation means that the first step, a C-H bond rupture together with a charge transfer, is the rate determining step. This is what is usually assumed, Tafel slope of approximately 120 mV dec^{-1} have been reported before in steady state measurements [19], but also other values had been found in literature [20, 21] as already discussed in chapter 1, part 1.7.2.

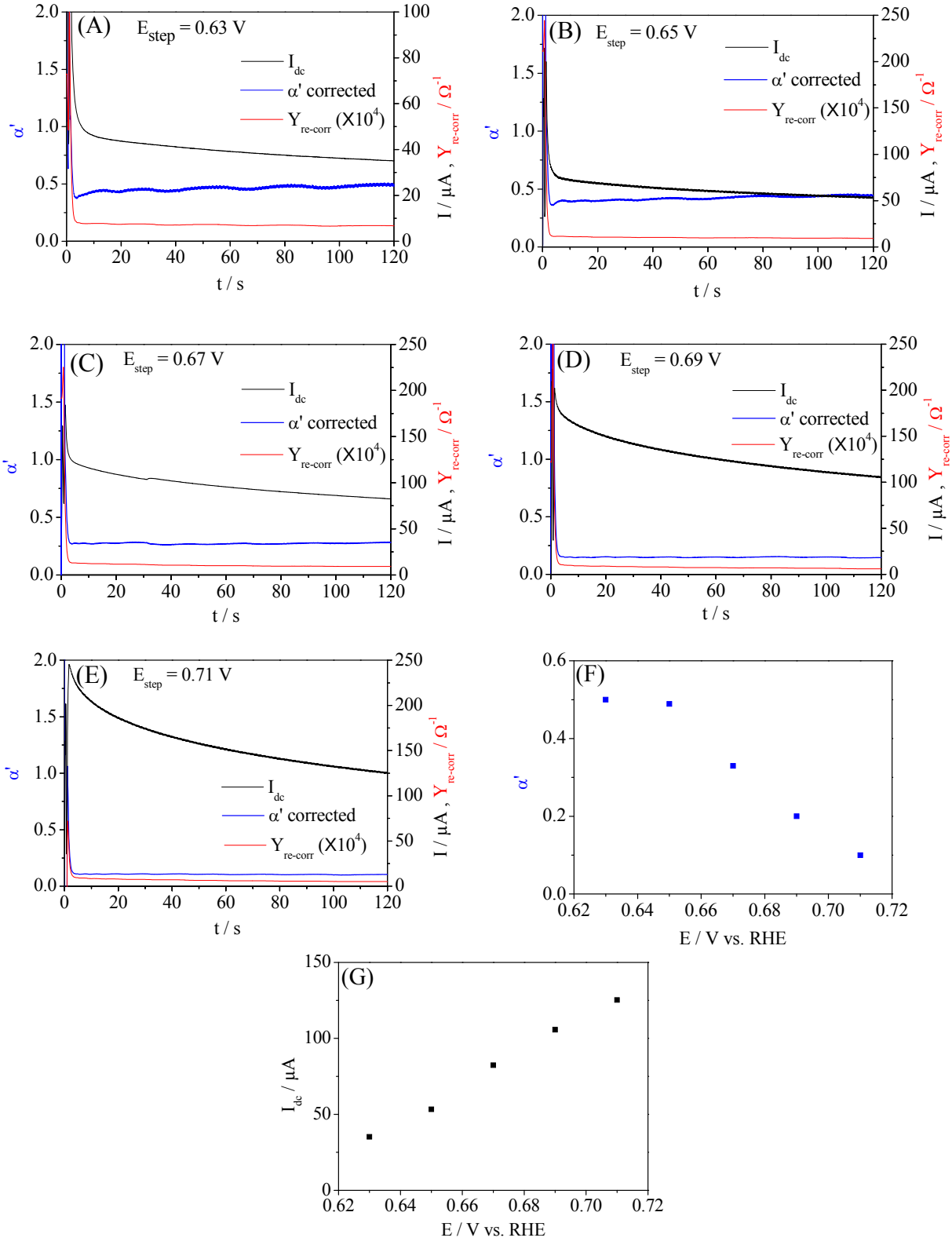

Figure 5-11 (A) The corrected apparent transfer coefficient for the oxidation of methanol at Pt(Poly) in 0.5 M H_2SO_4 at different potentials together with the dc and the corrected real part of the admittance transients (F) corrected α' values determined during 2 min of methanol oxidation at various step potentials and (G) Potential dependence of the dc current. u_{ac} = 3 mV, f = 33.5 Hz and electrolyte flow rate = 5 µLs^{-1}

Jusys and Behm et al. [22] found that the kinetic isotope effect for methanol oxidation is rather small and therefore concluded that not the C-H bond rupture is the rds, but the slow oxidation of adsorbed CO. Of course, the concept of rds is some what problematic in the case of surface reactions. In the usual determination of the Tafel slope in steady state measurements, the potential dependence of the current includes the rate of the "direct reaction path" via dissolved intermediates, which depends on the number of free sites on the surface and thus the coverage of adsorbed CO formed in the indirect pathway. Its steady state coverage depends on the rate constants of adsorption and desorption and therefore on analysis of the Tafel slope may be difficult. The ac voltammetry method presented here, however, has the advantage that the coverage within one period of the potential oscillation is constant. The Tafel slope (on apparent transfer coefficient) therefore directly reflects the potential dependence of the rate constants. Even if this method of the determination of α' cannot distinguish between the two reaction paths, the observed value of 0.5 strongly suggests that the rds is for both reactions the first reaction step.

5.2.4 Electrooxidation of methanol adsorption product

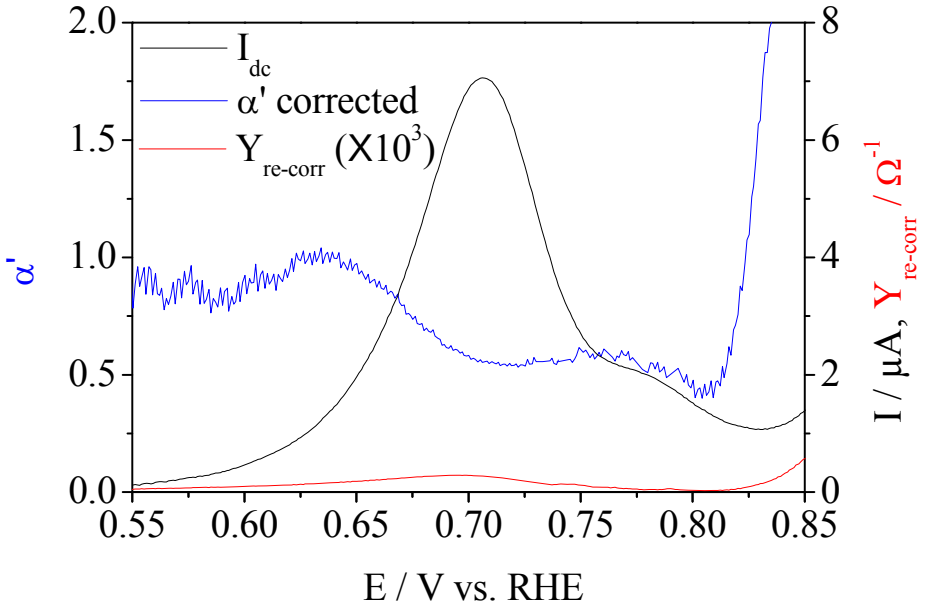

Figure 5-12 The corrected apparent transfer coefficient for the oxidation of methanol adsorption product at Pt(Poly) together with the dc current and the real part of the corrected admittance. u_{ac} = 1 mV, f = 33.5 Hz, E_{step} = 0.5 V, sweep rate = 10 mVs^{-1} and electrolyte flow rate = 5 μLs^{-1}.

Fig. 5-12 shows α' values (after correction) during a CV in which the adsorbate formed from methanol was oxidized in the supporting electrolyte as explained in chapter 2, part 2.2.2.2. The total charge density for the potentiodynamic oxidation of CO formed from methanol, calculated by integration from (0.55-0.85 V), is 260 μC cm^{-2} including the double layer charging. This is only about 70 % of the oxidation charge for adsorbed CO (from CO gas) demonstrating the lower coverage caused by the large number of adsorption sites needed for the methanol dehydrogenation. α' values around 0.5 were obtained at low potential.

α' values for the adsorbed CO formed from methanol were also determined during recording the current transients. To do so, after formation of the adsorbate, the electrolyte was exchanged for the supporting electrolyte and the potential was stepped to different potentials to oxidize the adsorbate. The oxidation charge densities of methanol adsorbate are almost constant around ca. 260 μC cm^{-2} and independent of potentials as shown in Table 5-3 except for low potentials, where a large error might occur due to the long integration time.

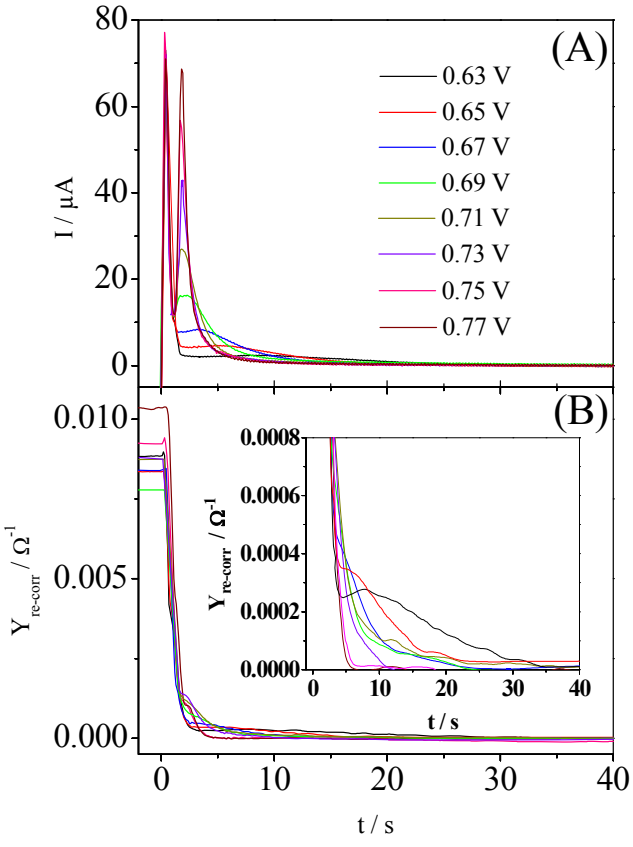

Figure 5-13 (A) The dc current transients, (B) corrected real part of the admittance transients for the oxidation of methanol adsorbate on Pt(Poly) at various step potentials in 0.5 M H_2SO_4. u_{ac} = 3 mV, f = 33.5 Hz, sweep rate = 10 mVs^{-1}, electrolyte flow rate = 5 μLs^{-1}. Inset in A: The real part of the ac current transients, inset in (B): Enlarged view of the corrected real part of admittance transients.

Table 5-3 Oxidation charge densities of methanol adsorbate at different potentials.

E_{step} / V	Q / μC cm^{-2}
0.63	186
0.65	165
0.67	193
0.69	261
0.71	269
0.73	247
0.75	240
0.77	256

The dc current transients recorded during the oxidation of methanol adsorbate at various potentials at Pt(Poly) are displayed in Fig. 5-13A, while the corrected real part of the admittance transients are displayed in Fig 5-13B. Again, with increasing potential, i_{max} increases while t_{max} decreases, also all transients start with a spike corresponding to the double layer charging current followed by the methanol adsorbate oxidation peak. In particular, at low potentials, the current is less peak-shaped than during the oxidation of adsorbed CO (cf. Fig. 5-5). This behavior was observed before [9]; it indicates a reaction order with respect to the adsorbate much lower than 1.

α' values calculated during the oxidation of methanol adsorption product at different potentials are shown in Fig. 5-14 (A-H) together with the dc and the real part of the corrected admittance as a function of time. As can be seen in Fig. 5-15, the apparent transfer coefficient values taken at the oxidation peak maximum are around 0.5.

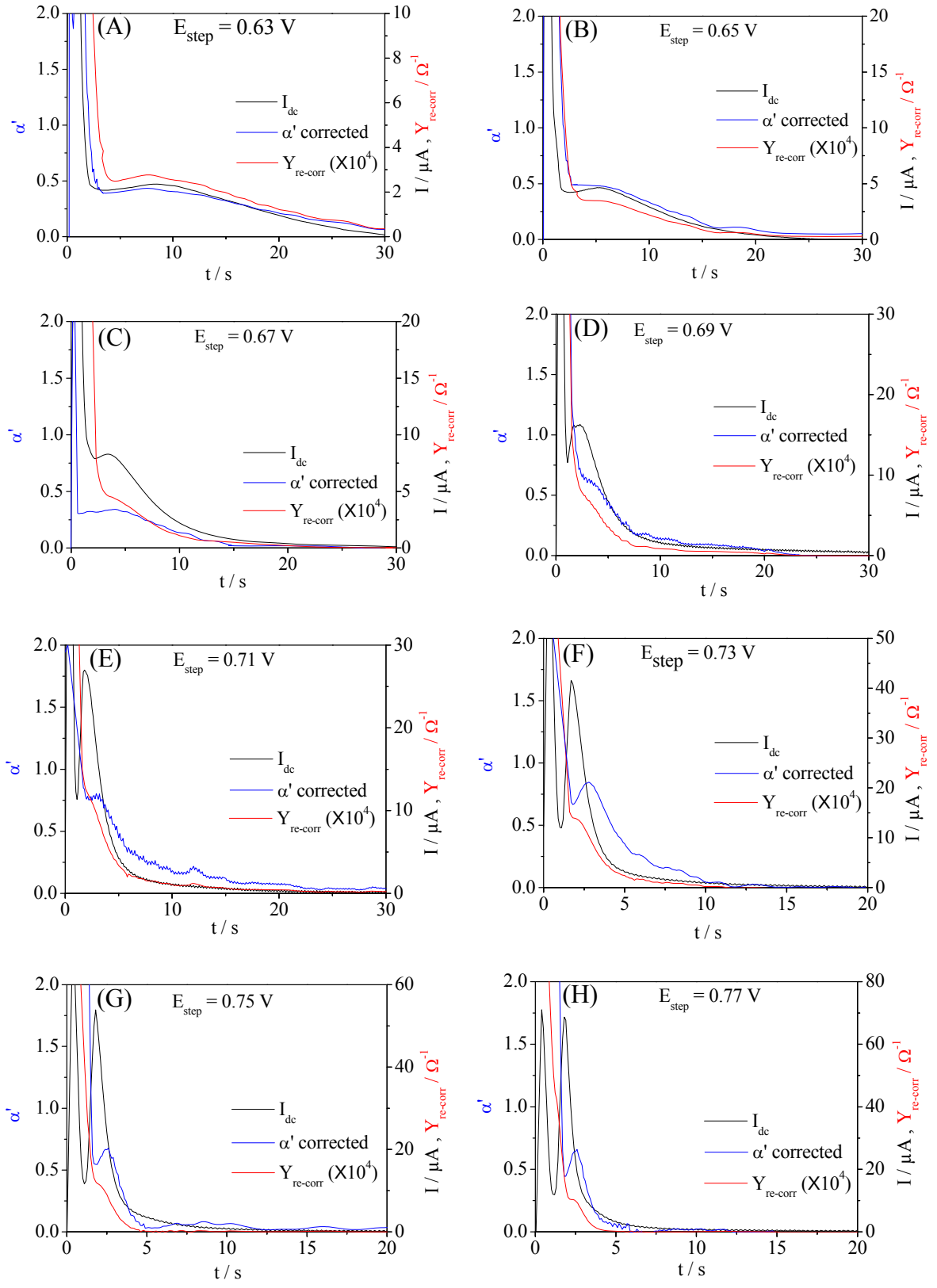

Figure 5-14 The corrected apparent transfer coefficient for the oxidation of methanol adsorbate at different potentials together with the dc and the corrected real part of the admittance transients in 0.5 M H_2SO_4, u_{ac} = 3 mV, f = 33.5 Hz and electrolyte flow rate = 5 μLs^{-1}.

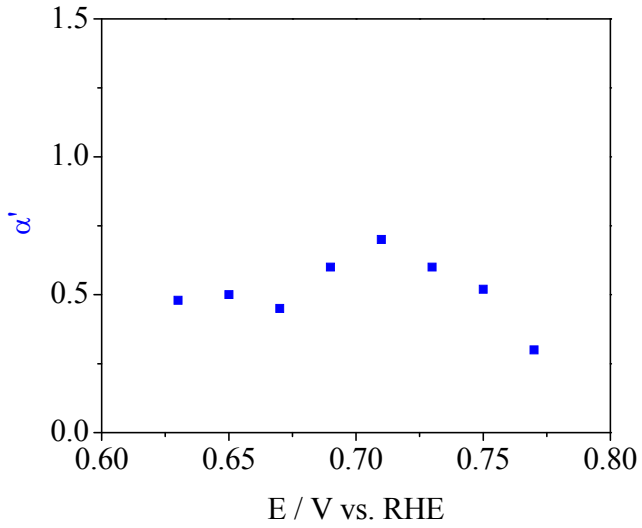

Figure 5-15 The apparent transfer coefficient for the oxidation of methanol adsorbate at Pt(Poly) at various potentials determined in the maximum of the current transients of potential step experiments and calculated after correction.

Tafel slope obtained according to the traditional methods are plotted in Fig. 5-16 using the values depicted in Table 5-4. From the plot of $log(j_{max})$ vs. E, Tafel slopes of 73 mV dec^{-1} at low potentials and 128 mV dec^{-1} at high potentials were calculated, whereas from the plot of $-log(t_{max})$ vs. E, a Tafel slope of 116 mV dec^{-1} was obtained at low potentials up to 0.7 V. At potentials higher than 0.71 V, t_{max} is not anymore decreasing with potential because of the high electrolyte resistance, but remains almost constant and hence the slope is not reasonable. I believe that the ac voltammetric determination of the Tafel slope (and transfer coefficient) is much more reliable, because not only the current and time of the maximum of the transient is used.

Table 5-4 t_{max} and j_{max} for the oxidation of methanol adsorbate at Pt(Poly) at various potentials.

E / V vs. RHE	t_{max} / s	-log t_{max}	j_{max} / µA cm^{-2}	log j_{max}	α' corrected
0.63	8.41	-0.9248	8.62	0.93551	0.42
0.65	5.51	-0.74115	16.61	1.22037	0.48
0.67	3.41	-0.53275	29.96	1.47654	0.32
0.69	2.3	-0.36173	57.6	1.76042	0.7
0.71	1.8	-0.25527	105.97	2.02518	0.76
0.73	1.82	-0.26007	151.45	2.18027	0.65
0.75	1.7	-0.23045	200.5	2.30211	0.54
0.77	1.8	-0.25527	242.76	2.38518	0.44

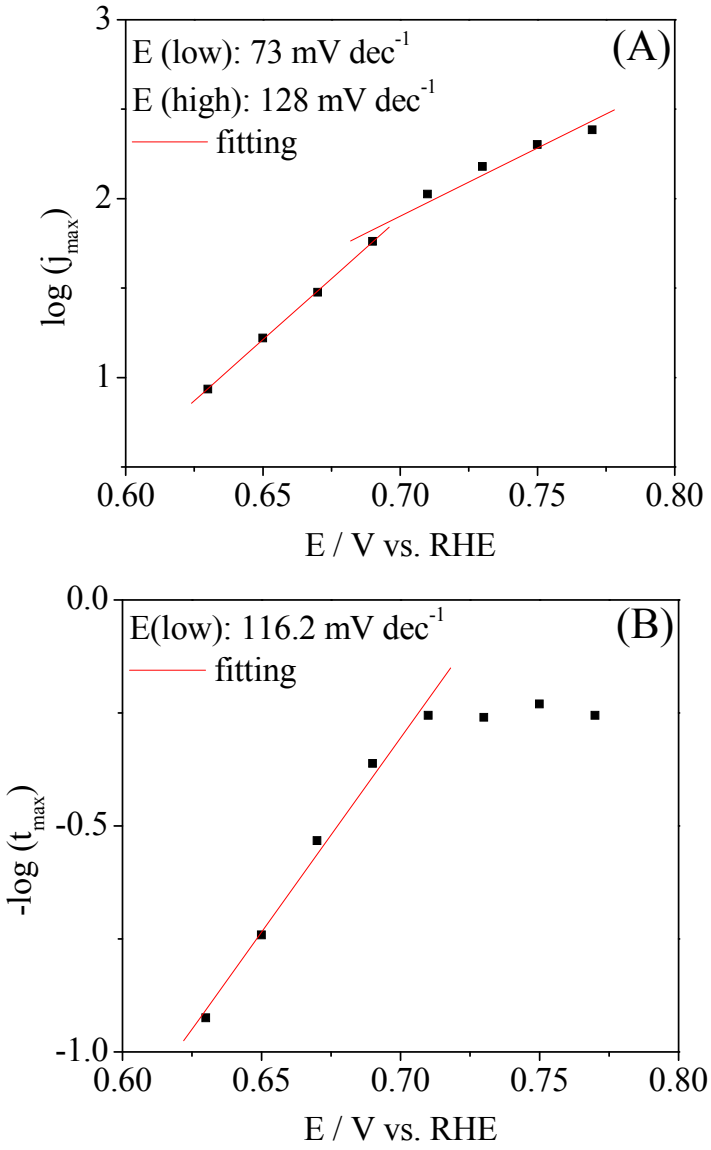

Figure 5-16 Tafel slopes for the oxidation of methanol adsorbate at Pt(Poly) measured by plotting –log(t_{max}) vs. E (A) and log(j_{max}) vs. E (B).

It is astonishing that the transfer coefficient for adsorbed CO formed from methanol differs from that observed for adsorbed CO (from CO gas): At all potentials, α' = 0.5, which means that at all potentials the first reaction step (formation of adsorbed OH) is rate determining. In reference [9], it has been already pointed out that, contrary to CO adsorbed from CO gas, the adsorbate formed from methanol is oxidized with a reaction order of zero with respect to the coverage. The reason for the different behavior might be the lower coverage of CO formed from methanol. However, in Fig. 5-3B and Fig. 5-6A it is obvious that α' is nearly constant and larger than 1 far below half coverage. According to reference [9], the 0th reaction order originates from the fact that oxidation occurs only at particularly active

sites (kinks and dislocations) to which the CO molecules diffuse. OH adsorption at such sites would then be the rate determining step, in accordance with $\alpha' = 0.5$.

A possible explanation for the different behavior of CO adsorbed from dissolved CO gas could be a slow surface diffusion of adsorbed CO. In the case of extremely slow diffusion, oxidation would proceed according to a nucleation and growth model. Then, the distribution of the CO molecules and the structure of the adsorbate layer would be different for a partially oxidized CO_{ad} layer (non homogeneous distribution of CO molecules) and the adsorbate formed from methanol. However, many papers compared the theoretical transients, obtained from Monte Carlo simulations for slow and fast surface diffusion, with experimental transients and the common conclusion was that CO diffusion on Pt is fast contrary to CO on Rh [10, 23-26]. Therefore, at this point, I cannot give a clear reason for this difference and more experiments are needed.

5.3 Conclusions

The ac voltammetry method has the advantage that the transfer coefficient can be determined at a single potential; a wide range of potentials with a constant Tafel slope is therefore not necessary. Moreover, the accurate determination is also possible for reactions of adsorbates. The high electrolyte resistance in the dual thin layer cell can be subtracted by applying a simple mathematical ac voltage correction. This correction has been applied during the determination of α' in the potential sweep and potential step oxidation of pre-adsorbed CO and methanol as well as bulk methanol oxidation at smooth Pt(Poly) electrode. As a control experiment and to test the validity of the correction method presented here, the oxidation of pre-adsorbed CO at Pt(Poly) performed previously in the H-cell was repeated here in the dual thin layer cell under flow through conditions. α'_{corr} and the corresponding Tafel slope obtained during the potential sweep and potential step experiments are in accordance with the results obtained before under stagnant conditions and negligible electrolyte resistance of 2 Ω cm^2 [1]. A transition of α'_{corr} from values around 1.5 at low potentials to 0.5 at high potentials was confirmed in the thin layer cell. All of the above proves the validity of the ac voltage correction presented here.

During the oxidation of methanol from the bulk at Pt(Poly), a typical α'_{corr} value of 0.5 (Tafel slope = 118 mV dec^{-1}) has been calculated at the onset potential of methanol bulk oxidation (ca. 0.6 V) demonstrating that the first charge transfer (according to $CH_3OH \rightarrow CH_2OH + H^+ + e^-$) is the rate determining step. Similar results were obtained in potential step

experiments in methanol containing electrolyte. During the oxidation of methanol, it is important to work under convection control (with a fast removal of intermediates from the interface), because otherwise the intermediates react further and their reaction cannot be separated from the reaction under study i.e. the oxidation of methanol itself. Previous determination of the Tafel slope often had been done in the absence of convection; that could be a further reason for differing results. Of course, in my measurement I cannot distinguish the two parallel reaction paths. Since the value determined according to the method presented here is not influenced by the potential dependence of adsorbate coverage, it is more reliable.

During the potential sweep or potential step oxidation of pre-adsorbed methanol (methanol adsorption product), α' value of 0.5±0.2 (Tafel slope 85-118 mV dec^{-1}) was obtained both at low and at high potentials. This is clearly different from the case of pre-adsorbed CO; and demonstrates the difference nature of an adsorbate layer from CO_{gas} and methanol in solution.

References

[1] H.-C. Wang, S. Ernst, and H. Baltruschat, Physical Chemistry Chemical Physics 12:2190 (2010).
[2] H. Wang, in Mathematisch-Naturwissenschaftlichen Fakultät, Rheinischen Friedrich-Wilhelms-Universität Bonn, Bonn, 2009.
[3] A. Cuesta, A. Couto, A. Rincon, M. C. Perez, A. Lopez-Cudero, and C. Gutierrez, Journal of Electroanalytical Chemistry 586:184 (2006).
[4] N. M. Markovic, B. N. Grgur, C. A. Lucas, and P. N. Ross, Journal of Physical Chemistry B 103:487 (1999).
[5] H. Massong, S. Tillmann, T. Langkau, E. A. Abd El Meguid, and H. Baltruschat, Electrochimica Acta 44:1379 (1998).
[6] E. Santos, E. P. M. Leiva, and W. Vielstich, Electrochimica Acta 36:555 (1991).
[7] E. Santos, E. P. M. Leiva, W. Vielstich, and U. Linke, Journal of Electroanalytical Chemistry 227:199 (1987).
[8] M. Bergelin, E. Herrero, J. M. Feliu, and M. Wasberg, Journal of Electroanalytical Chemistry 467:74 (1999).
[9] B. Lanova, H. Wang, and H. Baltruschat, Fuel Cells 6:214 (2006).
[10] H. Wang, Z. Jusys, R. J. Behm, and H. D. Abruña, The Journal of Physical Chemistry C 116:11040 (2012).
[11] F. J. Vidal-Iglesias, J. Solla-Gullón, J. M. Campiña, E. Herrero, A. Aldaz, and J. M. Feliu, Electrochimica Acta 54:4459 (2009).
[12] A. R. Kucernak and G. J. Offer, Physical Chemistry Chemical Physics 10:3699 (2008).
[13] L. Palaikis, D. Zurawski, M. Hourani, and A. Wieckowski, Surface Science 199:183 (1988).
[14] G. Garcia and M. T. M. Koper, Physical Chemistry Chemical Physics 10:3802 (2008).
[15] A. A. Abd-El-Latif and H. Baltruschat, Journal of Electroanalytical Chemistry 662:204 (2011).

[16] M. Krausa and W. Vielstich, Journal of Electroanalytical Chemistry 399:7 (1995).
[17] H. Wang and H. Baltruschat, Journal of Physical Chemistry C 111:7038 (2007).
[18] W. Vielstich, Fuel Cells, John Wiely & Sons Ltd., 1965.
[19] J. P. MacDonald, B. Gualtieri, N. Runga, E. Teliz, and C. F. Zinola, International Journal of Hydrogen Energy 33:7048 (2008).
[20] R. Inada, K. Shimazu, and H. Kita, Journal of Electroanalytical Chemistry 277:315 (1990).
[21] M. Umeda, H. Sugii, and I. Uchida, Journal of Power Sources 179:489 (2008).
[22] Z. Jusys and R. J. Behm, Journal of Physical Chemistry B 105:10874 (2001).
[23] N. P. Lebedeva, M. T. M. Koper, J. M. Feliu, and R. A. van Santen, Journal of Physical Chemistry B 106:12938 (2002).
[24] M. T. M. Koper, A. P. J. Jansen, R. A. v. Santen, J. J. Lukien, and P. A. J. Hilbers, Journal of Chemical Physics 109:6051 (1998).
[25] S. C. S. Lai, N. P. Lebedeva, T. H. M. Housmans, and M. T. M. Koper, Topics in Catalysis 46:320 (2007).
[26] T. H. M. Housmans, C. G. M. Hermse, and M. T. M. Koper, Journal of Electroanalytical Chemistry 607:69 (2007).

6. Application of the potential modulation method to study the oxygen reduction reaction

6.1 Introduction

The oxygen reduction reaction (ORR) has been studied in the dual thin layer flow through cell at Pt(Poly) in 0.5 M H_2SO_4 at different flow rates. As an application of the potential modulation method described in chapter 5, also here, the apparent charge transfer coefficient (α') and the corresponding Tafel slope for the ORR has been calculated and compared to the Tafel slopes obtained from the normal method. In addition to the correction of the high electrolyte resistance in the dual thin layer cell, the contribution from other adsorption processes presented by the adsorption resistance has been also subtracted. The effect of increasing convection on the obtained α' and Tafel slopes has been examined.

6.2 Results and discussion

6.2.1 Steady state oxygen reduction at Pt(Poly) in the dual thin layer cell

Fig. 6-1 shows the steady-state CVs for the ORR at three different flow rates (5, 25 and 50 μLs^{-1}) in 0.5 M H_2SO_4. The onset of ORR was around 0.95 V in all cases, which is the same potential region for platinum oxide formation [1], afterwards, the reduction current increases with increasing overpotential. A diffusion-mass transport mixed control current region is observed in the range (0.75-1.1 V) followed by a constant diffusion limited current region at potentials lower than 0.75 V typical to the ORR at platinum in acidic medium [2, 3]. As expected, a small hysteresis in the reduction currents was observed in the negative and positive-going sweeps which was attributed to the sluggish activity of the platinum oxide surfaces towards ORR as compared to the surface of platinum after complete reduction of the oxides [4]. I will therefore present and later analyze only the positive going sweeps. With increasing flow rate (convection), the values of the reduction currents increase, consequently more reactive species were transported from the bulk of the solution to the surface of the electrode and hence leading to higher current values. The mass transport limited ORR current at 0.2 V was plotted versus the cube root of the flow rate (cf. inset in Fig. 6-1). As it is well known for flow cell measurements [5, 6], the mass transport limited current decay with the cube root of the flow rate underlining that this relation is also valid here.

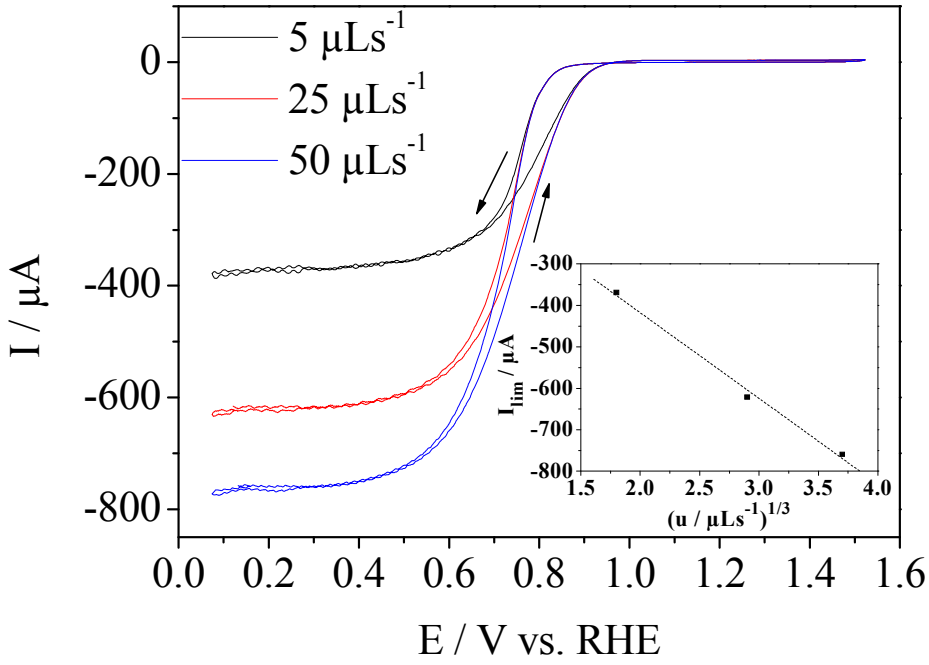

Figure 6-1 Steady-state CVs for oxygen reduction at Pt(Poly) in 0.5 M H_2SO_4 at different flow rates in the dual thin layer cell. Sweep rate: 10 mVs^{-1}. Arrows indicate the direction of the sweep. Inset: the mass transport limited ORR current at 0.2 V as a function of the cube root of the electrolyte flow rate in the dual thin layer flow through cell.

6.2.2 Apparent transfer coefficient for ORR and the negative Tafel slope

As shown in chapter 5, the high electrolyte resistance in the dual thin layer flow through cell obtained from impedance spectra has to be subtracted because it leads to high $i_{ac}R$ potential drop during the superimposed ac potential. To do so, an ac potential correction was applied.

The apparent transfer coefficient after correction is given by:

$$(\alpha'_{corr})_1 = \frac{RT}{F} \cdot \frac{Y_{re-corr}}{i_{dc}} \qquad (6\text{-}1)$$

Here, the subscript (1) indicates that only R_{el} was subtracted according to equation (5-1) to correct α'.

In reality, the adsorption resistance (R_{ad}) contributes to the real part of the admittance in the total measured potential difference. In order to exclude the contribution of R_{ad}, the corrected real part of the admittance $(Y_{re\text{-}corr})$ was calculated (as explained in chapter 5, part 5.2.1) in the supporting electrolyte saturated with argon giving ($Y^{Ar}_{re-corr}$) and with oxygen

giving ($Y_{re-corr}^{O_2}$). The difference gives the real part of the admittance corresponding to the ORR without the contribution from other adsorption processes according to:

$$Y_{re-corr}^{ORR} = Y_{re-corr}^{O_2} - Y_{re-corr}^{Ar} \tag{6-2}$$

The apparent transfer coefficient corresponding only to ORR is then given by:

$$(\alpha_{corr}^{'})_2 = \frac{RT}{F} \cdot \frac{Y_{re-corr}^{ORR}}{i_{dc}} \tag{6-3}$$

Here, the subscript (2) signifies that α' was corrected for of R_{el} and R_{ad}.

The well known Butler-Volmer equation was used to describe the kinetics of an activation-controlled reaction such as ORR [7]:

$$i = i_o(e^{\alpha_a \eta zF/RT} - e^{-\alpha_c \eta zF/RT}) \tag{6-4}$$

At high overpotential for ORR, equation (6-4) can be written as:

$$i = -i_o e^{-\alpha_c zF\eta/RT} \tag{6-5}$$

The Tafel slope *(b)* of the reaction is then given with a negative sign by:

$$\frac{\partial E}{\partial \ln|i_{dc}|} = \frac{RT}{-\alpha_c zF} = \frac{-RT}{zF} \cdot \frac{1}{\beta} \tag{6-6}$$

For a single electron transfer, the activation barrier is symmetric with β is very close to 0.5 at 25°C and a negative Tafel slope of -120 mV dec^{-1}.

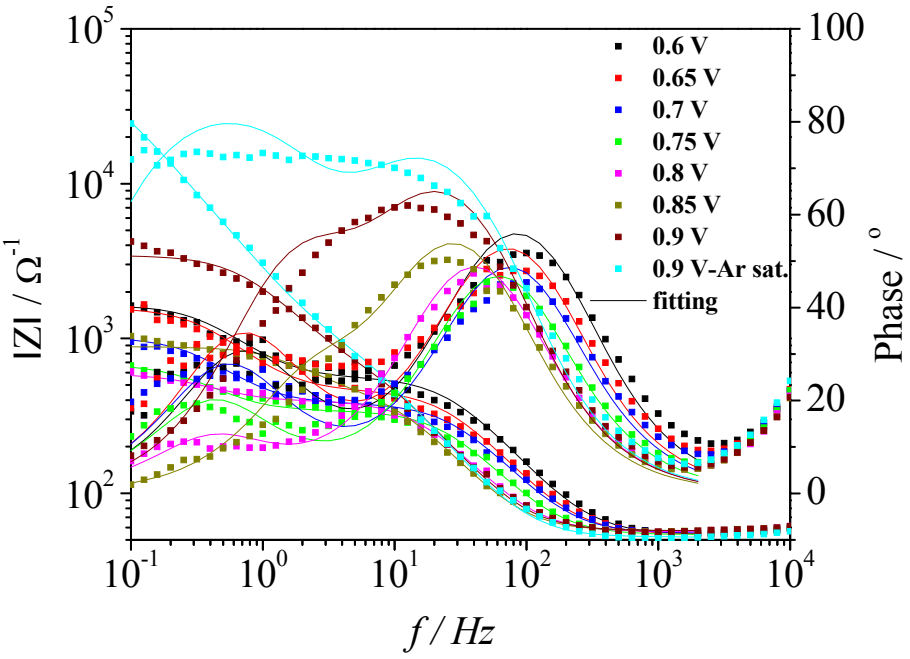

Figure 6-2 Impedance spectra of ORR at Pt(Poly) in the dual thin layer cell. Electrolyte flow rate: 5 μLs^{-1}.

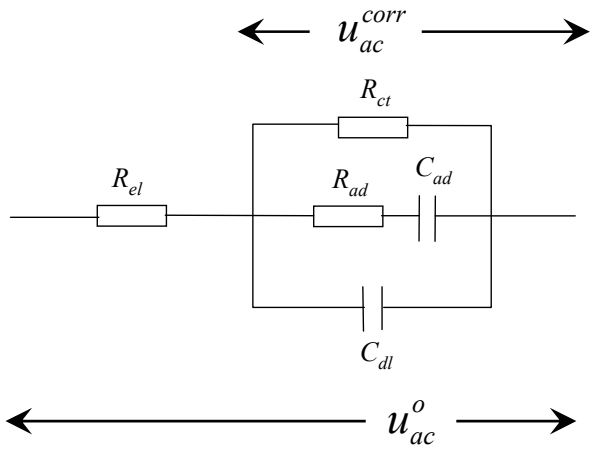

Figure 6-3 Equivalent circuit used for fitting of EIS data during ORR at Pt(Poly) in the dual thin layer cell.

Fig. 6-2 shows the impedance spectra of Pt(Poly) in an oxygen saturated supporting electrolyte at different potentials. (Note that: all impedance spectra were recorded in the positive going sweep, i.e. after switching the sweep to the anodic direction) to ensure complete reduction of surface oxides as shown above. The equivalent circuit shown in Fig. 6-3 was used for fitting of the EIS spectra (0.1 Hz - 2×10^3 Hz) and the results are listed in Table 6-1. It consists of a resistance (R_{el}) for the electrolyte resistance in series with a parallel combination of a capacitance (C_{dl}) for the double layer capacitance, another resistance (R_{ct}) for the charge transfer resistance and a resistance (R_{ad}) for the adsorption resistance which itself in series with a capacitor (C_{ad}) for adsorption capacitance.

As depicted in Fig. 6-2, at high frequencies (> 50 Hz), the impedance is simply represented by a series combination of R_{el} and C_{dl}. At low frequencies (≤ 50 Hz), however, the equivalent circuit in Fig. 6-3 holds, which includes the charge transfer resistance (R_{ct}) responsible for the determination of the oxygen reduction rate at Pt surface. For that reason, in all of the ac measurements presented here, I chose (3, 5 and 10 Hz) as appropriate frequencies.

The shape of the spectra was as expected for such equivalent circuit except at high frequencies (> 10^3 Hz). The reason is again the high iR drop and the bad current distribution in the thin layer cell. At potentials higher than 0.85 V, platinum oxide acts as a poison which inhibits the rate of ORR significantly (cf. Fig. 6-3, at 0.9 V). In addition to ORR represented by R_{ct}, adsorption of species other than oxygen occurs at Pt surface with an adsorption resistance (R_{ad}) and capacitance (C_{ad}) as depicted in Table 6-1. An electrolyte resistance in the

range 55-60 Ω cm^2 is obtained which leads to high $i_{ac}R$ drop during the superimposed ac voltage (as shown in chapter 5) and should be subtracted.

Table 6-1 Fitting data for impedance spectra of ORR at Pt(Poly).

E / V vs. RHE	R_{el} / Ω	R_{ad} / Ω	R_{ct} / Ω	C_{dl} / F	C_{ad} / F
0.6	54.3	779.8	1585	1.17×10^{-5}	1.6×10^{-4}
0.65	54.6	590.7	1524	1.52×10^{-5}	2×10^{-4}
0.7	55.2	512	959	1.7×10^{-5}	3.2×10^{-4}
0.75	54.1	546	625	2.23×10^{-5}	4.6×10^{-4}
0.8	56.5	960	533	3.04×10^{-5}	3.2×10^{-4}
0.85	57.3	1135	827	3.6×10^{-5}	4.5×10^{-5}
0.9	57.4	1603	3372	3.1×10^{-5}	2.7×10^{-5}
0.9 Ar-Sat.	52.2	2063	56456	3.12×10^{-5}	2.6×10^{-5}

Comparing the fitting data at 0.9 V in case of Ar and O_2 saturated supporting electrolyte shows that here, as pointed out before in chapter 5, part 5.2.1, a reliable impedance and ac data can be obtained in the dual thin layer cell also in case of ORR; whereas R_{ad} , C_{dl} and C_{ad} did not changes, R_{ct} in case of Ar saturated supporting electrolyte is ca. 10 times larger than in O_2 saturated one. This is not astonishing because this resistance should theoretically be infinite in pure supporting electrolyte. Also the higher time constant of the RC element in case of 0.9 V (Ar- saturated supporting electrolyte), corresponding to a frequency of 20 Hz, show that at a high frequency the current passes through the $R_{ad}C_{ad}$ elements in the equivalent circuit shown above, while at lower frequencies, it passes through the R_{ct}. Therefore, the ac voltammetry measurements should be done at such low frequencies.

Fig. 6-4 show the positive going sweep of the potential for the ORR at Pt(Poly) in oxygen saturated 0.5 M H_2SO_4 at different flow rates, 5, 25 and 50 μLs^{-1}. The reason behind selection of the positive going sweeps is again that the platinum surface is much more active after completely removing of oxides in the negative going sweeps. Underpotential deposited hydrogen (H_{UPD}) and oxide formation processes are taking place during the measurement of the ORR and their contributions are superimposed on the ORR curve [8]. It is obvious therefore to correct for the capacitive current from adsorption processes while keeping the sweep rate high enough to minimize the effect of impurities.

For comparison, the real part of the corrected admittance corrected by subtraction of R_{el} ($Y_{re\text{-}corr\ (1)}$) or by subtraction of R_{el} and R_{ad} ($Y_{re\text{-}corr\ (2)}$) is also displayed. The real part of the corrected admittance recorded in the supporting electrolyte, in oxygen saturated supporting electrolyte and the difference were also shown in Fig. 6-4 (A)'. The difference in the corrected real part of the admittance can be calculated using equation (6-2), which gives

the portion of the admittance after correction for the adsorption processes, especially that of OH^- adsorption at potentials higher than 0.8 V.

After correction for R_{el} and R_{ad} as explained above, at 3, 5 and 10 Hz, the area of interest for studying the ORR (0.8-0.9 V) exhibits a fairly constant apparent transfer coefficient (α') where the current is kinetically limited. In this region, (-(1-α) = ca. -0.5, i.e. α = 0.5) corresponding to a Tafel slope of -120 mV dec^{-1}. At potentials lower than 0.8 V, α' decreases with potential; obviously where the current is not kinetically rather diffusion limited. At potentials higher than 0.9 V, the ORR current is too low anyway due to the formation of platinum oxides and α' significantly increases with potential.

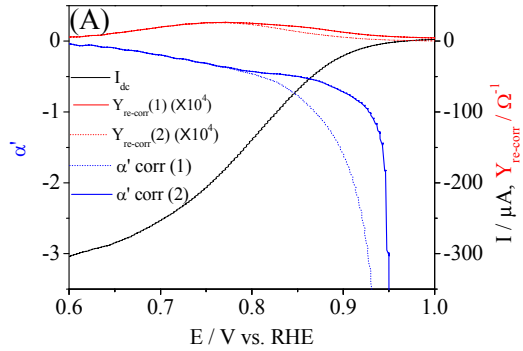

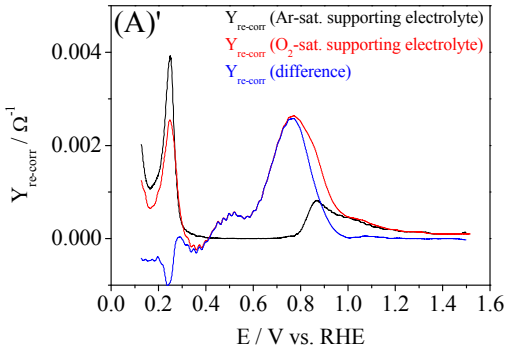

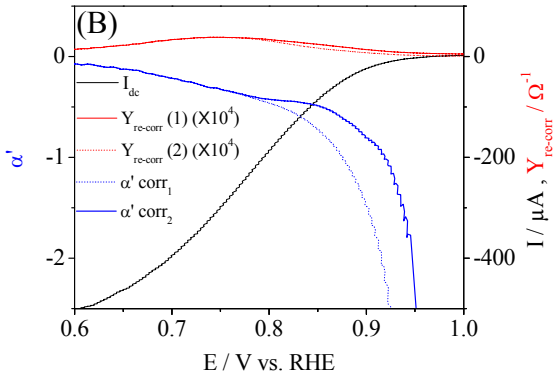

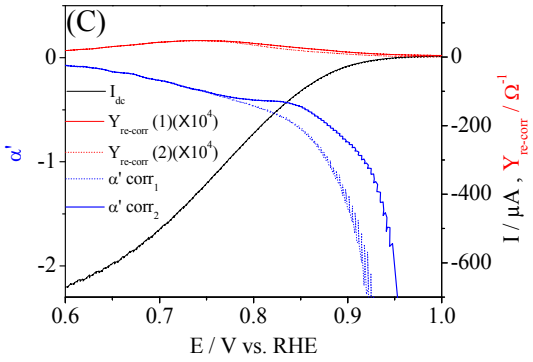

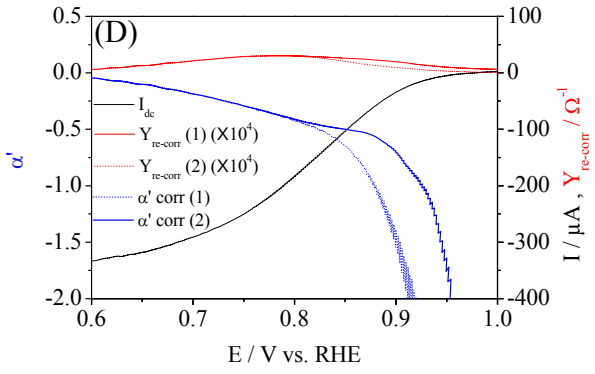

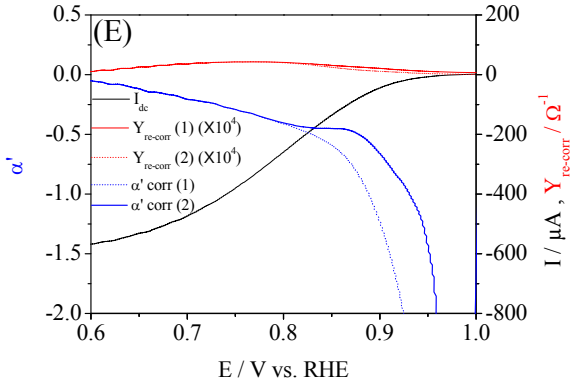

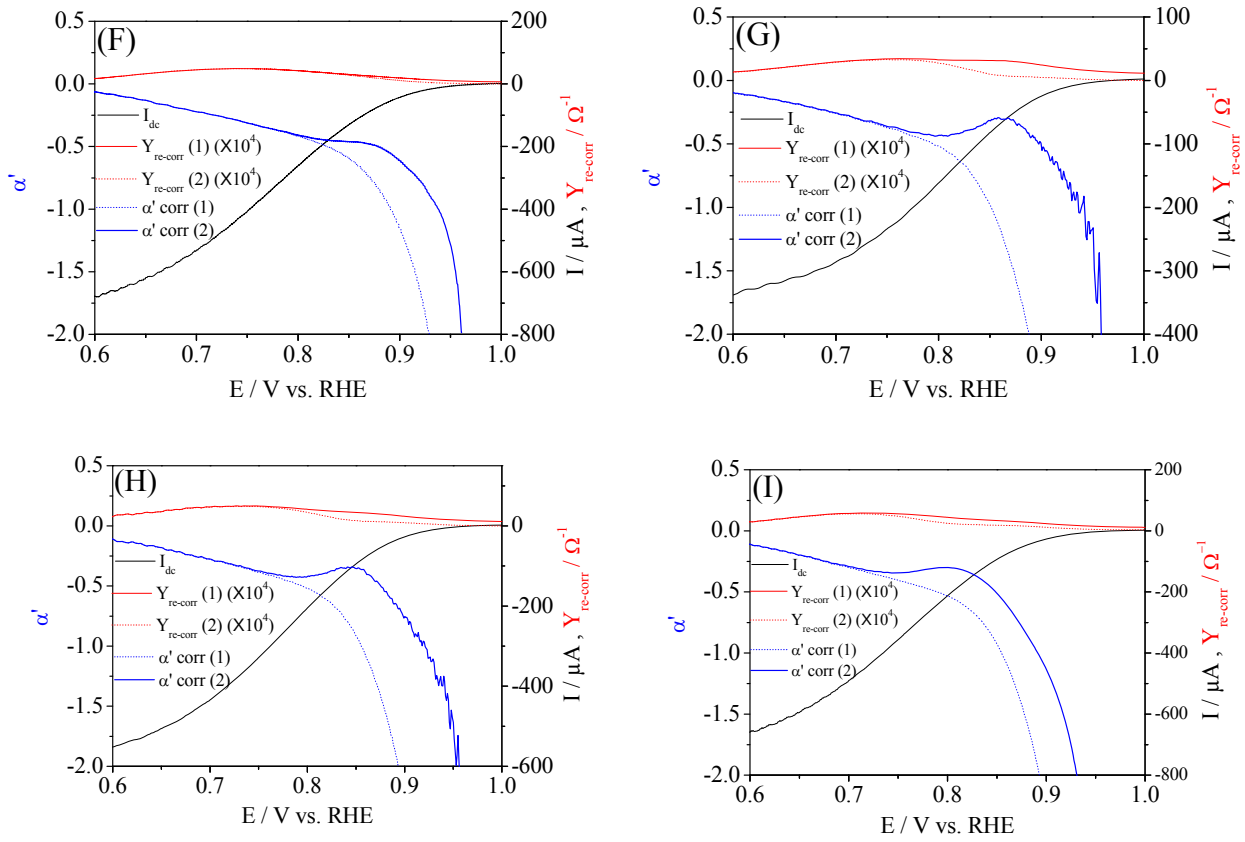

Figure 6-4 (A-C), (D-F) and (G-I), the apparent transfer coefficient after correction (blue), the dc currents (black) and the real part of the corrected admittance ($Y_{re\text{-}corr}$) (red) recorded during ORR at Pt(Poly) in 0.5 M H_2SO_4 with sweep rate = 10 mVs^{-1}, electrolyte flow rates = 5 μLs^{-1}, 25 μLs^{-1} and 50 μLs^{-1}, u_{ac} = 1 mV and f = 3, 5 and 10 Hz respectively. (A)', the real part of the corrected admittance in the Ar saturated supporting electrolyte (black), in O_2 saturated supporting electrolyte (red) and the difference (blue) at 5 μLs^{-1} and 3 Hz is shown as an example.

For comparison, the data extracted from the steady-state voltammogarms for ORR at Pt(Poly) were used to draw Tafel plot at different flow rates. At low potentials, the Tafel slope was around -120 mV dec^{-1} and at high potentials it was around -60 mV dec^{-1}, independent of the flow rate and in agreement with previous literature for ORR at platinum in acidic medium [9-12]. The change in the Tafel slope was attributed to the potential-dependent coverage of surface oxides that inhibit the adsorption of oxygen and intermediates as suggested previously [13]. It is well known that the low Tafel slope is due to ORR at platinum surface covered with oxides while the large slope is due to the same process at clean platinum surface [12]. Damjanovic et al. [14] reported that the change in the adsorption state of oxygen from Temkin-type to Langmuir-type due to the reduction of the surface oxides was the reason for

the change in the Tafel slope. A Tafel slope of -120 mV dec^{-1} with α' = 0.5 at all flow rates suggests that the first electron transfer to oxygen during ORR is the rate determining step as purposed before [12, 15, 16].

The difference between the Tafel slope obtained from ac voltammetry method (-120 mV dec^{-1}) at high potential region and that obtained from normal method (-60 mV dec^{-1}) is due to the fact that in case of ac voltammetry the coverage within one ac period is constant and the Tafel slope or the apparent transfer coefficient directly reflects the potential dependence of the reaction rate, i.e. the current is only a function of potential:

$$i = zFk_o e^{-\alpha_c F\eta/RT} \tag{6-8}$$

Then a Tafel slope of -120 mV dec^{-1} is obtained.

In the usual determination of the Tafel slope, the potential dependence of the rate is affected by the coverage since it is not constant and changed with changing the potential, i.e. depends on the number of free active sites (1-θ) and hence,

$$i = zFk_o e^{-\alpha_c F\eta/RT}(1-\theta) \tag{6-9}$$

This then leads to a non constant Tafel slope, which is decreasing with current density.

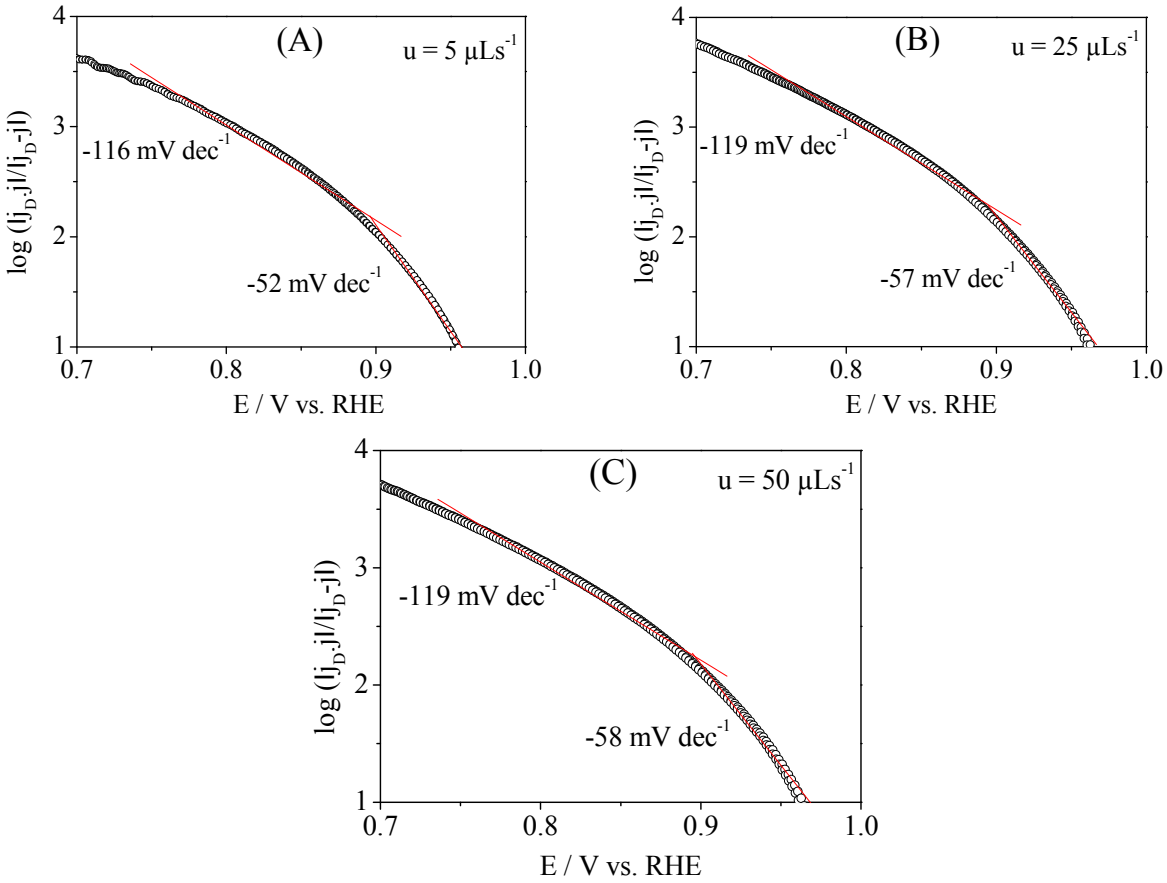

Figure 6-5 Tafel plots for ORR at Pt(Poly) electrode in 0.5 M H_2SO_4 at different flow rates.

6.3 Conclusions

The ORR has been studied in the dual thin layer flow through cell at Pt(Poly) electrode in 0.5 M H_2SO_4 at different flow rates. The potential modulation technique has been applied using three different frequencies. The high electrolyte resistance as well as the adsorption resistance has been subtracted giving a final admittance values correspond only to the ORR process. Apparent transfer coefficient values around -0.5 (Tafel slope = -120 mV dec^{-1}) were calculated in all cases independent of the frequency or the flow rate. Two different Tafel regions have been observed from the plot of log $|j_D.j|/|j_D-j|$ versus E; low Tafel slope (around -60 mV dec^{-1}) at high potential and high Tafel slope (around -120 mV dec^{-1}) at low potential in accordance with other previous investigations. The contradiction between the Tafel slopes calculated from ac voltammetry method and that from usual method at high potential is due to the influence of the coverage on the potential dependence of the rate in case of the usual method where the coverage is always changing with potential while in the ac voltammetry method the coverage is constant during the potential oscillation. From the above observation, at Pt(Poly), the first electron transfer to oxygen is the rate determining step.

References

[1] S. Strbac, Electrochimica Acta 56:1597 (2011).
[2] A. Sarapuu, A. Kasikov, T. Laaksonen, K. s. Kontturi, and K. Tammeveski, Electrochimica Acta 53:5873 (2008).
[3] N. M. Markovic, H. A. Gasteiger, and P. N. Ross, Journal of Physical Chemistry 99:3411 (1995).
[4] J. Jiang and K. Rajagopalan, Electrochimica Acta 58:717 (2011).
[5] S. G. Weber and J. T. Long, Analytical Chemistry 60:903A (1988).
[6] A. Bard and L. Faulkner, Electrochemical Methods: Fundamentals and Applications, John Wiley & Sons, New York, 1980.
[7] D. W. Banham, J. N. Soderberg, and V. I. Birss, The Journal of Physical Chemistry C 113:10103 (2009).
[8] D. van der Vliet, D. S. Strmcnik, C. Wang, V. R. Stamenkovic, N. M. Markovic, and M. T. M. Koper, Journal of Electroanalytical Chemistry 647:29 (2010).
[9] U. A. Paulus, T. J. Schmidt, H. A. Gasteiger, and R. J. Behm, Journal of Electroanalytical Chemistry 495:134 (2001).
[10] B. N. Grgur, N. M. Markovic, and P. N. Ross, Canadian Journal of Chemistry-Revue Canadienne De Chimie 75:1465 (1997).
[11] N. Markovic, R. Adzic, B. Cahan, and E. Yeager, Journal of Electroanalytical Chemistry 377:249 (1994).
[12] N. Wakabayashi, M. Takeichi, M. Itagaki, H. Uchida, and M. Watanabe, Journal of Electroanalytical Chemistry 574:339 (2005).
[13] N. Alexeyeva, K. Tammeveski, J. Solla-Gullón, and J. M. Feliu, Electrochimica Acta 55:794 (2010).
[14] A. Damjanovic and V. Brusic, Electrochimica Acta 12:615 (1967).

[15] N. M. Markovic, H. A. Gasteiger, B. N. Grgur, and P. N. Ross, Journal of Electroanalytical Chemistry 467:157 (1999).
[16] N. M. Markovic, T. J. Schmidt, V. Stamenkovic, and P. N. Ross, Fuel Cells - From Fundamentals to Systems 1:105 (2001).

7. Summary and outlook

The main challenge in the area of fuel cell research is to find a good catalyst that helps in complete oxidation of the fuel at the anode and reduction of the oxygen at the cathode at a low overpotential which consequently would give rise to the maximum cell efficiency. However, for the direct methanol fuel cell (DMFC) operating at low temperature, the main problem that arises at the anode is its poisoning (deactivation) due to the accumulation of the fuel adsorption product (CO_{ad}) which can only be oxidized at high potentials (> 0.7 V). For low temperature direct ethanol fuel cells (DEFCs), the main problem that arises at the anode, beside its poisoning by ethanol adsorption products (CO_{ad} and $CH_{x,ad}$), is the incomplete ethanol oxidation due to the difficulty of (C-C) bond breaking. In the previous types of fuel cells, a sluggish ORR kinetics was observed at the cathode which results in a large voltage drop. Such behavior is due to strong inhibition of the cathodic ORR, resulting in high overpotentials and therefore, significant deterioration in the energy conversion efficiency of the cell. The slow kinetic behavior stems from the difficulty of (O=O) bond breaking.

In order to model the conditions of continuous oxidation/reduction in a fuel cell, the continuous mass transfer to the electrode surface is necessary. Therefore, mass spectrometry and ac voltammetry measurements presented here were done using the thin layer flow through cell. This thesis aims at a determination of the rate constant of single reaction steps during the oxidation of CO, methanol and ethanol at different platinum surfaces. Towards that aim, I investigated the electrocatalytic oxidation and adsorption rate of methanol (chapter 3) and the electrocatalytic oxidation of ethanol (chapter 4) at different Pt surfaces, using DEMS. In chapter 5, the potential dependence of the bulk and adsorbed methanol oxidation reaction rate (presented by the apparent transfer coefficient, α') and the corresponding Tafel slope of the reaction have been determined under convection conditions using a potential modulation ac voltammetry technique. Finally, as an application of the method presented in chapter 5, my work in chapter 6 aims at the determination of the apparent transfer coefficient and Tafel slope of the ORR at Pt(Poly) electrode.

The electrooxidation of methanol proceeds via the dual pathway mechanism. The first pathway (named "indirect pathway") involves the dehydrogenation of methanol to adsorbed CO followed by its oxidation to CO_2. The second pathway (named "direct pathway") involves the formation of dissolved intermediates as HCHO and HCOOH which are transported away from the electrode surface by convection. CO_2 current efficiencies and the degree of surface

poisoning with CO_{ad} have been shown to be independent of the electrolyte flow rate; both confirm the parallel pathway mechanism.

As shown above, since CO_{ad} is the main poison of the anode catalyst layer in the direct alcohol fuel cell, it is better to catalytically oxidize it at a low overpotential. In the present thesis, it has been shown that Ru electrodeposited at Pt is better catalyst than pure Pt. It promotes the oxidation of CO_{ad} at low potentials according to bifunctional and electronic mechanisms, at high potentials, however, Ru losses its co-catalytic activity. On such bimetallic surfaces, Ru is preferentially adsorbed at steps. Complete blocking of the Pt step sites with Ru shifts the oxidation to the direct pathway (non-CO-pathway) and thus results in low CO_2 current efficiency. It leads also to the inhibition of the methanol oxidation current due to the blocking of the most active Pt step sites necessary for methanol adsorption and oxidation.

Methanol adsorption rates have been determined: at Pt(Poly), the adsorption rate increases with increasing methanol concentration and adsorption potentials. At Pt(331) and Pt(332) electrodes, methanol adsorption rate was doubled with double step density, higher with higher Ru coverage and increase by a factor of 10 per 0.1 V. Increasing step density however lead to a decrease in methanol adsorption rate from 2.2 MLs^{-1} at Pt(100) to only 1.8 MLs^{-1} at Pt(11,1,1) due to the geometric ensemble effect and the much smaller activity of (111) sites as compared to (100) sites.

A detailed evaluation of the CO_2 and acetaldehyde current efficiencies during ethanol oxidation at Pt(Poly), Pt(11,1,1) and Pt(311) as well as the same single crystal surface modified with Sn has been investigated. Under flow through conditions, during the potentiostatic ethanol oxidation, the amount of CO_2 is negligible. There is no further oxidation of the soluble product at the surface and acetaldehyde is the main oxidation product (current efficiency close to 100 %). At a Pt(311) electrode, a small amount of CO_2 is observed due to the oxidation of the ethanol adsorption product and not due to the oxidation of bulk ethanol as proved by a separate potential step experiments. Acetic acid in addition to acetaldehyde (current efficiency of ca. 50 %) are the main oxidation products. The onset of ethanol oxidation at Sn modified Pt(311) electrode is shifted negatively by 0.2 V. This shift is not associated with CO_2 production; rather acetaldehyde and acetic acid are the main oxidation products.

At the above surfaces, the experimentally determined acetaldehyde current efficiencies are too high if calibration is simply achieved by an electrolyte with a known concentration of the product due to incomplete mixing in the dual thin layer flow through

cell. By performing other experiments with i-propanol, I determined a correction factor for that: In that case, the product (acetone) with a faradaic current efficiency of 100 % has a similar diffusion coefficient and volatility as acetaldehyde.

The apparent transfer coefficient (α') and consequently the corresponding Tafel slopes were determined quasi continuously as a function of potential or time (i.e. in the CV or in the potentiostatic experiments) for the oxidation of pre-adsorbed CO, and methanol as well as bulk methanol at Pt(Poly) electrode under convection conditions. This method involves a sinusoidal modulation of the potential and simultaneous recording of the ac and the dc current. This method has the advantage that the transfer coefficient can be determined at a single potential; a wide range of potentials with a constant Tafel slope is therefore not necessary. In control experiments, using adsorbed CO, values previously determined using the H-cell were reproduced. This demonstrates that the method is applicable to the thin layer cell despite of the high electrolyte resistance which was subtracted by applying a simple ac mathematical ac voltage correction. Contrary to the case of the oxidation of adsorbed CO, where the transfer coefficient varies from about 1.5 at low potentials to 0.5 at high potentials due to a change of the rate determining step, the apparent transfer coefficient for the methanol adsorption product is around 0.5 (Tafel slope of 118 mV dec^{-1}) at all potentials, suggesting that at all potentials the first reaction step, the adsorption of OH, is the rate determining step and not in equilibrium.

As an application of the above mentioned ac voltammetry method, the apparent transfer coefficient and the Tafel slope have been also determined for the ORR at Pt(Poly) electrode under convection conditions. In addition to the high electrolyte resistance, also a correction for the adsorption resistance was performed. Apparent cathodic transfer coefficient of ca. 0.5 (Tafel slope of ca. –120 mV dec^{-1}) were calculated in all cases independent of the frequency and the electrolyte flow rate. This suggests that, at Pt(Poly) the first electron transfer to oxygen is the rate determining step.

For future work, the following experiments would be most interesting:

1. Determination of the apparent transfer coefficient for ORR for some other ORR catalysts, e.g., metal oxide based catalysts.
2. Electrocatalytic oxidation of methanol on Sn modified surfaces vicinal to (100) plane, e.g., Pt(11,1,1) and Pt(311) in order to examine what would be the effect of Sn on the current efficiency for CO_2 during methanol oxidation.

3. Electrooxidation of CO at Ag modified Pt(311) electrodes whereas Ag is much stable adatom at Pt electrode. In this respect, it would be interesting to check what would be the behavior of adsorbed CO at these surfaces, where CO molecules could adsorb and what would be the effect of Ag on the CO coverage at the surface.

A C K N O W L E D G E M E N T S

I would like to express my deepest gratitude to my advisor **Prof. Dr. Helmut Baltruschat** for his support, guidance and assistance in all the work I have accomplished. Above all the most needed, he provided me unflinching encouragements in various ways. I am indebted to him more than he knows.

My appreciation is also extended to the other member of my thesis committee, **Prof. Dr. Wandelt**, **Prof. Dr. Mader** and **Prof. Dr. Maier**. I would like to thank them for their willingness to take the time to oversee the development and evaluation of my thesis.

Especial thanks to **Dr. Ernst** for his valuable discussions in both theoretical and experimental areas. I really enjoyed the work with **Dr. Abd El Aziz** (my old brother), his help and encouragements are gratefully acknowledged. I thank also my present and former colleagues in the electrochemistry group for their help on struggling against the difficulties both in experiments and living, **Dr. H. Wang**, **Ipek**, **Ahmet**, **Izet**, **Johannes**, **Xu**, **Nicky**, **Ana**, **Hatem**, **Shahid**, **Nikolay**, **Sevda**, **Mehdi**, **Christoph Molls**, **Christoph Bondü**, **Claudia**, **Jan**, **Sabina** and **Markus**. The friendship and help of Mrs. Kleine and Mrs. Rossignol are gratefully appreciated.

I would like also to thank all members in the mechanical, electronic and glass workshops, especially **Mr. Königshofen**, **Mr. Backhausen**, **Mr. Böhmer** and **Mr. Langen**, for their help, support, repairing and reconstructing fine glasses and electronics devices. Many thanks also to the computer expert **Mr. Knut Hintzen** for his kind help.

I thank also the Egyptian Government (Ministry of High Education and Research - MOHE) for the financial support of this research for four years. I express my thanks to all members in the Egyptian Culture Office in Berlin, especially; **Prof. Dr. Sayed Tag El Din**, **Prof. Dr. Mamdouh Eldamaty**, **Mr. Imad** and **Mrs. Iman** for their kind help and support.

I would like to thank my parents, my sister, all of my family members and my friends in Bonn. They were always encouraging me and supporting me with their best wishes.

Many thanks to my lovely wife for her patience, love and motivational support that helped me reach all of my aims so far. She was always there carrying me up and stood by me through good and bad times. The joy of my lovely daughter **(Jana)** and my little son **(Ahmed)** helped me a lot.
Finally, without the help of **ALLAH**, this work would not have been completed.

Ehab Mostafa

CURRICULUM VITAE

UNIVERSITY EDUCATION

2008-2012 PhD in Bonn University, Germany

Dissertation: *Electrocatalysis and Kinetics of the Direct Alcohol Fuel Cells: DEMS and ac Voltammetry Studies*

Supervisor: Prof. Dr. Helmut Baltruschat

2002-2005 M.Sc. in Mansoura University, Egypt

Dissertation: *Preferential solvation of some drugs and their metal complexes in aquo-organic mixtures*

Supervisors: Prof. Dr. Gaber M. Abu El-Reash, Prof. Dr. Ibrahim S. Shehatta and Prof. Dr. Usama El Ayaan

2001-2002 Post graduate courses as partial fulfillment of the requirements of the M.Sc. degree, Faculty of Science, Mansoura University, Egypt

1997-2001 B.Sc. Chemistry (Excellent with honor, 85 %), Mansoura University, Egypt

WORK EXPERIENCE

2008-2012 Egyptian scholarship for PhD study in electrochemistry
Bonn University, Germany.

2005-now Assistant lecturer in Chemistry department, Faculty of Science, Mansoura University, Egypt.

2001-2005 Demonstrator in Chemistry department, Faculty of Science, Mansoura University, Egypt.

PUBLICATIONS

1. Electrooxidation of Ethanol at Polycrystalline and Platinum Stepped Single Crystals: A Study by Differential Electrochemical Mass Spectrometry; Electrochim. Acta, 55(2010) 7951-7960.
2. Quantitative DEMS Study of Ethanol Oxidation: Effect of Surface Structure and Sn Surface Modification; Phys. Chem. Chem. Phys., 2012, 14, 16115–16129

3. Quasi Continuous Determination of the Apparent Transfer Coefficient of Methanol Oxidation using a Potential Modulation Technique under Convection Conditions; Submitted.
4. Electrocatalytic Oxidation and Adsorption Rate of Methanol at Different Platinum Surfaces: a DEMS Study; in preparation.
5. Application of the Potential Modulation Technique to Study the ORR at different Platinum catalysts; in preparation.

CONFERENCES AND POSTER CONTRIBUTION

1. 8th and 9th International Conference on Chemistry and its Role in Development, Sharm El Sheikh, Egypt.
2. **Electrooxidation of Ethanol on Pt(332) and Ru Modified Pt(332) Electrodes: DEMS Study,** Bunsentagung 2009 ''Physical chemistry of solids: The Science behind Material Engineering'', 21-23 May 2009, Universität zu Köln.
3. **Ethanol and Methanol: Adsorption Rates and Rates of Intermediate Formation at Pt Single Crystal Electrodes,** 216th ECS meeting with EuroCVD 17 and SOFC XI-11th International symposium on Solid Oxide Fuel Cells, 4-9 October 2009, Vienna, Austria.
4. **Step Decoration with Cocatalysts for CO and Methanol Oxidation: Effect on Transfer Coefficient and Mechanism,** 216th ECS meeting with EuroCVD 17 and SOFC XI-11th International symposium on Solid Oxide Fuel Cells, 4-9 October 2009, Vienna, Austria.
5. **DEMS Study on Methanol Electrooxidation at Monocrystalline Platinum Electrodes: The Effect of Adsorption Time, Surface Structure, Ru Adatom and Potentia,** Electrochemistry from biology to physics, the 61st Annual Meeting of the International Society of Electrochemistry, 26th September -1st October 2010, Nice, France.
6. **Vacuum Technique Workshop** - Universität zu Köln.
7. **Alcohol Adsorption and Oxidation at Modified Stepped Pt Electrodes,** Doktorandenworkshop, Template Funktionale Chemische Schablonen SFB 624, 17-18 June 2010, Bad Honnef, Germany.
8. Emin Dikman 1st National Applied Electrochemistry Summer School, 14-17 September 2010, Izmir, Turkey.
9. **Quasi Continuous Determination of the Symmetry Factor by Potential Modulation Technique under Convection Conditions,** Electrochemistry for Advanced Materials,

Technologies and Instrumentation, the 63rd Annual Meeting of the International Society of Electrochemistry, 19-24 August, 2012, Prague – Czech Republic.

LECTURE CONTRIBUTIONS

1. **DEMS Study on Methanol Electrooxidation at Monocrystalline Platinum Electrodes: The effect of Adsorption time, Surface Structure, Ru Adatom and Potential,** Winter School of Electrochemistry, 6-11 February 2010, Kleinwalseltal, Austria.
2. **DEMS Study on the Oxidation of Ethanol at Poly- and Single Crystal Platinum Surfaces,** Electrocatalysis: Present and Future, an ELCAT Meeting, 14-17 November 2011, Alicante, Spain.
3. **DEMS Study on the Oxidation of Ethanol at Poly- and Single Crystal Platinum Surfaces,** Winter School of Electrochemistry, 24-29 February 2012, Kleinwalseltal, Austria.